UNIVERSITÀ DEGLI STUDI DI CATANIA

Dipartimento di Scienze Biologiche, Geologiche e Ambientali

Dottorato in Scienze Geologiche, Biologiche e Ambientali - XXXII ciclo

Ph.D. Thesis

Presented to obtain the rank of
INTERNATIONAL DOCTOR

RACHELE LOMBARDO

Role of Granitoid Magmatism in the Growth and Evolution of the Continental Crust: A Petrological and Geochronological Study of Quartz-Diorites and Tonalites from a type section of Late-Paleozoic Continental Crust (Serre Batholith, Southern Italy).

Tutor:
Prof.ssa Patrizia Fiannacca

Co-tutor:
Prof. Miguel A. Stipp Basei
Prof. Rosolino Cirrincione

Table of Contents

Introduction

The widespread abundance of granitoid rocks and their metamorphic equivalents highlights that granitic magmatism plays a fundamental role in the genesis and evolution of the continental crust throughout all the Earth history. Nevertheless, the origin of granitic magmas is much controversial and any study devoted to this topic includes several parameters to be determined, such as source nature and composition, causes and mechanisms of melting and processes of magmatic differentiation. The relative contribution of the mantle and crustal sources in granite generation represents essential information to be acquired.

The mantle has undoubtedly played an important role in the primordial continental crust differentiation. Despite, the current larger portion of the continental crust is made up of quartz-feldspathic composition, namely granite and granodiorite (Dhuime *et al.,* 2011; Hawkesworth *et al.,* 2010; Rudnick and Gao, 2003), that are not in equilibrium with the ultramafic mantle assemblage. It suggests that granitoid rocks cannot be directly derived from mantle melting (Rudnick, 1995). In fact, once mafic magmas leave their source, differentiation processes (fractional crystallization, peritectic entrainment, restite unmixing, magma mixing) and assimilation (AFC) of pre-existing crust modify the primitive composition. In this view, two main mechanisms have been invoked to explain granitic magmatism:

1) partial melting of felsic meta-sedimentary or meta-igneous rocks either containing free water or the contribution of hydrous minerals (Chappell & White, 1974; 2001);
2) differentiation of mantle-related magmas (Bonin *et al.,* 2005; Moyen *et al.,* 2017).

It makes it possible to discriminate between granites derived from intracrustal differentiation and those that, including mantle components, represent new additions to the continental crust. Furthermore, to realize the mechanisms and the interval times necessary to build granite batholiths is also critical to understand how crust grows and evolves (Moyen *et al.,* 2017).

In the geodynamic setting plays a central role in granite generation:

1. subduction-related granitoids usually have a significant contribution from mantle magmas;
2. late- to post-orogenic settings are more favourable to granite generation by re-melting of pre-existing continental crust in a “very hot” system (e.g., Moyen et al., 2017; and references therein).

The crust of arc environment is formed through differentiation of mafic melts (basaltic to andesitic magmas derived by fluxed-melting of the mantle) with heat transfer linked to magma advection.

The late-orogenic location represents a complex magmatic activity with the formation of (i) crust-derived granites referred to the extensional setting. The partial melting of lower and middle crust produces melts at relatively low temperatures (water present or with muscovite breakdown) or higher temperatures (biotite breakdown); (ii) Mg-K mafic melts. The source is the mantle contaminated by crustal material producing a hybrid magma (Moyen *et al.,* 2017).

Besides, mafic magmas (e.g., gabbros and diorites) made up a small part of a granitoid batholith, they can represent the keystone to understand the probable contribution of the mantle. They have been explained as mantle-derived parental magma (LeBel *et al.,* 1985; Jung *et al.,* 2015), end-member in mixing and assimilation processes (Reid *et al.,* 1983; De Paolo, 1981), materials of lower crustal regions (Gromet & Silver, 1987) and the heat source for the melting of the underlying continental crust (Pitcher, 1982; van de Flierdt *et al.*, 2003).

The Capo Vaticano Promontory (CVP), representative of late-orogenic magmatism, has been selected for this study since it represents a part of the deepest portion of the Serre Batholith, where the quartz diorites are the most mafic end members, as well as the deepest and oldest magmatic units of a 12-km thick granitoid batholith forming the middle portion of an almost complete and intact late Palaeozoic crustal section, exposed in the Serre Massif-Capo Vaticano Promontory in central Calabria (southern Italy). They crop out with a wide variety of compositions and microstructural features, varying degrees of interaction with the migmatite host rocks, varying proportions of totally preserved to totally disaggregated MME, as well as very good exposure conditions and state of preservation. All these conditions make the CVP an ideal study area for investigating batholith-forming processes and, ultimately, the processes involved in the growth/differentiation of the continental crust.

The aim of this study is to achieve a better knowledge on the processes of growth and evolution of the continental crust. To assess these process we carried out an isotope study an isotope study (Rb-Sr, Sm-Nd, Pb-Pb for the whole-rock and U-Pb and Hf in the zircon crystals) of lower crustal quartz diorites yield reasonable proof about recycling of old crust or new mantle addition during late orogenic processes. The combination of major/trace element and whole-rock isotopic composition permit to determine the magma source and the differentiation processes. Finally, SHRIMP U-Pb ages provide time constrain about anatectic processes, emplacement age of the magma and late-recrystallization processes.

1. Geological background

1.1 The Western European Variscan Belt

In Europe, the time span between 430 to 330 Ma was characterized by the convergence of Gondwana and Laurentia-Baltica supercontinents (Behr et al., 1984; Matte,1986; Burg et al., 1987; Ledru et al., 1989; von Raumer & Stampfli, 2002; 2003) with the closure of oceanic basins and micro-plates docked to Laurentia-Baltica (Matte, 2001). The final collision is dated at 340-330 Ma (late Carboniferous; Caggianelli *et al.,* 2007; Angì *et al.,* 2010), leading tothe formation of Pangea (c. 300 Ma), with the amalgamation of Gondwana, peri-Gondwana and Laurussia (e.g., von Raumer, 2013). The late-Variscan stage was characterized by a transtensional/transpressional tectonic setting producing widespread partial melting of the continental crust (320 – 280 Ma). This was explained by slab roll-back of Paleo-Tethys oceanic lithosphere (von Raumer *et al.,* 2003; Angì *et al.,* 2010). Afterwards, a fast uplift (1 mm/year)and rapid erosion affected the intracontinental detrital basin in the Late Carboniferous (Capuzzo e Bussy, 2000). The area was interested by a metamorphic evolution, where the U-Pb monazite dating indicated an in-situ decompression melting at around 320 ± 1 Ma for the paragneisses and at around 327 ± 2 Ma for the metapelites (von Raumen *et al.,* 2003). A bimodal Carboniferous granite magmatism was recorded in the Mont-Blanc/Aiguilles Rouges area. It is characterized by the Al-rich, crustal-derived melts and mantle-derived mafic melts with variable amounts of crustal contamination. Their emplacement is influenced by lithospheric-scale transcurrent faults (Burg et al., 1994). Minor volumes of anatectic melts have been also produced by in situ decompression melting.

Clockwise P-T (pressure-temperature) paths tracked the previous tectonic lithospheric evolution: burial and heating during crustal thickening (Devonian–Carboniferous), followed by nearly isothermal decompression and final isobaric cooling (Late Carboniferous–Permian, i.e., late Variscan stage; Caggianelli *et al.,* 2007 and reference therein). Associated to the clockwise P-T path large volumes of granitoids were emplaced, defining the European Variscan belt. Well exposed outcrops are located in north-eastern Sardinia (Ricci, 1992; Di Vincenzo et al., 2004), Central French Massif (Gardien et al., 1997), Bohemian Massif (Buttner and Kruhl, 1997) and the Calabria massifs (Schenk, 1989; Rottura et al., 1990; Fiannacca et al., 2015). Late Variscan stages are characterized by contemporaneous LP-HT metamorphism and widespread magmatism (e.g. Ricci, 1992; Krohe, 1998; Graessner *et al.,* 2000; Ledru *et al.,* 2001).

1.2 The Calabria-Peloritani Orogen

Remnants of the European Variscan Chain are well preserved in the Calabria-Peloritani Orogen (CPO), an arcuate Alpine mountain belt linking the nowadays southern Apennines and the Sicilian Maghrebides, in southern Italy (Fig. 1.1). The CPO architecture is the result of Cretaceous-Paleogene Europe verging Eo-Alpine chain, constituted by basement nappe and ophiolite-bearing tectonic units that built the Apennine orogenic belt in the Neogene (Cirrincione *et al.,* 2015). The present-day location of CPO is related to the progressive back-arc opening of the Tyrrhenian sea together with thrusting promoted by slab roll-back of African subducting plate and the south-eastward migration of the entire belt towards the nowadays geographical location (Rossetti *et al.,* 2001; Cifelli *et al.,* 2008; Carminati *et al.,* 2010). Tectonically, the Curinga Girofalco line (Fig. 1.1) separates two different sectors: the Sila Massif and Catena Costiera in the northern part and the Serre Massif, Aspromonte Massif and Peloritani Mountains in the southern region.

The CPO consists of a poly-metamorphic basement for which opposing hypothesis have been proposed by different authors. Variscan metamorphism was suggested by Atzori *et al.* (1984) and Ioppolo & Puglisi (1989), whereas other authors (Acquafredda *et al.,* 1994; Ferla, 2000; De Gregorio *et al.,* 2003; Ferla & Meli, 2007; Micheletti *et al.,* 2007; Williams *et al.,* 2012; Fiannacca *et al.,* 2013) have indicated, especially for the rocks of CPO southernmost sector, a pre-Variscan origin or the assemblage of pre- and syn-Variscan terranes during the late-orogenic Variscan stages, and a final reworking during the Alpine-Apennine orogenesis (e.g., Cirrincione et al., 2015; and references therein). The late-Variscan stage was characterized by the emplacement of large volumes of granitoid magmas at c. 300 Ma, forming batholiths in the northern (Sila Batholith in the Sila Massif) and central parts (Serre Batholith and Capo Vaticano Promontory covering an area of 1250 Km^2) of the CPO (e.g., Schenk, 1980; Rottura *et al.,* 1989; 1990; 1991; Ayuso *et al.,* 1994; Fornelli *et al.,* 1994; Graessner et al., 2000; Fiannacca *et al.,* 2005, 2008, 2017, 2019; Langone et al., 2014). Minor strongly peraluminous leucogranodiorite–leucogranite plutons, and small weakly peraluminous trondhjemite plutons, in the Aspromonte Massif and Unit and north-eastern Sicily are associated with the larger batholith intrusion.

Thermobaric data for the Variscan basement indicate an ill-preserved stage of initial thickening episode, owing to the subsequent nearly complete equilibration at peak metamorphic conditions. However, the occurrence of earlier metamorphic events is revealed by 450 ± 20 Ma age (Schenk, 1989) obtained for the Serre lower crust and 330–326 Ma age (Acquafredda et al., 1991, 1992) for the Sila mid to upper crust. LA-ICP-MS U-Pb zircon ages of mafic granulites in Serre lower crust have recorded various Variscan stages ranging from 357 ± 11 Ma to 279 ± 10 Ma (Fornelli *et al.*, 2011a; 2014). Clustering of the ages tells a story about crustal thickening (347-340 Ma), peak metamorphism (323-318 Ma) and multistage decompression (300-294 Ma). The dating of a deformed quartz-monzodiorite dike suggests a 323 ± 5 Ma as the minimum age of the magmatism. Altogether, a 60-70 Ma time was indicated as the persisting of the granulitic facies metamorphism and the anatectic conditions (Fornelli *et al.,* 2011a). Similar LA-ICPMS and SIMS ages were reported by Micheletti *et al.* (2008) for the Serre lower crustal metapelitic complex (340 to 260 Ma). A crustal thickening event occurred between 340 and 300 Ma (associated with water-fluxed melting producing trondhjemitic leucosomes), followed by LP/HT metamorphism, mica-dehydration melting and crustal extension between 300 and 260 Ma. In this view, a diachronic evolution is supported for the deep and upper parts of Serre lower crust.

Youngerages, about 135 Ma, in the calc-alkaline granitoids have been releted to Alpine tectonism, provoking the uplift and outcropping of different portions of the Variscan basement (Borsi *et al.,* 1976; Del Moro *et al.,* 1986). A successive Rb-Sr biotite age interpretation (Del Moro *et al.,* 2000) refers the age of 135 Ma to Tethys opening with extensional shear zones interesting the granitoids and metamorphites of southern Calabrian arc. The closure of the Tethys was associated with a compressive regime that started at around 80-90 Ma and is continued during the Tertiary. In the Serre massif, the crustal section was upon the Mammola unit at around 48 Ma.

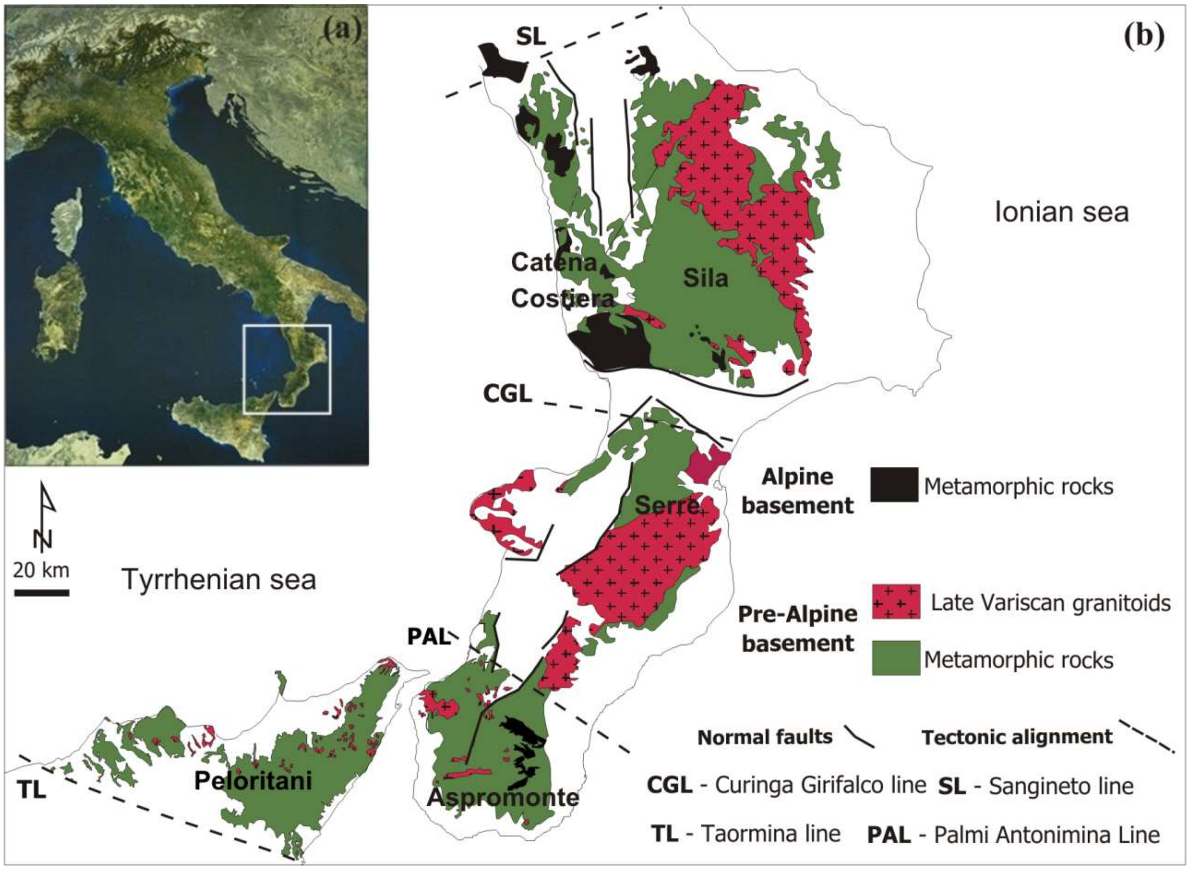

Figure 1.1- Sketch map of Calabrian-Peloritani Orogen (CPO). a) CPO localization; b) Distribution of pre-Alpine (pre- or syn-Hercynian) and Alpine basement with the main tectonic alignment (modified from Angì et al., 2010).

1.3 The Serre Batholith

The Serre Massif (SM; Fig. 1.2) represents a rare and spectacular opportunity to investigate a continue cross-section of continental crust. The complete tilting has permitted the exposition from the lower crust (in the northern sector) thought granitoid middle batholith to the upper crust (southern sector). Albeit Capo Vaticano Promontory (CVP) and Serre Batholith (SB) are separated by the Mesima graben, the field, structural, petrographic, geochemical and geochronological analogies have led to defining them as the same batholith (e.g., Bonfiglio, 1963; Caggianelli et al., 2007; Fiannacca *et al.* ,2015).

The SM consists of a continuous cross-section of late-Paleozoic continental crust, about 25 km thick (Schenk 1980; 1990), made up of three different crustal segments (lower, middle and upper crust) exposed in continuity from NW to SE (Figs. 1.2, 1.3). Mafic granulites are present in the lower crustal portion (about 7-8 km thick; Fig. 1.3) with minor metagabbros, felsic granulites, metabasites, metaperidotites, fine-grained metapelites and metacarbonates overlain by a metapelitic complex consisting of coarse-grained migmatitic paragneisses and Opx-Bt-Grt granulites, with intercalated metabasites, rare marbles and with felsic orthogneisses occurring at the top (Schenk, 1984; 1989; Acquafredda *et al.,* 2006; 2008; Festa *et al.,* 2013). The middle portion is represented by the Serre Batholith (SB; Fiannacca et al., 2015; and references therein) (Figs. 1.2, 1.3). It consists of foliated and unfoliated tonalites, granodiorites and granites with minor quartz-diorites and rare quartz-gabbros. The granitoids were emplaced in an extensional regime at different depths (from ~23 to ~ 6 km; Caggianelli *et al.,* 2000). The foliated quartz-diorite and tonalites represent the deepest portion of the batholith, producing a migmatitic border zone at the contact with the lower crustal metapelites (Rottura *et al.,* 1990). Two-mica porphyritic granodiorites and granites (BMPG), characterized by K-feldspar megacrysts ranging from 2 to 12 cm, form the intermediate portion of the batholith. The shallower level is made up of two-mica equigranular granodiorites and granites (BMG) passing upward to biotite ± amphibole granodiorites (BAG). Langone *et al.* (2014) suggested an over accretion model dating a tonalite and granodiorite corresponding to the bottom and the top of the batholith. The LA-ICPMS U-Pb ages have been clustered for both lithotypes in two main groups: a 306 Ma age (*emplacement age*) and 295 Ma for the tonalite; a 295 Ma (*emplacement age*) and an older age at 306 Ma for the shallower granodiorite. The opposite ages indicate a reciprocal influence of the magmatic pulses during the emplacement. The younger granodioritic pulse was emplacement at 295 Ma and during the arise had incorporated older zircon. The tonalite was emplacement at 306 Ma and was affected by fluid circulation producing a 295 Ma overgrowth. Recent SHRIMP U-Pb zircon dating (Fiannacca *et al.*, 2017) indicated an incremental multipulse over-accretion of the batholith, in a time range of ca. 5.1 ± 4 Ma; a crystallization age of 297.3 ± 3.1 Ma has been obtained for the deep quartz-diorite and tonalites and age of 292.2 ± 2.6 Ma for the shallow weakly peraluminous granodiorites (BAG). The intermediate levels yielded an age of 296.1 ± 1.9 Ma and 294.9 ± 2.7 for the BMG, close to the contact with BAG and BMPG, respectively, while the porphyritic rocks have an age of 294.2 ± 2.6 Ma. The uppermost crustal segment (Figs. 1.2; 1.3) consists of two metamorphic complexes (Stilo-Pazzano and Mammola, respectively) that were brought in contact along with a low-angle tectonic detachment before being intruded by granitoids (Angì *et al.,* 2010; Festa *et al.,* 2013). The Stilo-Pazzano complex comprises low greenschist-facies phyllites with minor marbles, quartzites and metavolcanic layers (e.g., Acquafredda *et al.,* 1994; Navas-Parejo *et al.,* 2009). The Mammola complex contains amphibolite-facies paragneisses, with subordinate leucocratic gneiss and amphibolites. Both the granitoids and the upper crustal metamorphic rocks are intruded by late- to post-orogenic rhyolitic to andesitic dykes (Romano et al., 2011) announcing the early Pangea fragmentation (Barca et al., 2010; Cirrincione et al., 2014, 2016).

The CVP setting is influenced by recent tectonics, as suggested by the 1905 earthquake, characterized by several normal faults, striking NE-SW and WNW-ESE, bording the CVP and also occurring in the Tyrrhenian offshore (e.g., Monaco and Tortorici, 2000). Only the uppermost portion of the lower crust section and the deep-intermediate portion of the Serre Batholith are exposed in the CVP. In the SW area, the upper part of the Serre lower crustal section is represented by migmatitic metapelites (kinzingitic gneisses; Maccarrone *et al.,* 1983; Schenk, 1984; Rottura *et al.,* 1991). The granitoids crop out discontinuously beneath a Miocene-Quaternary carbonate and terrigenous cover (Burton, 1971) over an area of about 270 km^2. Their compositions range from metaluminous/weakly peraluminous quartz-diorites and tonalites to strongly peraluminous porphyritic granodiorites with minor granites (Rottura *et al.,* 1990; 1991; Fiannacca *et al.,* 2015). The most mafic rocks, cropping out in Santa Maria and Ioppolo localities, are quartz diorites of two different types (Rottura *et al.,* 1990; 1991). The first-type is plagioclase-rich (An_{47-57}; 65 vol. %), showing cumulitic structure with interstitial biotite, quartz and amphibole (cummingtonitic and tschermakitic in composition) and some accessories phases. The second type contains mainly cumulus of biotite (up to 45 vol. %) and plagioclase (An_{46-60}; about 40 vol. %), with minor quartz and cummingtonite-hornblende intergrowths. The plagioclase-rich quartz diorites contain cm- to m-sized amphibolite and metapelite xenoliths related to the upper part of the Serre lower crust (Maccarrone *et al.,* 1983; Schenk, 1984; 1989). Large crystals of garnet are also abundantly present, especially in proximity to metapelitic xenoliths and have been interpreted as peritectic phases produced by partial melting of the enclosed metasedimentary rocks (Clarke & Rottura, 1994). Strongly foliated tonalites are exposed in the northern and southern part of the Promontory, at various localities (e.g., Briatico, Santa Maria and Ioppolo). Weakly foliated tonalites (Capo Vaticano and Parghelia types), containing biotite-hornblende-bearing enclaves of quartz dioritic to tonalitic compositions, are intruded by porphyritic granitoids (Rottura *et al.,* 1990; 1991). The latter consist of two mica porphyritic granodiorites and granites (BMPG; Fiannacca et al., 2015) with some preferred orientation of K-feldspar megacrysts, 1-10 cm-long (Rottura *et al.,* 1991; Cirrincione et al., 2013).

Strongly foliated tonalites and quartz diorites were intruded earlier into the kinzingitic gneisses, producing partial melting of country rocks (Caggianelli *et al.,* 1991; Rottura *et al.,* 1990). The weakly foliated tonalites and granodiorites were intruded later, in a more brittle domain (Rottura *et al.,* 1991).

Different petrogenetic interpretations have been proposed for the CVP granitoids in the last three decades. Rottura *et al.* (1989; 1990) stated an origin through fractional crystallization from different magma batches for the CVP tonalites, with the lower ε_{Nd} values in CVP quartz-diorites respect to tonalites excluding them as cumulates deriving from a single tonalitic parental magma. The

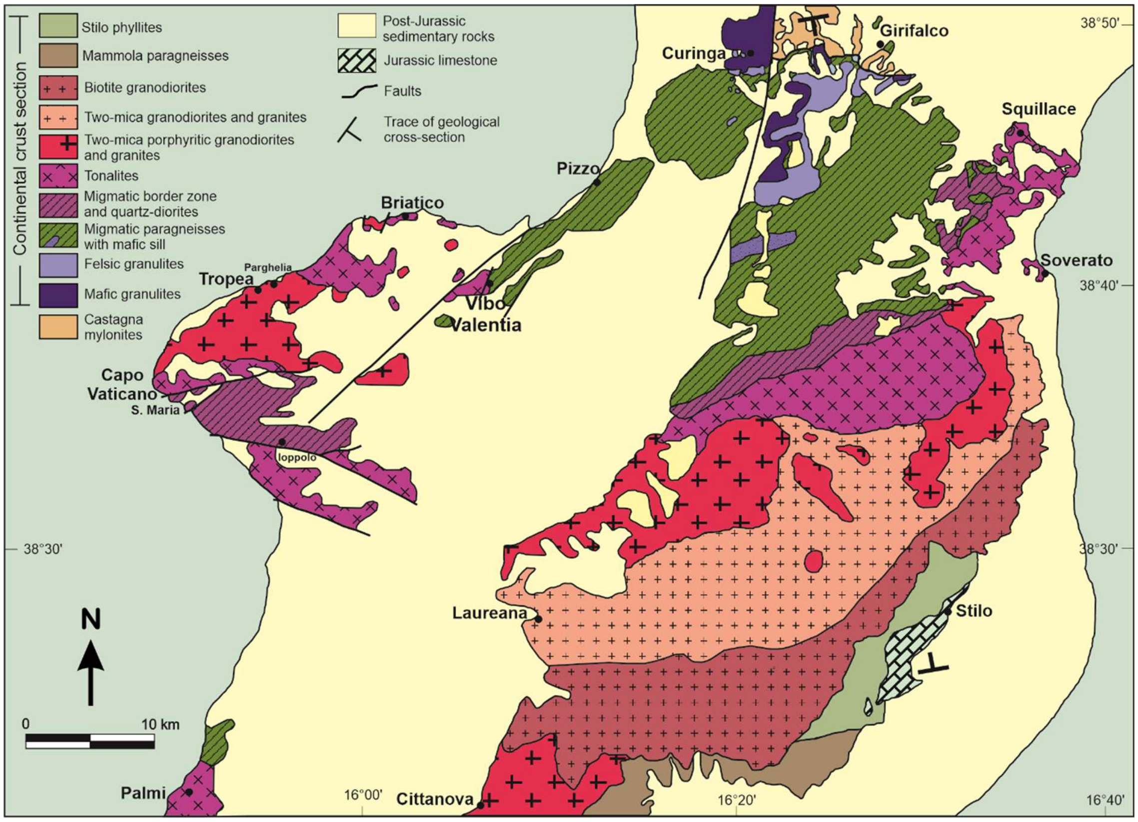

Figure 1.2 - Geological sketch map of Serre massif and Capo Vaticano Promontory with distribution of the main lithotypes (after Fiannacca et al., 2015; and references therein).

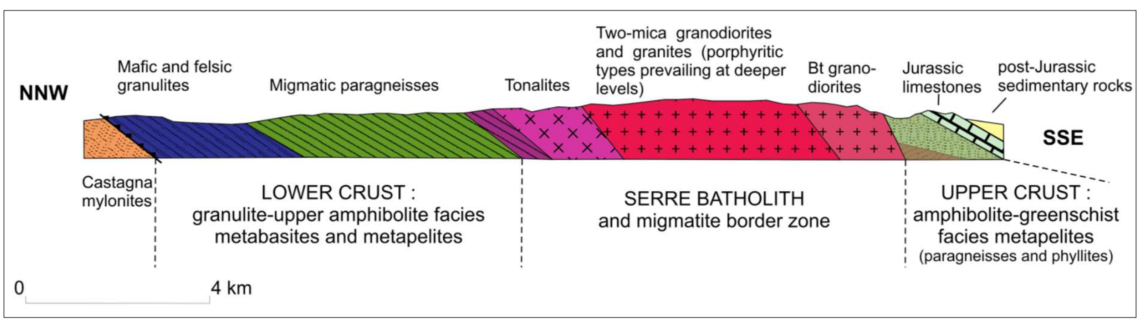

Figure 1.3 - Schematic geological cross-section of Serre Massif continental crust (after Fiannacca et al., 2015 and references therein).

proposed source is a hydrous basaltic crust that, during melting processes, produced an intermediate magma. Crustal contamination, mingling and fractionation processes might all have contributed to the observed geochemical variations within the granitoids. In 1991, Rottura *et al.* indicate a strong crustal contribution for the CVP tonalite with a mantle contribution diluted by crustal assimilation. Mafic enclaves could be proof of the mantle role. Tonalite evolved from a calc-alkaline intermediate magma by fractional crystallization with a variable degree of assimilation. The strongly peraluminous porphyritic rocks have been considered both in terms of I-type and S-type sources (Rottura *et al.,* 1990) or as the product of mixing between two felsic melts or between crustal and mantle magmas

(Rottura *et al.,* 1991). Fiannacca *et al.* (2015) proposed that the different granitoid types resulted from the partial melting of different crustal sources, producing diverse magma batches reflecting the various nature of the melted rocks. I-type (metabasalts) and S-type (mafic metapelites) sources have been proposed for tonalites-quartz-diorites and porphyritic granodiorites and granites, respectively.

Lombardo *et al.* (2020) suggested a multi-steps fractional crystallization model to explain the three different cumulates compositions of the CVP quartz-diorites and tonalites, drawing inflexed descent lines. From the differentiation of a tonalitic parental magma, the Bt-rich quartz-diorites represent the first cumulates obtained after F=10%, the second step models an intermediate cumulate between Bt-rich and Pl-rich quartz-diorites (F=20%); the third corresponds to the Pl-rich quartz-diorites after F=30%. The fractional crystallization process was suggested as the main process in CVP S-type granodiorite to granite evolution. However, it also is consistent with Peritectic Assemblage Entrainment (Clemens & Stevens, 2012) modelling obtained by partial melting of a metapelitic source with entrainment of 20 to 5 % vol. of a peritectic assemblage made of orthopyroxene and garnet.

2. Quartz-diorite and tonalite from the CVP: sampling and field features

New 35 samples of quartz-diorite, tonalite and associated MME (CVP labeled; Fig. 2.1) have been collected from different areas of the Capo Vaticano Promontory. The sampling was planned to pick up representative unaltered mafic samples with variable composition and emplacement depth. Most of the sampling took place in coastal outcrops due to the extensive occurrence of soil, sedimentary and vegetal covers in the more internal areas of the CPV. The sample selection has been made at distant from the underlying high-grade metasedimentary boundary and the overlying two-mica porphyritic granodiorites and granite to avoid probable contamination.

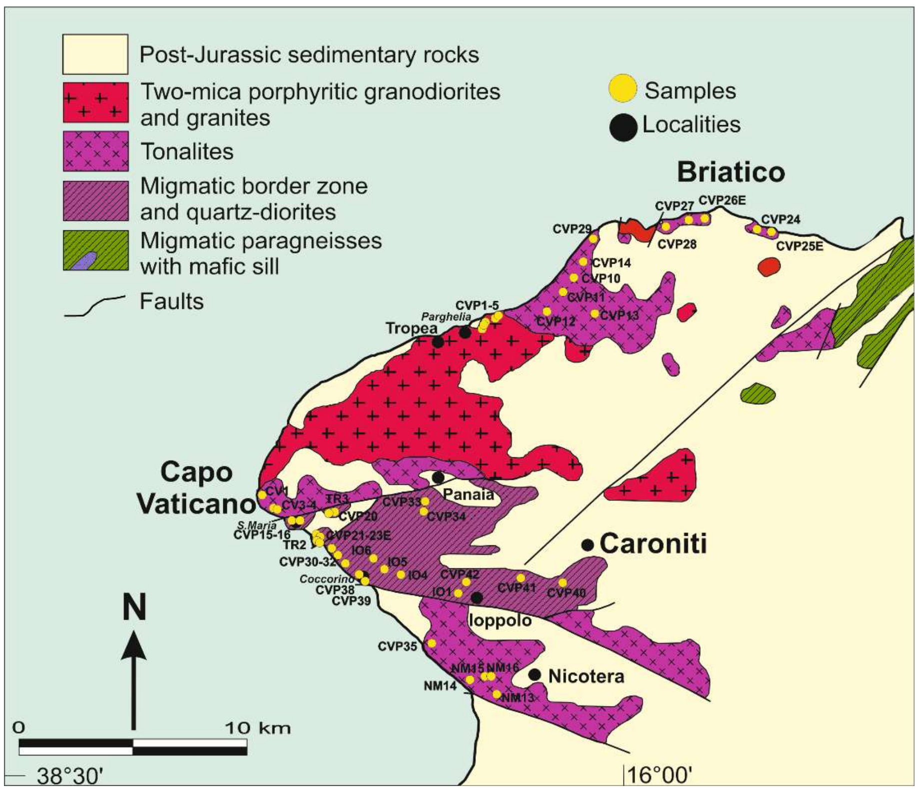

Figure 2.1 - Geological sketch map of CVP granitoids with sample locations (modified from Fiannacca et al., 2015; NM, TR and CV sample are from Fiannacca et al., 2015).

2.1. Quartz-diorites

Quartz-dioritic lithotypes crop out exclusively in the CVP southern sector. The transitional contacts between quartz-diorites and the lower crustal metapelitic basement (Fig. 2.2) ascribe them as the deepest lithology in the granitoids sequence. Magma intrusion into the metapelites, promoting the partial melting of the basement, is testified by migmatites. Evidence of mixing/mingling processes are represented in the outcrops by anatectic rocks cm-sized peritectic garnets and cm- to m-sized restitic metapelitic enclaves (Fig. 2.2 a-d). Hybrid quartz-diorites have been originated by an advanced commixture (mixing/mingling processes) between quartz-dioritic magma and residual anatectic melt (Fig. 2.2d).

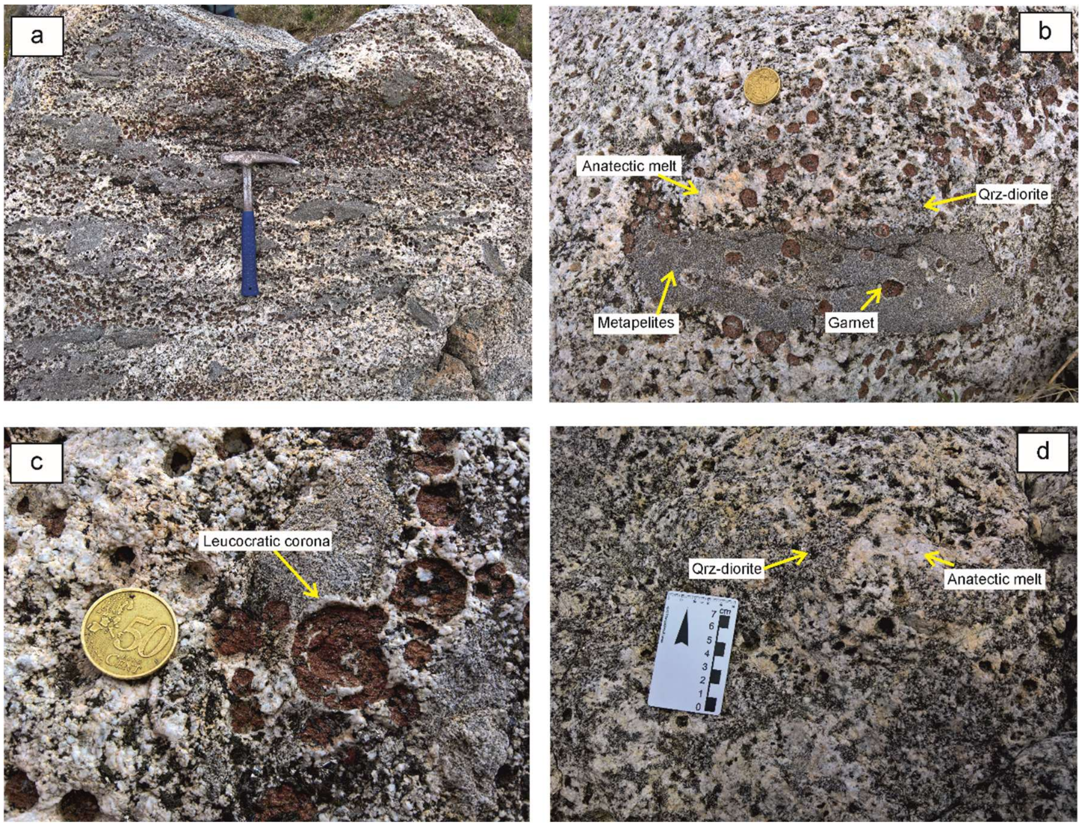

Figure 2.2 - Border zone features at the outcrop scale. a) Overview of the mingled area with leucocratic levels (anatectic melt) and melanocratic levels (metapelitic enclaves); b,c) Closer inspection of restitic enclaves, anatectic melt, peritectic garnet and quartz-dioritic magma; a leucocratic corona of anatectic melt surrounding the garnet is shown in the fig. c; d) hybrid rock created by progressive mingling between anatectic melt and quartz-dioritic magma.

Quartz-diorite s.s. (Fig. 2.3 a-d) shows an inequigranular structure with a medium-coarse grain-size. Biotite, amphibole and mafic enclave alignment highlight a well-marked magmatic foliation, consistent with their emplacement along a deep shear-zone (Fig. 2.3 a). Biotite (up to 10 mm), amphibole (up to 2 mm), plagioclase (up to 7 mm), quartz (up to 5 mm) are the main mineral phases. Mafic microgranular enclaves of quartz-dioritic/tonalitic composition with variable sizes (cm up to 1 m) and with lobate shape are abundantly dispersed in the host (Fig. 2.3 a, c). Depending on the size, MME has been partially assimilated by the quartz-dioritic magma, whereas mineral transfer from the host to the MME is widely present (Fig. 2.3 c). Locally, pegmatites cross-cut the quartz-diorites (Fig. 2.4 d).

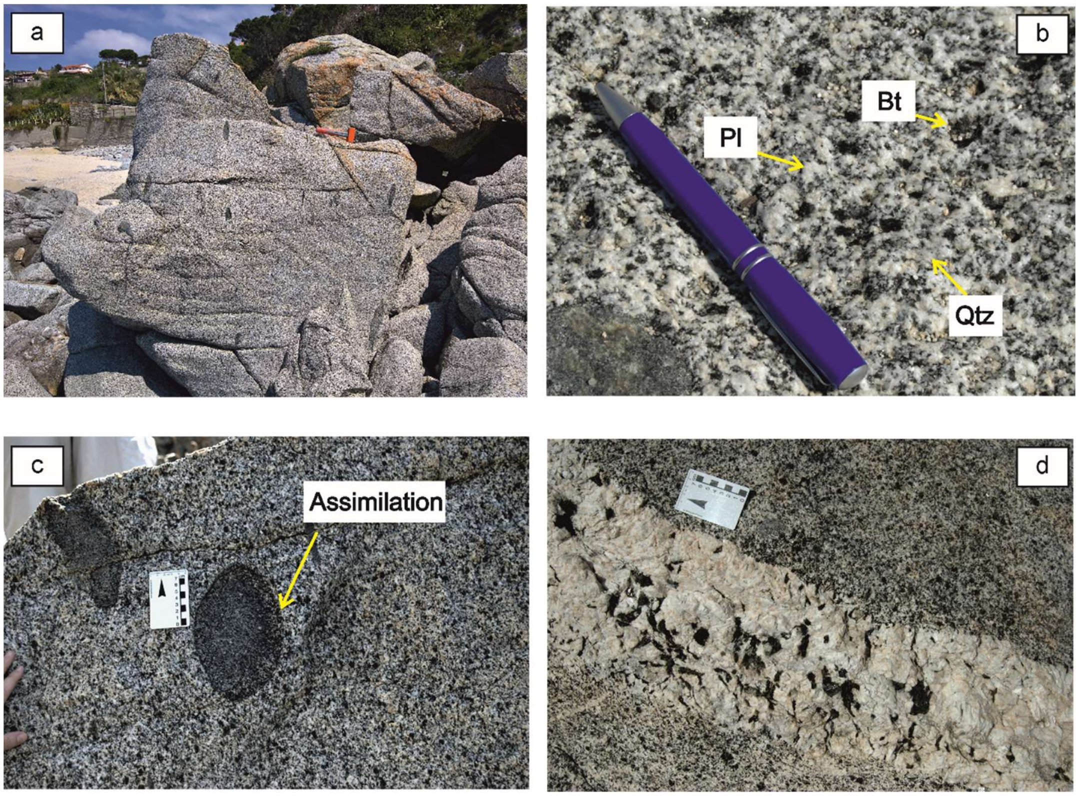

Figure 2.3 - Quartz-diorites features in the outcrop. a) Magmatic foliation in quartz-diorite marked by iso-oriented MME; b) Detail of the main mineral phases observable in the field; c) enclave affected by assimilation and amalgamation with the host; d) quartz-diorite and pegmatite sharp contact.

2.2. Tonalites

Tonalites show the similar features of quartz-diorites. They crop out both in the northern and southern parts of the CVP, presenting a strong and sporadically weak foliation, respectively.

The Cenozoic intensive tectonics, that has particularly affected the southern CVP sector, does not permit an accurate reconstruction of the relationships between the different bodies ., Weakly foliated tonalites (Fig. 2.4 a, b) with sporadically schlieren texture (Fig. 2.4 b), sometimes surrounded by massive pegmatites (Fig. 2.4 d) have been recognized in the Coccorino locality.They host mafic microgranular enclaves reaching metric dimensions and rarely cm-sizes (Fig. 2.4 b, c). These rocks exhibit a medium-to coarse-grained hypidiomorphic texture (Fig. 2.4 e, f) and are constituted by biotite (up to 10 mm), plagioclase (up to 8 mm), amphibole (up to 2 mm) and quartz (up to 8 mm).

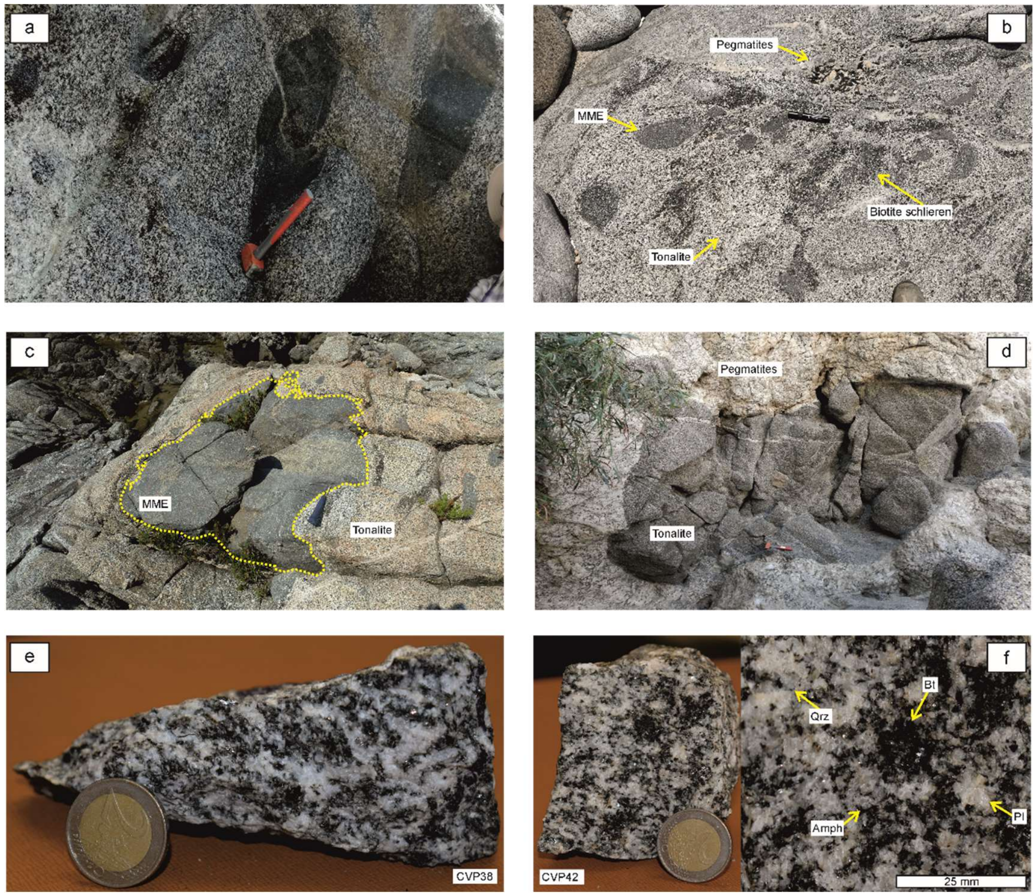

Figure 2.4 - Tonalite from the southern sector of the CVP (Coccorino-Panaia area). a) Weakly foliated tonalite with iso-oriented lobate mafic enclaves; b) Mingled tonalitic rocks with partly assimilated enclaves, biotite schlieren and pegmatite; c) Partly digested metric MME; d) Block of tonalite included in pegmatite; e,f) hand specimens and main minerals (CVP38 and CVP42 samples, respectively).

Tonalites with a strong foliation characterize the northern sector of CVP batholith. Despite the paucity of outcrops, it is possible to recognize an evolutive sequence passing from melanocratic tonalites (biotite- and amphibole-rich) to more leucocratic varieties cropping out close to the contact with the overlying porphyritic granodiorites and granites. The Briatico tonalites (Fig. 2.5 a-d) show a strong foliation indicative of an intense deformation at high depth (Fig. 2.5 a, b), associated with deformed and partly digested enclaves (Fig. 2.5 b, c). Inequigranular texture and medium grain size characterize the lithotypes. Plagioclase (up to 7 mm), biotite (up to 5mm), amphibole (up to 3 mm) and quartz (up to 4 mm) are the minerals observable at outcrop scale.

Parghelia tonalites (Fig. 2.6 a-d) exhibit an inequigranular medium-coarse grained texture with a grainsize increment of plagioclase (up to 10 mm) and quartz (up to 5 mm), decrement of biotite in size and modal abundance (up to 3 mm) and total absence of amphibole. The evolved character of these

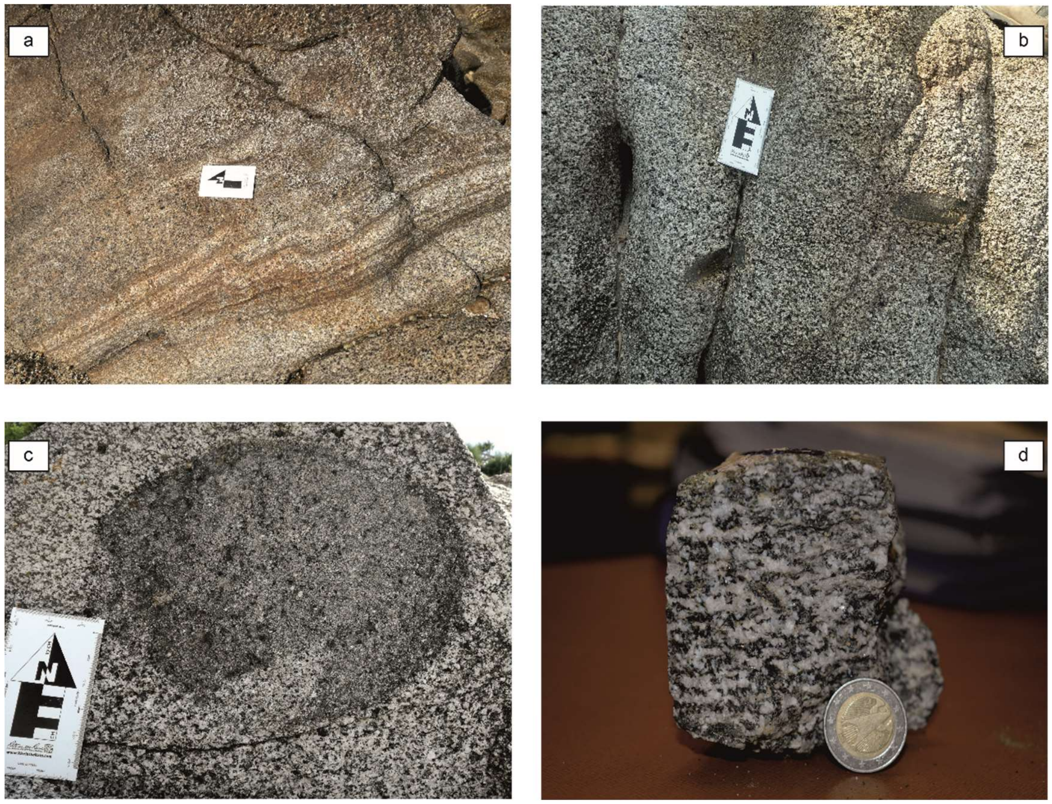

Figure 2.5 - Tonalite from Briatico area. a) Strongly foliated and folded tonalite with alternation of light - and dark layers; b) Characteristic outcrop appearance; c) partly resorbed and hybridized enclaves with irregular outline and magmatic transfer of different minerals; d) hand specimen (CVP29) with strong magmatic foliation.

rocks is shown by their leucocratic appearance. They are unfoliated, with a minor presence of mafic microgranular enclaves, up to a few cm-long (Fig. 2.6 a). Sharp magmatic contacts are observed between the Parghelia tonalites and the BMPG (Fig. 2.6 b), with the rare occurrence of K-feldspar minerals into tonalitic rocks. At the same time, strong disaggregation of the tonalites by the intrusion of the porphyritic granitoid magmas is also locally documented in the field (Fig. 2.6 d).

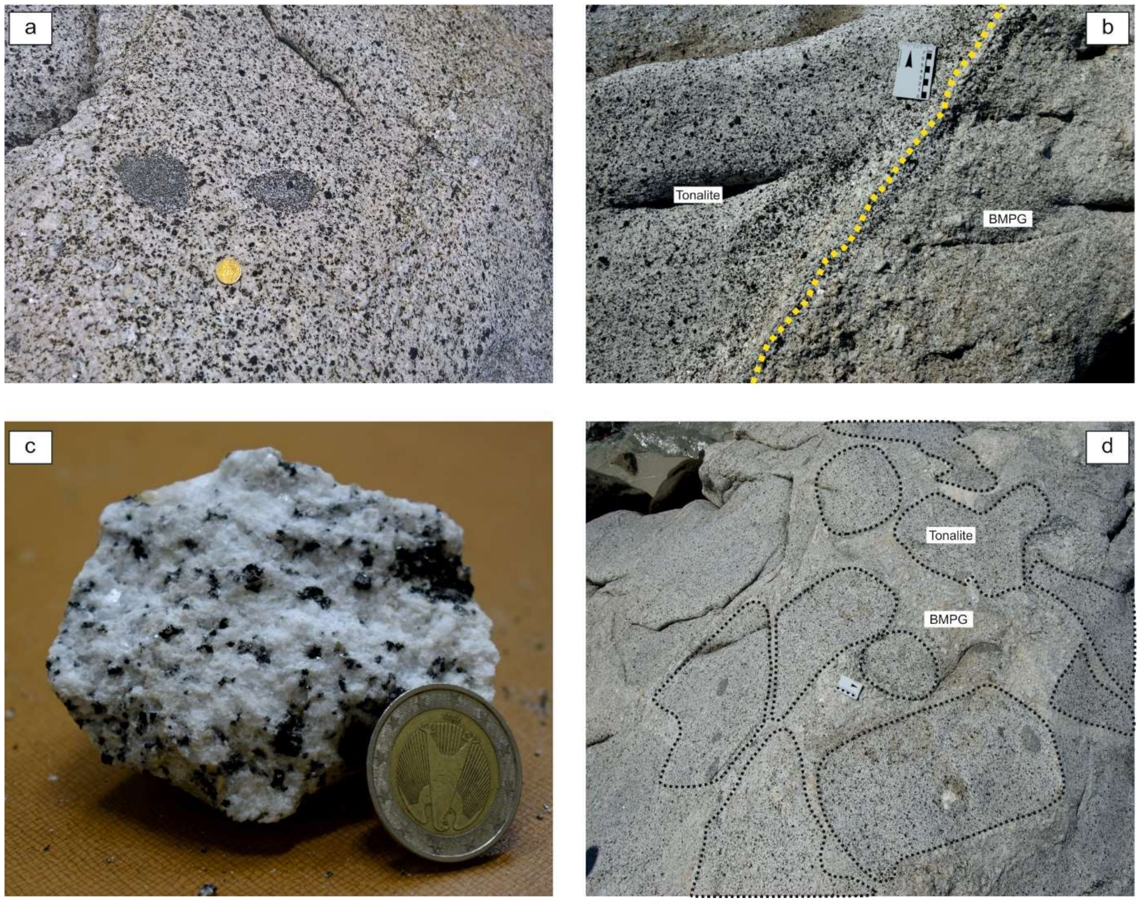

Figure 2.6 - Parghelia leuco-tonalite. a) Characteristic field appearance with ellipsoidal and partly digested enclaves. b) Sharp contact between BMPG and leucotonalite; c) Hand sample of leucotonalite (CVP5); d) Intrusion of the granodioritic magma into tonalites, pulling apart them in sharp or rounded blobs. The contoured area (dotted line) represents the tonalite, the remaining part the granodiorite.

2.3 Mafic Microgranular Enclaves

As discussed above, the MMEs are abundant in both quartz diorites and tonalites, showing cm- to m-sizes (Fig. 2.7 a-d). They exhibit lobate and ellipsoidal shape (Fig. 2.7 a) and undefined contacts with the host (Fig. 2.7 c). In fact, some portions are entirely or partly assimilated by the quartz-dioritic/tonalitic magmas, and also presenting some xenocrysts deriving from the host through magma transfer processes. These features may have masked the original composition of the mafic magma, but the amount of contamination depends on the MME size. The texture is inequigranular porphyritic, with a fine-medium grained groundmass composed of mafic minerals (biotite and amphibole) and minor plagioclase. The phenocrysts are represented by plagioclase and biotite, reaching the size of few millimeters (up to 2-3 mm).

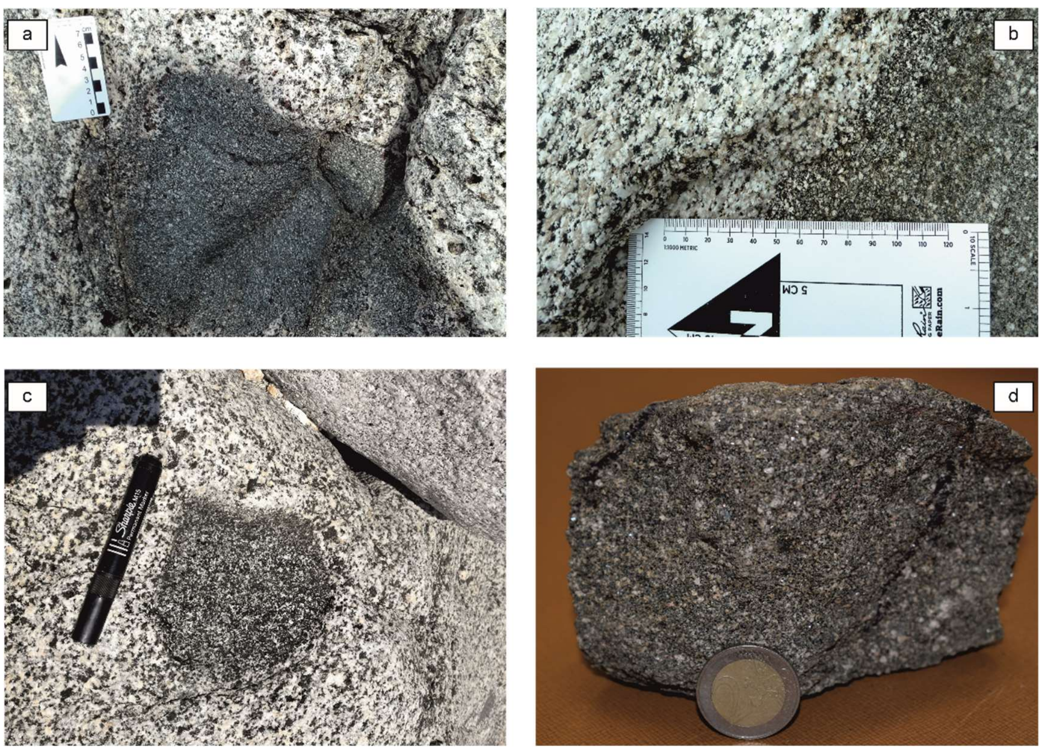

Figure 2.7 - Field features of the mafic microgranular enclaves. a) Enclave preserving sharp contact with quartz-diorite, while some portions are resorbed (S. Maria locality). Mineral transfer occurs between host and MME; b) Detail of tonalite-MME contact (Briatico locality); c) Partly digested enclave at the Coccorino locality; d) MME hand sample (CVP25E – Briatico locality).

2.4 The magmatic sequence at Capo Vaticano Promontory

Field observations highlighted affinities and local differences in the lithotypes constituting the CVP crustal cross-section. As reported above, the primary magmatic contact between *quartz-diorite and tonalite* is not well preserved due to a Cenozoic to recent tectonic activity. The two lithotypes are found juxtaposed only through tectonic contacts and exclusively in the southern part of the CVP. The reconstructed CVP cross-section is made up, from the bottom to the top, by the following magmatic sequence (Fig. 2.8):

1. *Quartz-diorites with restitic metapelitic enclaves, anatectic melts and peritectic garnet.*
2. *Hybrid quartz-diorites.*
3. *Quartz-diorites, tonalites and Parghelia (leuco-)tonalites.*
4. *Porphyritic granodiorites and granites*.

Hybrid- and s.s.- quartz-diorites-types have been observed in the southern sector of CVP. The first is characterized by two recognizable portions, an anatectic melt and a quartz-dioritic magma, absence of foliation and the rare occurrence of MME. The second-type exhibits mafic minerals and medium-large sizes MME strongly iso-orientated.

Different kinds of tonalites have been recognized (e.g., Rottura et al., 1983; 1990; 1991): strongly foliated in the northern areas (Briatico), weakly foliated in the southern areas (Nicotera, Coccorino, Ioppolo and Caroniti) and unfoliated leucotonalites. The first type is characterized by a biotite and amphibole iso-orientation, indicating a syn-magmatic foliation in a deep ductile regime. The second and third type suggests relatively higher emplacement depths and less efficient ductile domain. The microgranular mafic enclaves (quartz-dioritic and tonalitic in composition) develop an ellipsoid shape parallel to the syn-magmatic foliation experiencing the same deformative processes at a deep depth. In addition, MMEs are very abundant and larger at the bottom of the magmatic sequence, decreasing both in abundance and size toward the contact with the overlying two-mica granitoids.

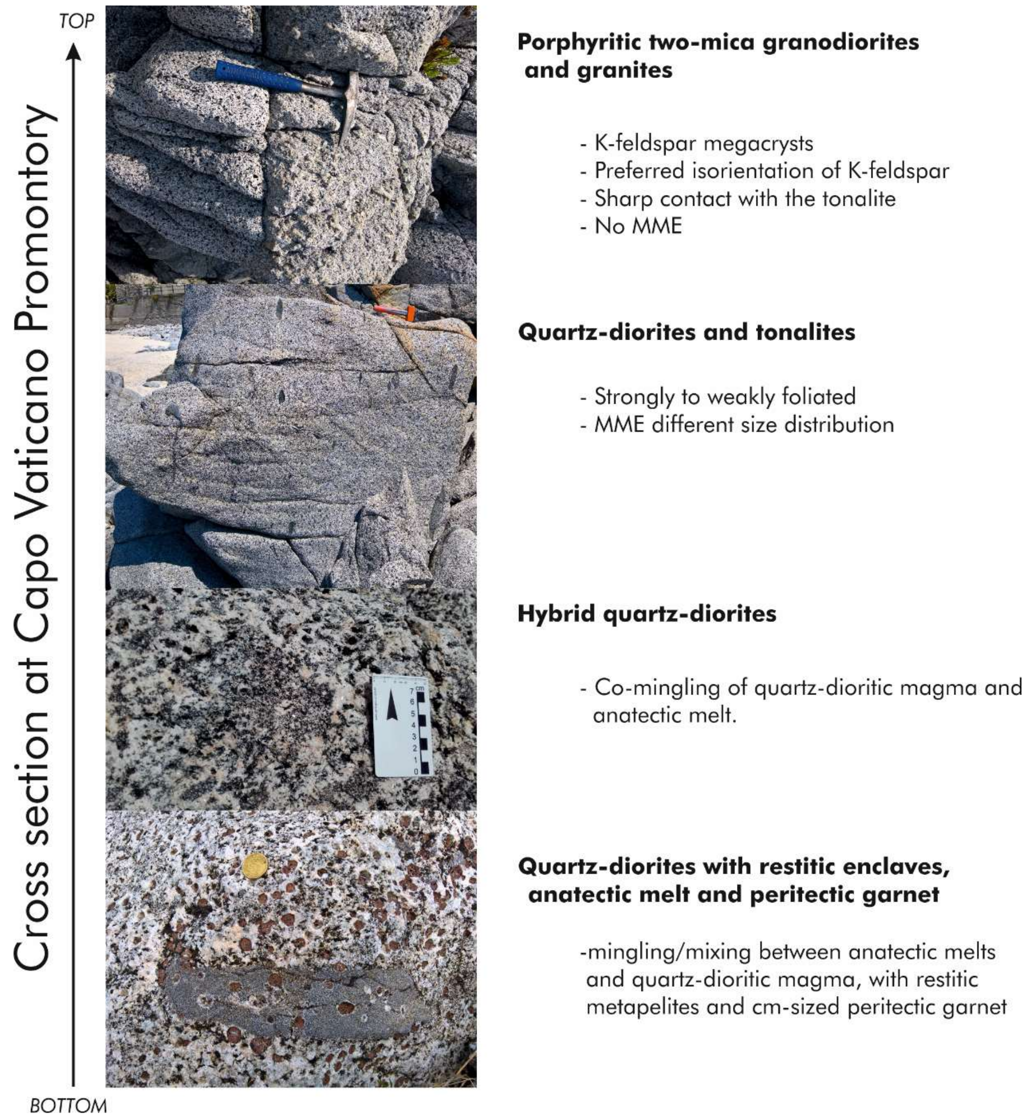

Figure 2.8 - Reconstructed cross-section at Capo Vaticano Promontory. See details in the text.

3. Petrography of quartz-diorite, tonalite and MME

3.1 General features

The modal abundances (Table 1 in Appendix) of the minerals constituting the CVP samples classify them as quartz-diorites, tonalites (including also the MME) and leucotonalites (M < 10%). All granitoids, expect for MME, show a medium-coarse grain-size and an equigranular (usually in the evolved terms) to inequigranular texture (in the less evolved rocks).

Plagioclase, amphibole, biotite, quartz are the primary phases, epidote, allanite, apatite, zircon and ilmenite the accessories. K-feldspar and muscovite appear only in the evolved terms with modal abundances that do not exceed 5vol. %.

The variation of the modal abundances in the studied rocks reflects the reconstructed cross-section described in the second chapter. In fact, the deepest lithotypes are the more mafic in composition with amphibole up to 15 vol. % and biotite up to 25 vol. %, passing to the leucotonalites, with quartz up to 30 % in vol, low biotite content (< 10 % in vol.) and absence of amphibole.

The mafic enclaves show medium-fine grain-size porphyritic inequigranular texture with phenocrysts of plagioclase and biotite enclosed in a fine matrix constituted by the same mineralogy plus epidote, ilmenite, apatite and quartz.

The petrographic features will be therefore described in the following section taking into account quartz-diorite s.s., tonalite, leucotonalite and the MME. The quartz-diorite rocks from the migmatite border zone and the hybrid quartz-diorite have been excluded for the purposes of this PhD thesis.

3.2 Quartz-diorites

The quartz-diorites have heterogranular orthocumulitic texture with medium-coarse grain-size. They show a pronounced anisotropy with biotite, amphibole, plagioclase and quartz as main phases. Epidote and allanite are the more abundant accessory phases, but apatite, ilmenite and zircon are present.

Plagioclase, building a cumulitictexture, exhibits euhedral/subhedral shape, albite-pericline and Carlsbad twinning and weak to absent oscillatory zoning (Fig. 3.1 a). Epidote and zircons are common inclusions, while sometimes sericite and secondary epidote can be alteration phases in the deformed crystals (Fig. 3.1 b). Some small and rounded crystals have been found in amphibole, indicating a fast crystallization.

Amphibole displays a subhedral to anhedral shape, usually twinned with straight contact with biotite and irregular with plagioclase; frequently, it contains quartz, biotite, apatite and titanite (Fig.

3.3 c, d). It is occasionally replaced by biotite, indicating the reaction Hbl + melt → Bt (Fig. 3.1 c, d). The typical pleochroism is green. There are also large-medium crystals with anhedral shape and resorbed portions (usually re-filled by quartz) that present double pleochroism: the first changing to green up to green-bluish and the second from pale-green to colourless. They correspond to two calcic amphiboles: hornblende and cummingtonite, respectively.

Biotite constitutes small and medium crystals (isolated or in clots) with subhedral to anhedral shape (Fig. 3.1 e, f). Mineral inclusions are zircon, apatite, epidote, allanite and allanite-epidote coronae. Rarely it presents smaller rounded inclusions of quartz and hornblende. Biotite can be replaced by chlorite and crypto-crystalline phases. Along the grain-boundaries, when biotite is in contact with plagioclase, processes of softening and reaction between the two minerals produce secondary phases such as oxides, muscovite, ilmenite and apatite. Indeed, ductile and fragile deformations are testified by kink bands and fractures filled by quartz.

Anhedral *quartz* is frequently present in interstitial position, with plagioclase inclusions and displaying deformation microstructures (chessboard and undulatory extinction; Fig. 3.1 a, c).

Epidote is the main accessory phase, exhibiting euhedral shape in contact with biotite and resorbed/irregular boundaries with plagioclase (Fig. 3.1 g), while allanite forms typical coronitic structure with the epidote (Fig 3.1 h). The epidote s.s. shows perfect zoning and simple twinning proving its magmatic origin.

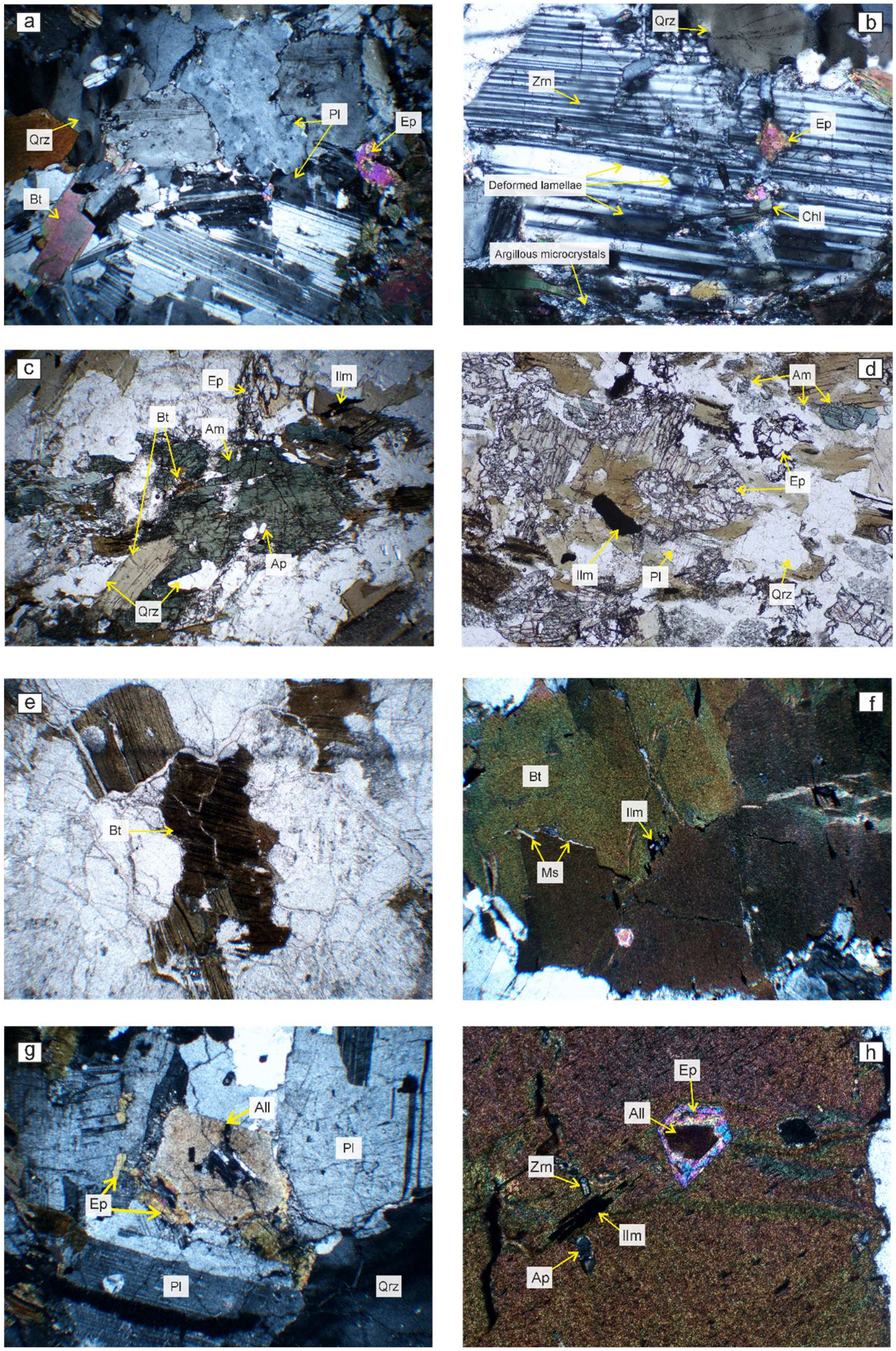

Figure 3.1 - Quartz-diorite textures. a) Cumulitic plagioclase with occasionally interstitial biotite, quartz and epidote (5X, CVP30 sample); b) Euhedral plagioclase with deformed lamellae and fractures filled by secondary epidote, chlorite and argillaceous minerals (10X, CVP30); c) Subhedral amphibole with simple twinning, partly resorbed and replaced by biotite (5X, CVP30); d) Detail of skeletal amphibole replaced by biotite, highlighting the reaction between amphibole and liquid. The epidote is associated with biotite (10X; CVP30) e) Subhedral isolated biotite (2.5X; CVP20); f) Biotite with muscovite developing at the grain boundaries (2.5X; CVP20); g) Subhedral allanite surrounded by anhedral epidote (2.5X; CVP20); h) Accessory minerals included in biotite (10X; CVP20). Mineral abbreviations in figures from Siivola e Schmid, 2010.

3.3 Tonalite and leucotonalite

Hypidiomorphic heterogranular texture with the medium-coarse grain is highlighted in tonalite (Fig. 3.2) and leuco-tonalites. The ***tonalites*** present the same mineralogy of the quartz-diorites, but with scarce or absent amphibole and with muscovite and orthoclase present in the more evolved terms. Allanite, epidote, apatite, titanite, ilmenite, zircon are the accessory phases (Fig. 3.2).

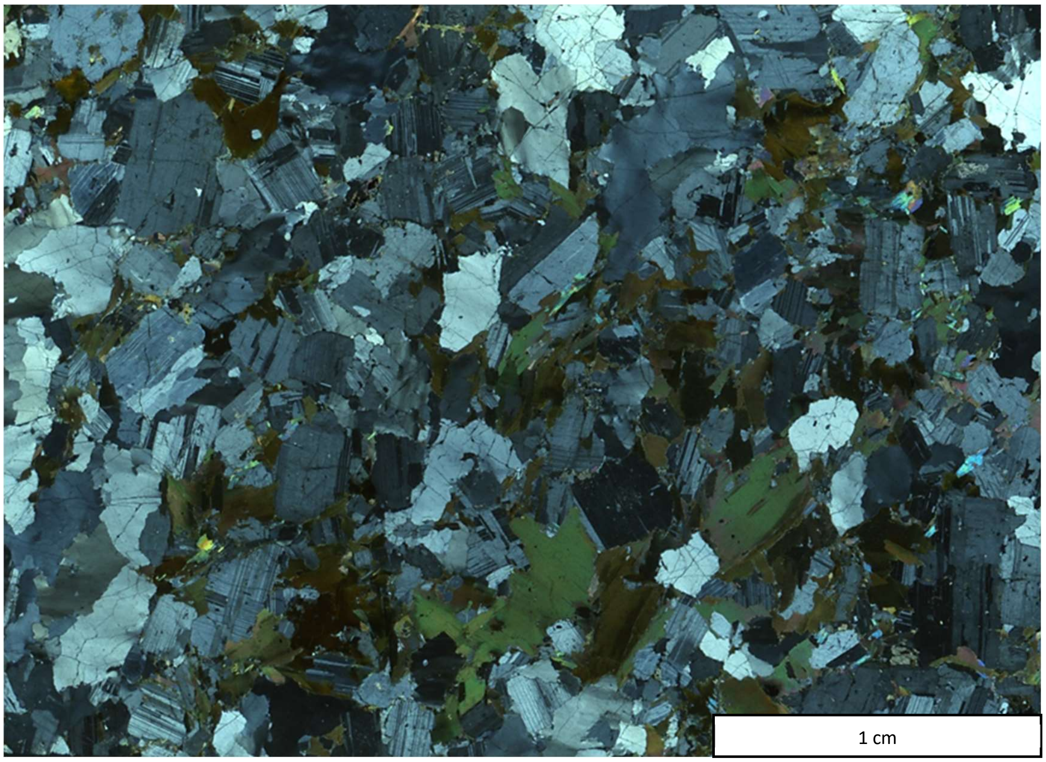

Figure 3.2 – Microphotograph of a tonalite (CVP10 sample). A weakly isorientation is highlighted by plagioclase and biotite.

In detail, euhedral to subhedral ***plagioclase*** crystals (Fig. 3.3 a,b) are sometimes arranged in a cumulitic structure. Smaller crystals of amphibole, biotite and, rarely, epidote can be included in feldspar phases. Simple and multiple (albite, Carlsbad, albite-pericline) twinning and absent to weak zoning are common features in all samples. Tapered, deformed and new generation twins indicate low-temperature subsolidus deformations (Fig. 3.3 a,b).

Biotite crystals (Fig. 3.3 c,d) are usually arranged in clots, but can also form large euhedral to anhedral individual crystals. Accessory phases such as zircon, ilmenite, epidote, apatite, and sporadically plagioclase parallel to the cleavage are the common inclusions. Intergrowths between amphibole and biotite are present and, exceptionally, also biotite mantling hornblende. Kink bands and cleavage bending occurred (Fig. 3.3 c). Associated with biotite, well-shaped primary ***muscovite*** crystals are present. In the amphibole-free types, the interaction between plagioclase and biotite produces reaction zones with the biotite resorption and replacement by secondary muscovite, ilmenite and titanite, while plagioclase shows a zoning border with different birefringence respect the inner zones and without twin's growth (Fig. 3.3 d).

When *amphibole* is present, it shows a skeletal structure (Fig. 3.3 e), after replacement by biotite. Some "missing portions" can be filled by microcrystalline quartz, indicating that resorption took place during late recrystallization stage.

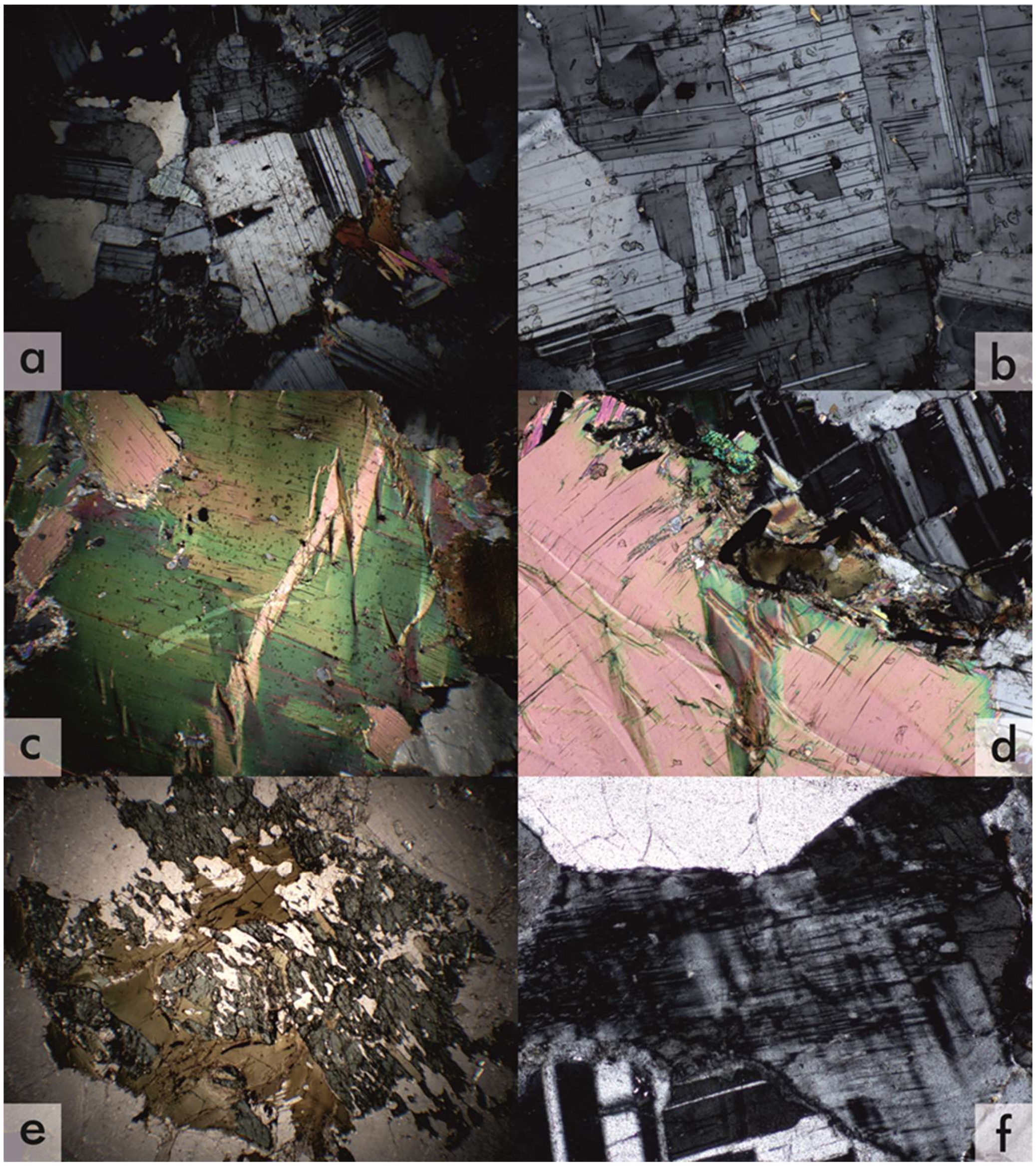

Figure 3.3 – Tonalite's minerals. a,b) Euhedral to subhedral plagioclase with primary and secondary twinning (2.5X); c) Subhedral biotite with kink bands (2.5X); d) Biotite rim replaced by epidote, titanite and oxides (10X); e) Hornblende partly replaced by biotite (2.5x); d) Interstitial K-feldspar (10X).

Quartz abundance ranges from 15 to 20 vol%; crystal forms anhedral bands with undulatory extinction, sometimes surrounded by microcrystalline grains. In other cases, quartz exhibits lobate grain boundaries and subgrains, indicating high-temperature deformations. Tiny quartz crystals surround the subgrains, showing a re-crystallization process at a lower temperature.

Occasionally, small interstitial crystals of *K-feldspar* (Fig. 3.3 f) are present with anhedral shape and perthitic exsolution.

Epidote is the main accessory phase also in the tonalite. The euhedral shape is preserved in contact with biotite (as inclusions or at the grain boundaries), while a resorbed and irregular shape is shown in contact to the quartz-feldspathic matrix. The magmatic nature is testified, in addition to the euhedral shape, by magmatic zoning and coronitic structures with allanite crystals. In some samples, epidote has been preserved in small relicts of amphibole, surrounded by biotite crystals.

Allanite is the second accessory phase in abundance with euhedral to subhedral habits, well-developed zoning and usually associated with biotite.

Apatite, *zircon*, *ilmenite* are the main inclusion phases.

The *leucotonalites* are characterized by a mafic content <10 % vol. with the absence of amphibole and less abundant biotite. The texture is heterogranular with medium-coarse grain-size (Fig 3.4).

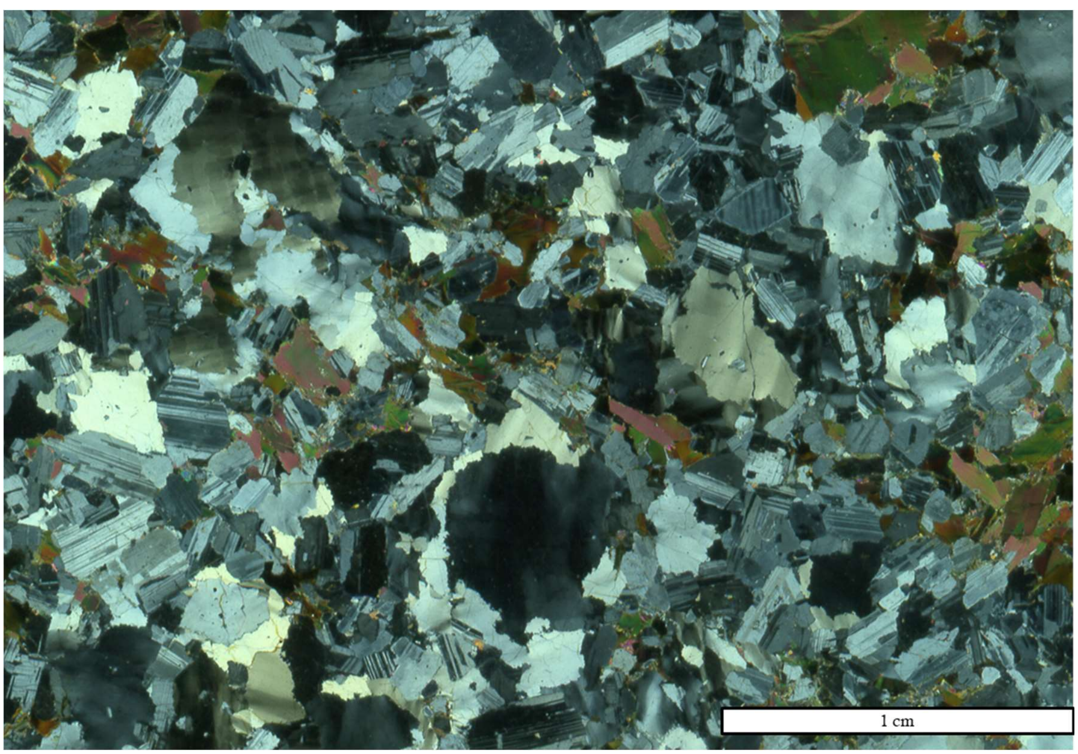

Figure 3.4 - Microphotograph of a leuco-tonalite.

Plagioclase presents well-shaped boundaries, good twinning and regular zoning. There are plagioclase clots, showing a similar aspect to rare cumulitic structure, with a straight shape and only interstitial quartz. At the same time, there are medium/coarse plagioclases with rounded and irregular shape usually in contact with large quartz crystals. Where twinning is well-defined (Carlsbad, albite, and pericline), deformation processes are highlighted: acicular and/or lamellae with no regular width preserve information about ductile processes; fractures, filled by less anorthitic plagioclase or argillaceous minerals indicate late-deformative processes probably during the last stage of cooling. Patchy and irregular zoning is the main feature in the coarse crystals together with an incipient substitution by sericite and muscovite lamellae in crystal-core or marking the crystal zoning. Based on previous considerations, two generations of crystals can be distinguished: the first characterized by crystals with coarse size, euhedral shape, weak and patchy zoning, abundant replacement by secondary phases (muscovite and sericite), small biotite inclusion in the core, myrmekitic intergrowth in contact to orthoclase and less abundant microcline. The less abundant second generation is referred to as crystals of medium size, subhedral to anhedral shape (rarely euhedral), well-developed twinning, absent zoning and alteration, forming a cumulitic structure.

Biotite varies in abundance, grain size and quantities of inclusions. It can occur as clots or isolated crystals, subhedral and anhedral shape and partly replaced by muscovite. The most common inclusions are zircon, apatite, ilmenite and quartz.

K-feldspar constitutes the rocks only for 5 % vol. Orthoclase and rarely microcline are founded in interstitial positions. Different types of perthite are present: exsolution of albite lamellae referred to the decrement of temperature, flame and patchy perthites linked to deformation or interaction with fluids. It can be affected by late-magmatic to solid-state replacement with plagioclase (myrmekite). Symplectitic intergrowths have been observed between muscovite and K-feldspar.

Muscovite occurs as tabular lamellae included in biotite (replacement product) and as small interstitial crystals in contact with the quartz-feldspathic phases (primary muscovite).

Quartz features (undulatory and chessboard extinction, subgrain deformation and rare recrystallization processes presenting triple joints) are typical in all samples, whereas the modal abundance and grain size are variable. Some minerals (plagioclase, biotite and, rarely, accessory phases) can be included in quartz and itself form inclusion in biotite, plagioclase and K-feldspar.

The accessory phases are zircon, apatite, ilmenite.

3.4 Mafic microgranular enclaves

The MME show medium-fine grain-size with an inequigranular porphyritic texture (Fig. 3.5). The phenocrysts (plagioclase and rarely biotite) are relatively scarce (2-5% vol.) and rarely exceed 2 mm. They are enclosed in a fine matrix constituted by the same mineralogy plus epidote, ilmenite, apatite and quartz. The grain size is variable but smaller than the magmatic host, with coarser euhedral grains, that may derive by crystal transfer from the host to the mafic magma, and subhedral to anhedral constituting the groundmass minerals.

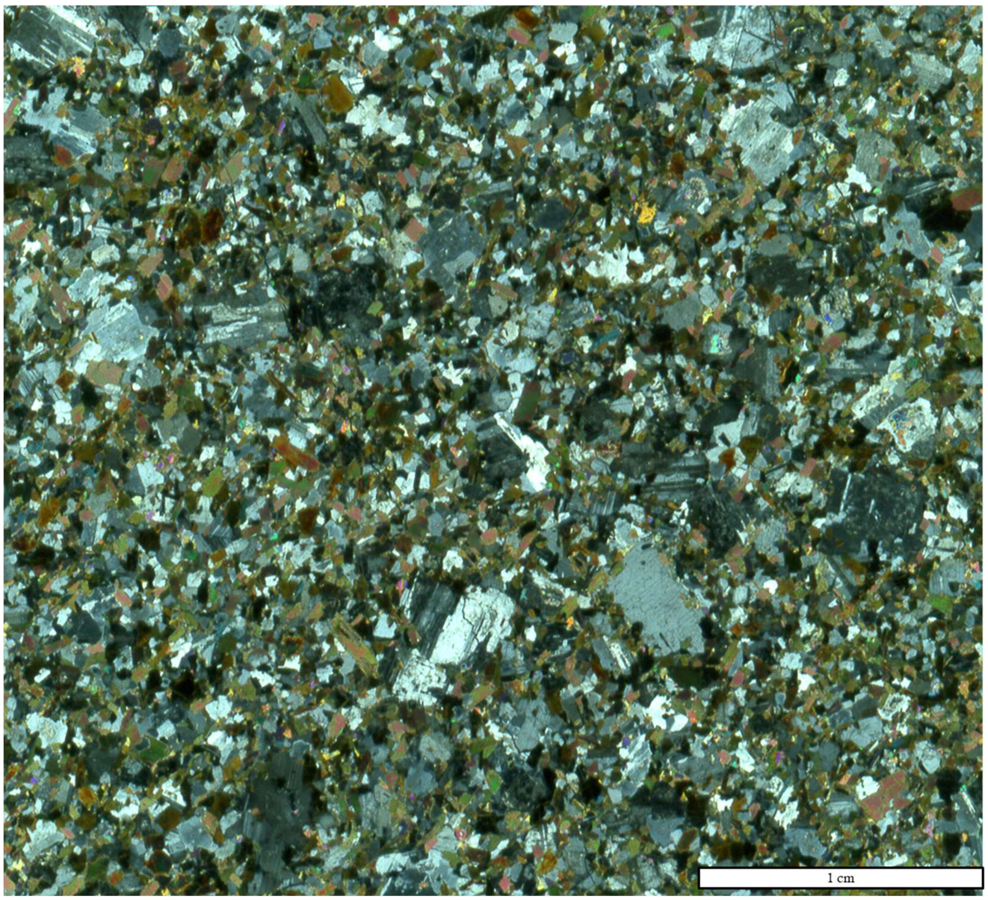

Figure 3.5 - Microphotograph of a mafic microgranular enclaves.

Large euhedral ***plagioclase*** crystals do not show twinning or zoning and contain small inclusions of amphibole, biotite and rarely epidote arranged parallel to elongation. Crystals can be wholly replaced, except in the rim, by sericite, secondary muscovite and clinozoisite. Subhedral smaller crystals exhibit well-developed polysynthetic twinning (albite-pericline) with rare inclusions and absence of zoning.

Subhedral ***amphibole*** is hornblende. It is more abundant than in the tonalite, but in some MME can be exclusively found as an anhedral inclusion in plagioclase crystals. It is usually replaced by biotite for reaction with the liquid.

Biotite shows subhedral to anhedral shape, with inclusions of euhedral epidote, epidote-allanite coronae, apatite and zircon. It constitutes most of the matrix, forming aggregates and clots.

Quartz (< 5 vol %) occurs in interstitial position, showing chessboard extinction. It is present in subgrains and tiny crystals with different orientations.

4. Mineral chemistry

4.1 Introduction

Mineral composition analyses have been conducted on different samples representative of any lithotype at the Laboratório de Microssonda Eletrônica of the University of São Paulo, Geosciences Institute (CPGeo – USP). Major elements of main and accessory phases are reported in Table 2 (see appendix) together with the description of the methodology. In this chapter, the mineralogical characterization is described jointly to highlight the similitude and/or difference between the lithotypes.

4.2 Plagioclase

Figure 4.1 shows as the feldspar compositions are relatively similar in all CVP lithotypes.

Labradorite to oligoclase plagioclase characterizes both quartz-diorite and tonalite, with a slightly wider range in the latter. The oscillatory zoning is reverse, with anorthite content ranging from An_{33} to An_{54} in the less evolved rock and from An_{25} to An_{61} in the evolved ones. Small patchy zoning in the crystal core with a more albitic composition (An_{8-21} in quartz-diorite and An_{14-23} in tonalite) can be indicative of decompression in the magma chamber, creating reabsorption of the inner feldspar portions.

Leuco-tonalite displays two generations of plagioclase: the first characterized by a reverse oscillatory zoning defined by core-to-rim An contents ranging from 32% to 47 %; the second is normal zoning (An_{22-50}) characterizing the medium/small crystals.

MME's plagioclase composition varies from An_{23} to An_{60}, in agreement with the plagioclase contents of quartz-dioritic and tonalitic hosts. Plagioclase shows normal zoning, from labradorite–andesine core to fresh oligoclase (An_{23}–An_{29}) rims.

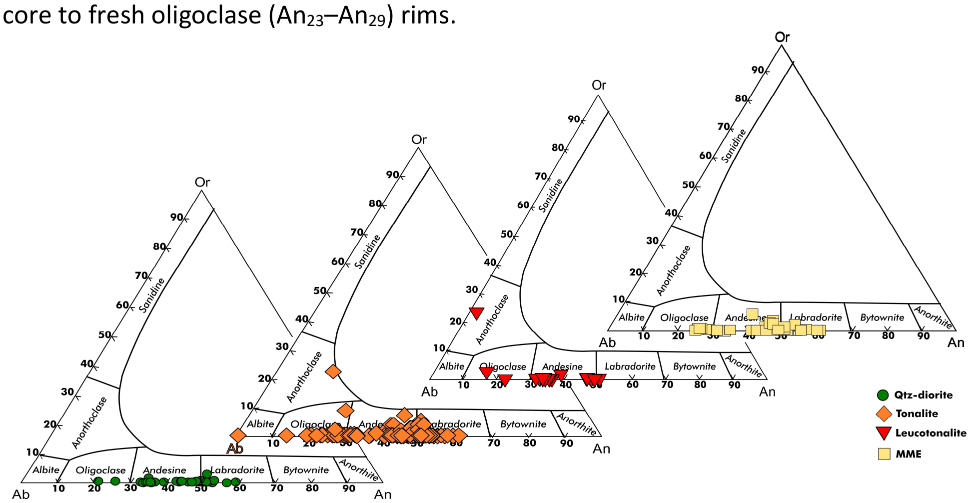

Figure 4.1- Plagioclase classification diagram for CVP lithotypes (Deer et al., 1963). Symbol as in the legend.

4.3 Biotite

Biotite shows enrichment in Al^{IV} atoms p.f.u. Gathering the samples based on the lithotypes and area of sampling, different features have emerged (Fig. 4.2). In the southern region (S. Maria), quartz-diorite has the highest values in $Fe/(Mg+Fe^{2+})$ and lowest aluminum content. Conversely, the quartz-diorite of the Briatico area exhibits the highest amounts of Al^{IV}. A bimodal distribution of Al^{IV} contents is also highlighted in the microgranular mafic enclaves. MME enclosed in the quartz-diorite (S. Maria) are enriched in aluminum, than the MME hosted in tonalite (Briatico). Despite what was expected, the comparing of MME biotite content with the respective host does not match. It suggests that although field study pointed out a partly digestion and/or mineral transfer, the biotite composition has not been undermined.

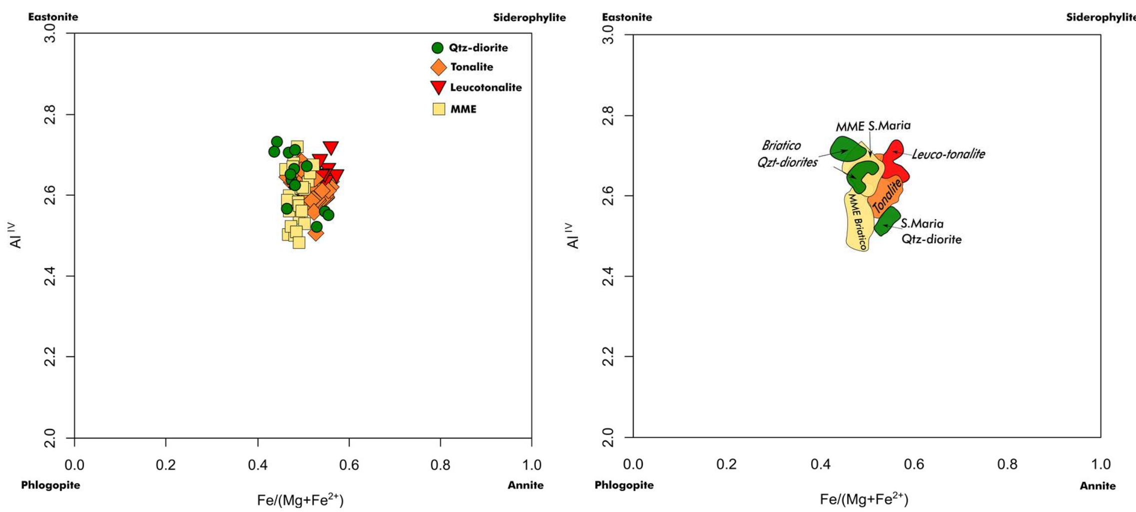

Figure 4.2 - Al^{IV}vs. $Fe/Mg+Fe^{2+}$ classification diagram of biotite (left diagrams). The right diagram shows the contour of the CVP sample referred to the area of sampling.

In the Abdel-Rhaman (1994) diagrams (Fig. 4.3), biotite plots at the boundary between the calc-alkaline and the peraluminous fields. Calc-alkaline field (C) corresponds to biotite deriving from I-type magmas in an orogenic-subduction setting. In contrast, the peraluminous field (P) is indicative of biotite deriving from S-type magmas in a collisional environment. The use of Al-Mg diagram seems to be the most discriminating tool for the estimation of the granite magma nature based on mineral criteria (Stussi & Cuney, 1996). In this way, a calc-alkaline affinity is more reliable.

Mg# [Mg/(Mg+Fe)] ratio is homogenous for tonalites (0.44-0.56), leuco-tonalite (0.43-0.46),and MME (0.48-0.54). As described above, the quartz-diorite can be divided into two different groups outcropping in the CVP's northern and southern area (despite they exhibit similar Mg# such as the previous lithotypes)the Briatico quartz-diorites (0.46-0.56)and the S. Maria quartz-diorites (0.45-0.47), respectively.

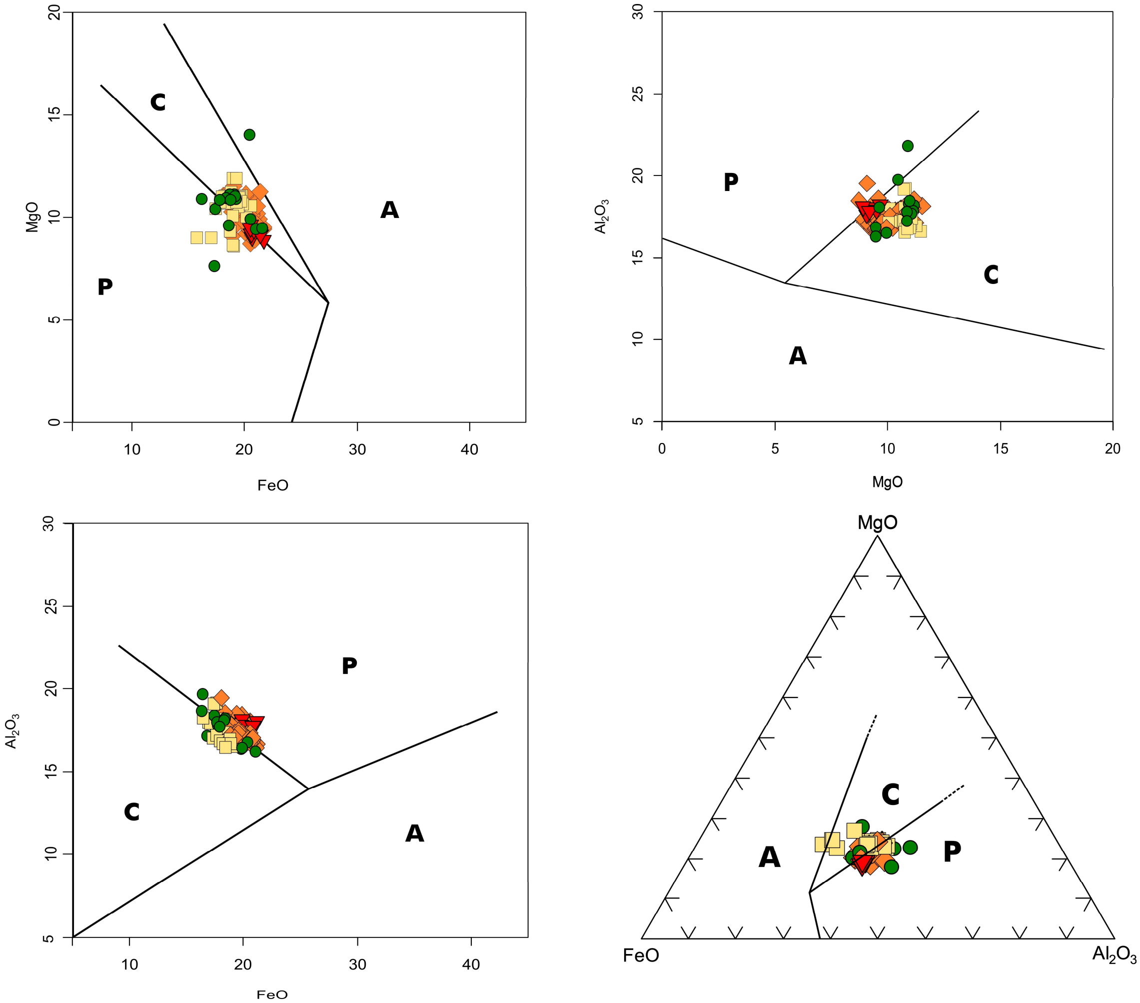

Figure 4.3 - Biotite discrimination diagrams using major elements (modified by Abdel-Rhaman, 1994). Symbols as in fig. 4.4; P = peraluminous, C = calc-alkaline, A = alkaline.

Inversely, Al^{IV} values are slightly similar for all rocks: in S. Maria quartz-diorites varies from 2.52 to 2.56, Briatico quartz-diorites from 2.57 to 2.73, tonalite from 2.58 to 2.68, leucotonalite from 2.64 to 2.72, S. Maria MME from 2.61 to 2.72 and Briatico MME from 2.48 to 2.71.

Due to the very scarce presence of *muscovite* in CVP lithotypes, only a few crystals in the evolved rocks (tonalite and leucotonalite) have been analysed. Muscovite from the leucotonalites plots in the field of primary magmatic muscovite, while most of the muscovite from the tonalites derives from the alteration of the main minerals, especially the biotite (Fig. 4.4). Primary muscovite is enriched in BaO (1.64-1.81 wt. %) and TiO_2 (0.66 – 3.41 wt. %) and depleted in K_2O (9.44 – 10.48 wt. %) in the tonalite than leucotonalite (BaO = 0.22-0.39 wt%, TiO_2 =0.81 – 1.71 wt% and K_2O = 10.48 – 11.53 wt. %).

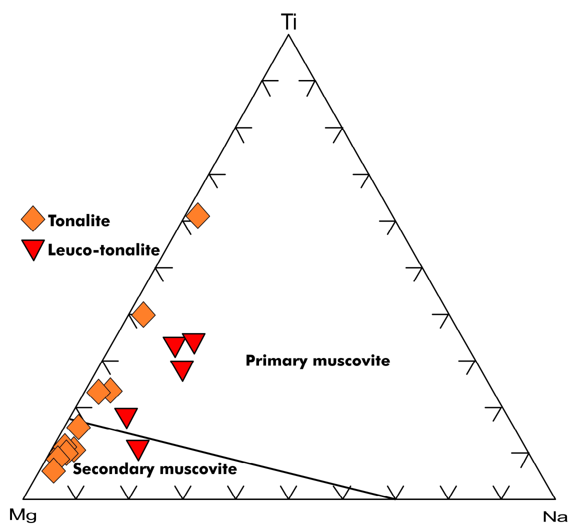

Figure 4.4 - Mg – Ti – Na classification for muscovite (from Miller et al., 1981).

4.4 Amphibole

Monoclinic amphibole is present in the studied lithotypes with the main composition ranging from Mg- and Fe-hornblende to Fe-Tschermakite hornblende. A gradual substitution Mg → Fe with the decrement of Si (a.p.f.u.) is illustrated in Fig. 4.5. In detail, a core-rim compositional changing from Mg-Hbl → Fe-Hbl → Fe-Tsch Hbl is common to S. Maria quartz-diorite, tonalite and Briatico MME. Mg-rich amphibole characterizes the Briatico quartz-diorites with the broad compositional range (from actinolite to Mg/Fe Tschermakite) and S. Maria enclave (from Mg-Hbl to Tsch-Hbl). The actinolite and actinolitic hornblende composition, found mainly in the rim, have been considered as alteration products.

Excluding the Briatico quartz-diorite with the wide Mg# range (0.38-0.68), the content is quite constant in all granitoids analysed: 0.48-0.52 in the S. Maria quartz-diorite, 0.44-0.52 in the tonalites, 0.47 – 0.54 in the Briatico MME and 0.50 – 0.53 in the S. Maria MME. The high $Mg/Mg+Fe^{2+}$ ratio of the amphibole compared with the biotite states an earlier crystallization of the calcic amphibole.

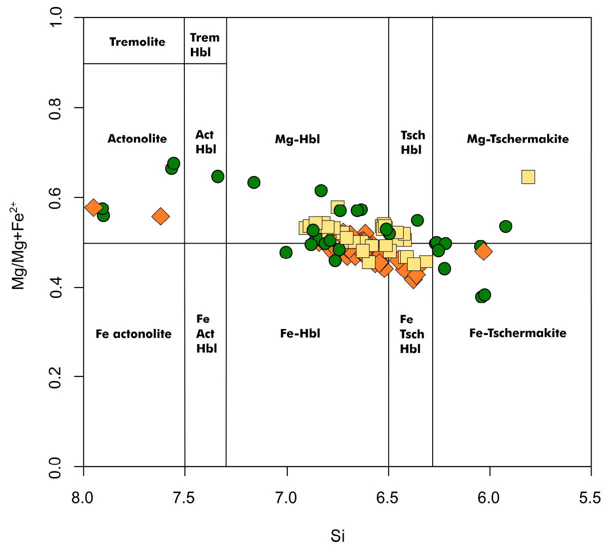

Figure 4.5 - Hornblende classification diagram (Leake, 1978) of CVP granitoids. Symbols as in Fig. 4.5.

The microprobe analysis detected an decrement in Al_2O_3 (9.43 – 12.14 wt. %) and MgO (7.06 – 8.64 wt. %) of S. Maria quartz-diorite compared with the Briatico ones (Al_2O_3 = 11.74 – 21.74 wt%). Higher contents in Na_2O (0.99 -1.21 t%) , K_2O (0.47 – 0 .76 wt. %) and F (0.06 -0.19 wt%) for the enclave sampled in the S. Maria area than the northern CVP area (Na_2O = 0.68 – 0.10 wt. %., K_2O = 0.88 – 1.05 wt. %, F = 0.03 – 0.11 wt%) have been highlighted.

4.5 Epidote

WinEpclas software (Yavuz et al., 2018) was used to calculate the name of the most abundant accessory phase presents in the studied rocks. The classification uses epidote-supergroup minerals based on the IMA subcommittee report (Armbruster *et al.,* 2006) with discovered and IMA-approved new epidote minerals since then (see Yavuz *et al.,* 2018). Based on the predominant cation in the A, T, M sites with redistributions in the key sites (A1, A2, M1, M2, M3, O4; Table 1) the mineral was classified as epidote and a minor part as clinozoisite, allanite(-Ce) and dissakisite(-Ce).

Another classification considers the allocation of the cation in the M1, M2 and M3 sites, respectively. The Fe^{3+}- Al^{VI} – Me^{2+} diagram (Fig. 4.6) permits to classify epidote minerals, considering the isomorphic transition between REE-poor and REE-rich minerals. Unfortunately, despite the petrographic study highlighted allanite in the quartz-diorite, the thin section analysed exhibit only epidote minerals. Epidote, clinozoisite and allanite are the common accessory minerals present in the tonalites.

[A1]Dominant cation	[A2]Dominant cation	[M1]Dominant cation	[M2]Dominant cation	[M3]Dominant cation	[O4]Dominant anion	[Epidote subgroup]	[Epidote name]
Ca	Ca	Al	Al	Fe3+	O	Clinozoisite subgroup	Epidote
Ca	Ca	Al	Al	Al	O	Clinozoisite subgroup	Clinozoisite
Ca	(REE)3+	Al	Al	Fe2+	O	Allanite subgroup	Allanite-(Ce)
Ca	(REE)3+	Al	Al	Fe3+	O	Allanite subgroup	Dissakisite-(Ce)

Table 1 - Cations distribution in the main crystallographic sites in the epidote and corresponding classification (from Yavuz et al., 2018).

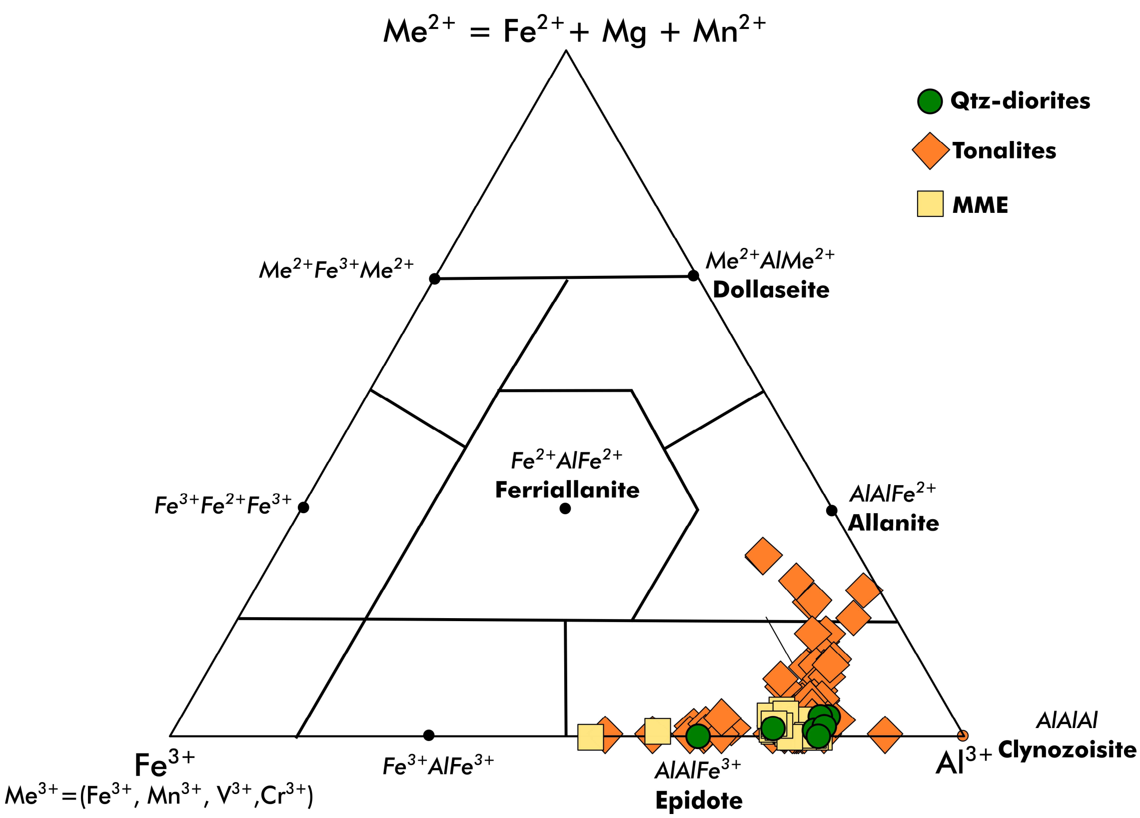

Figure 4.6 - Classification diagram for REE-bearing members of the epidote group based on crystallochemical data (modified from Kartashov 2014).

4.6 Summary

Combining petrographic and minerochemical features, a cogenetic nature is suggested for all the studied lithotypes from Capo Vaticano Promontory. The main crystallization sequence is characterized by plagioclase and amphibole, followed by biotite and epidote, quartz and rare orthoclase. Specifically, quartz-diorites s.s., tonalite and MME crystallization sequence is made by amphibole/plagioclase -> epidote -> biotite -> quartz (amphibole decreasing from quartz-diorites to tonalite); leuco-tonalite by plagioclase -> biotite -> muscovite -> quartz -> orthoclase. Biotite is the mineral phase showing the widest difference in the lithotypes, especially in Mg# and Al content. Table 2 displays a list of the main feature of primary mineral phases in the CVP lithotypes.

Table 2 - Main mineral chemistry features of Pl, Amph and Bt from the studied CVP lithotypes.

Lithotypes	Plagioclase	Amphibole	Biotite
Quartz-diorites	An_{54-43} An_{21-18} (resob.core)	Fe-Hbl/Hbl (S.Maria) $Mg/Mg+Fe^{2+}$ 0.47-0.54 More varieties (Briatico) $Mg/Mg + Fe^{2+}$ 0.50-0.53	Al^{IV}= 2.48-2.71 $Mg/Mg+Fe^{2+}$ 0.45-0.47 Al^{IV}= 2.61-2.72 $Mg/Mg + Fe^{2+}$ 0.49-0.56
Tonalites	An_{59-30} (coarse crystals) An_{22} (resorbed portion)	Mg-Hbl/Fe-Hbl Fe-Tsch Hbl $Mg/Mg+Fe^{2+}$ 0.44-0.52	Al^{IV}= 2.58-2.68 $Mg/Mg + Fe^{2+}$ 0.44-0.53
Leuco-tonalites	An_{42-37} (coarse crystals) An_{50-22} (medium crystals)	-	Al^{IV}= 2.64-2.72 $Mg/Mg + Fe^{2+}$ 0.43-0.46
MME	An_{60-25}	Mg-Hbl/Fe-Tsch Hbl (Briatico) $Mg/Mg+Fe^{2+}$ 0.50-0.53 Mg-Hbl/Tsch Hbl (S.Maria) $Mg/Mg+Fe^{2+}$ 0.47-0.54	Al^{IV}= 2.61-2.72 $Mg/Mg + Fe^{2+}$ 0.48-0.53 Al^{IV}= 2.48-2.71 $Mg/Mg + Fe^{2+}$ 0.49-0.54

5. Geochemistry

5.1 Introduction

Major and trace elements have been obtained for all CVP lithotypes sampled during the Ph.D. study. Whole-rock major- and trace-element compositions of 32 samples (eight quartz-diorites, sixteen tonalites, four leucotonalites and four mafic microgranular enclaves; Appendix.Table 6) have been achieved at ALS Laboratory. ICP-AES and ICP-MS techniques have been used to detect major (wt.%) and trace elements (ppm), respectively. The methods consist of the fusion of each bead followed by acid digestion. The Sr-Nd-Pb isotopic composition (Appendix. Table 7) has been acquired at CPGeo (Centro de Pesquisas Geocronológicas) laboratory at Universidade de São Paulo through the MC-ICP-MS technique. In particular, for the whole-rock Sm-Nd and Rb-Sr isotope study, 16 samples (4 quartz-diorites, 10 tonalites and 2 MME) were selected, while the Pb-Pb systematics have been applied to three quartz-diorites, four tonalites and two enclaves. The data have been plotted together for better visualization and figuring out geochemical variations and/or analogies between lithotypes. Geochemical data have been managed using the GCDKit software (Janousek et al., 2006; 2016).

5.2 Major elements

A continuous evolutionary trend from gabbroic diorite to granodiorite is displayed in the Middlemost (1994) diagram (Fig. 5.1 a). In particular, the geochemical classification agrees with the petrographic classification for quartz-diorites and tonalites. In contrast, MME and leuco-tonalite are categorized as gabbroic diorite and granodiorite, respectively. The previous geochemical characterization is confirmed by R_1-R_2 diagram (De La Roche *et al.,* 1980; Fig. 5.1 b). In the diagram of Frost et al. (2001; Fig. 5.2 a,b) the CVP rocks follow the magnesian and cal-alkalic to calcic trend.The

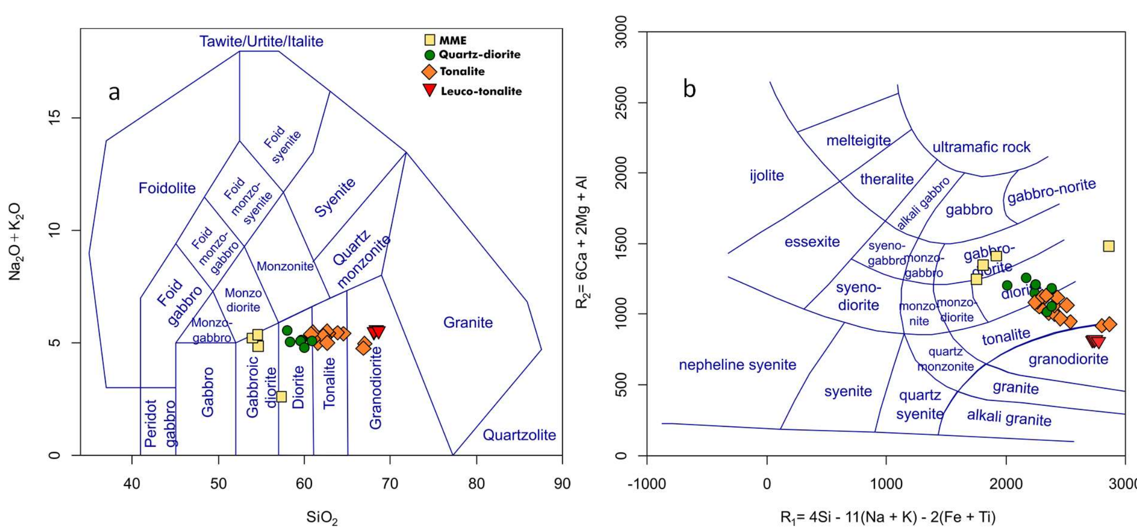

Figure 5.1 - Plutonic classification of CVP lithotypes projected in the TAS diagram in the left (Middlemost, 1994) and R_1-R_2 plot in the right (De La Roche et al., 1980). Symbols as in legend.

Shand diagram (1943; Fig. 5.2c) all granitoids exhibit weakly peraluminous except for the MME, showing a metaluminous affinity. Similarly, the B-A plot (Debon and Le Fort, 1983; Fig. 5.3 a) confirm the dominant mineralogy (Bt ± minor Amph) with a homogenous alumina content.

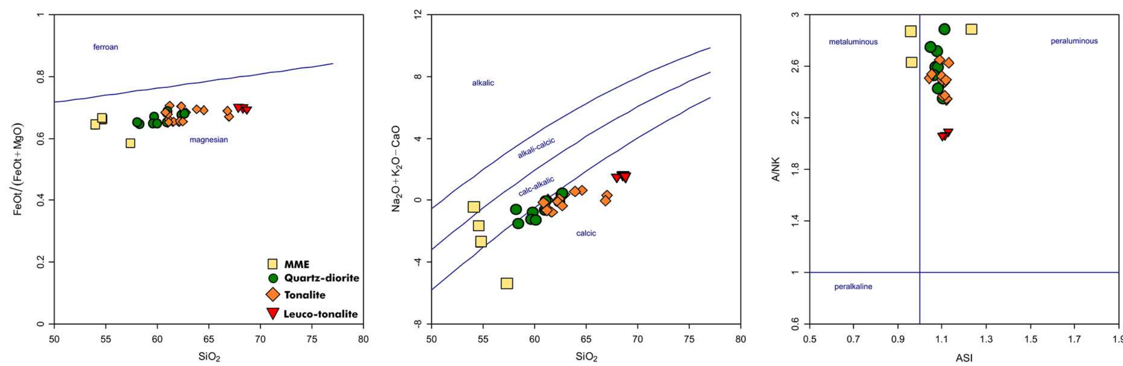

Figure 5.2 - CVP lithotypes project in the Frost et al. (2001, 2006) diagram. a) Feo_t/(FeO_t+MgO) vs SiO_2 diagram; b) Na_2O +K_2O – CaO vs. SiO_2 diagram; c) A/NK vs Alumina saturation index (ASI)) diagram.

A moderate enrichment in K_2O is showed in the Peccerillo and Taylor diagram (1972; Fig. 5.3), indicating a K-rich calc-alkaline series evolving to calc-alkaline series for the SiO_2 enriched tonalite and leuco-tonalite.

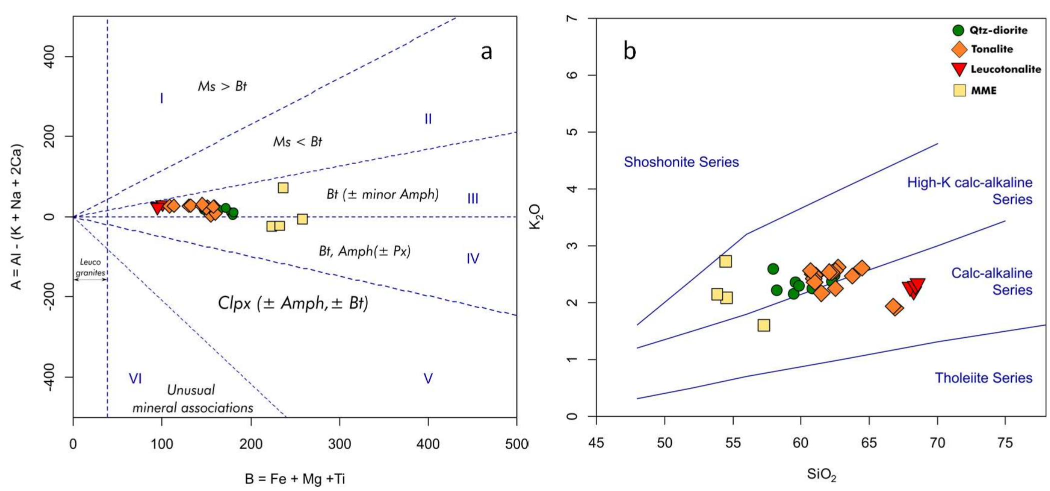

Figure 5.3 - a) A-B plot (Debon and Le Fort, 1983); b) K_2O vs. SiO_2 diagram (Peccerillo and Taylor 1972). Symbol as in the legend

Harker diagrams for major elements, even with some scatter in some components, depict linear trends for quartz-diorite, tonalite and leuco-tonalite (Fig. 5.4). Al_2O_3, TiO_2, FeO_{tot}, MgO, CaO, MnO and P_2O_5 define a strong negative correlation with the silica content. K_2O defines a scattered positive trend, whereas Na_2O demonstrates an approximately flat pattern with an enrichment towards the leuco-tonalite.

Mafic micrograular enclaves show a wide compositional range in major elements (Fig. 5.4). As expected, the MMEs are enriched in MgO, FeO_{tot}, CaO and MnO respect to the quartz-diorite/tonalite main trends. A slight impoverishment is shown for K_2O and P_2O_5.

The general tendency of the major elements (Fig. 5.4) is consistent with results obtained for the CVP rocks by Rottura *et al.* (1989; 1990) and Fiannacca *et al.* (2015).

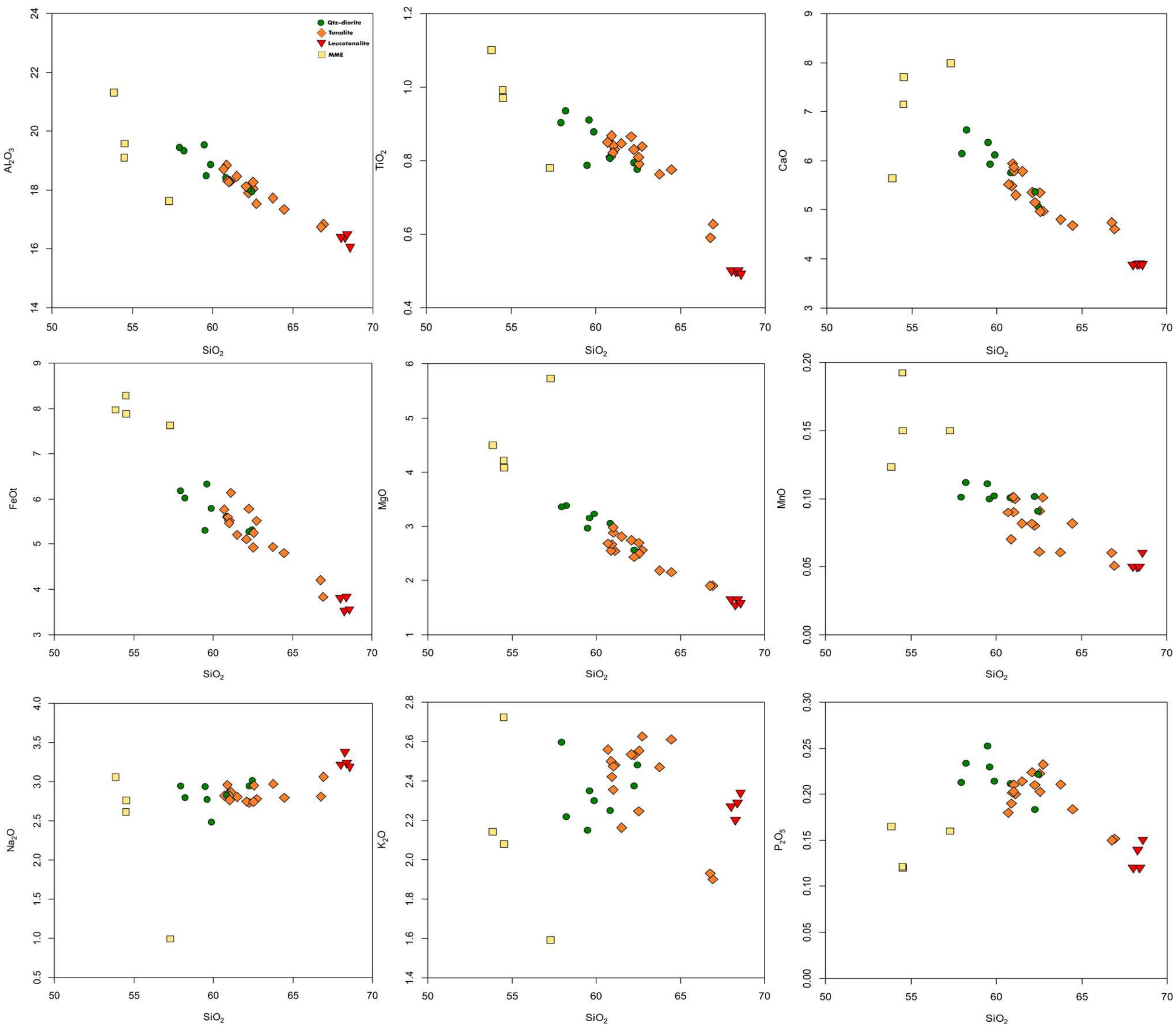

Figure 5.4 – Harker diagrams of the major elements in the CVP lithotypes.

5.3 Trace elements

Except for a few trace elements, ill-defined trends characterize the CVP rocks (Fig. 5.5). General negative correlations with silica can be observed for Ba, Sr, Eu and V from the less evolved quartz-diorite s.s. to the evolved leucotonalites (Fig. 5.5). A closer examination highlights an enrichment in Rb (68.8 - 93.5 ppm), Zr (173 – 251 ppm), Th (0.91 – 17.1 ppm), Ce (22.4 – 141.5 ppm), Hf (4.3 – 6.1 ppm) and depletion in Y (0.73 –1.93 ppm) in the tonalites and leuco-tonalite compared with the quartz-diorites.

The mafic enclaves exhibit dissimilar concentrations in trace elements without defining a clear trend. In general, they show homogeneous enrichment in Eu and V and are depleted in Ce (28.4 – 59.6 ppm), Zr (129 – 173 ppm), Th (0.45 – 10.6 ppm) and Hf (3.2 -4.6 ppm) compared with the quartz-diorite and tonalite. A wider range is shown by Ba (589 – 815 ppm), Sr (236 – 344 ppm), Rb (58.5 – 93 ppm) and Y (18.5 -67.5 ppm).

Primitive mantle-normalized multi-element diagrams (Fig. 5.6) show similar patterns in all CVP

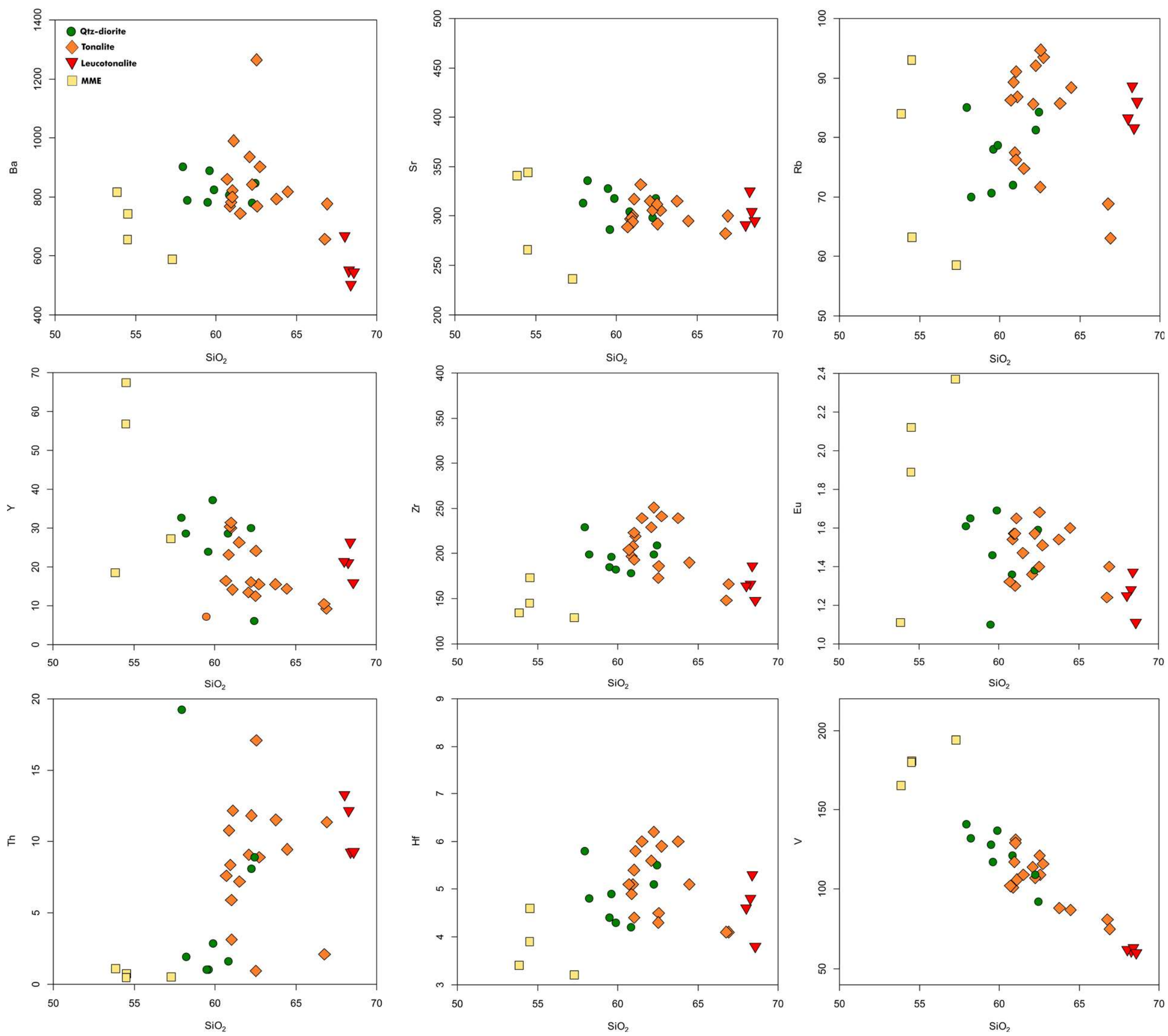

Figure 5.5 – Trace elements distribution in CVP quartz-diorites, tonalite, leucotonalite and MME.

lithotypes. LIL elements are enriched respect to HFSE, although a wide variability is shown in the quartz-diorite and tonalites (e.g. La, Ce and Pr). U-positive anomaly is weakly evident compared with the CVP quartz-diorite and tonalite studied by Rottura *et al.* (1989; 1990) and Fiannacca *et al.* (2015).

All quartz-diorites, tonalites and leuco-tonalites highlight Nb, Ta, Sr, P, Zr, Ti troughs, although Nb and Ta negative anomalies are less marked in the evolved tonalites. In addition, a slight Ba depletion is present in the leuco-tonalite pattern.

Mafic microgranular enclave patterns do not reveal any difference from the host. Cs, Rb and Ba are enriched compared with the HFSE and HREE. The latter outlines a quasi-flat pattern with small Th, Ta, Sr, P, Zr and Ti negative anomalies.

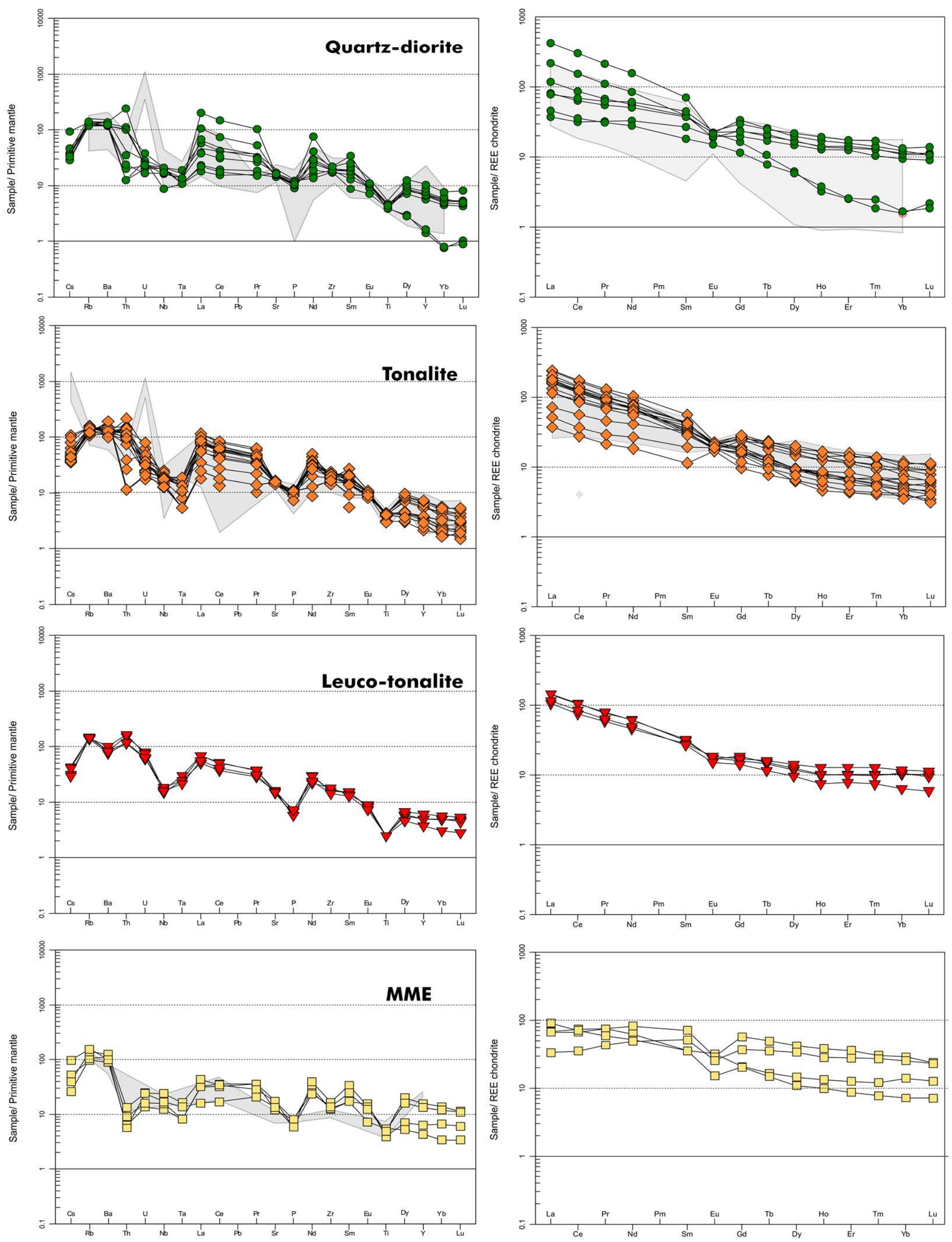

Figure 5.6 - Multi-element diagram for CVP lithotypes. In the left: Primitive mantle normalized patterns (McDonough and Sun (1995)); in the right: REE-chondrite normalized pattern (Boyton, 1984). Shadow area are CVP literature sample from Rottura et al. (1989; 1990) and Fiannacca et al. (2015). Symbols as in Fig. 5.5.

Chondrite-normalized REE patterns exhibit different inclination in each lithotype (Fig. 5.6). In general, strong to weak LREE/HREE fractionation is gradually observed with the increasing of the silica content (quartz-diorite → tonalite → leucotonalite). The enclaves are the only rocks showing a flat REE pattern. In fact, $(La/Yb)_N$ average ratios vary from 33.3 in quartz-diorite, 25.6 in tonalite, 13.7 in leuco-tonalite and 5.3 in the mafic enclaves. Negative Eu anomalies are well evident in each lithotype, but less-marked positive anomalies are shown in quartz-diorite (Eu/Eu* = 1.03) and more marked in tonalite (Eu/Eu* = 1.25-1.64). The gradual enrichment in ΣREE is well highlighted with the increment of the silica content (Fig. 5.7) with tonalites showing the strong enrichment. In addition, LREE contents (quartz-diorites = 60 -225 ppm, tonalite = 47 -295 ppm, leucotonalite = 128 -177 ppm, MME = 73 – 132 ppm) are present in more quantities than the HREE (quartz-diorites = 1.35 – 7.37 ppm, tonalite = 2.21 – 2.65 ppm, leucotonalite = 3.95 -6.92 ppm).

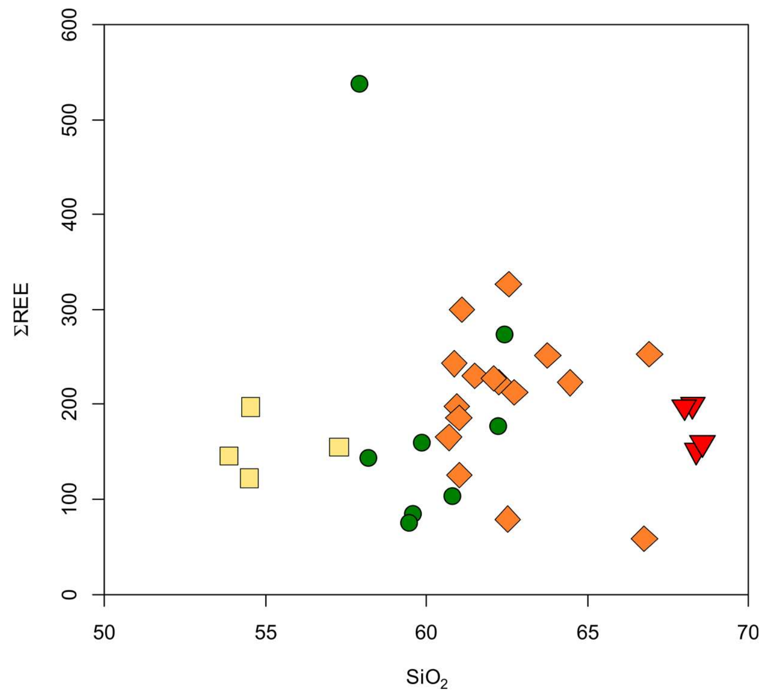

Figure 5.7 - ΣREE vs SiO_2 diagram of Capo Vaticano Promontory lithotypes. Symbols as in Fig. 5.5.

5.4 Isotope geochemistry

Sixteen samples have been selected for the Sr-Nd isotope characterization, whereas nine samples have been chosen for the Pb-Pb systematics. These correspond to a selection of CVP lithotypes analyzed for the major and trace elements.

Sr and Nd isotopic ratios have been recalculated to a crystallization age of 298 Ma, obtained by U-Pb SHRIMP analysis for these rocks (see geochronology chapter). Homogenous $^{87}Sr/^{86}Sr$ initial ratio are in the range 0.7097 – 0.7103 for the studied CVP rocks, whereas a wider range (from -5.88 to -7.43) is shown by εNd values (Fig. 5.8 a, b). The Nd ratio defines a vertical array, as already reported by Rottura *et al.* (1989; 1990) and Fiannacca *et al.* (2015) for the granitoids of the Serre Batholith. As shown in Fig. 5.8 b, studied samples are all characterized by a highly unradiogenic Nd isotopic signature, in contrast with less negative εNd literature values obtained for three tonalites (+ 0.04/-1.62 and -3.66, respectively; Rottura et al., 1989; 1990 and reference therein). Interestingly, the εNd variation observed in studied samples does not exhibit a correlation with the major element composition and the possible origin of the different rock types. In particular, if the mafic enclaves derived from mantle magma, their Nd signature should be less unradiogenic than that in the granitoids. On the contrary, the MME are characterized by the most unradiogenic εNd value.

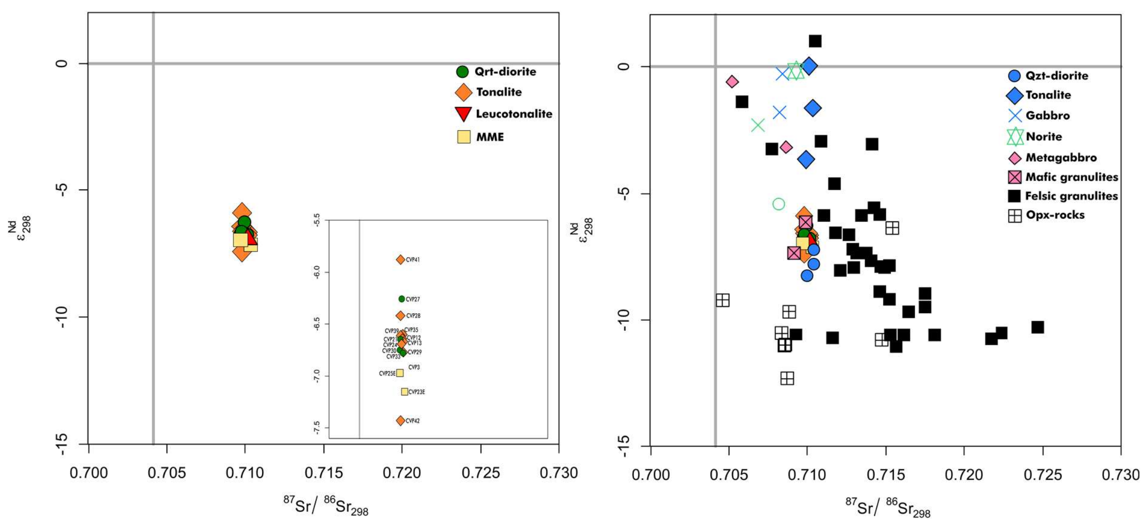

Figure 5.8 - Sr initial ratio versus εNd ratio recalculated at 298 Ma. a) Sr_i and εNd ratios fro CVP lithotypes of present study; b) CVP compared with literature data of granitoids (from Rottura et al., 1989; 1990) and lower crustal basement of CVP area (Caggianelli et al., 1991; Del Moro et al., 2000). New data symbols as reported in legend. Blue filled symbols: granitoids rock from Serre and CVP (from Rottura 1989; 1990); green: magmatic rock from Sila Batholith; fuchsia: metaigneous rocks (after Caggianelli et al, 1991); black: metagreywackes migmatites (Del Moro et al., 2000) and Opx-bearing rocks (Caggianelli et al., 1991).

The $^{206}Pb/^{204}Pb$, $^{207}Pb/^{204}Pb$ and $^{208}Pb/^{204}Pb$ ratios range in quartz-diorite, tonalite and MME from 17.97 to 18.34, from 15.60 to 15.65 and from 37.93 to 38.60, respectively. In $^{207}Pb/^{204}Pb$ and $^{208}Pb/^{204}Pb$ versus $^{206}Pb/^{204}Pb$ diagrams, they plot directly above the Pb growth curve (proposed by Stacey and Kremers, 1975), indicating a U/Pb and Th/Pb enrichment in the source (e.g., Jung *et al.,* 2015).

Comparison with the lower crustal rocks of the Serre Batholith shows a strong affinity with mafic granulites.

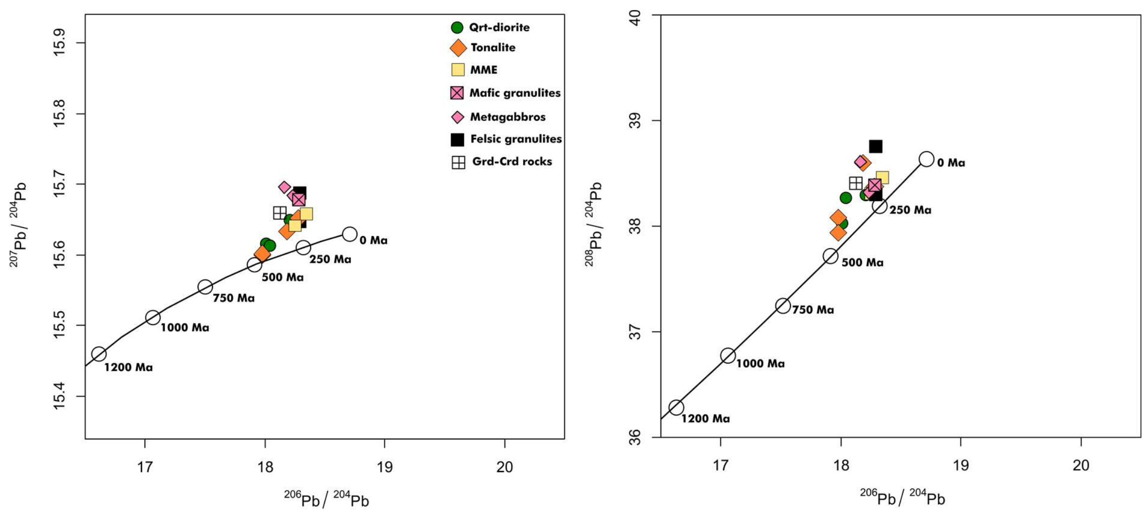

Figure 5.9 – $^{207}Pb/^{204}Pb$ and $^{208}Pb/^{204}Pb$ versus in $^{206}Pb/^{204}Pb$ ratios in CVP granitoids and lower crustal basement. Symbols as in Figure. Curve represent Pb growth by Stacey and Kremers, 1975). For references see Fig. 5.8.

6. Zircon U-Pb zircon geochronology and Lu-Hf isotope constrains

6.1 Zircon sampling and analysis

Two quartz-diorites, six tonalites and two MME samples, collected at various distances from the lower crustal basement rocks across the whole CVP area, have been selected to extract information about the age of batholith construction (SHRIMP U-Pb data) and to evaluate the presenceof late Paleozoic melt-precipitated zircon crystallised from magmas of different compositions, as a clue for possible mixing between crustal and mantle-related melts. Previous zircon geochronology of a small number of analysed quartz diorite and tonalite samples (Schenk, 1989; Langone et al., 2014; Fiannacca et al., 2017) indicated significant inheritence within the intrusives with zircon displaying inherited cores. In this study the analysed zircon grains all show simple structure without evidence for older/inherited cores.

Information on the relative contribution of crustal and mantle sources in the genesis of the different granitoid rocks was investigated through analysis of the Hf composition from the same spots of the dated zircon crystals.

Overall, 123 zircon crystals analysed with the SHRIMPII-e at the Geochronological Research Center of the University of São Paulo, Geosciences Institute (CPGeo – USP). Lu-Hf isotope systematics were analysed on the same zircon spots (134) analysed for the U-Pb systematics and in CVP33 tonalitic sample (not previously dated) by LA-MC-ICP-MS at CPGeo-USP. Results are reported in Appendix Tables 8 and 9).

Zircon crystals have been extracted from sievedcrushate, using magnetic and heavy liquid separation methods. During the picking, the zircon was arranged in rows, plaster in epoxy resin and polished to show internal structure. CL and transmitted images have been performed and used to choose the spot location. The SHRIMP II was employed using the procedures based on Compston et al. (1984), Williams (1998), Stern (1998) and Sircombe (2000) and described by Sato *et al*. (2014). Temora 2 was used as a standard to the $^{206}Pb/^{238}U$ age reference (416.78 Ma, Black et al. 2004). Raster time is 2 – 3 minutes with spot size = 50µm, plus 0.5 minutes of burning time fixed at the center. The age reported in figures are given with one sigma precision, and the average ages reported in the text are weighted-mean $^{238}U/^{206}Pb$ ages, with 95% confidence limits. The Tera-Wassemburg diagrams were prepared by using Isoplot/Excel (Ludwig 2003).

Neptune multicollector inductively coupled plasma mass spectrometer equipped with an Analyte G2 excimer laser ablation system was used for Lu-Hf analysis. The laser spot parameters were: 35 µm in diameter; ablation time of 60s; repetition rate of 7 Hz and He was used as the carrier gas. ^{171}Yb, ^{173}Yb, $^{174}(Hf+Yb+Lu)$, ^{175}Lu, $^{176}(Hf+Yb+Lu)$, ^{177}Hf, ^{178}Hf, ^{179}Hf and ^{181}Ta were collected simultaneously. A decay constant for ^{176}Lu of 1.867 x10^{-11} y^{-1} (Söderlund et al. 2004), the present–day chondritic ratios of $^{176}Hf/^{177}Hf$=0.282772 and $^{176}Lu/^{177}Hf$=0.0332 (Blichert-Toft & Albarède 1997) and the depleted mantle values of $^{176}Hf/^{177}Hf$=0.283225 and $^{176}Lu/^{177}Hf$=0.0385 (Vervoort & Blichert-Toft 1999) were adopted to calculate εHf values. A bulk earth $^{176}Lu/^{177}Hf$=0.0150 was also considered for data reduction (Griffin et al. 2002). The analytical procedure consists in one blank analysis followed by two GJ standards. Eleven samples are then measured. At the end, two more GJ standards are analyzed. After data correction, a Python program renormalizes the sample's ^{176}Hf /^{177}Hf ratio, based on the difference between the average value of the GJ standard and its expected value (0.282015; Y.S. Liu et al., 2010). This Python program calculates εHf and two stage DM model age using formulas from Yang *et al.,* 2007.

6.2 U-Pb-Th systematics

6.2.2 Quartz-diorites

Zircon extracted from the CVP27 sample consists of subhedral grains (120-310 µm) with a well-developed prismatic shape compared to the pyramidal facets (Fig.6.1). Usually, smaller grains have a lower aspect ratio (2:1) than larger ones (5:1). CL images clarify the internal structural complexity of the zircon crystals: most of the zircons are characterized by tight oscillatory zoning and recrystallization edges. The recrystallization may completely obliterate the original magmatic zoning. No discordant cores are visible in the quartz-diorites suggesting an exclusively magmatic origin of the zircons.

On a total of 15 spots, 13 targeted grains have been analysed in the middle and edge parts of the crystals showing tight oscillatory zoning and 2 in the center of homogenous bright CL areas (Fig. 6.1). Th and U range and Th/U ratio are narrow in the normal oscillatory zoning (U=132-278 and Th = 97-210 ppm, Th/U=0.40-0.92), except for a crystal with high U (532 ppm) and Th (398 ppm) and similar Th/U ratio = 0.74. The bright homogenous zircons exhibit a more constant composition (U = 100-129 ppm, Th = 42-48 ppm, Th/U = 0.37-0.40). $^{206}Pb/^{238}U$ ages and Tera-Wasserburg Concordia have been used, because zircon crystal ages are younger than 1.5 Ga. Taking into account the Th/U contents, the internal microtexture and the U-Pb age, three main events have been recognized: a *crystallization age* at 303± 1 Ma, older age at 314 ± 3 Ma, tentatively considered as an *anatectic age,* and a *recrystallization age* at 296± 1 Ma (Fig. 6.2).

Zircons on the CVP30 sample are euhedral to subhedral (116 -336 µm) prismatic grains (Fig. 6.1) with aspect ratio range from low (2:1) to high (6:1). The CL images show well-developed magmatic oscillatory zoning and a bright edge. Elongated zircon constitutes a specific population (around the 40%), exhibiting banded zoning. Eleven spots have been located in the main igneous oscillatory zoning, whereas one spot was located in the homogenous bright crystal. The U and Th contents measured in the oscillatory zoned domains are in the range 230-699 and 139-501 ppm with a narrow Th/U ratio (0.51-0.81). The homogenous bright portion has U = 94 ppm, Th = 71 ppm and Th/U= 0.75. Once again, three different ages have been obtained (Fig. 6.2): the older as recording the anatectic conditions (308 ± 2 Ma), a *crystallization age* (297± 2 Ma), followed by a late magmatic episode (289 ± 1 Ma*; late recrystallization*) that affect partly or totally the zircon surface.

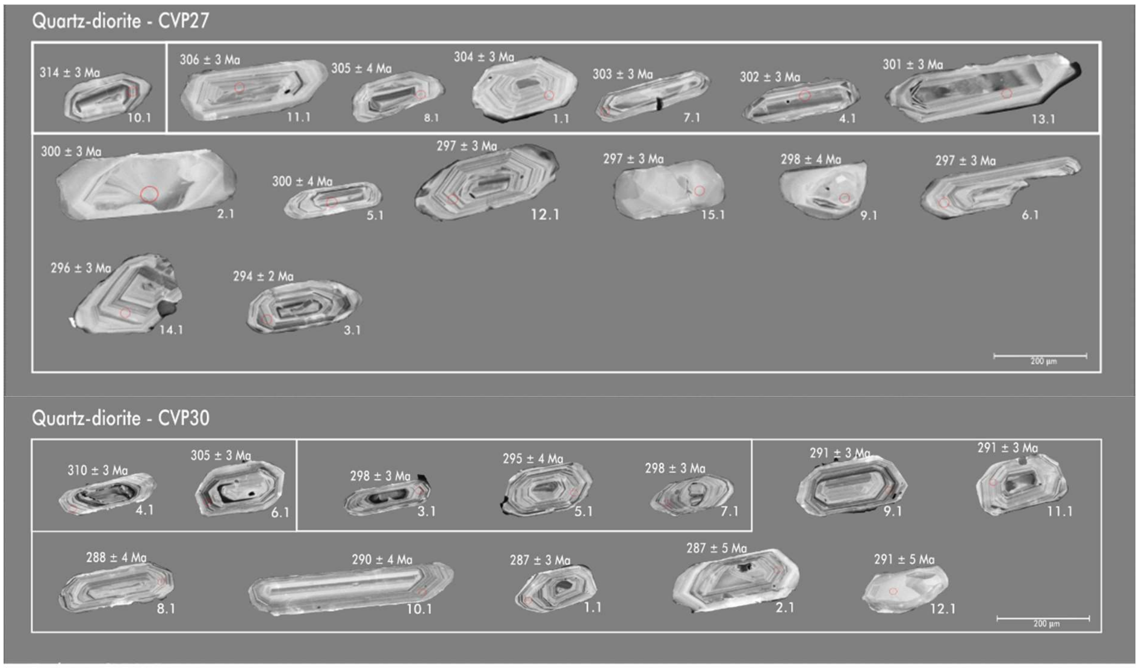

Figure6.1 - CL images of the analysed zircons in the quartz-diorites (CVP27 and CVP30 samples) from the CVP. The red n circles represent the analysed spots, with the associated $^{206}Pb/^{238}U$ ages obtained by SHRIMP dating. The boxs represent zircon spots used to obtain the anatectic, emplacement and recrystallization ages, respectively.

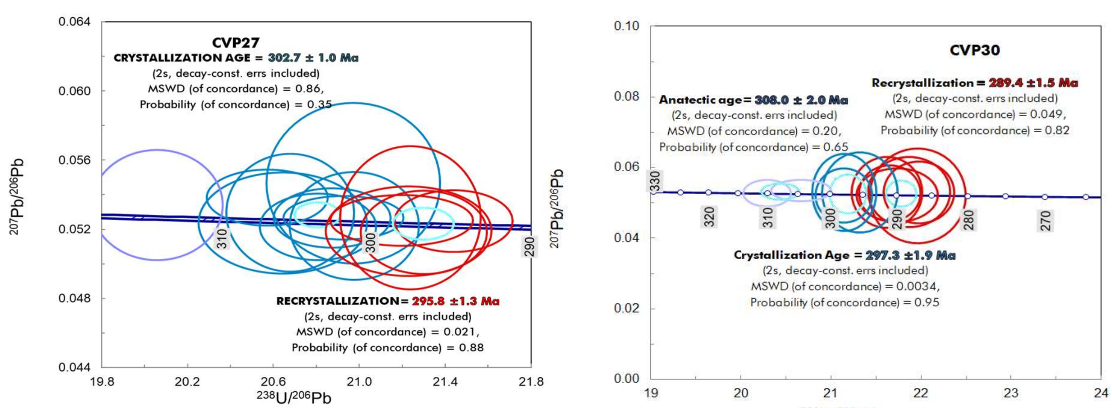

Figure 6.2 - U-Pb Tera-Wasserburg concordia diagram for zircon grains from the quartz-diorites (CVP27 and CVP30). Calculated with Isoplot v. 4.15 (Ludwig 2011).

6.2.2 Tonalites

The zircon grains in the tonalites show wide variability. The sample description follows a possible depth of emplacement.

Sample CVP42 exhibits thick prismatic zircons with some bipyramidal terminations and minor elongated grains (Fig. 6.3). Compared with zircon grains of the quartz-diorite, the zircon size is smaller, ranging from 60 to 260 µm and with a dominant low aspect ratio population (2:1). The 90% of the grains exhibit well-defined oscillatory zoning from the inner to the outer parts, whereas the remaining 10% displays a wider bright and homogenous edge, indicating U-poor portions; Fig. 6.3). Only two crystals seem to contain a possible older core with a rounded and irregular shape, both homogenous, one darker and the other brighter (Fig. 6.3). Sixteen spots have been analysed: 9 spots located in the middle portion, in correspondence to the normal zoning (U = 170-392 ppm, Th =55-234 ppm, Th/U = 0.27 – 0.68), 3 spots located in the center (U = 97-431 ppm, Th =53-135ppm, Th/U = 0.31 – 0.54), one in the core (U = 22 ppm, Th = 25 ppm, Th/U = 1.13) and one bright edge (U = 129 ppm, Th = 63 ppm, Th/U = 0.49). Two analyses with high uncertaintieswere rejected (2.1 and 2.2 spots). The U-Pb data have been clustered in two main groups, based on igneous zoning and Th/U ratio providing: an older age of 303.5 ± 1.4 Ma, interpreted as indicating anatectic conditions in the source region, and a magmatic age of 297.3 ± 1.3 Ma (Fig. 6.4). Only one core provides a confidently Paleo-proterozoic age of 2562 ± 42 Ma, surrounded by a recrystallized edge (291 ± 4 Ma; Figs. 6.3, 6.4).

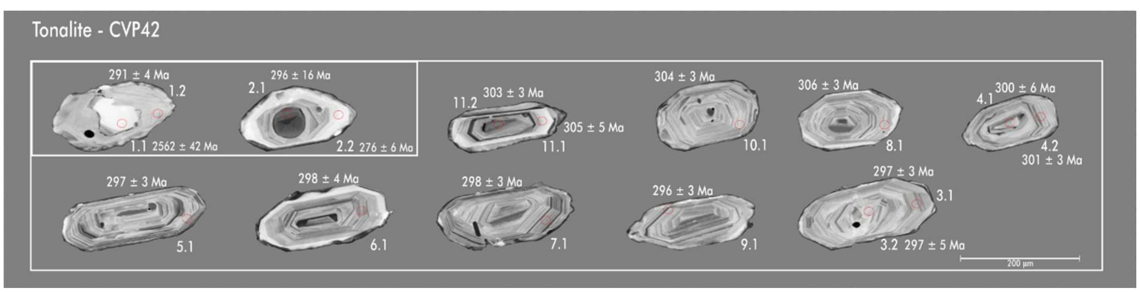

Figure 6.3 - CL images of the analysed zircons in the CVP42 tonalite. The red open dots represent the analysed spot and the $^{206}Pb/^{238}U$ ages obtained by SHIRIMP method.

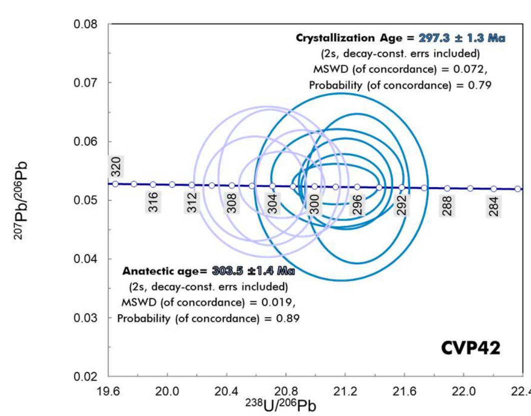

Figure 6.4 - U-Pb Tera-Wasserburg concordia for zircon grains in the CVP42 tonalite. Calculated with Isoplot v. 4.15 (Ludwing 2011).

Zircons from *CVP35* sample are small prisms with well-shaped bipyramidal terminations (Fig. 6.5). The CL images yield different sizes and internal textures compared with the other tonalites. The grain size range from 120 to 350 µm but three main clusters can be recognized: 120-150 µm (60%), 230-250 (20%) µm and 300-350 µm (20%). The oscillatory-zoned domains are darker, indicating U-enrichment. Large crystals (size > 200 µm) exhibit disturbed oscillatory zoning in the center, surrounded by U-rich portions and homogenous bright edges (Fig. 6.5). Banded zoning is also present in the smaller crystals. Twelve spots have been dated: 6 representing the oscillatory zoning (U = 114-1017 ppm, Th= 81 - 505 ppm, Th/U = 0.50 -1.20), one the inner banded zoning (U =211 ppm, Th= 282 ppm, Th/U = 1.33) and 5 CL homogenous bright edges (U = 79 - 705-79 ppm, Th = 39-141 ppm, Th/U = 0.14 -0.56). Unexpectedly, one grain with oscillatory zoning has provided a date corresponding to the magmatic age obtained from the previous sample (298.2 ± 2.8 Ma; spot 7.1), while the other crystals have the same radiogenic $^{206}Pb/^{238}U$ age within analytical uncertainty (MSWD = 0.15), giving a weighted mean age of 291.2 ± 1.3 Ma, referred to recrystallization processes (Fig. 6.6). Two analyses have been rejected because they gave dates younger than 280 Ma, interpreted as reflecting Pb loss. Analysis on the homogenous rims of three grains yielded older ages (356 ± 5 Ma, 341 ± 7 Ma, 333 ± 10 Ma) and narrow Th/U ratio (0.14-0.50), these are interpreted to be xenocrysts

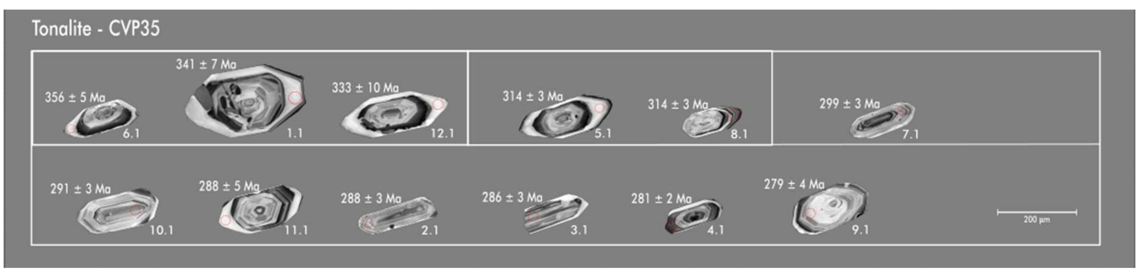

Figure 6.5 - CL images of the analysed zircons in the CVP35 tonalite. The red open dots represent the analysed spot and the $^{206}Pb/^{238}U$ ages obtained by SHIRIMP method.

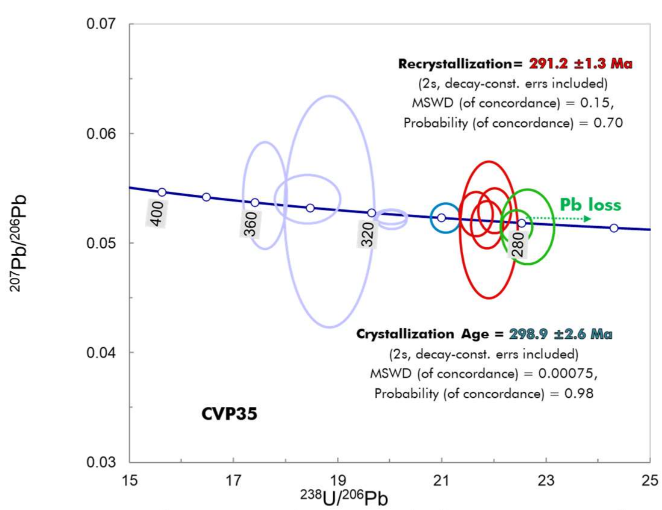

Figure6.6 - U-Pb Tera-Wasserburg concordia for zircon grains in the CVP35 Calculated with Isoplot v. 4.15 (Ludwing 2011).

The zircons picked up from sample *CVP39* mostly consist of subhedral small prismatic crystals (95-180 µm) with the sporadic occurrence of rounded pyramidal terminations. No possible inherited cores have been detected (Fig. 6.7). Large grains (250 – 310 µm) contain numerous inclusions, usually in correspondence of fractures. Fragmented zircons are present in both populations. Well-developed oscillatory zoning is shown in all CL images. Twelve spots were analysed for the U-Pb-Th in correspondence of magmatic zoning. The narrow Th/U ratios (0.34 -0.91) and U and Th contents (136-420 ppm and 49-384ppm, respectively), are consistent with precipitation of all zircons from a single magma. Six spots gave a magmatic emplacement age of 297 ± 1.1 Ma (Fig. 6.9), whereas a clusters at weighted U-Pb age of 284.7 ± 1.5 Ma, has been interpreted as Pb loss.

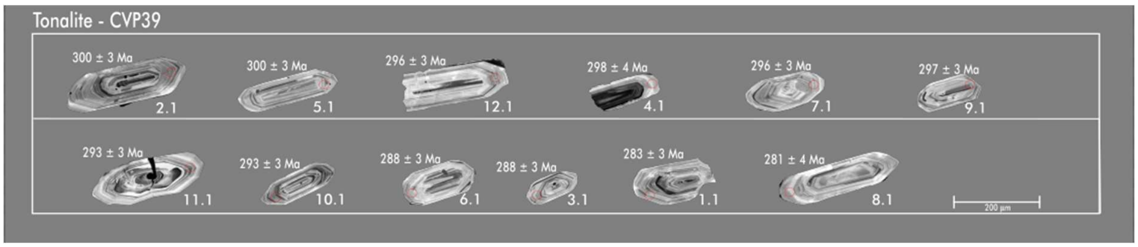

Figure 6.7 - CL images of the analysed zircons in the CVP39 tonalite. The red open dots represent the analysed spot and the $^{206}Pb/^{238}U$ ages obtained by SHIRIMP method.

Similarly to the previous samples, zircon from *CVP28* tonalite (Fig. 6.8) occurs as subhedral prisms with a well-defined tight concentric zoning, with occasional irregular growth patterns and rarely truncated by a late recrystallization (9.1). Of 14 dated spots, twelve have been located in the oscillatory-zoned portions (U = 120-426 ppm, Th =55- 362 ppm, Th/U = 0.40-0.72, except for spot 8.1 with a higher Th/U ratio of 1) and two in the centers (U = 114-448 ppm, Th =73-300 ppm, Th/U = 0.64-0.67). Even though rims and cores with apparent magmatic zoning have been analysed, ages obtained are different (Fig. 6.9). Three analyses (4.1, 5.2, 6.1) gave an age of 306 ± 2 Ma indicative of anatectic processes in the source before magma emplacement. $^{206}Pb/^{238}U$ dates from remain spots provided a weighted mean age of 298.1 ± 1 Ma, in accord with the previous sample's magmatic crystallization age (Fig. 6.9).

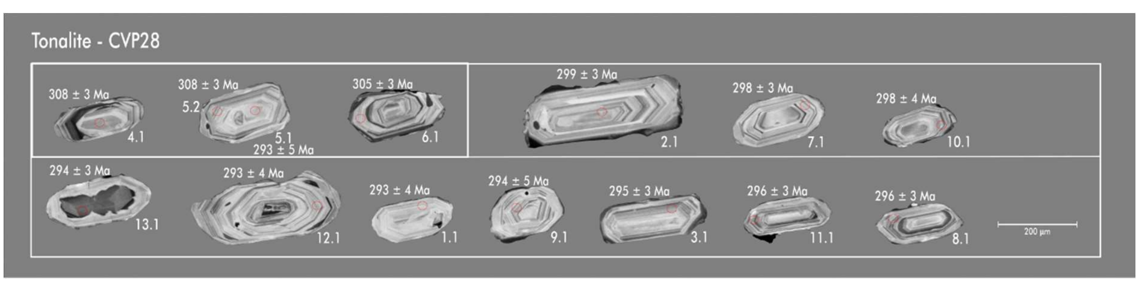

Figure6. 8 - CL images of the analysed zircons in CVP28 tonalites. The red open dots represent the analysed spot and the $^{206}Pb/^{238}U$ ages obtained by SHIRIMP method.

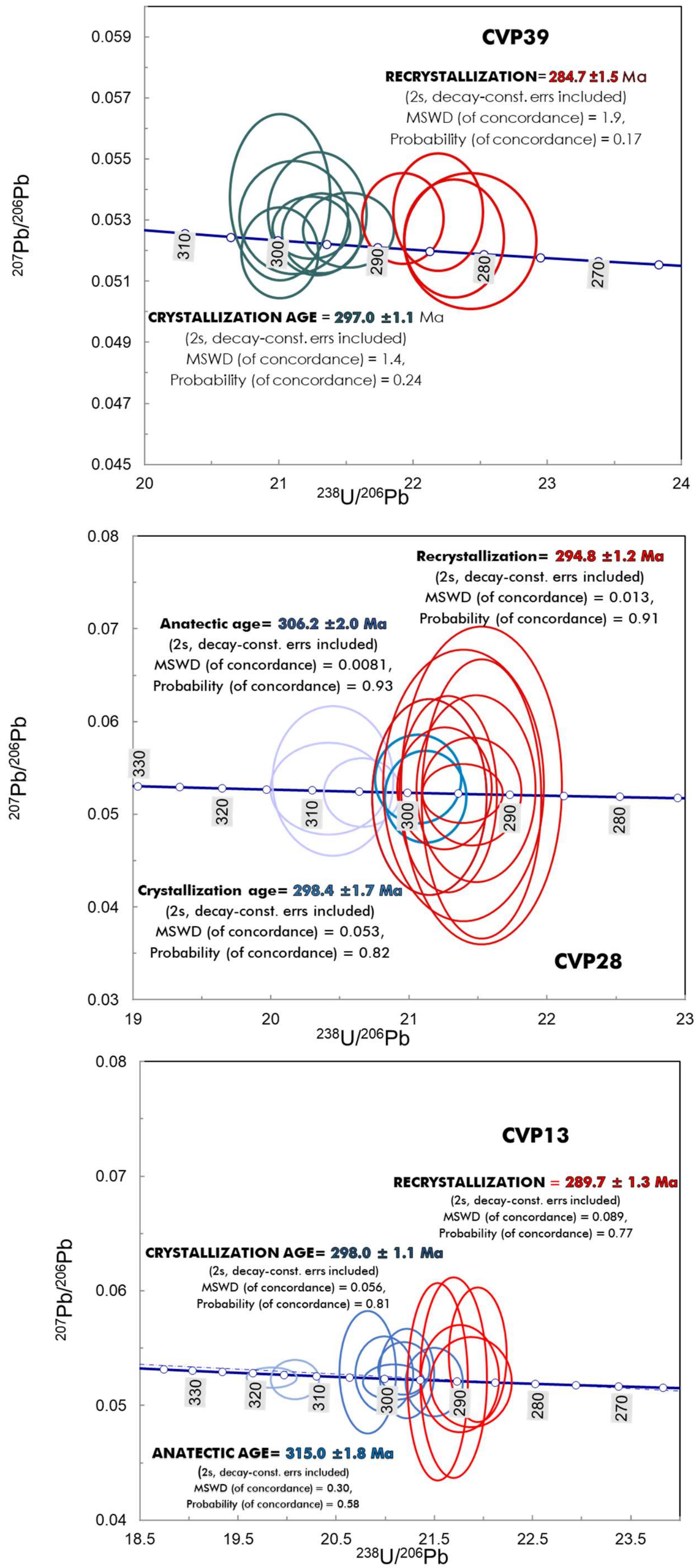

Figure 6.9 - U-Pb Tera-Wasserburg concordia for zircon grains in the tonalite (CVP39, CVP28 and CVP13). Calculated with Isoplot v. 4.15 (Ludwing 2011).

Zircon crystals extracted from sample *CVP13* are euhedral to subhedral with an elongated prismatic shape and bipyramidal terminations sometimes truncated or overgrown by bright rims (Fig. 6.10). Grain size range from 100 to 200 µm and from 250 to 320 µm. Crystals commonly exhibit oscillatory zoning with U-rich portions, as it is evident from dark color in the CL images, but some U-poor centers are present (<1%). On fourteen spots analysed, eight targed spots are located in the tight oscillatory zoned rim, one in the magmatic center, five in the CL bright rims or in the disturbed oscillatory zoning. Of the eight rims analysed from the oscillatory-zoned portions, six rims present a wide range in U (294-952 ppm) and Th (99-491 ppm), but relatively narrow Th/U ratios (0.15-0.49), while two rims show higher U (1043- 1188 ppm) and Th (423-451 ppm) contents with similar Th/U ratio (0.35-0.43). The only center analysed (14.1 spot) shows comparable U, Th and Th/U values (324 ppm, 225 ppm and 0.69), pointing to an origin of the crystals from a single parental magma. In contrast, the peripheral regions yielded lower values (U = 216-380 ppm, Th = 38-142 ppm, Th/U = 0.18 – 0.37) indicating zircon crystallization/recrystallization in a different chemical environment. The U-Pb systematics in accord with the Th and U contents and the other tonalite samples (Fig. 6.9) shows: an older age (315 ± 1.8 Ma) referred to anatectic process (U-Th rich edges), a middle-age (298 ± 1.1 Ma) representative of the magmatism event (relatively lower U-Th contents in the rim) and a youngerage (289.7 ± 1.3 Ma) indicated as recrystallization (U-rich rims).

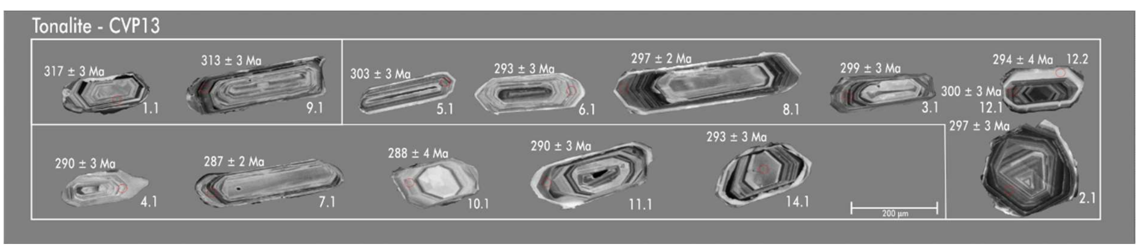

Figure 6.10 - CL images of the analysed zircons in CVP13 tonalites. The red open dots represent the analysed spot and the $^{206}Pb/^{238}U$ ages obtained by SHIRIMP method.

The last sample (*CVP3*) represents an evolved leucotonalite, containing euhedral prismatic grains with well-shaped bipyramidal terminations (Fig. 6.11). Three main populations have been clustered on the basis of the sizes: 100-180 µm, 270 -300 µm and rare 350 -360 µm. Most of the grains of small and medium sizes show prismatic shape with bypiramidal terminations and irregular oscillatory zoning from the inner to the outer parts and rare banded zoning. The magmatic oscillatory

ANATECTIC

zoning is well-developed in the large crystals (Fig. 6.11). CL images reveal irregular cores, rounded or with irregular oscillatory zoning. It was impossible to date these crystals for their high U-contents. Nine analyses of the igneous oscillatory zoned zircon in the outer portions revealed narrow U (88-349ppm), Th (57-311ppm) contents and Th/U range [0.30-0.77 except for spots 3.1 (0.95)] indicating once again direct precipitation from a single magma. One spot was located in the banded zoned, presenting similar U and Th contents (136 and 177 ppm, respectively) and high Th/U ratio (1.21). All the analyses plot in a single cluster, giving a weighted age of 296.8 ± 1 Ma (MSDW=0.17; Fig. 6.9).

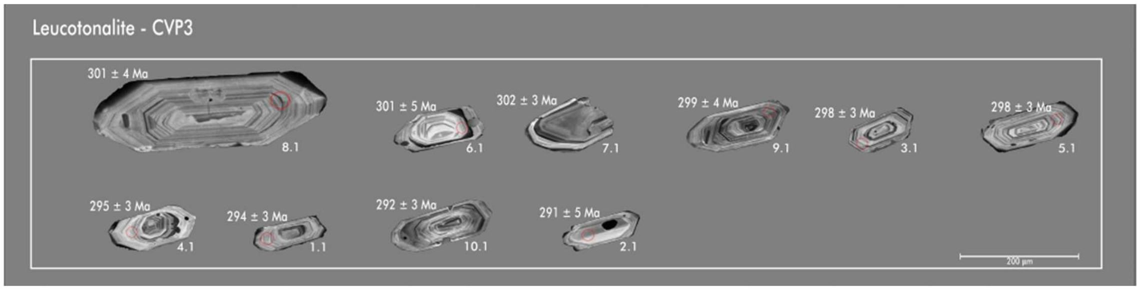

Figure 6.11 - CL images of the analysed zircons in CVP3 tonalites. The red open dots represent the analysed spot and the $^{206}Pb/^{238}U$ ages obtained by SHIRIMP method.

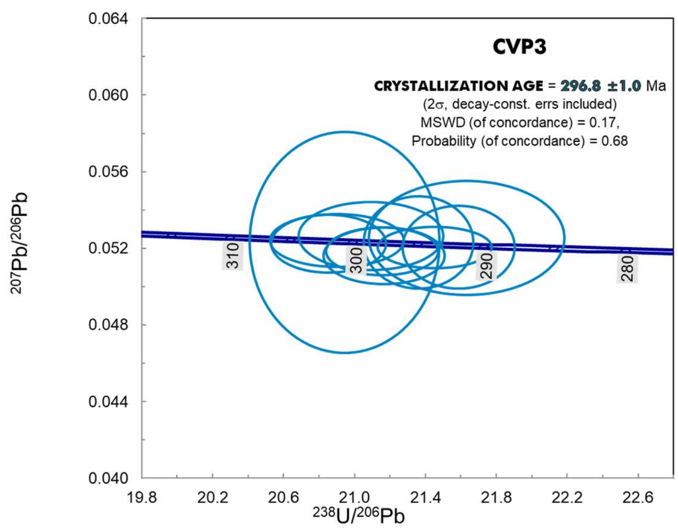

Figure 6.12 - U-Pb Tera-Wasserburg concordia for zircon grains in the leucotonalite (CVP3). Calculated with Isoplot v. 4.15 (Ludwing 2011).

6.2.3 Mafic microgranular enclaves

Two predominant zircon typologies wereextracted from sample CVP25E (Fig. 7.13). The first one includes subhedral fragmented grains (90%), variable in size (50-250 µm), with CL homegenous dark color (U-rich) or banded zoning (Fig. 6.13). The second group (10%) is represented by few prismatic grains sometimes fragmented, with rounded bipyramidal terminations and tight oscillatory zoning (Fig. 6.13). Sixteen spots have been analysed: nine spots in edge with marked oscillatory zoning, five darker portion and two centers (one brighter and one with banded zoning). Zircon with oscillatory zoning has narrow trace elements contents (U = 148-304 ppm, Th = 79-300 ppm, Th/U= 0.54-0.99) with the spot 1.1 showing U=636 ppm, Th=294 and Th/U ratio = 0.46; dark homogenous crystals have a wide range in U (194-676 ppm) and Th (227-995 ppm) with a narrow Th/U ratio (1.06 – 1.47). Conversely, the two analyzed centers have similar U and Th contents (203-225 ppm and 188-204ppm, respectively) and Th/U ratio (0.91-0.93). Obtained ages for this sample can be grouped in three main clusters as in the quartz-dioritic/tonalitic host (Fig. 6.14): a weighted age of 302 ± 1.6 Ma recording *anatectic processes (*corresponding with the Th/U richer crystals*)*; an *emplacement age* of 295 ± 1.2 Ma (grains with lower Th and U contents) and a *recrystallization age of* 286.8 ± 2 Ma (homogenous Th and U contents). The MME emplacement and recrystallization ages are relatively younger respect to quartz-diorite and tonalite, suggesting a late intrusion into the host.

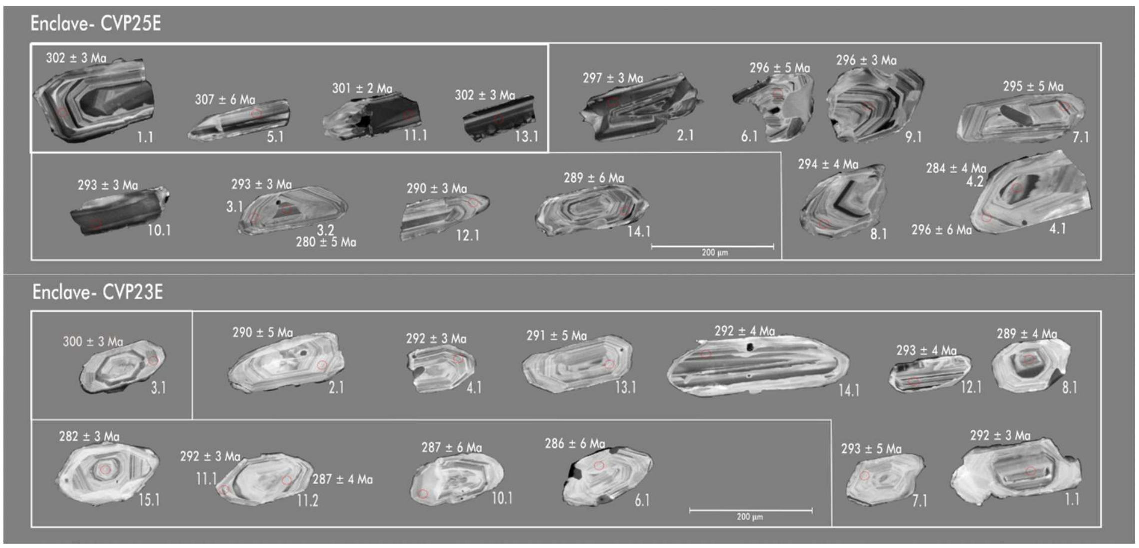

Figure 6.13 - CL images of the analysed zircons in mafic microgranular enclaves (CVP23E and CVP25E). The red open dots represent the analysed spot and the $^{206}Pb/^{238}U$ ages obtained by SHIRIMP method.

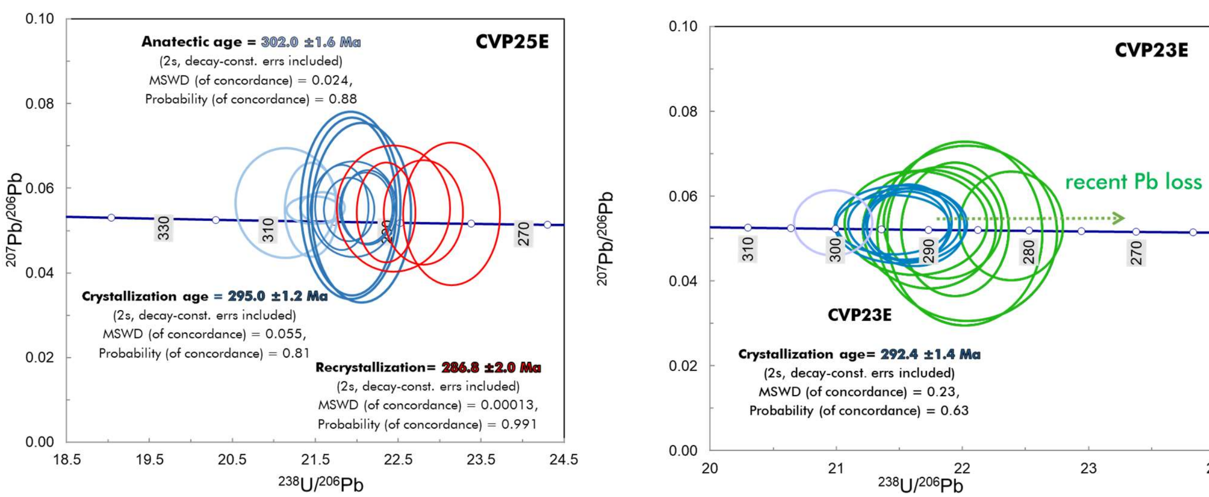

Figure 6.14 - U-Pb Tera-Wasserburg concordia for zircon grains in the MME (CVP23E and CVP25E). Calculated with Isoplot v. 4.15 (Ludwing 2011).

Zircons from the second enclave (*CVP23E*) show a subhedral shape with fine concentric zoning, sometimes masked by a white homogenous recrystallization (Fig. 6.13). Zircon crystals appear similar to quartz-dioritic and tonalitic crystals. Larger crystals (250-300 µm) are prismatic with tight oscillatory zoning and U-poor edges. The smaller grains (120-170 µm) are elongated or prismatic, showing irregular oscillatory zoning and rare banded zoning and homogenous dark portions. The spots locations were planned as follows: 7 oscillatory zoning in the edges, three irregular oscillatory zoning and four centers with CL white appearance. Of all spots analysed, the oscillatory zoning having U = 156-278 ppm, Th =73-294 ppm contents and Th/U = 0.43-0.89 ratios. Only four centers have been dated, giving a narrow composition (U = 135-191, Th = 90-151 and Th/U = 0.66 – 0.78), such as the irregular oscillatory zoning (U =119- 233 ppm, Th = 52-162 ppm, Th/U = 0.42-0.69). Omitting some analyses considered Pb loss, two concordia ages have been obtained (Fig. 7.14): a *crystallization age* (292.4 ± 1.4 Ma) and an *anatectic age* (300.2 ± 1 Ma).

6.3 Hf results

The Hf analyses were performed on all the previous samples and one additional tonalitic rock (CVP33). The Lu-Hf investigation has been conducted in a total of 133 spots, close to or in the same spots used to obtain the $^{238}U/^{206}Pb$ ages. Precedence has been given to the measurements considered as reflecting magmatic crystallization, but some spots referred to anatectic and recrystallization

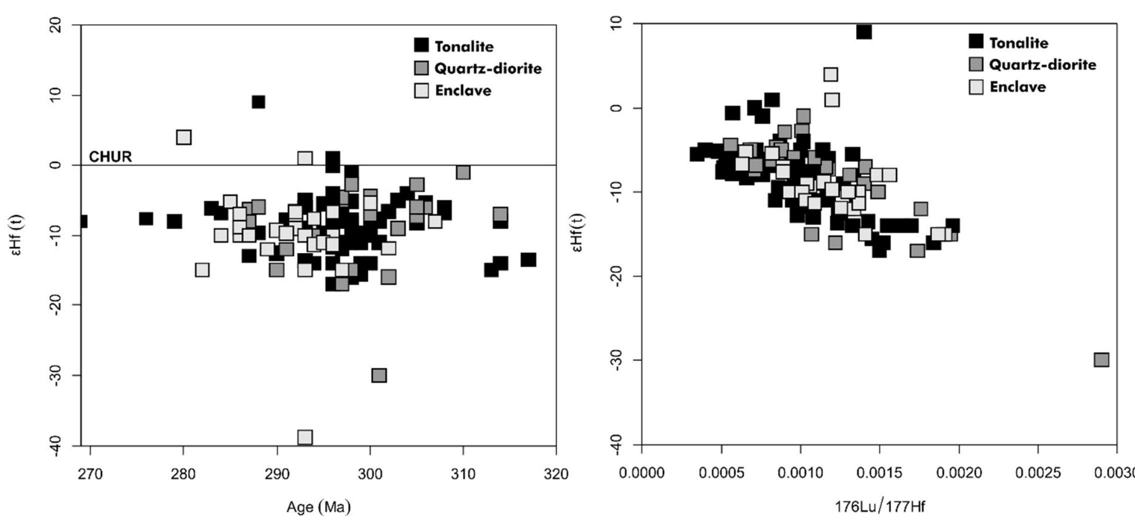

Figure6.14 - εHf vs $^{238}U/^{206}Pb$ ages (left diagram) and εHf vs $^{176}Lu/^{177}Hf$ (right diagram) for the CVP rocks.

events have also been analysed.

On the whole, widespread εHf values characterize CVP lithotypes, with a similar range, for the magmatic zircon in three rock types from -2.7 to -17, +1 to -16, -6 to -15 for the quartz diorites, tonalites and MME, respectively (Fig. 6.14). Few spots show radiogenic values close to or above the CHUR, whereas εHf negative values dominate, suggesting a significant contribution of an old continental crust. Low $^{176}Lu/^{177}Hf$ (0.0001-0.0020; Fig. 6.14) and $^{176}Hf/^{177}Hf$ ratios (0.28116-0.28246) together with Hf T_{DM} model ages from 2230 to 1178 Ma are also indicative of homogenous crustal sources. Zircon $^{176}Hf/^{177}Hf$ ratios vs. magmatic crystallization ages is used to understand if crustal

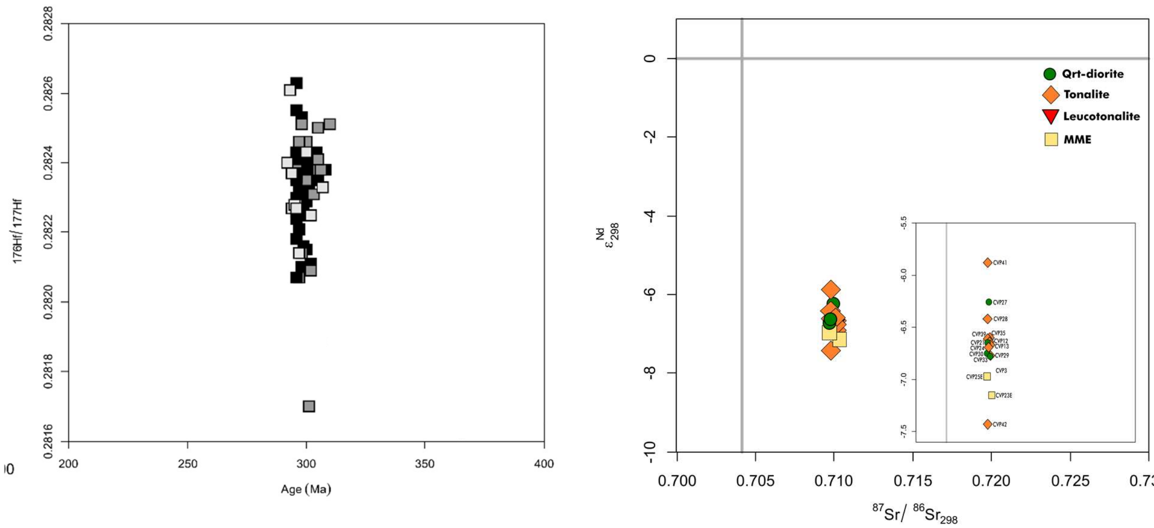

Figure 0.15 - $^{176}Hf/^{177}Hf$ vs U-Pb age. Left diagram: $^{176}Hf/^{177}Hf$ values for magmatic zircon; Right: εNd vs $^{87}Sr/^{86}Sr_{298}$ trend.

reworking occurred (e.g., Spencer *et al., in press*). Fig. 6.15 shows as $^{176}Hf/^{177}Hf$ ratios vs. U-Pb ages for the magmatic crystallization age revealed a vertical array. The similar whole-rock Nd isotopic trend in Sr_i and εNd diagrams (Fig. 6.15) constraints the plausible hypothesis of the recycling of a continental crust.

Specifically, quartz-diorites have εHf ratio ranging from -17 to -1, except for one highly negative value (-30) in the CVP27 sample (Fig. 6.16; Appendix.Table 9). The Hf T_{DM} model age span in

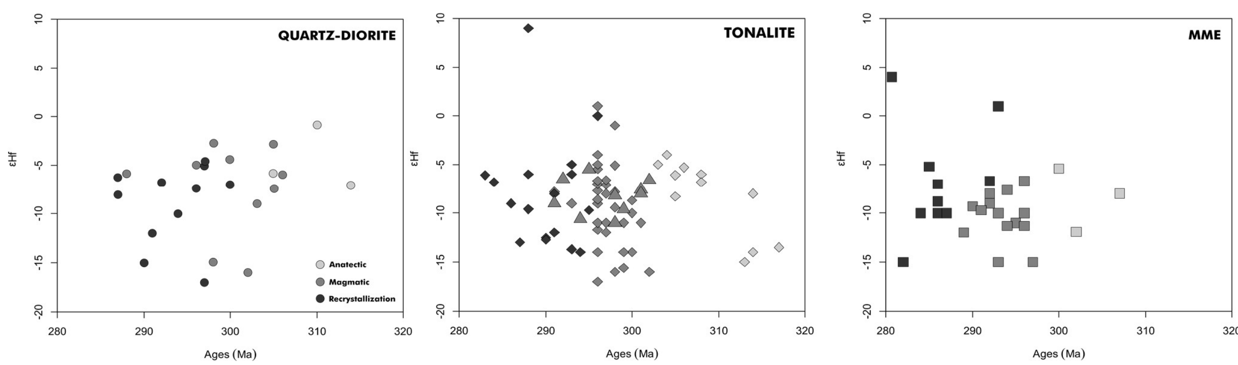

Figure6.16 - εHf versus anatactic, magmatic and recrystallization ages for quartz-diorites, tonalite and mafic microgranular enclaves.

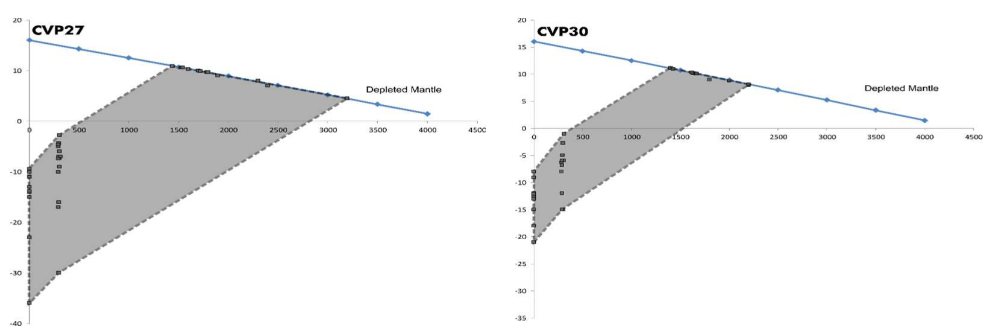

Figure6.17 - εHf versus ages (Ma) with reported T_{DM} ages for the zircons analysed in the CVP quartz-

a broad range from 1.4 Ga to 2.4 Ga, reaching 3.0 Ga for the spot with the lowest εHf value obtained (Figs. 6.17). Nd T_{DM} model age shows a close-range (1.5 and 2.0 Ga) than Hf T_{DM} values (Fig. 6.18).

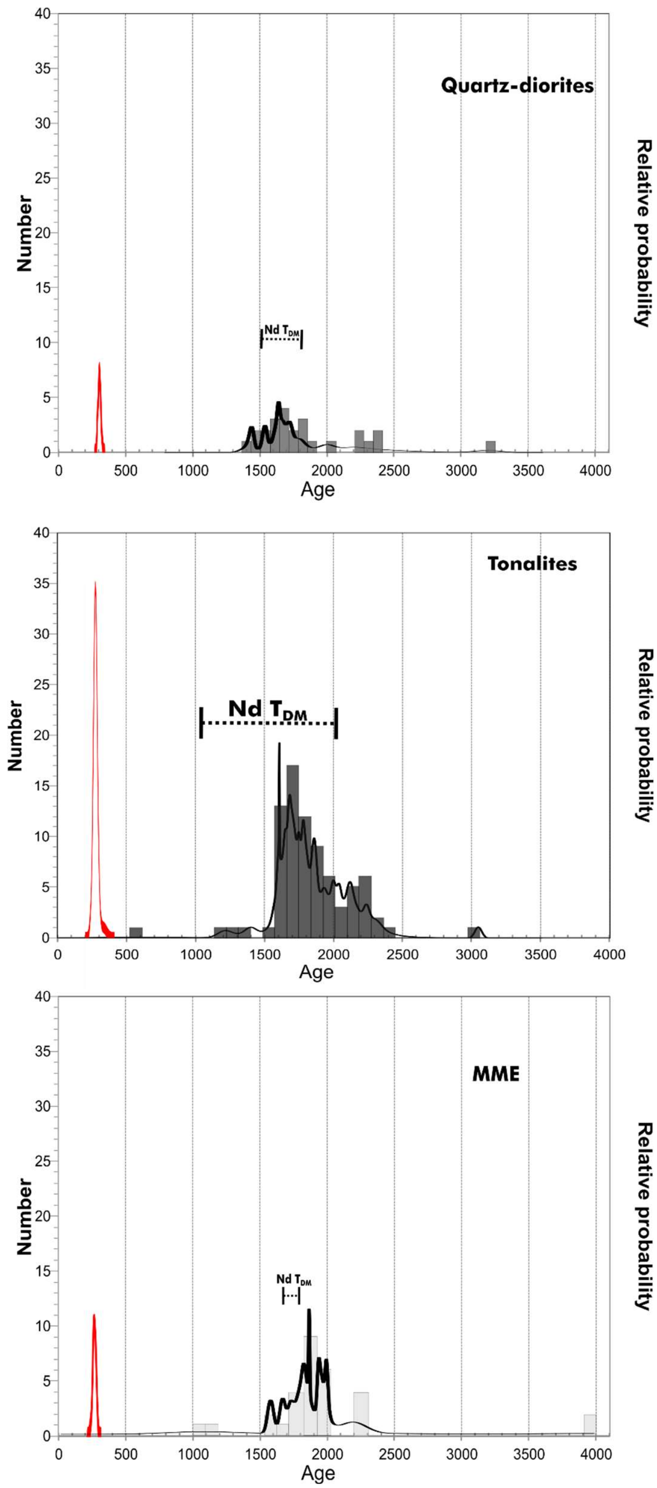

Figure6.18 - Relative distribution of the Hf T_{DM} model ages in the zircons with the associated Nd T_{DM} whole-rock age. Red trends indicate the U-Pb age in all CVP lithotypes; the black trend is the cumulative gaussian curve for an assemblage of data and relative errors (calculated with Isoplot v. 4.15, Ludwing 2011).

The result complies with Hueck *et al.* (2020), suggesting that Sm and Nd systematics, giving a mean value of whole-rock, aren't as effective at identifying potentially different melt sources when compared with the Lu-Hf systematics in the zircon.

In the tonalites, the Hf results indicate more variability in each sample (Appendix.Table 9). Overall, the εHf value varies from -16 to +9 (Fig. 6.16). Three positive values (0 and +1 for a magmatic age about 296 and +9 for a recrystallization age c. 288 Ma), representing a potential contribution of juvenile magma, have been exclusively detected in one tonalite sample . In contrast to negative values with a T_{DM} model age ranging from 1530 to 2300 Ma for the magmatic zircon (Fig. 6.19), the Hf model age of the radiogenic component is younger (c. 600 and 1200 Ma) If we exclude mantle input, in agreement with several studies (Patchett *et al.* (1981), Smith *et al.,* 1987; Corfu and Stott, 1993, Pain *et al.*, 2016), the slightly positive values can be explained as crustal contamination by juvenile input or as the presence of zircon xenocrysts (Bhattacharya *et al.,* 2015). The unique inherited zircon crystal found in CVP42 tonalite (Fig. 6.3; c. 2500 Ma) registers εHf close to CHUR value (-0.6) and has a Hf T_{DM} model age of about 3.0 Ga. As the quartz-diorite, Nd model ages (1.5 - 1.8 Ga) for the tonalite designate younger ages compared with the Hf model age (600-3040 Ma; Fig. 6.18).

Finally, εHf values obtained for the MME do not differ significantly (Figs 6.16). The strong affinity with tonalites and quartz-diorites is well represented by the similar εHf values as well as by the Hf T_{DM} model ages for the magmatic ages (1.8 to 2.2 Ga) (Fig 6.20). In the same way, the slightly more radiogenic values (+1 and +4) exhibit different ages as the tonalite (c. 293 and 280 Ma, respectively). εNd and εHf T_{DM} model age comparison (Fig. 6.18) indicates again the robustness of the zircon (1.6 -1.7 and 1.0-2.2 Ga, respectively).

The εHf and the T_{DM} model age corroborate heterogenous old crust as the source of studied granitoids. Similar observations can also indicate for MME. In fact, a wide variation in εHf in a single magmatic suite is an inherited feature of the heterogeneity of the magma sources (e.g., Smith *et al., 1987).*

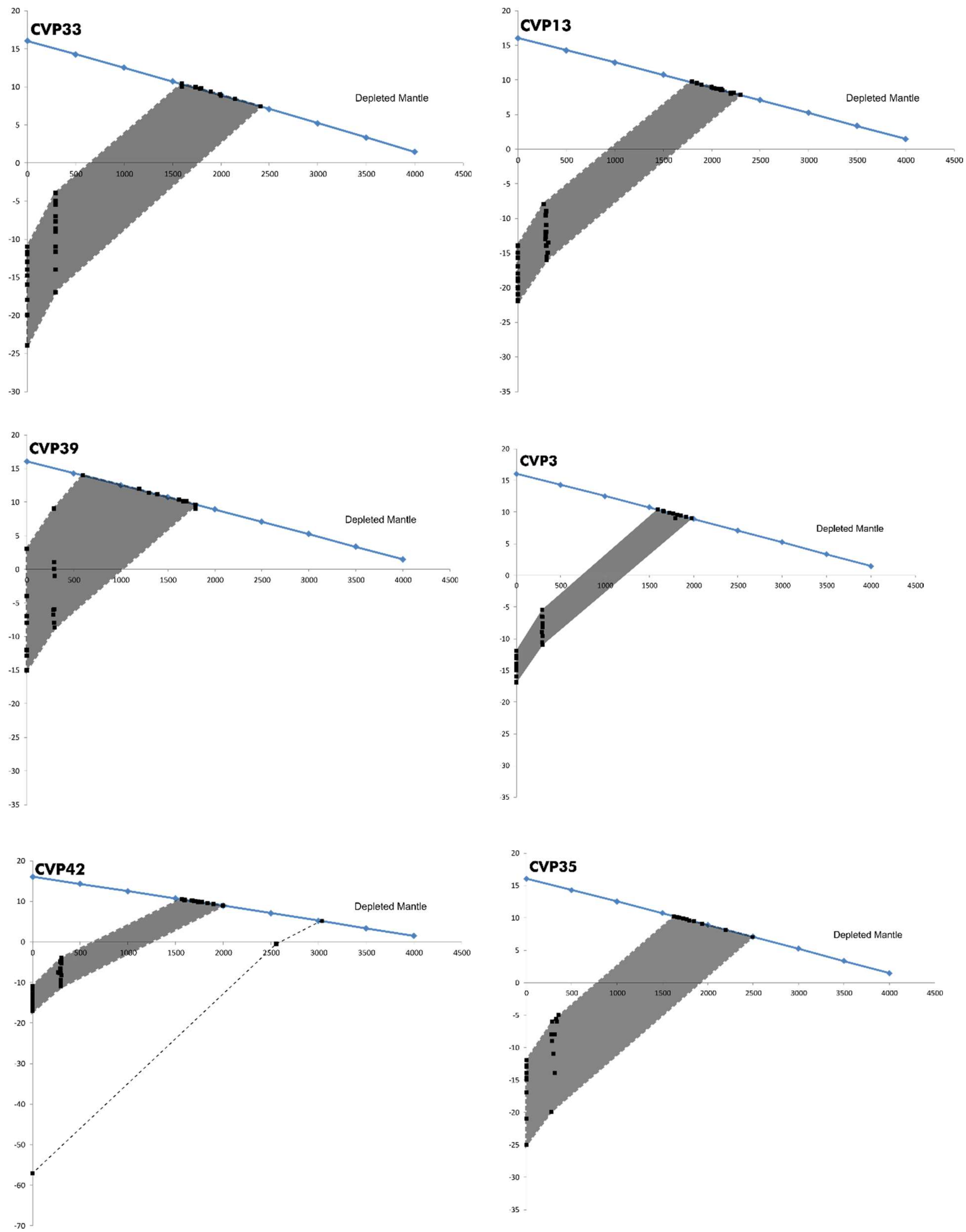

Figure 6.19 - εHf versus ages (Ma) with reported T_{DM} ages for the zircons analysed in the CVP tonalites.

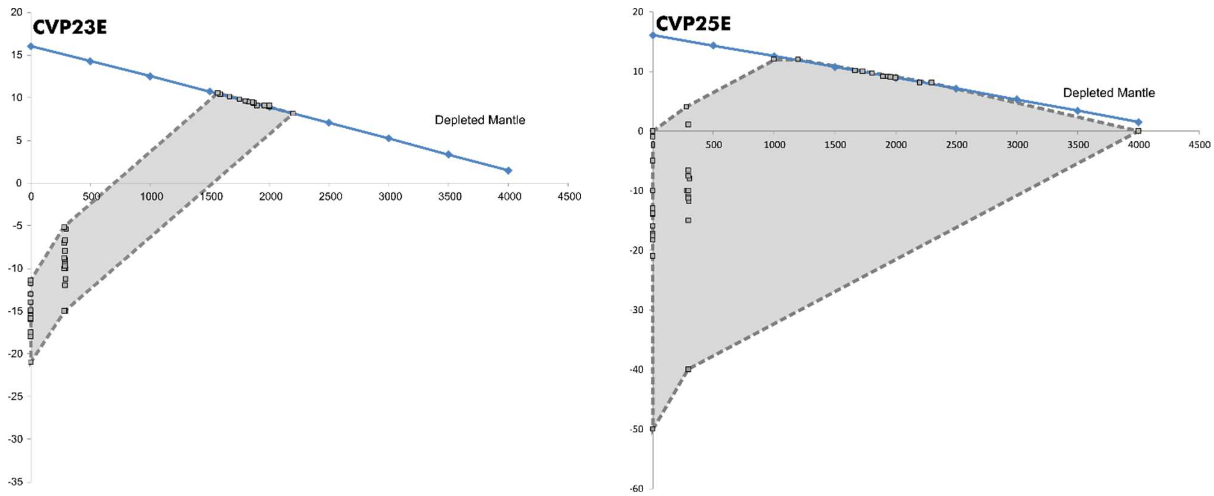

Figure 6.10 - εHf versus ages (Ma) with reported T_{DM} ages for the zircons analysed in the CVP MME.

6.4 Th/U ratio vs. Lu/Hf systems: crustal growth versus source information

The aptitude of zircon to incorporate in the crystal lattice different concentration of the elements during melting or crustal genesis together with the extraordinary resistance to survive in many petrogenetic processes allow registering important information during geological earth time. If Th and U concentrations particularly permit to reconstruct crustal growth (Scherer *et al.,* 2007), Lu-Hf accommodation imparts informationabout protolith age, juvenile mantle addition, crustal reworking or mixing of both (Payne et al., 2016).

Th/U ratio and εHf ratio have been compared using a $^{206}Pb/^{238}U$ age to evaluate the role of both components in the CVP evolution. Moreover, the CL zircon textural features and spot locations were chosen as a further discriminant. If the partial melting process of a homogenous source has been confirmed by εNd (Fig. 5.8), the variability of the source is strengthened by Th/U and εHf ratios (Fig. 6.21). The wide Th/U range (0.4 -1.5) corresponds with the magmatic oscillatory zoning and with minor homogenous dark portions and banded zoning. A similar trend is observed for the εHf, ranging from +1 to -15. The high Th/U and εHf variability registered during magma crystallization can be referred to a combination of partial melting of heterogeneous crustal sources.

The older ages, tentatively defined as *"anatectic",* show dispersed Th/U ratio with a consistent cluster at 0.6 and narrow εHf range (-2 to -8; Fig. 6.21). The tight data suggest an evolution in a closed system.

Furthermore, similar values have been observed in metamorphic xenocrysts. U-Pb ages obtained here, have also been reported by Fornelli et al. (2011) for the Variscan metamorphism of the Serre lower crust in the range 357-340 Ma and 323-318 Ma (crustal thickening and peak metamorphism, respectively). The older anatectic U-Pb age recorded in this study was about 315 Ma.

Fiannacca *et al.* (2017) reported a c. 305 Ma anatectic age of two-mica monzogranites and porphyritic granodiorite of the adjacent Serre Batholith. The Th/U and εHf analogies do not permit to discriminate between the two events clearly.

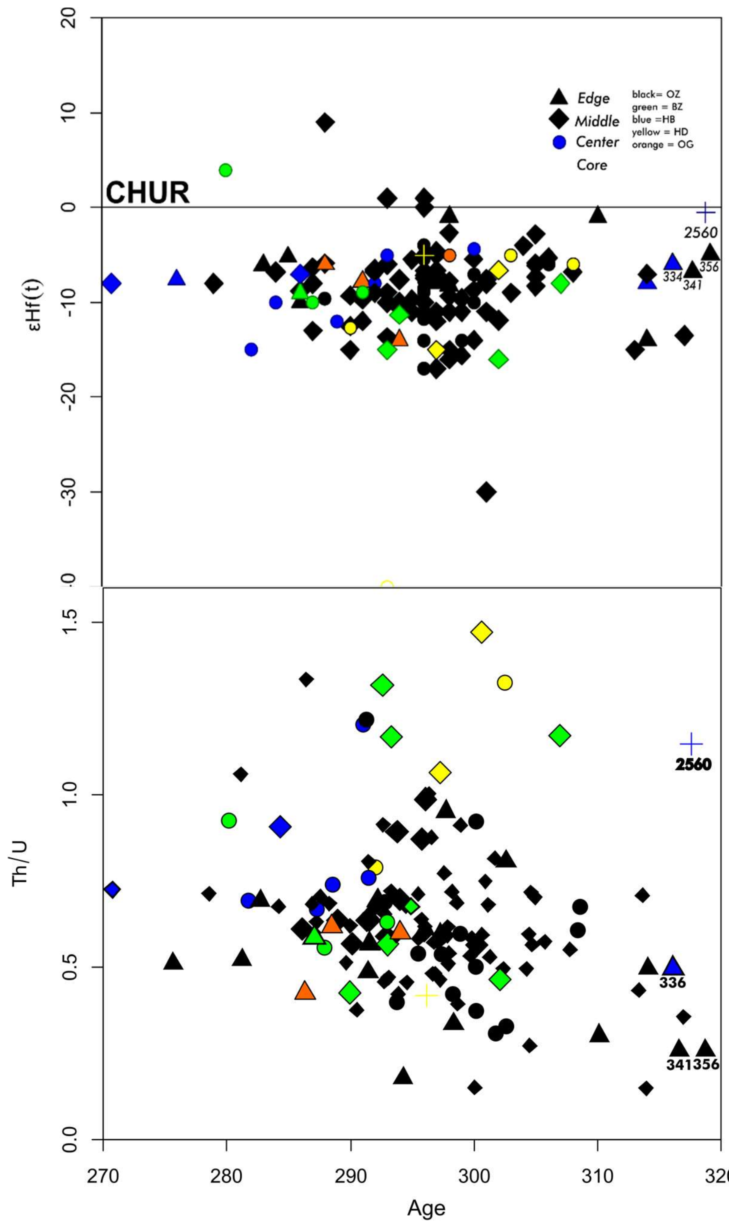

Figure 6.21 - εHf and Th/U vs. U-Pb age. OZ= oscillatory zoning; BZ = banded zoning; HB=homogenous bright; HD = homogenous dark; OG= recrystallization. See text for explanation.

Late crystallization ages highlight a relatively homogenous range in Th/U ratio and εHf. The greatest part of the analysed spots was located in oscillatory zoning and minor in CL homogeneous bright edges. Thick to wide bright rims are common in CVP lithotypes, but sometimes observed in the center or completely covering the crystals. The same CL texture has been reported from Zeck &

Whitehouse (2002; introducing the terms "white pest") and Peressini *et al.* (2007). In accord with the latter authors, the recrystallization occurred in the presence of high-T deformation and interstitial fluid during the late stage of magmatic growth. The Th/U ratio and εHf approximately constant and close to the magmatic event are caused by slow recrystallization. The apparently magmatic zoning is undermined by the late process, recording the younger ages.

Finally, Th/U and εHf ratios are well-correlated with the zircon-textural features showing a good relationship with the U-Pb age (anatectic, crystallization and recrystallization). The two parameters indicate a strong variability of the magmatic zircon derived by the partial melting of an old heterogeneous continental crust with the undefined minor juvenile contribution.

6.5 Registered processes in the magma chamber

The magmatic age of the CVP quartz-diorites and tonalites is homogenous (296 ± 1 Ma), whereas one tonalite indicates a relatively older age (302.7 ± 1 Ma; CVP27 sample). SHRIMP U-Pb data for the CVP agree with the emplacement age of 297.3 ± 3.1 Ma obtained by Fiannacca *et al.* (2017) for a quartz-diorite from the adjacent Serre Massif using the same method. The older ages of c. 302 Ma can be considered close to a 306 Ma age obtained by Langone *et al.* (2014), dating a tonalite of Serre Massif. A narrow Th/U range (0.30 – 0.81) and the almost exclusively negative εHf indicates, as discussed above, the participation of an old heterogeneous crustal source. The data align with the Th/U ratio (0.45-0.81) and $\delta^{18}O$ (7.3–8.3‰) describe by Fiannacca *et al.* (2017) for the Serre Massif quartz-diorite. The slightly positive εHf values (0 and +1) refer to two tight oscillatory zoned rims, with an assigned crystallization date of 296 ± 3 Ma for both and similar U/Th ratios (0.58-0.59), deriving from a tonalite sample (CVP39). These features would suggest a minor contribution of juvenile magma.

MME's crystallization age is younger than the age of the quartz-dioritic and tonalitic host (295 ± 1.2 Ma and 292 ± 1.4 Ma, respectively), in accord with the intrusion of the more mafic magmas into the crystallizing granitoid. Although an enrichment in Th is generally indicative of a mafic input, the unradiogenic Hf isotopic signature, similar to quartz-diorite and tonalite, is in agreement with the field, petrography, geochemical and whole-rock features. In fact, the sporadic presence of sharp contacts and mineral transfer from the host into the enclave are indicative of high magmatic temperature that had permitted the partial digestion of MME inside the granitoids. Besides, as discussed in the petrogenesis chapter, similar mineralogy and Sr_i values and the less unradiogenic εNd values reveal the co-genetic affinity. In the more mafic enclave (CVP25E), two radiogenic Hf values (+4 and +1) have been observed in a unique zircon crystal with a magmatic age and late recrystallization age, respectively. The late emplacement of MME could be concerned with the emplacement of the two-mica granodiorites (BAG) in the adjacent Serre Massif. The BAG represents the uppermost intrusion and the final stage of batholith construction. An age of 295 ± 1.4 (Langone *et al.,* 2014) and 292.2 ± 2.6 Ma (Fiannacca *et al.,* 2017) was reported for BAG, that is the crystallization age obtained for the CVP MME. Langone *et al.* (2014), dating the top (BAG) and bottom (tonalite) of the Serre Massif obtained two clusters of age. A dominant age of about 306 Ma for the tonalite and the minor of 295 Ma interpreted as disturbance of the isotopic systems by a successive magma pulse. The granodiorite recorded a dominate age of 295 Ma (emplacement age) and a minor cluster of 306 Ma age interpreted as zircon incorporation from tonalite.

Recrystallization is widely present in all lithologies studied. This process did not affect exclusively zircon edges but all the crystal portions, particularly the centers.

Zircon rims from three grains yielded significantly older ages. These correlated to Variscan orogenesis, with U-Pb zircon dates of c. 356, 341,334, Ma, have been observed exclusively in the tonalite CVP35 sample. The zircon crystals are like the zircon founded in the lower crustal mafic granulites exposed in the adjacent Serre Massif (Fornelli *et al.,* 2011). Crustal thickening was dated to happen between 347-340 Ma, whereas the ages comprised between 323 and 318 Ma were considered as indicative of metamorphic peak (Fornelli *et al.,* 2011). At the same time (347-325 Ma), crustal melting started in the whole CPO (Fornelli et al., 2002, 2011; Appel et al., 2011). The late-Varsiscan multistage decompression had involved the partial melting of the mafic and felsic granulites followed by magma ascent and emplacement at different crustal depths.

6.6 Crustal reworking

As mentioned in the previous chapters, a predominantly crustal signature is indicated by many features such as whole-rock geochemistry, Sr and Nd isotopes, modelling and lastly by Lu-Hf isotopes in zircon. In fact, the three main dated events, the negative Hf signature and the HfT_{DM} model ages, strongly support a crustal reworking. The paucity of metamorphic crystals and inherited cores indicate as high-temperature has affected in the lower crust, reabsorbing the zircon of the source and producing new generation crystals. The data confirm Zr saturation modeling, calculated taking into account the bulk composition, with tonalitic magma reaching the highest temperature (about 800°C), unsaturated-zircon magma and consequently fractionation (F=25%).

Contemplating the crustal origin, it is necessary to think about the probable source. No Hf data have been obtained in the literature regarding the Serre lower crust, but Nd and Sr isotopes, partial melting modeling and experimental data confirm amphibolite as the source. How, in this point of view, can explain the radiogenic Hf values? There are two potential ways: the first one is a marginal contribution of the mantle; the second one is exclusively the melting of a hydrous and heterogenous lower crust with no mantle input. If the mantle played a minor role, its signature could have been masked by the continuous melting of the mafic crust and successive assimilation of metasediments.

The progressive magma homogenization can produce a more consistent unradiogenic signature (Payne *et al.,* 2016). It is well known that the breakdown of biotite and amphibole generate melt in the crust. High degrees of partial melting leave behind a nearly anhydrous rock, such as the felsic and mafic granulites preserved in Serre lower crust, giving direct evidence of intense melting processes with progressive melt extraction and emplacement of different magma pulses. The heat necessary to melt mafic crust was likely furnished by asthenosphere upwelling and crustal thinning without any volatile fertilization in the lower crust, as suggested by Annen *et al.* (2006) in a deep crustal hot zone. Melting of the heterogeneous crust could have given the broader isotopic εHf values preserving a slightly mafic evolution. As reported by Fiannacca *et al.* (2015), the vertical spread in εNd reflects heterogeneous sources, deriving from the combination of mature sedimentary components and recent igneous rock and sediments derived from the rapid erosion.

6.7Summary

The U-Pb ages had permitted to distinguish three main events in all quartz-dioritic and tonalitic rocks: a probable *anatectic* age (c. 308 ± 2 Ma), a *crystallization* age of about 298 ± 1.5 Ma and recrystallization process at around 290 ± 1.5 Ma for quartz-dioritic and tonalitic magmas in the Capo Vaticano Promontory. The U-Pb ages are well-correlated with the U/Th contents, textural features and εHf.

εHf results present a wide range during the magmatic events, but predominant negative values agree with the εNd, indicating an old continental crust as the source. The slightly positive values can be related to a limited juvenile contribution but still remain to evaluate the mantle role in the batholith construction or as a result of direct transfer of Hf isotope budget from inherited (xenocryst) zircon (Dahlquist *et al.* 2020). In general, the positive values could reflect a metabasic source less contaminated, whereas more negative can represent a contaminated metaigneous or vulcanites sequence or hybrid sources. Also, a mantle magma as a heat source is extensively accepted, producing a large volume of magma able to leave the source and arise to the emplacement location (Fiannacca *et al.,* 2017).

Three main processes characterize mafic microgranular enclaves as the hosts: *anatectic* (302 ± 1.6 Ma), *crystallization* (293.7 ± 1 Ma) and *recrystallization* (286.8 ± 2 Ma) ages. The mafic inputs have been emplacement later in the quartz-dioritic and tonalitic semi-solid framework, but still hot. Partial digestion and contamination of the MME from the quartz-dioritic and tonalitic magmas are well-documented in the field observations. However, they maintain the original crustal imprinting, as highlighted by εHf and εNd. The emplacement age has suggested an affinity with the two-mica granodiorite (BAG) of the nearby Serre batholith with whom they also share similar mineralogy. In addition, MMEs are widely present in the BAG.

7. Granitoid genesis and evolution in Capo Vaticano Promontory

7.1 A co-genetic origin for the CVP granitoids?

The data and observations presented above indicate that all of the studied phases can be considered to have formed as part of a single, evolving system. The petrographic study has highlighted a mineralogical sequence passing from quartz-diorites through tonalites and to leucotonalite. Amph / Pl → Bt and Ep → (Ms) → (K-feld) → Qtz is the crystallization sequence (minerals in brackets are found in the evolved lithotypes). Amphibole occurs in quartz-diorite and tonalite, whereas it is absent in the evolvedlithotypes. The averaged Mg/Fe Kd ($[X_{Mg}/X_{Fe}]_{Bt}/[X_{Mg}/X_{Fe}]_{Hbl}$) between amphibole and biotite ranges from 0.97 and 1.07 in the quartz-diorite and tonalite, respectively. The occurrence of skeletal amphibole associate with biotite clots and thedistribution coefficient values close to unity suggested a late appearance of the biotite as replacement product of amphibole (Hbl + liq → Bt) during the liquid magmatic evolution (Speer et al., 1987; Christofides et al., 2007). It is also highlighted by occasionally biotite-mantled amphibole.

Variation diagrams in major and trace elements show collinear trends (Figs. 5.1 – 5.5) for quartz-diorites, tonalite and leucotonalite. Negative trends in Al_2O_3, TiO_2, CaO, FeO_{tot}, MgO, MnO, P_2O_5, V, Ba, Eu and Sr (Figs. 5.4 - 5.5) are consistent with fractionation of plagioclase, amphibole, biotite and apatite. K_2O, Rb, Th, Ce, Zr and Hf (Figs. 5.4 - 5.5) exhibit a positive correlation with an inflection before the compositional gap (SiO_2 = 64 – 67%) and negative trends for two tonalites and the leuco-tonalites, in according to late crystallization of biotite, zircon and epidote. Y defines two different populations: Y-rich and Y-poor, considered to relate to as amphibole abundances. Strong to weak LREE-HREE fractionation is highlighted moving from the less differentiated quartz-diorites to more evolved leucotonalite reforcing the cogenetic affinity. The initial $^{87}Sr/^{86}Sr$ ratio and negative εNd isotope values support a derivation from an old continental crustal. The tight overlap with the restitic mafic granulite of the Serre lower crust strongly confirms the crustal signature. Despite lead and hafnium isotopes permits to extrapolate similar conclusions, they indicate the involvement of more heterogeneous crustal material compared to Sr and Nd isotope ratios.

Finally, the U-Pb SHRIMP ages have indicated a contemporaneous emplacement age (from 302 ± 1 Ma to 297 ± 2 Ma) and the superimposition of multiple processes (an older anatectic age and a younger recrystallization age) for all granitoids, indicating a contemporaneous origin.Collectively, all of these characteristics are consistent with a co-genetic relationship between quartz-diorites, tonalites and leucotonalite.

Mafic microgranular enclaves are quartz-dioritic and tonalitic in composition with main (oligoclasic-labradoritic plagioclase, Mg-hornblende/Fe-Tschermakitic amphibole) and accessory phases (epidote and allanite) similar to the host. Despite this similarity, the biotite shows enrichment in Al^{IV} contents compared to the biotite in the granitoid host. From the geochemical point of view, they are characterized by higher values in FeO^{tot}, MgO, Al_2O_3, TiO_2, CaO, MnO, V and Eu according to their mineralogy, whereas a heterogeneity is shown in trace element abundances, showing samples enriched and depleted in specific elements (such as Y, Rb, Sr). This variability could be referred to as a different fractionation of amphibole, biotite and plagioclase. In fact, amphibole can be absent in the mineralogy and the high Rb content indicates the strong fractionation of the biotite. Except for one MME enclave, the REE patterns show depleted LREE due to the epidote fractionation and Eu negative anomalies. The strong isotopic affinity with the granitoids rocks for the whole-rock and zircon data suggests a common source. The younger U-Pb emplacement age (295 ± 2Ma 292 ± 1 Ma) defines a late intrusion into the granitoids rocks. All previous features are again consistent with a co-geneticaffinity with the granitoid host. .

7.2 Source of the CVP parental magmas

As previously indicated, various interpretations about the source have been reported for the quartz-diorite and tonalite of CVP. A hydrous basaltic crust has been proposed as the magma source of the quartz-diorites and tonalites from the Serre Batholith rocks; minor processes (crustal contamination, mixing and fractionation) might all have contributed to the observed geochemical variations within the granitoids (Rottura *et al.,* 1990; Fiannacca et al. 2015). Rottura *et al.* (1991) proposed an origin related to the interaction between mantle magmas and crustal rocks.

In granitoid petrogenesis, the nature of the magma source is considered to exert a strong control on the melt composition (Chappell & White, 1974; 2001; Fiannacca et al., 2015; Moyen et al., 2017). If the parental magma, in general thinking, is considered as an image of the source, subsequent multiple processes such as fractional crystallization (Bowen, 1912; 1928), combined assimilation and fraction crystallization (AFC; De Paolo, 1981), magma mixing, restite unmixing (White and Chappell, 1977; Chappell and White, 2001) and peritectic assemblage entrainment (PAE; Stevens et al., 2007; Clemens e Stevens, 2012) can mask the original features.

Whole-rock and in-situ isotopic compositions (Rb-Sr, Sm-Nd, Pb-Pb, Lu-Hf and O) can be powerful tools to constrain the nature of the source and to trace the evolution of the produced magmas for a wide diversity of granitoids. Conversely, they can provide misleading information in the case of hybrid sources. For example, a hybrid magma (e.g., mantle contaminated by crust) will have enrichment in incompatible elements strongly controlled by the minor crust components. In this scenario, the volumetrically major role of the mantle is obscured (e.g., Moyen et al., 2017; and references therein). Any supposition about the relative contribution of mantle and crust and the effective creation of new crust and/or recycling crust needs various strategies to identify the nature of the source and petrogenetic mechanisms involved (Moyen et al., 2017).

The study of the mafic rock in a complex batholith can permit to uncover the probable genetic link with mantle and consequent crustal growth. Quartz-diorite and tonalite represent the best candidates.

7.2.1. The mantle role

The role of the mantle can be revealed by quarzt-diorite and MME that represent the more-suitable mafic end-member in the CVP. The highly negative εNd values preclude the role of the mantle and strongly confirm the involvement of old crustal components in the genesis of studied granitoids.

If the mafic microgranular enclaves can be the differentiation product of a mantle magma, the original signature has been completely masked by contamination of crustal material. Field observation has highlighted a possible contamination/hybridization by interaction with the host magma with sporadically mineral transfer processes. However, metaluminous affinity (ASI = 0.95 - 1), mineral compositions closer to the host, systematic change in major and trace elements and absence of significant variation in the isotopic feature (Fig. 5.8) indicate a co-genetic affinity with the quartz-dioritic/tonalitic hosts (Dodge and Kistler (1990), Pin *et al.* (1990), Donaire *et al.,* 2005, Moita *et al.,* 2015).

Quartz-diorites can be excluded as parental magma due to their high silica (about 58 wt. %) and low Cr (20 ppm) contents that are not in equilibrium with melts derived from the mantle. In addition, the absence of mafic minerals such as orthopyroxene and clinopyroxene supports the previous features. The Nb-Ta-Ti signature, the enrichment in LILE (Fig. 5.6) and Sr_i and εNd are in accordance with an origin from crustal sources.

7.2.2 Crustal sources

No isotope data variations have been observed across 20 wt% of SiO_2, implying a single source or an isotopically homogenous system. This rules out most scenarios for the mixing of crust and mantle magmas and the differentiation through a liquid line descent/fractional crystallization process of a mafic magma.

Many geochemical markers can help to identify distinct magma sources. Alumina saturation index (ASI) has been used by different authors to discriminate the probable source (e.g., Shand, 1943; Chappell & White, 1974, 2001; Debon & Le Fort, 1983; Villaseca et al., 1998; Patiño-Douce, 1999; Moyen et al., 2017).

In particular, Chappell & White (1974; 2001) set a separation between I-type (metaluminous to weakly peraluminous) and S-type (strongly peraluminous) granitoids at an ASI value of 1.1. There is no overlap in the more mafic I-type and S-type. When granites become more felsic, the ASI values of most felsic unfractionated I-type granites converge to 1.0–1.1, which overlap with S-type values ranging from 1.01 to 1.25 (Chappell et al., 1992).

Quartz-diorites, tonalite and leucotonalite of Capo Vaticano Promontory show a weak enrichment in ASI (1.02 -1.11) with the increment of the silica defined by an initial positive trend in the less evolved quartz-diorite tending to a flatter tendency in the tonalite and leucotonalite. This gradual increment is in concordance with the fractionaction of the biotite and its high Al^{IV} contents. Overall,the dominant calc-alkaline affinity, as indicated in Abdel and Rhaman (1994) and Frost et al. (2001) diagrams, and the ASI values determine an I-type origin of CVP quartz-diorites,tonalites and leucotonalites.

In the projection from biotite of the Shand diagram of Moyen *et al.* (2017; Fig. 7.1), the CVP lithotypes describe liquids derived from the same source pointing to the granite minimum. The horizontal line corresponds to A/CNK = 1 and most of the experimental liquids plot above the line (this means that are all peraluminous), while the grey line separates liquid derived from mafic and felsic sources. The CVP trend overlaps with the composition of the experimental melts derived from mafic sources (basalts and andesites).

CVP lithotypes in Fig. 7.2 (Laurent et al., 2014) fall in the field of the low-K mafic source enriched in CaO with an evolutive trend pointing to Al_2O_3/MgO+FeO_{tot} vertex. A comparison with experimental melts in the diagrams of Patino-Douce (1999) confirms an amphibolite as a potential source (Fig. 7.2).

MFW diagram (Mafic rocks – Felsic rocks - Weathering index; Ohta and Arai, 2007; Fig. 7.3), is used to highlight the effect of the differentiation and the alteration on the mafic rocks. The CVP lithotypes perfectly fit along with the differentiation trend of andesitic-dacitic melt.

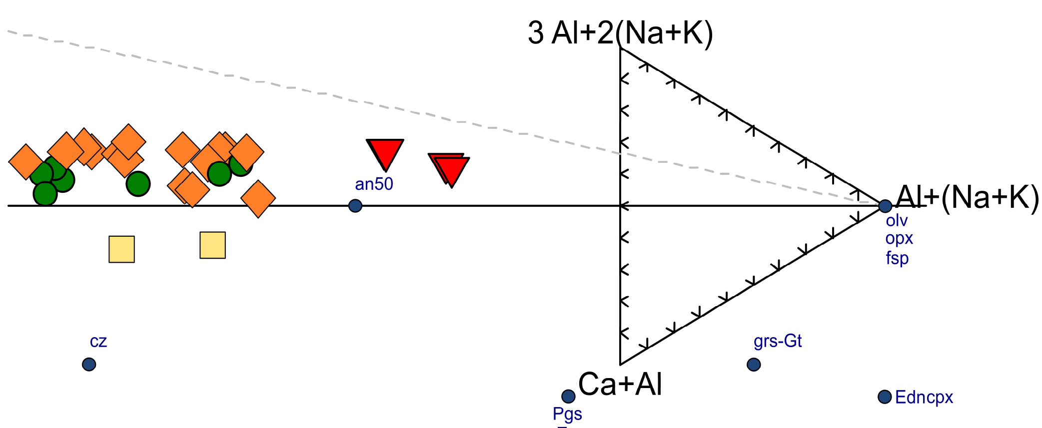

Figure 7.1 - Biotite projection diagram. The samples are plotted along the Ca+Al-3Al+2(Na+K)-Al+(Na+K) plan. The line pointing to Al+(Na+K) vertex corresponds to A/CNK=1; the 2:1 grey line between the vertexes 3 Al+2 (Na+K) and Ca+Al separates the mafic sources (basalt and andesite) from the felsic sources (meta-granitoids or meta-sediments). After Moyen et al. (2017). Symbols as in Fig. 6.2.

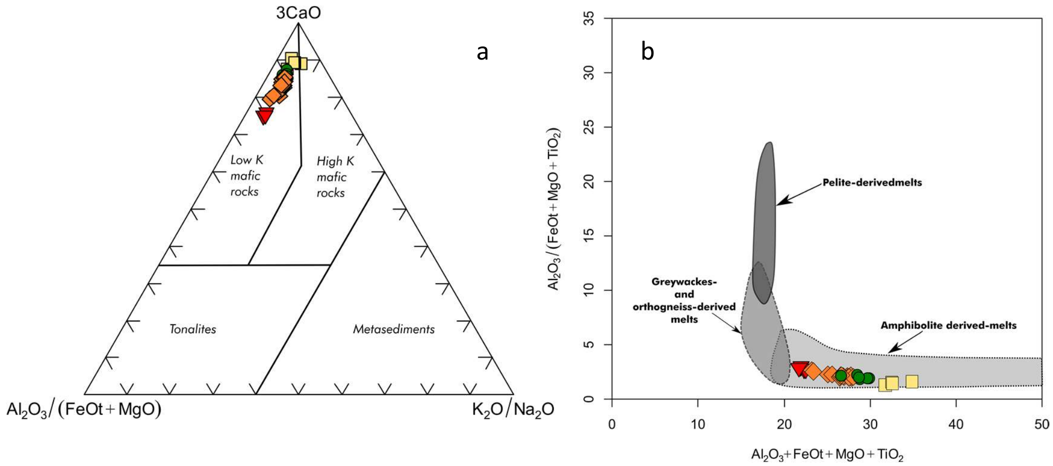

Figure 7.2 – Comparison between CVP sample and experimental melts. a) Ternary diagram 3CaO – $Al_2O_3/(FeO_{tot}$ + MgO) – K_2O/Na_2O with plotted CVP lithotypes (after Laurent et al., 2014 and reference therein). *b) Al_2O_3 +FeO_t + MgO +TiO_2 vs. $Al_2O_3/(FeO_t$ + MgO + TiO_2) diagram (from Patino Douce, 1999). CVP granitoids symbols are as in Fig. 6.2.*

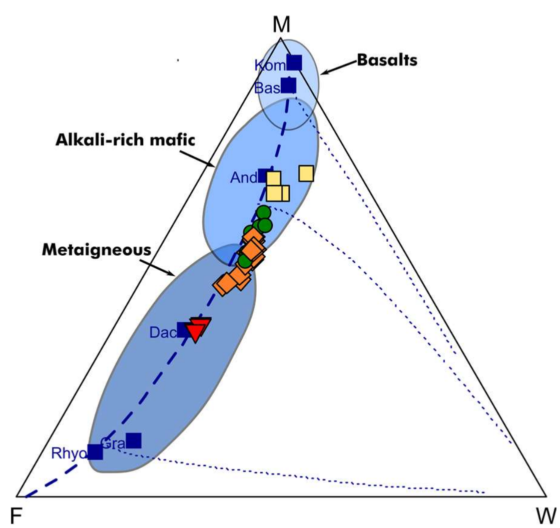

Figure 7.3 - MFW diagram. The diagram shows the differentiation and the various degree of weathering for the mafic rocks. F = Felsic rock, M = Mafic rock, W = weathered composition (Ohta e Arai, 2007). Filled coloured fields represent experimental melts with different compositions. M=− 0.395 × ln(SiO_2) + 0.206 × ln(TiO_2) − 0.316 × ln(Al_2O_3) + 0.160 × ln(Fe_2O_3) + 0.246 × ln(MgO) + 0.368 × ln(CaO∗) + 0.073 × ln(Na_2O) − 0.342 × ln(K_2O)+ 2.266. F = 0.191 × ln(SiO_2) − 0.397 × ln(TiO_2) + 0.020 × ln(Al_2O_3) − 0.375 × ln(Fe_2O_3) − 0.243 × ln(MgO) + 0.079 × ln(CaO∗) + 0.392 × ln(Na_2O) + 0.333 × ln(K_2O) − 0.892.W=0.203 × ln(SiO_2) + 0.191 × ln(TiO_2) + 0.296 × ln(Al_2O_3) + 0.215 × ln(Fe_2O_3) − 0.002 × ln(MgO) − 0.448 × ln(CaO∗) − 0.464 × ln(Na2O)+ 0.008 × ln(K_2O) − 1.374. Where CaO denotes CaO corrected for apatite and carbonates (modified from Moyen et al., 2017).*

Finally, in the A-B plot of Debon and Le Fort (1983), modified by Villaseca *et al.* (1998; Fig. 7.4), CVP granitoids are classified as moderately peraluminous granitoids (m-P; field not shown), with slightly negative trends and peraluminosity increasing with the maficity decrement. In a crustal setting, there are three types of source rocks that can produce peraluminous melts: pelites, metaigneous and/or greywackes and amphibolites (Fig. 6.6). Production of peraluminous granitoid melts by dehydration melting of metaluminous metabasalts at lower crustal depth has been documented by many experimental studies (e.g., Beard & Lofgren 1991; Wolf & Wyllie 1994; Patino Douce & Beard 1995; Springer & Seck 1997).

Clearly depicted by isotope signature and the experimental melts, a crustal metabasite is the probable source of quartz-diorites, tonalite, leucotonalite and enclaves. The restitic nature of the lower crust of Capo Vaticano Promontory (Caggianelli et al., 1991; Fornelli et al., 2011) supports the granitic melts extraction. The Serre lower crust is composed of two different complexes: a deep portion characterized by mafic granulites (comprising metagabbros, metaperidotites and minor metapelites, felsic granulites and metacarbonates) and an uppermost portion made up of felsic granulites (migmatitic paragneisses and Opx-Bt-Grt granulites with minor metabasites and rare marbles and felsic orthogneisses). Comparison with this basement and CVP in Sr_i, εNd and Pb isotopes shows a strong isotopic correlation of CVP granitoids with the mafic granulites (Figs. 5.8).

Amphibolites have been reported in the literature as xenolith in Pl-rich quartz-diorites (Rottura *et al.,* 1990) in the CVP area. More extensive outcrops of amphibolite are located in Palmi-Bagnara area (Puglisi & Ioppolo, 1994), ca. 20 Km southernmost of CVP and it is considered part of the Serre Batholith. The Palma-Bagnara metamorphic complex is made up of a tonalitic gneiss with associated metasediment and amphibolite, metamorphosed to high-amphibolitic facies (Puglisi &

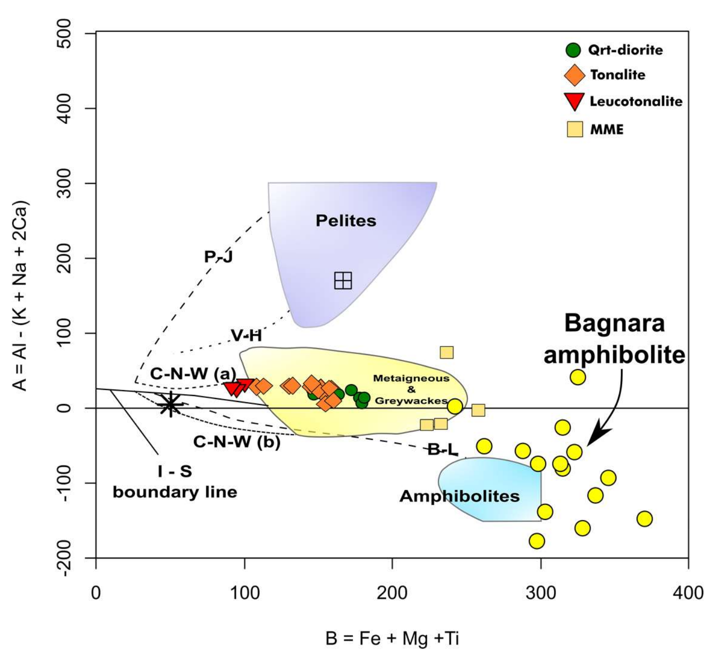

Figure7.4 - A-B diagram (Debon e Le Fort, 1983, modified by Villaseca et al., 1998). The probable source able to produce peraluminous melt in crustal setting a reported in figure. Palmi-Bagnara sample from Puglisi & Ioppolo, 1994.

Ioppolo, 1994). In the A-B plot, the more mafic granitoids produced by partial melting of a metabasic source or by coeval basaltic magma correspond to the higher degree of partial melting or mixture of melt with restitic/peritectic phases (Chappell et al., 1987; Stevens et al., 2007; Fiannacca *et al.,* 2019) Plotting the Palmi-Bagnara amphibolite in the Villaseca diagrams (Puglisi & Ioppolo, 1994; Fig. 7.6) the CVP lithotypes depict a trend ascribable to partial melting of Palmi-Bagnara amphibolite.

Furthermore, as shown in the Harker diagrams (Fig. 5.6), two populations of quartz-diorites have been differentiated: Y-poor and -rich. Interestingly, Ioppolo & Puglisi (1994) have observed two populations of amphibolite: Y- and HREE-rich and Y- and HREE-poor, respectively. The authors suggested mantle melting at moderate LP outside the stability field of the garnet (due to low MREE/HREE fractionation) for the origin of the pre-Variscan basaltic protolith of the Y-rich amphibolite and a deeper garnet-rich mantle partial melting for the protolith of the Y-poor amphibolite. In this scenario, a progressive partial melting from the Y-poor to Y-enriched amphibolite is in accordance with the genesis of granitoids.

7.3 Magma differentiation

Quartz-dioritic to leucotonalitic linear trends can be the proof of vary differentiation processes such as fractional crystallization (Bowen, 1912; 1928), magma mixing, restite unmixing (Chappell et al., 1977) and assimilation fractional crystallization processes (AFC; De Paolo, 1981). They will be addressed on a case-by-case.

7.3.1 Fractional crystallization

As discussed above, the resemblance of major and trace element patterns in quartz-diorites and tonalite reinforce the genetic affinity between the lithotypes. Quartz-diorite with the less evolved silica content and the higher abundance of mafic phases could be the parental magma responsible for the differentiation though a fractional crystallization process. On the other hand, the cumulitic plagioclase and Eu positive anomalies suggest a quartz-diorite as a cumulate derived from fractionation crystallization of an more evolved magma. The few presences of positive Eu peaks, although an orthocumulitic structure has been well-observed in petrography study, could be related to the contemporaneous fractionation of amphibole and plagioclase.

Initial Sr_i, εNd and $^{207}Pb/^{206}Pb$ isotopes are homogenous and show systematic behavior with major elements. Figures 7.5 and 7.6 show as all isotopes developed flat trends confirming the genetic affinity between CVP granitoids. Once again, these features indicate that a possible evolution by fractional crystallization in a closed-system could be responsible for the geochemical variability in the CVP suites.

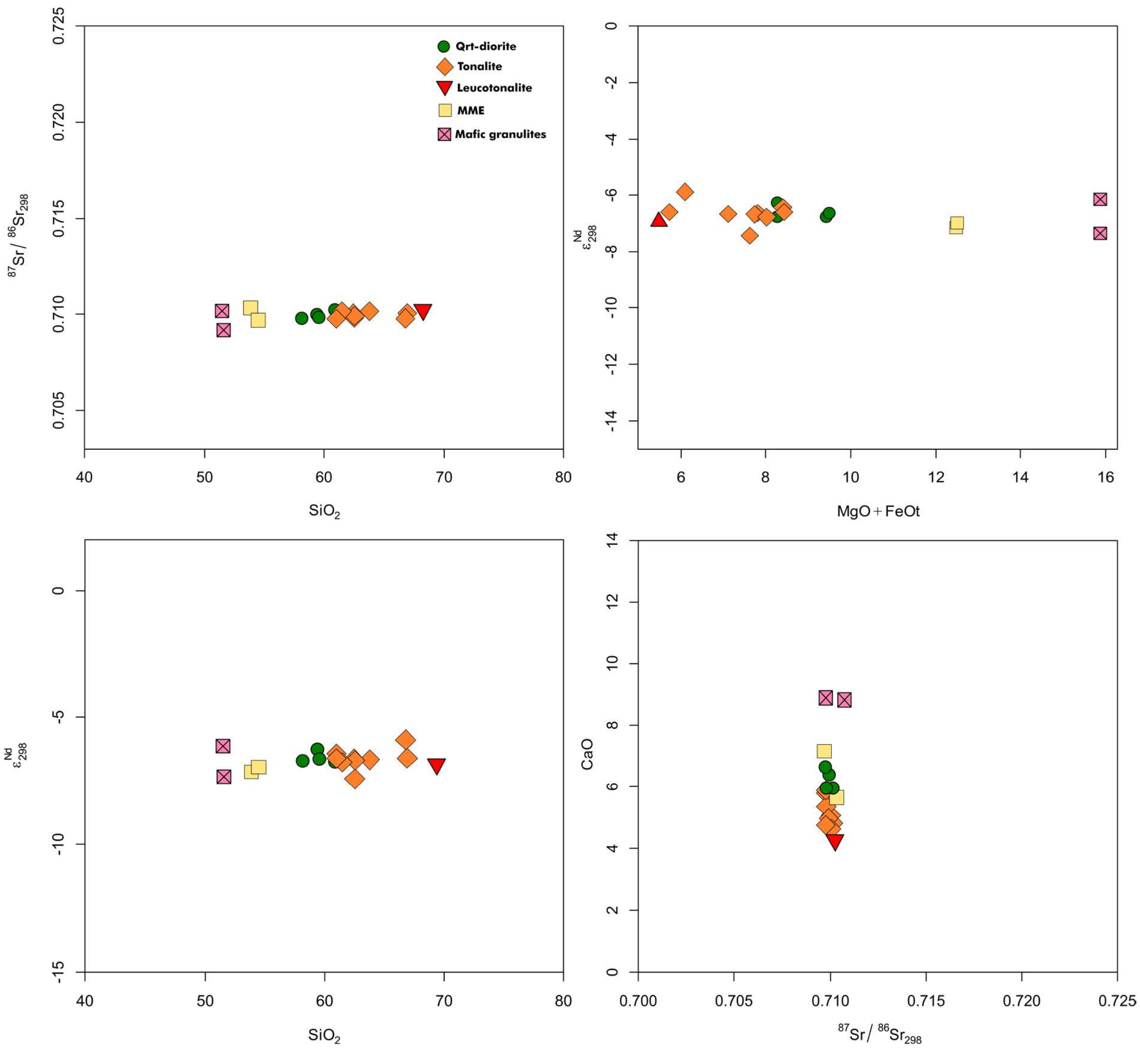

Figure 7.5 - Variation diagrams Sr_i versus SiO_2 and CaO and εNd_{298} versus SiO_2 and MgO+Feo_{tot}. The flat trend indicates the closed-system fractional crystallization of mafic granulites (from Caggianelli et al., 1991).

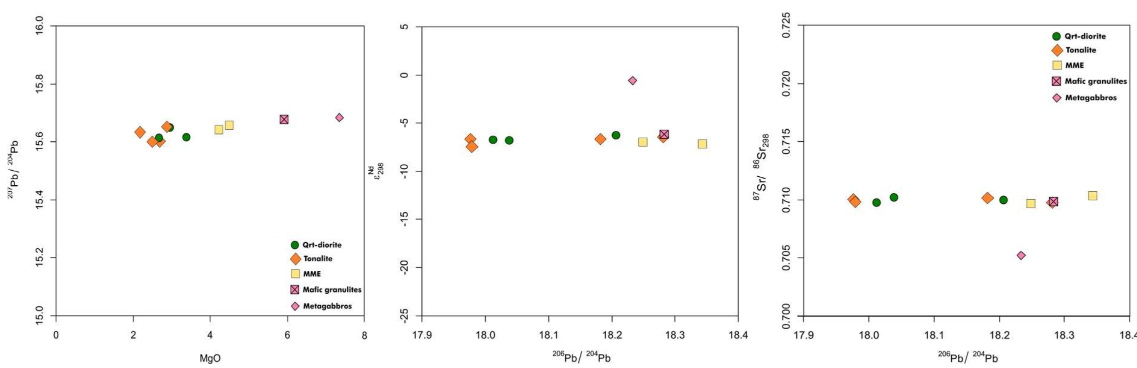

Figure 7.6 - Variation diagrams of $^{207}Pb/^{204}Pb$ versus MgO and $^{206}Pb/^{204}Pb$ versus εNd and Sr_i. The flat trend indicates an fractional crystallization in a closed system. The mafic granulites is collinear with the granitoids (from Caggianelli et al., 1991).

7.3.2 Assimilation and fractional crystallization

Field relationships have highlighted the intrusion of quartz-dioritic magma into the metapelites. The assimilation of the basement has produced at least two types of quartz-diorites: the first associated with the partial melting-derived products (restitic enclaves, anatectic melt and peritectic garnet), the second is a hybrid quartz-diorites originated by continuous mixing/mingling between quartz-dioritic magma and anatectic melts.

Despite the lack of heterogenous petrographic and geochemical evidence in the lithotypes collected away from the migmatitic border zone, two different hypotheses can be proposed:

1. The AFC processes cannot be completely excluded. The data collected until now could be the result of a strong homogenization that has completely erased the traces of that process.

2. The magma emplacement has affected only some portion of the basement, as testified by an exclusive outcrop in the southern sector of CVP (S. Maria locality).

7.3.3 Magma mixing

Mixing between mantle and crustal magmas is also able to explain linear trends in Harker diagrams. The mafic end-member could be the mafic microgranular enclaves associated with the rocks. Although correlation exists in some major elements, the absence of noticeable trends in trace elements excludes it. Secondly, more importantly, the Sr_i and εNd isotopic signature (Fig. 5.8a) should draw a curvilinear trend with the more mafic rock exhibiting the less unradiogenic values. The similar Sr_i ratio (0.7097 -0.7103) and the relatively larger εNd values (-5.88 to -7.43) depict a vertical array ascribable to a contribution of a quite homogenous old crustal source in the granitoids genesis, strongly rejecting this hypothesis.

7.3.4 Restite unmixing process

The restitic unmixing process seems to play a minor role in the quartz-diorite/tonalite evolution. The Nb-Ta-Ti and P troughs in the primitive-mantle normalized patterns (Fig. 5.6) can indicate the retention of restitic phases in the source, such as ilmenite, titanite, apatite. On the other hand, the restitic phases suggested by the authors (Chappell et al., 1987) to support the model, such as An-rich core in plagioclase, inherited zircon and mafic phases (orthopyroxene and clinopyroxene, although ordinarily involved in partial melting processes) are absent. Besides, any source exposed to partial melting would leave a restite. As proposed in Lombardo et al. (2020) for the CVP quartz-diorite and tonalite, the partial fitting with the mafic granulites of the Serre lower crust could indicate an early-stage restite fractionation regime responsible for geochemical variation, followed by a fractional crystallization regime masking the original features (Chappell *et al.,* 1987).

7.3.5 Modelling partial melting

An intermediate composition of Bagnara amphibolite (Puglisi & Ioppolo, 1994) has been considered as representative of the composition for the source rocks. A batch melting modeling of the major elements permits to obtain the parental magma after 36% of partial melting with a restite composed by Pl=48%, Opx = 49% and Qrz = 3%. The modal abundance of restitic phases coincides with assemblages catalogued by Schenk (1984) for the mafic granulites present in the Serre lower crust. Beard & Lofgren (1991) have demonstrated experimentally that 30% of the partial melting of an amphibolite source produces a tonalitic melt. Depending on bulk composition, dehydration melting of amphibolite yields 10–60% quartz dioritic to tonalitic melt at 900°-1000° C (Jung et al., 2015).

7.3.6 Modelling fractional crystallization

The differentiation processes described above have highlighted how the fractional crystallization is the main process acting in the granitoids evolution. Based on petrographic and geochemical features, the cumulitic plagioclase and well-marked Eu anomalies indicate how some quartz-dioritic and tonalitic samples represent the cumulitic products of a more evolved liquid. The tonalitic sample CVP39, representing the magma obtained by partial melting of the Bagnara amphibolite, is now used as parental magma.

The mass-balance formula ($C_0=F*C_L + (1-F)*C_S$) was used to calculate the major elements model, whereas the Rayleigh law was applied ($CL = C0*F^{(D-1)}$) for the trace modeling. Choosing the CVP39 tonalite as the parental magma (C_0), CVP4 leuco-tonalite as the evolved liquid (C_L) and the mineral compositions of phases present in the less evolved quartz-diorite (Pl, Amph, Bt, Ep, Ilm and Ap), major element modeling produces the evolved composition (CVP4) after 30% of fractional crystallization (Fig. 7.7). The cumulate is constituted by the following mineral assemblage: Pl = 52%, Amph = 12%, Bt = 30%, Ep = 2%, Ilm =1 %, Ap = 2%. The results are reported in Tab. 7.1.

Primitive mantle- and chondrite-normalized patterns have been modelled, considering the results obtained with the previous modeling. Kd values for Pl, Amph, Bt and Ilm are for dacitic melt (from GERM website).

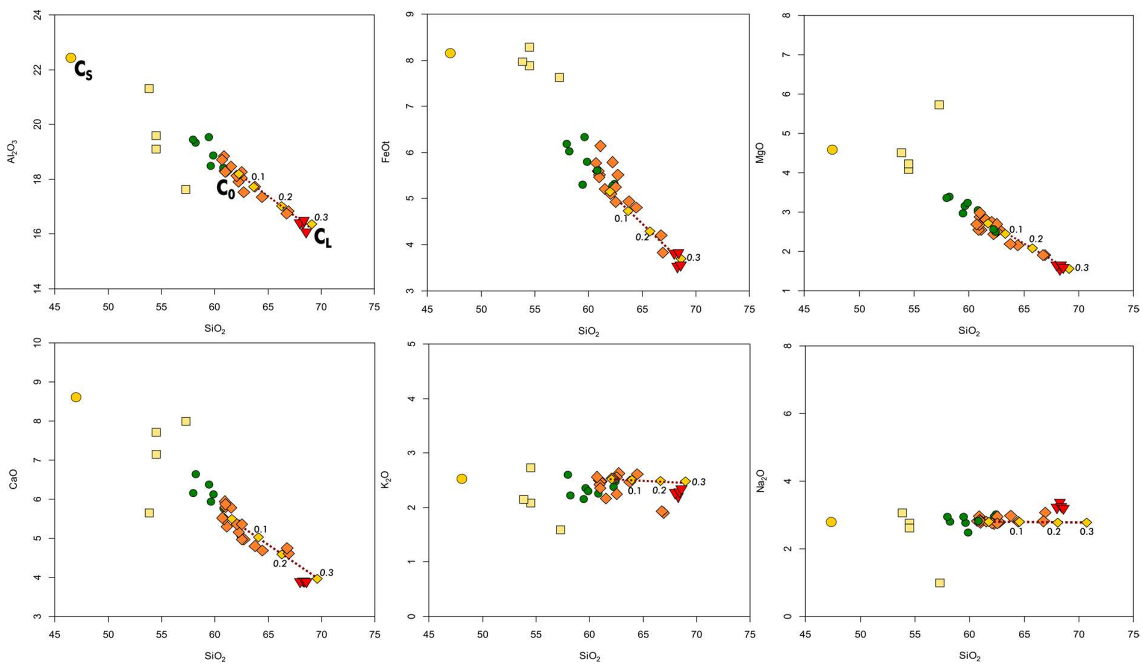

Figure 7.7 - Major elements fractional crystallization modelling for CVP quartz-diorite, tonalite and leucotonalite. C_0=parental magma; C_L= liquid composition; C_S= cumulate composition. Dotted lines represent the liquid line evolution with numeric values indicating the degree of fractionaction (F = 0.1, 0.2, 0.3, respectively).

	CVP39 (C_0)	Pl	Amph	Bt	Ep	Ilm	Ap	Tt	Cumulate	Dif.magma	CVP4 (C_L)
SiO_2	62.09	54.25	45.21	34.29	38.67	0	0	31.28	44.7	68.54	68.57
Al_2O_3	18.12	29.07	12.23	18.73	26.32	0.06	0	3.95	22.73	16.14	16.06
FeOt	5.1	0.13	17.01	17.21	9.74	32.92	0.21	1.93	7.8	3.94	3.56
CaO	5.35	10.59	11.11	0.18	22.01	0	52.4	27.85	8.38	4.05	3.89
MgO	2.74	0	10	10.36	0	0	0.54	0.04	4.32	2.06	1.59
Na_2O	2.75	5.26	1.08	0.11	0	0	0	0.04	2.9	2.69	3.19
K2O	2.53	0.05	0.45	9.59	0	0	0	0.03	2.96	2.35	2.34
TiO_2	0.87	0.05	0.19	1.94	0.19	52	0	33.33	1.15	0.75	0.49

Table 7.1 – Fractional crystallization results obtained for the major elements of CVP granitoids.

Modeling the cumulate and the liquid evolved from the parental magma (CVP39), the leuco-tonalitic liquid (CVP4, green trend) fits with REE elements, confirming fractional crystallization as the main process in quartz-diorite/tonalite differentiation (Fig. 7.8).

The mismatch with some elements, e.g., La, Ce, Zr, might be due to the presence of the accessory minerals that have not been considered in the model (Ap and Ep was excluded in this phase for the higher Kd values).

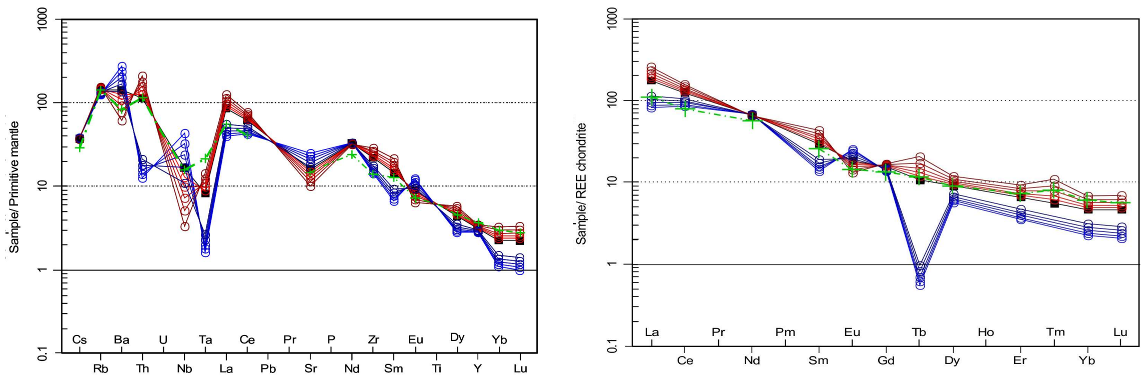

Figure7.8 - Primitive mantle and chondrite- normalized multi-elements diagrams with the red line representing the liquid evolution and the blue line the solid evolution. Black trends = parental magma; green trend = evolved liquid.

6.3.7 Modelling with accessories

When granitoid magmas are zircon-saturated at the source, zirconium concentration in a melt is referred to as zircon saturation systematics (Watson and Harrison, 1983; Miller *et al.,* 2007). It is commonly observed that strongly peraluminous granites (typically S-type) contain abundant inherited zircon and low total Zr, whereas metaluminous to weakly peraluminous granitoids (usually I-type) tend to be poor in inherited zircon and often somewhat richer in Zr (Miller *et al.,* 2007). The zircon saturation index, in addition to the Zr concentration in the melt, is related to the temperature. Mafic hotter magmas usually are undersaturated and can dissolve a large quantity of zircon. Felsic colder magmas are less able to dissolve zircon and can contain inherited crystals (Zr-saturated magma).

Zr versus SiO_2 (Fig. 5.6) diagram shows, in general, an incompatible behavior, although it is well-constrained for a tonalite group, with increasing silica and a sudden drop at around SiO_2 = 64%. The change of tendency denotes the saturation point and the equivalent passage from an undersaturated-Zr magma to a saturated. Appling theZr solubility model of the Watson & Harrison (1983)), the Zr saturation level calculated (Zr_{calc}) shows a similar Zr concentration in whole-rock (Zr_{obs}), indicating that magma is close to Zr-saturation (Fig. 7.9). Considering a Zr-saturated magma, the granitoids should be contain inherited crystals (antecrysts or xenocrysts). The univocal emplacement age obtained for CVP granitoids rocks (297 Ma) and the absence of inherited crystals suggests Zr-unsaturated magma. The igneous rock with silica content less than 64 wt% have been considered as Zr-unsaturated. If the zircon is present, it should be inherited or have crystallized from late-stage highly differentiated melt domains more silicic than the bulk-rock composition (Siegel *et al.,* 2018). This is supported by interstitial and included zircon in biotite in the CVP rocks. The temperature calculated with zircon saturation is higher (820 °C) for the tonalite and the slightly colder for quartz-diorite and leuco-tonalite (ca. 760 °C). The higher T and Zr_{obs} contents in some tonalites support the idea that the initial parental magma was tonalitic (Fig. 7.9). The quartz-diorite represents the cumulates and the leuco-tonalite, the evolved liquid.

If the whole-rock were modelled via fractional crystallization, zircon could not be thought of as independently for the whole-rock. In this view, a zircon fractional crystallization was modeled (for reference see Janousek *et al.,* 2016).

Modeling accessory minerals is difficult because the K_D can change rapidly and it is controlled by temperature and melt composition (C_L). In this view, zircon could be considered as a function of the bulk rock and modeled using the Raleigh law. Mineral chemistry and the correspective Kd, the modal proportion of the cumulate, whole-rock dataset, a likely parental magma composition (C_0) and liquid composition (C_L) are parameters used in the model.

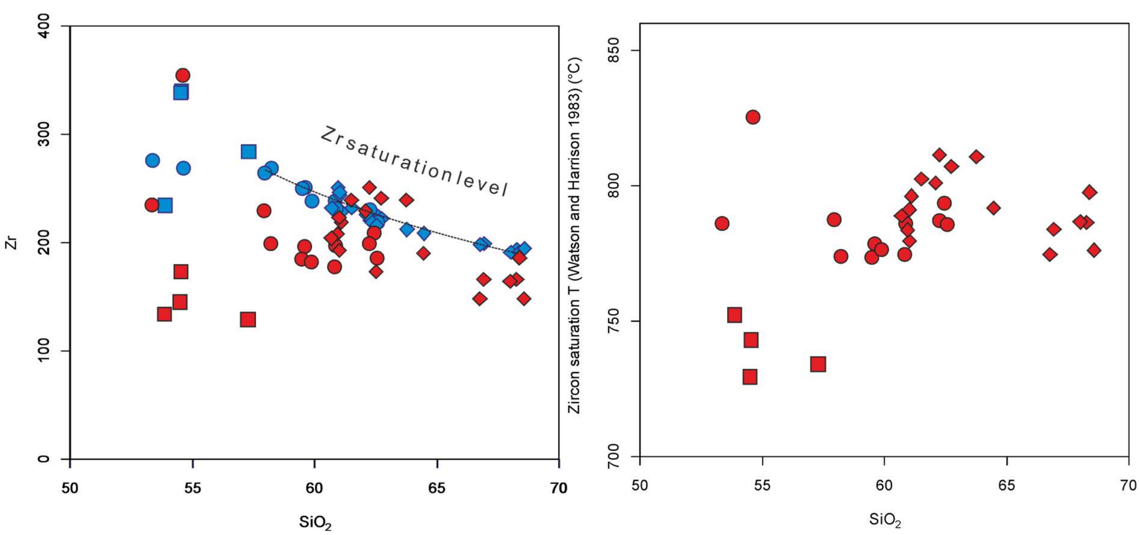

Figure 7.9 - Zr versus SiO_2 diagrams. Left: Zr concentrations necessary to saturate quartz-dioritic/tonalitic melt compared with the whole-rock Zr content; Right: Zr saturation temperature calculated according to Watson & Harrinson (1983). Squares: MME; circles: quartz-diorites, diamonds: tonalite and leucotonalites.

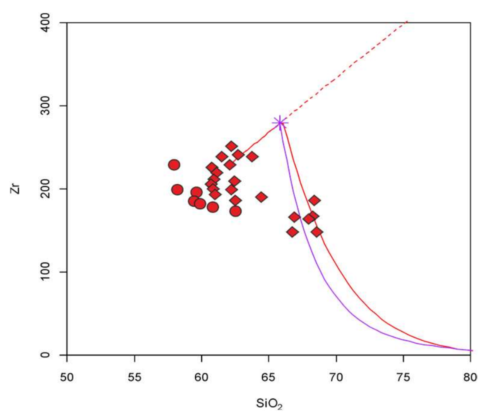

Figure 7.10 – Zircon fractional crystallization using the solubility (red curve) and the Kd values (purple line). See text for the explanations (modified by Janousek et al., 2006).

Modelling permits to calculate the fractional crystallization taking into account the solubility parameter and the Kd values applying the Rayleigh law. Assigning CVP39 as the C_0, the model calculates a new C_0 (the purple star) representing the saturation point (Fig. 7.10). The fractional crystallization curves will represent the liquid evolution with solubility (red) and Kd (purple) methods crystallizing 0.2% of zircon.

The results of the modelling show that the saturation point is reached at about 250 ppm of Zr, indicating undersaturated magma until 68 % wt. with SiO_2 with similar trends of zircon fractional crystallization for both methods (with a degree of fractionation corresponding to 25%, approaching the degree of fractionation obtained for whole-rock major and trace elements).

The new model supports the SHRIMP U-Pb ages obtained for CVP samples, indicating that high-temperature magma completely dissolves inherited-source zircons. Zircon in quartz-dioritic/tonalitic magma is a new phase precipitated directly from the magma during fractional crystallization processes at around 297 Ma.

8. Conclusions

The role of mantle or crust as possible sources in the genesis of the granitoid batholith has been crucial to understanding how the continental crust grows and evolves in geological times. The wide compositional variability of the granitoids is referred to as a differentiation processes occurred up until the emplacement level. This can obliterate the real contribution of the source in the magma production.

Mafic granitoids represent the more suitable lithotypes to investigate the probable contribution of the mantle in the composite batholith. As a case study, the quartz-diorite and tonalite of Capo Vaticano Promontory, representing lower crustal magmatic units of a complete late Paleozoic crustal section, are the best candidates to explore the role of the mantle or the crust in a late-orogenic batholith.

The petrographic, geochemical and isotopic (Nd, Sr,Pb and Hf) and U-Pb ages evidence delineate a genetic affinity between quartz-diorites, tonalites and leucotonalite.

SHRIMP U-Pb data confirm a late-Variscan age for the quartz-diorite and tonalite (302 ± 1 Ma to 297.4 ± 1.6 Ma). The presence of older ages (from 315 ± 1.8 Ma to 306 ± 2 Ma), defined here tentatively as anatectic, places a limit for the lower crustal anatectic processes. Fiannacca *et al.* (2017) proposed a range from 305 to 302 Ma for the peraluminous granites of the nearby Serre Massif. Similar εHf values obtained for the anatectic ages and metamorphic xenocrysts does not allow to differentiate well between the two events. Surely, it is possible that the anatectic process of the mafic granulites started earlier, because quartz-diorite and tonalite represent the earliest and the deepest intrusion within Capo Vaticano Promontory. A late recrystallization process (c. 290 Ma ± 1 Ma) is indicative of a high temperature and interstitial fluid.

The cumulitic nature of quartz-diorites suggests a differentiation from a tonalitic parental magma and a liquid evolution towards the leucotonalitic terms. Fractional crystallization has been invoked as the main process responsible for the geochemical variations in the quartz-diorites and tonalite. In fact, modelling of major and trace elements produces their evolved composition after F=30% and a cumulate with a mineral assemblage of Pl= 53%, Amph=12%, Bt=30%, Ep=2% and Ilm =1%. However, a minor role of restite unmixing processes and the AFC are not completely excluded.

A mafic granulite is suggested as the restitic source for the quartz-diorite based on Sr, Nd, Pb isotopic data.. Comparing with the experimental data strongly confirm an amphibolite as the source. The Palmi-Bagnara amphibolite, constituting a part of Serre Massif located about 20 Km southernmost of CVP, was used for batch melting model. The model was able to produce the tonalitic parental magma after 36 % of partial melting of the amphibolite with a restite assemblage composed by Pl, Opx and Qtz.

The εHf in the zircon confirms a crustal source, but the wide range indicates a major heterogeneity. The presence of some positive values does not exclude a marginal role of the mantle. The mafic input can be related to a metabasaltic source less contaminated or probably with a minor contamination of metasediments during its rise.

MME have been considered as co-genetic with quartz-diorites and tonalites based on their mineralogical and isotopic analogies. In fact, comparison with the experimental melts supports a mafic granulites as the source. Modeling the MME evolution is not simple, because of the contamination with the host magma that had modified the original features. The emplacement of MME into the granitoids is dated at around 292 ± 1 Ma.

Finally, all the data support a strong a crustal signature for the evolution of the quartz-diorite, tonalite and MME in the Capo Vaticano Promontory.

References

Abdel-Rahman, A.-F.M. (1994) - Nature of biotites from alkaline, calc-alkaline, and peraluminous magmas - Journal of Petrology 35 (2): 525–541. https://doi.org/10.1093/petrology/35.2.525

Acquafredda, P., Lorenzoni, S., Zanettin Lorenzoni, E., Barbieri, M., Trudu, C. (1991) – The age of volcanisn and metamorphism of the Bocchigliero Paleozoic sequence (Sila – southern Italy) – Rendiconti Linei 2: 145-156.

Acquafredda, P., Caggianelli, A., Piccaretta, G. (1992) – Late magmatic to subsolidus coronas in gabbroic rocks from the Sila massif (Calabria, Italy) – Mineralogy and Petrology 46: 229 – 238.

Acquafredda, P., Lorenzoni, S., Zanettin Lorenzoni, E. (1994) - Paleozoic sequences and evolution of the Calabrian–Peloritan Arc (Southern Italy) - Terra Nova 6: 582–594.

Acquafredda, P., Fornelli, A., Paglionico, A., Piccarreta, G. (2006) - Petrological evidence for crustal thickening and extension in the Serre granulite terrane (Calabria, southern Italy) - Geological Magazine 143: 145–163.

Acquafredda, P., Fornelli, A., Piccarreta, G., Pascazio, A. (2008) - Multi-stage dehydration–decompression in the metagabbros from the lower crustal rocks of the Serre (southern Calabria, Italy) - Geological Magazine 145: 397–411.

Angì, G., Cirrincione, R., Fazio, E., Fiannacca, P., Ortolano, G., Pezzino, A. (2010) - Metamorphic evolution of preserved Hercynian crustal section in the Serre Massif (Calabria–Peloritani Orogen, southern Italy) - Lithos 115: 237–262.

Annen, C., Blundy, J. D., & Sparks, R. S. J. (2006). The genesis of intermediate and silicic magmas in deep crustal hot zones. Journal of Petrology, 47(3), 505-539.

Appel, P., Cirrincione, R., Fiannacca, P., Pezzino, A., 2011. Age constraints on Late Paleozoic evolution of continental crust from electron microprobe dating of monazite in the Peloritani Mountains (southern Italy): another example of resetting of monazite ages in high-grade rocks. International Journal of Earth Sciences 100, 107–123

Armbruster, T., Bonazzi, P., Akasaka, M., Bermanec, V., Chopin, C., Gieré, R. & Pasero, M. (2006). Recommended nomenclature of epidote-group minerals. European Journal of Mineralogy, 18(5), 551-567.

Atzori, P., Ferla, P., Paglionico, A., Piccarreta, G., Rottura, A. (1984) - Remnants of the hercynian orogen along the 'calabrian-peloritan arc', southern italy: A review - Journal of the Geological Society, 141 (1): 137-145.

Ayuso, R.A., Messina A., De Vivo, B., Russo, S., Woodruff, L.G., Sutter, J.F., Belkin, H.E. (1994) - Geochemistry and argon thermochronology of the Variscan Sila Batholith, southern Italy: source rocks and magma evolution - Contributions to Mineralogy and Petrology 117(1): 87-109.

Barca, D., Cirrincione, R., De Vuono, E., Fiannacca, P., Ietto, F., and Lo Giudice, A. (2010) - The Triassic rift system in the northern Calabrian-Peloritani Orogen: evidence from basaltic dyke magmatism in the San Donato Unit - Per. Mineral. 79: 61–72. doi: 10.2451/2010PM0010

BEARD, J. S., & LOFGREN, G. E. (1991). Dehydration melting and water-saturated melting of basaltic and andesitic greenstones and amphibolites at 1, 3, and 6. 9 kb. Journal of Petrology, 32(2), 365-401.

Behr, H.-J., Engel, W., Franke, W., Giese, P., Weber, G. (1984) – The Variscan Belt in Central Europe: main structures, geodynamic implications, open questions – Tectonophysics 109 (1-2): 15-40.4

Bhattacharya, S., & Janwari, S. (2015). A Short Review on Lu-Hf Isotope System in Zircon: Implications for Crustal Evolution. Journal of the Indian Institute of Science, 95(2), 147-158.

Black, L. P., Kamo, S. L., Allen, C. M., Davis, D. W., Aleinikoff, J. N., Valley, J. W. & Foudoulis, C. (2004). Improved 206Pb/238U microprobe geochronology by the monitoring of a trace-element-related matrix effect; SHRIMP, ID–TIMS, ELA–ICP–MS and oxygen isotope documentation for a series of zircon standards. Chemical Geology, 205(1-2), 115-140.

Blichert-Toft, J., & Albarède, F. (1997). The Lu-Hf isotope geochemistry of chondrites and the evolution of the mantle-crust system. Earth and Planetary Science Letters, 148(1-2), 243-258.

Bonfiglio, L. (1963) - Plutoniti, migmatiti e metamorfiti della Calabria meridionale - Mem. Soc. Geol. It, 4: 79-95.

Borsi, S., Heike Merlin, O., Lorenzoni, S., Paglionico, A., Zanettin Lorenzoni, E. (1976) – Stilo Unit and “dioritic-kinzigitic” unit in Le Serre (Calabria). Geological, petrological and geocronological characters – *Boll. Soc. Geol. Ital.,* **95**: 219-244.

Boynton, W.V. (1984) - Cosmochemistry of the rare earth elements: meteorite studies - In: Henderson P (eds) Rare Earth Element Geochemistry. Elsevier, Amsterdam, pp 63-114.

Bowen, N.L. (1912) - The order of crystallization in igneous rocks - J Geol 20:457–468.

Bowen, N.L. (1928) - The evolution of the igneous rocks - Princeton University Press, Princeton.

Burg, J.P., Bale, P., Brun, J.P., Girardeau,J. (1987) - Stretching lineation and transport direction in the Ibero-Armorican arc during the Siluro-Devonian collision – Geodinamica Acta 1 (1): 71-87.

Burton, A.N. (1971) - Relazione generale, carta geologica della Calabria. Cassa per il Mezzogiorno, Roma, 120 pp.

Buttner, S & Kruhl, J.H. (1997) - The evolution of a late-Variscan high-T/low-P region: the southeastern margin of the Bohemian massif – Geologische Rundscau 86: 21-38.

Caggianelli, A., Prosser, G., Rottura, A. (2000) - Thermal history vs. fabric anisotropy in granitoids emplaced at different crustal levels: an example from Calabria, southern Italy - Terra Nova 12: 109–116.

Caggianelli, A., Liotta, D., Prosser, G., Ranalli, G. (2007) - Pressure-temperature evolution of the late Hercynian Calabria continental crust: compatibility with post-collisional extensional tectonics - Terra Nova 19: 502–514.

Caggianelli, A., Del Moro, A., Paglionico, A., Piccarreta, G., Pinarelli, L., Rottura, A. (1991) - Lower crustal granite genesis connected with chemical fractionation in the continental crust of Calabria (Southern Italy) - European Journal of Mineralogy 3: 159–180.

Carminati, E., Petricca, P. (2010) – State of stress in slabs as a function of large-scale plate kinematics – Geochemestry, Geophisysics, Geosystems 11 (4).

Chappell, B.W. & White, A.J.R. (1974) - Two contrasting granite types - Pacific Geology 8: 173–174.

Chappell, B.W. & White, A.J.R. (2001) - Two contrasting granite types: 25 years later - Australian Journal of Earth Sciences 48: 489–499.

Chappell, B.W., White, A.J.R., Wyborn, D. (1987) - The importance of residual source material (restite) in granite petrogenesis - Journal of Petrology, 28 (6): 1111-1138.

Christofides, G., Perugini, D., Koroneos, A., Soldatos, T., Poli, G., Eleftheriadis, G. & Neiva, A. M. (2007). Interplay between geochemistry and magma dynamics during magma interaction: an example from the Sithonia Plutonic Complex (NE Greece). Lithos, 95(3-4), 243-266.

Cifelli, F., Mattei, M., Porreca, M. (2008) - New paleomagnetic data from Oligocene–upper Miocene sediments in the Rif chain (northern Morocco): Insights on the Neogene tectonic evolution of the Gibraltar arc – Journal of geophysical research 113 (B2).

Cirrincione, R., Fiannacca, P., Ortolano, G., Pezzino, A., Punturo, R. (2013) - Granitoid stones from Calabria (Southern Italy): petrographic, geochemical and petrophysical characterization of ancient quarries of Roman Age – Periodico di Mineralogia 82 (1): 41-59.

Cirrincione, R., Fiannacca, P., Lustrino, M., Romano, V., and Tranchina, A. (2014) - Late Triassic tholeiitic magmatism in Western Sicily: a possible extension of the Central Atlantic Magmatic Province (CAMP) in the Central Mediterranean area? - Lithos 188: 60–71. doi: 10.1016/j.lithos.2013.10.009

Cirrincione, R., Fazio, E., Fiannacca, P., Ortolano, G., Pezzino, A., and Punturo, R. (2015) - The Calabria–Peloritani Orogen, a composite terrane in Central Mediterranean; its overall architecture and geodynamic significance for a pre- Alpine scenario around the Tethyan basin - Per. Mineral. 84: 701–749. doi:10.2451/2015PM0446

Cirrincione, R., Fiannacca, P., Lustrino, M., Romano, V., Tranchina, A., and Villa, I. M. (2016) - Enriched asthenosphere melting beneath the nascent North African margin: trace element and Nd isotope evidence in middle–late Triassic alkali basalts from central Sicily (Italy) - Int. J. Earth Sci. 105: 595–609. doi: 10.1007/s00531-015-1190-2

Clarke, D.B., Rottura, A. (1994) - Garnet-forming and garnet-eliminating reactions in a quartz diorite intrusion at Capo Vaticano, Calabria, Southern Italy - The Canadian Mineralogist 32: 623–635.

Clemens, J.D., Stevens, G. (2012) - What controls chemical variation in granitic magmas? Lithos 134–135, 317–329.

Compston, W., Williams, I. S., & Meyer, C. (1984). U-Pb geochronology of zircons from lunar breccia 73217 using a sensitive high mass-resolution ion microprobe. Journal of Geophysical Research: Solid Earth, 89(S02), B525-B534.

Corfu, F., & Stott, G. M. (1993). Age and petrogenesis of two late Archean magmatic suites, northwestern Superior Province, Canada: zircon U–Pb and Lu–Hf isotopic relations. Journal of Petrology, 34(4), 817-838.

De La Roche, H., Leterrier, J., Grandclaude, P., & Marchal, M. (1980). A classification of volcanic and plufonic rocks using r1r2-diagram and major-element an al yses-its relationships with current nomenclature. Chemical geology, 29, 183-210.

De Gregorio, S., Rotolo, S.G., Villa, I.M. (2003) - Geochronology of the medium to high grade metamorphic units of the Peloritani Mts., Sicily - International Journal of Earth Sciences 92: 852–872.

Debon, F., & Le Fort, P. (1983). A chemical–mineralogical classification of common plutonic rocks and associations. Earth and Environmental Science Transactions of the Royal Society of Edinburgh, 73(3), 135-149.

Del Moro, A., Paglionico, A., Piccarreta, G., Rottura, A. (1986) – Tectonic structure and evolution of the Serre, Calabrian Arc, southern Italy: geological, petrological and radiometric evidence – *Tectonophysics,* **124**: 223-238. Del Moro, A., Fornelli, A., Paglionico, A. (1994) - K-feldspar megacrystic suite in the Serre (Southern Calabria–Italy) - Periodico di Mineralogia 63: 19–33.

Del Moro, A., Fornelli, A., Piccarreta, G. (2000) - Disequilibrium melting in granulite–facies metasedimentary rocks of the Northern Serre (Calabria—Southern Italy) - Mineralogy and Petrology 70: 89–104.

De Paolo, D.J. (1981) - Trace element and isotopic effects of combined wallrock assimilation and Fractional crystallization - Earth Planet Sci Lett 53:189–202.

Deer, W.A., Howie, R.A., Zussman, J.(1963). Rock-Forming Minerals. Vol. 4: Framework Silicates. Longman, London, 435 pp

Dhuime, B., Hawkesworth, C., Cawood, P., 2011. When continents formed. Science 331,154–155.

Di Vincenzo, G., Carosi, R., Palmeri, R. (2004) - The Relationship between Tectono-metamorphic Evolution and Argon Isotope Records in White Mica: Constraints from *in situ* ^{40}Ar–^{39}Ar Laser Analysis of the Variscan Basement of Sardinia - *Journal of Petrology* 45 (5):1013–1043, https://doi.org/10.1093/petrology/egh002

Dodge, F., Kistler, R., (1990) - Some additional observations on inclusions in the granitic rocks of the Sierra Nevada. Journal of Geophysical Research 95, 17841–17848.

Donaire, T., Pascual, E., Pin, C., Duthou, J.-L., (2005) - Microgranular enclaves as evidence of rapid cooling in granitoid rocks: the case of the Los Pedroches granodiorite, Iberian Massif, Spain. Contributions to Mineralogy and Petrology 149, 247–265.

Ferla, P. (2000) - A model of continental crustal evolution in the geological history of the Peloritani Mountains (Sicily) - Memorie della Società Geologica Italiana 55: 87–93.

Ferla, P. & Meli, C. (2007) - Petrogenesis of tourmaline rocks associated with Fe-carbonate-graphite metapelite, metabasite and strata-bound polymetallic sulphide mineralisation, Peloritani Mountains, Sicily, Southern Italy - Lithos 99 (3-4): 266-288.

Festa, V., Caggianelli, A., Langone, A., Prosser, G. (2013) - Time-space relationships among structural and metamorphic aureoles related to granite emplacement: A case study from the Serre Massif (southern Italy) - Geological Magazine, 150 (3): 441-454.

Fiannacca, P., Brotzu, P., Cirrincione, R., Mazzoleni, P., Pezzino, A. (2005a) - Alkali metasomatism as a process for trondhjemite genesis: evidence from Aspromonte Unit, northeastern Peloritani, Sicily. Mineralogy and Petrology 84: 19–45.

Fiannacca, P., Williams, I. S., Cirrincione, R., Pezzino, A. (2008) – Crustal contributions to Late-Hercynian peraluminous magmatism in the Southern Calabria-Peloritani Orogen, Southern Italy: petrogenetic inferences and the Gondwana connection. – *Journ. Petrol.* **48***:* 1497-1514

Fiannacca, P., Williams, I.S., Cirrincione, R., Pezzino, A. (2013) - The augen gneisses of the Peloritani Mountains (NE Sicily): granitoid magma production during rapid evolution of the northern Gondwana margin at the end of the Precambrian - Gondwana Research 23: 782–796.

Fiannacca, P., Cirrincione, R., Bonanno, F., Carciotto, M.M. (2015) - Source-inherited compositional diversity in granite batholiths: The geochemical message of Late Paleozoic intrusive magmatism in central Calabria (southern Italy) - Lithos 236–237: 123–140.

Fiannacca, P., Williams, I.S., Cirrincione, R. (2017) - Timescales and mechanisms of batholith construction: Constraints from zircon oxygen isotopes and geochronology of the late Variscan Serre Batholith (Calabria, southern Italy) - Lithos 277: 302-314.

Fiannacca, P., Williams, I.S., Cirrincione, R., Pezzino, A. (2019) - Poly-orogenic melting of metasedimentary crust from a granite geochemistry and inherited zircon perspective (southern calabria-peloritani orogen, Italy) - Frontiers Earth Sci., https://doi.org/10.3389/feart.2019.00119

Fornelli, A., Caggianelli, A., Del Moro, A., Bargossi, G.M., Paglionico, A., Piccarreta, G., Rottura, A., (1994) - Petrology and evolution of the Central Serre granitoids (Southern Calabria–Italy) - Periodico di Mineralogia 63: 53–70.

Fornelli, A., Langone, A., Micheletti, F., & Piccarreta, G. (2011). Time and duration of Variscan high-temperature metamorphic processes in the south European Variscides: constraints from U-Pb chronology and trace element chemistry of zircon. Mineralogy and Petrology, 103(1-4), 101-122.

Fornelli, A., Langone, A., Micheletti, F., Pascazio, A., Piccarreta, G. (2014) – The role of trace element partitioning between garnet, zircon and orthopyroxene on the interpretation of zircon U–Pb ages: an example from high-grade basement in Calabria (Southern Italy) – International Journal of Earth Sciences (Impact Factor: 2.26). 03/2014; 103(2).

Fornelli, A., Piccarreta, G., Del Moro, A., & Acquafredda, P. (2002). Multi-stage melting in the lower crust of the Serre (Southern Italy). Journal of Petrology, 43(12), 2191-2217.

Frost, B.R., Frost, C.D. (2008). A geochemical classification for feldspathic igneous rocks - Journal of Petrology 49: 1955–1969.

Frost, B. R., Barnes, C. G., Collins, W. J., Arculus, R. J., Ellis, D. J., Frost, C, D. (2001) - A geochemical classification for granitic rocks – J. Petrol. 42: 2033-2048.

Gardien, V., Lardeaux, J.-M., Ledru, P., Allemand, P., Guillot, S. (1997) - Metamorphism during late orogenic extension: insights from the French Variscan belt- Bulletin de la Société Géologique de France 168 (3): 271–286.

Graessner, T., Schenk, V., Brocker, M., Mezger, K. (2000) - Geochronological constraints on the timing of granitoid magmatism, metamorphism and post- metamorphic cooling in the Hercynian crustal cross-section of Calabria - Journal of Metamorphic Geology 18: 409–421.

Griffin, W., Wang, X., Jackson, S., Pearson, N., O'Reilly, S. Y., Xu, X. & Zhou, X. (2002) - Zircon chemistry and magma mixing, SE China: in-situ analysis of Hf isotopes, Tonglu and Pingtan igneous complexes. Lithos, 61(3), 237-269.

Gromet, P., & Silver, L. T. (1987) -REE variations across the Peninsular Ranges batholith: Implications for batholithic petrogenesis and crustal growth in magmatic arcs. Journal of Petrology, 28(1), 75-125.

Hawkesworth, C., et al., 2010. The generation and evolution of the continental crust. Journal of the Geological

Hueck, M., Basei, M. A. S., & de Castro, N. A. (2020) - Tracking the sources and the evolution of the late Neoproterozoic granitic intrusions in the Brusque Group, Dom Feliciano Belt, South Brazil: LA-ICP-MS and SHRIMP geochronology coupled to Hf isotopic analysis. Precambrian Research, 338, 105566.

Ioppolo, S., Puglisi, G. (1989) - Petrological study of some Hercynian metamorphics from the NE Peloritani Mountains, Sicily [Studio petrologico di alcune metamorfiti erciniche dei Monti Peloritani Nord Orientali (Sicilia)] - Rendiconti - Società Italiana di Mineralogia e Petrologia, 43 (3): 643-656.

Janoušek, V., Farrow, C.M., Erban, V. (2006) - Interpretation of whole-rock geochemical data in igneous geochemistry: Introducing Geochemical Data Toolkit (GCDkit) - Journal of Petrology 47(6): 1255-1259.

Janoušek, V., Moyen, J.-F., Martin, H., Erban, V., Farrow, C.M. (2016) - Geochemical Modelling of Igneous Processes – Principles And Recipes in R Language – Springer Geochemistry.

Langone, A., Caggianelli, A., Festa, V., Prosser, G. (2014) – Time Constrain on the Building of the Serre Batholith: Consequences for the Thermal Evolution of the Hercynian Continental Crust Exposed in Calabria (Southern Italy) – *The Journal of Geology,* **122**: 183-199.

Leake, B.E (1978) – Nomenclature of amphiboles – American Mineralogist63 (11-12): 1023-1052.

LeBel L., Cocherie A., Baubron J.C., Fouillac A.M., Hawkesworth C.J. (1985) - A high-K, mantle derived plutonic suite from 'Linga', near Arequipa (Peru) - J. Petrol., 26 (1985), pp. 124-148

Ledru, P., Lardeaux, M., Santallier, D., Autran, A., Quenardel, J.M., Floc'h, J.P., Maillet, N., Marchand, Ploquin, A. (1989) - Où sont les Nappes dans le Massif Central Francais? Bulletin de la Societe Geologique de France - 5 (3): 605–618.

Liu, Y., Hu, Z., Zong, K., Gao, C., Gao, S., Xu, J., & Chen, H. (2010). Reappraisement and refinement of zircon U-Pb isotope and trace element analyses by LA-ICP-MS. Chinese Science Bulletin, 55(15), 1535-1546.

Lombardo, R., Fiannacca, P., & Cirrincione, R. (2020). Modellistica geochimica della diversità del magma granitoide al Promontorio di Capo Vaticano (Serre Batholith, Italia meridionale). Geochimica , 125599.

Ludwig, K. R. (2003). Isoplot 3.00: A geochronological toolkit for Microsoft Excel. Berkeley Geochronology Center Special Publication, 4, 70.

Ludwig, K. R. (2011). Isoplot/Ex Version 4: A Geochronological Toolkit for Microsoft Excel: Geochronology Center. Berkeley, California, USA.

Maccarrone, E., Paglionico, A., Piccarreta, G., Rottura, A. (1983) - Granulite-amphibolite facies metasediments from the Serre (Calabria, Southern Italy): their protoliths and the processes controlling their chemistry – Lithos 16 (2): 95-111.

Matte, P., 1986. Tectonics and plate-tectonics model for the Variscan Belt of Europe. Tectonophysics 126 (2–4), 329–374.

McDonough, W. & Sun, S.S. (1995) - The composition of the Earth - Chem Geol 120: 223-253.

Micheletti, F., Barbey, P., Fornelli, A., Piccarreta, G., Deloule, E. (2007) - Latest Precambrian to Early Cambrian U–Pb zircon ages of augen gneisses from Calabria (Italy), with inference to the Alboranmicroplate in the evolution of the peri-Gondwana terranes - International Journal of Earth Sciences 96: 843–860.

Micheletti, F., Fornelli, A., Piccarreta, G., Barbey, P., & Tiepolo, M. (2008). The basement of Calabria (southern Italy) within the context of the Southern European Variscides: LA-ICPMS and SIMS U–Pb zircon study. Lithos, 104(1-4), 1-11.

Middlemost, E. A. (1994). Naming materials in the magma/igneous rock system. Earth-Science Reviews, 37(3-4), 215-224.

Miller, J. S., Matzel, J. E., Miller, C. F., Burgess, S. D., & Miller, R. B. (2007). Zircon growth and recycling during the assembly of large, composite arc plutons. Journal of Volcanology and Geothermal Research, 167(1-4), 282-299.

Miller, C.F., Stoddard, E.F., Bradfish, L.J., Dollase, W.A. (1981) - Composition of plutonic muscovite: genetic implications - The Canadian Mineralogist 19 (1): 25–34.

Moita P., J.F. Santos, M.F. Pereira, M.M. Costa, F. Corfu (2015) - The quartz-dioritic Hospitais intrusion (SW Iberian Massif) and its mafic microgranular enclaves — evidence for mineral clustering Lithos, 224-225 (2015), pp. 78-100

Monaco, C. & Tortorici, L. (2000) – Active faulting in the Calabrian arc and eastern Sicily – Journal of Geodynamics 29 (3-5): 407:424.

Moyen, J.-F., Laurent, O., Chelle-Michou, C., Couzinié, S., Vanderhaeghe, O., Zeh, A., Villaros, A., Gardieng, V. (2017) - Collision vs. subduction-related magmatism: Two contrasting ways of granite formation and implications for crustal growth – Lithos 277: 154-177.

Navas-Parejo, P., Somma, R., Martín-Algarra, A., Perrone, V., Rodríguez-Cañero, R. (2009) - First record of Devonian orthoceratid-bearing limestones in southern Calabria (Italy) - Comptes Rendus Palevol 8: 365–373.

Ohta, T., & Arai, H. (2007). Statistical empirical index of chemical weathering in igneous rocks: A new tool for evaluating the degree of weathering. Chemical Geology, 240(3-4), 280-297.

Payne, J. L., McInerney, D. J., Barovich, K. M., Kirkland, C. L., Pearson, N. J., & Hand, M. (2016). Strengths and limitations of zircon Lu-Hf and O isotopes in modelling crustal growth. Lithos, 248, 175-192.

Patchett, P. J., & Tatsumoto, M. (1981). A routine high-precision method for Lu-Hf isotope geochemistry and chronology. Contributions to Mineralogy and Petrology, 75(3), 263-267.

Patiño-Douce, A. E.. What do experiments tell us about the relative contributions of crust and mantle to the origin of granitic magmas?. Geological Society, London, Special Publications, 1999, 168.1: 55-75.

Patiño Douce, A. E., & Beard, J. S. (1995). Dehydration-melting of biotite gneiss and quartz amphibolite from 3 to 15 kbar. Journal of Petrology, 36(3), 707-738.

Peressini, G., Quick, J. E., Sinigoi, S., Hofmann, A. W., & Fanning, M. (2007). Duration of a large mafic intrusion and heat transfer in the lower crust: a SHRIMP U–Pb zircon study in the Ivrea–Verbano Zone (Western Alps, Italy). Journal of Petrology, 48(6), 1185-1218.

Pin, C., Binon, M., Belin, M., Barbarin, B., Clemens, J., (1990) - Origin of microgranular enclaves in granitoids: equivocal Sr–Nd evidence from Hercynian rocks in the Massif Central (France). Journal of Geophysical Research 95, 17821–17828.

Pitcher K.W., (1982) – in: Hsu, K. (ed.), Mountain Building Processes. Academic Press, London, pp. 19-40.

REID, J., EVANS, O. C., FATES, D. G. (1983) – Magma mixing in granitic rocks of the central Sierra Nevada: How important is it? – *Geology*, **21:** 587-590.

Ricci, C.A. (1992) - From crustal thickening to exhumation: petrological, structural and geochronological records in the crystalline basement of the northern Sardinia -Contribution to Geology of Italy 276(5): 187-197.

Romano, V., Cirrincione, R., Fiannacca, P., Lustrino, M., Tranchina, A. (2011) - Late-Hercynian post-collisional dyke magmatism in central Calabria (Serre Massif, southern Italy) - Periodico di Mineralogia 80: 489–515.

Rossetti, F., Faccenna, C., Goffè, B., Monié, P., Argentieri, A., Funiciello, R., Mattei, M. (2001) - Alpine structural and metamorphic signature of the Sila Piccola Massif nappe stack (Calabria, Italy): Insights for the tectonic evolution of the Calabrian Arc – Tectonics 20 (1): 112-133.

Rottura, A., Bargossi, G.M., Caironi, V., Del Moro, A., Maccarrone, E., Macera, P., Paglionico, A., Petrini, R., Piccarreta, G. (1989) - Petrology and geochemistry and Sr, Nd isotopes of contrasting Hercynian granitoids from the southern Calabrian Arc (southern Italy) - Mineralogica et Petrographica Acta 32: 1–36.

Rottura, A., Bargossi, G.M., Caironi, V., Del Moro, A., Maccarrone, E., Macera, P., Paglionico, A., Perrini, R., Piccarreta, G., Poli, G. (1990) - Petrogenesis of contrasting Hercynian granitoids from the Calabrian Arc, Southern Italy - Lithos 24: 97–119.

Rottura, A., Del Moro, A., Pinarelli, L., Petrini, R., Peccerillo, A., Caggianelli, A., Bargossi, G.M., Piccarreta, G. (1991) - Relationships between intermediate and acidic rocks in orogenic granitoid suites: petrological, geochemical and isotopic (Sr, Nd, Pb) data from Capo Vaticano (southern Calabria, Italy) - Chemical Geology 92: 153–176.

Rudnick, R.L., 1995. Making continental crust. Nature 378, 571–578

Rudnick, R.L., Gao, S., 2003. Composition of the continental crust. In: Holland, H.D.,Turekian, K.K. (Eds.), Treatise of Geochemistry. Elsevier, Amsterdam, pp. 1–64.

Sato, K., Tassinari, C. C. G., Basei, M. A. S., Siga, O., Onoe, A. T., & De Souza, M. D. (2014). Sensitive High Resolution Ion Microprobe (SHRIMP IIe/MC) of the Institute of Geosciences of the University of São Paulo, Brazil: Analytical method and first results. Geologia USP - Serie Cientifica, 14(3), 3–18. https://doi.org/10.5327/Z1519-874X201400030001

Shand, S.J. (1943) - Eruptive rocks. Their genesis, composition, classification, and their relation to ore-deposits with a chapter on meteorite - John Wiley & Sons, New York.

Schenk, V. (1980) - U-Pb and Rb-Sr radiometric dates and their correlation with metamorphic events in the granulite–facies basement of the Serre, Southern Calabria (Italy) - Contributions to Mineralogy and Petrology 73: 23–38.

Schenk, V. (1984) - Petrology of felsic granulites, metapelites, metabasics, ultramafics and metacarbonates from southern Calabria (Italy): prograde metamorphism, uplift and cooling of a former lower crust - Journal of Petrology 25: 255–298.

Schenk, V. (1989) - *P-T-t* path of the lower crust in The Hercynian fold belt of southern Calabria - Geological Society, London, Special Publications, 43: 337-342.

Schenk, V. (1990) - The exposed crustal cross section of southern Calabria, Italy: structure and evolution of a segment of Hercynian crust - In: Fountain, D.M., Salisbury, M.H. (Eds.), Exposed Cross-Sections of the Continental Crust. Kluwer, Dordrecht The Netherlands, pp. 21–42.

Scherer, E. E., Whitehouse, M. J., & Munker, C. (2007). Zircon as a monitor of crustal growth. Elements, 3(1), 19-24.

Siégel, C., Bryan, S. E., Allen, C. M., & Gust, D. A. (2018). Use and abuse of zircon-based thermometers: a critical review and a recommended approach to identify antecrystic zircons. Earth-Science Reviews, 176, 87-116.

Sircombe, K. N. (2000). Quantitative comparison of large sets of geochronological data using multivariate analysis: a provenance study example from Australia. Geochimica et Cosmochimica Acta, 64(9), 1593-1616.

Smith, P. E., Tatsumoto, M., & Farquhar, R. M. (1987). Zircon Lu-Hf systematics and the evolution of the Archean crust in the southern Superior Province, Canada. Contributions to Mineralogy and Petrology, 97(1), 93-104.

Söderlund, U., Patchett, P. J., Vervoort, J. D., & Isachsen, C. E. (2004). The 176Lu decay constant determined by Lu–Hf and U–Pb isotope systematics of Precambrian mafic intrusions. Earth and Planetary Science Letters, 219(3-4), 311-324.

Speer, J. A. (1987). Evolution of magmatic AFM mineral assemblages in granitoid rocks; the hornblende+ melt= biotite reaction in the Liberty Hill Pluton, South Carolina. American Mineralogist, 72(9-10), 863-878.

Springer, W., & Seck, H. A. (1997). Partial fusion of basic granulites at 5 to 15 kbar: implications for the origin of TTG magmas. Contributions to Mineralogy and Petrology, 127(1-2), 30-45.

Stevens, G., Villaros, A., Moyen, J.F. (2007) - Selective peritectic garnet entrainment as the origin of geochemical diversity in S-type granite - Geology 35 (1): 9-12.

Stussi, J. M., & Cuney, M. (1996). Nature of biotites from alkaline, calc-alkaline and peraluminous magmas by Abdel-Fattah M. Abdel-Rahman: a comment. Journal of Petrology, 37(5), 1025-1029.

Traversa, G., Ronca, S.S., Del Moro, A., Pasquali, G., Buraglini, N. & Giancarlo Barabino, G. (2003) - Late to post-Hercynian dyke activity in the Sardinia-Corsica Domain: A transition from orogenic calc-alkaline to anorogenic alkaline magmatism - Boll. Soc. Geol. It., Volume speciale n. 2: 131-152.

Van de Flierdt, T., Hoernes, S., Jung, S., Masberg, P., Hoffer, E., Schaltegger, U., & Friedrichsen, H. (2003). Lower crustal melting and the role of open-system processes in the genesis of synorogenic quartz diorite–granite–leucogranite associations: constraints from Sr–Nd–O isotopes from the Bandombaai Complex, Namibia. Lithos, 67(3-4), 205-226.

Vervoort, J. D., & Blichert-Toft, J. (1999). Evolution of the depleted mantle: Hf isotope evidence from juvenile rocks through time. Geochimica et cosmochimica acta, 63(3-4), 533-556.

Villaseca, C., Barbero, L., & Herreros, V. (1998). A re-examination of the typology of peraluminous granite types in intracontinental orogenic belts. Earth and Environmental Science Transactions of The Royal Society of Edinburgh, 89(2), 113-119.

von Raumer, J.F., Stampfli, G.M., Bussy, F. (2002) – Organization of pre-Variscan basement areas at the north-Gondwana margin – Intern. J. of Earth Science 91: 35-52.

von Raumer, J.F., Stampfli, G.M., Bussy, F. (2003) – Gondwana-derived microcontinents – the constituents of the Variscan and Alpine collisional orogens – Tectonophysics 365(1-4): 7-22.

von Raumer, J.F., Bussy, F., Schaltegger, U., Schulz, B., Stampfli, G.M. (2013) - Pre-Mesozoic Alpine basements-their place in the European Paleozoic framework - Bulletin of the Geological Society of America 125: 89–108.

Watson, E. B., & Harrison, T. M. (1983). Zircon saturation revisited: temperature and composition effects in a variety of crustal magma types. Earth and Planetary Science Letters, 64(2), 295-304.

White, A.J.R. & Chappell, B.W. (1977) - Ultrametamorphism and granitoid genesis – Tectonophysics 4 (1–2): 7-22.

Williams, I.S., Fiannacca, P., Cirrincione, R., Pezzino, A. (2012) - Peri-Gondwanan origin and early geodynamic history of NE Sicily: a zircon tale from the basement of the Peloritani Mountains - Gondwana Research 22: 855–865.

Wolf, M. B., & Wyllie, P. J. (1994). Dehydration-melting of amphibolite at 10 kbar: the effects of temperature and time. Contributions to Mineralogy and Petrology, 115(4), 369-383.

Yavuz, F., Yildirim, D.K. (2018) – A Windows program for calculation and classification of epidote-supergrup minerals – Periodico di Mineralogia 87 (3).

Zeck, H. P., & Whitehouse, M. J. (2002). Repeated age resetting in zircons from Hercynian–Alpine polymetamorphic schists (Betic–Rif tectonic belt, S. Spain)—a U–Th–Pb ion microprobe study. Chemical Geology, 182(2-4), 275-292.

APPENDIX – Methods

1.1 ICP-AES and ICP-MS

The whole-rock geochemical analysis have been performed at the ALS Laboratory of Laughrea (Ireland).

The Inductively Coupled Plasma Atomic Emission Spectrometer (ICP-AES) was used to obtain the major rock-forming elements, whereas the Inductively Couple Plasma Mass Spectrometer (ICP – MS) was used for the trace elements.

Two different sample preparation have been followed for both methods.

To obtain the major elements, a prepared sample (0.200 g) was added to lithium metaborate/lithium tetraborate flux (0.90 g), mixed well and fused in a furnace at 1000°C. The resulting melt is then cooled and dissolved in 100 mL of 4% nitric acid/2% hydrochloric acid. This solution is then analyzed by ICP-AES and the results are corrected for spectral inter-element interferences.

To obtain the trace elements, a Lithium Borate ($LiBO_2/Li_2B_4O_7$) fusion have been applied. A powder prepared sample (0.100 g) is added to lithium metaborate/lithium tetraborate flux ($LiBO_2/Li_2B_4O_7$), mixed well and fused in a furnace at 1025°C. The resulting melt is then cooled and dissolved in an acid mixture containing nitric, hydrochloric and hydrofluoric acids. This solution is then analyzed by inductively coupled plasma - mass spectrometry.

The data are certificated by ISO 17205:2005.

1.2 Microprobe analysis

The mineralogical analysis was obtained at Laboratorio da Microsonda Elettronica in Sao Paulo (USP).

Thin section of about 100 µm was preparated in the Laboboratio de tratamento de amostra and covered by a 25 nnm thick carbon coat. The analysis was carried using a JEOL JXA-FE-8530 probe and a NORAN/Voyager EDS and WDS automation system. Instrumental conditions were set at 15 kV, 300 nA, and 2-5 mm for the accelerating voltage, beam current, and diameter, respectively, in order to improve the spatial resolution, X-ray signals and absorption corrections.

1.3 Geochronology: U-PB SHRIMP analysis and LA-ICP-MS

Zircon crystal was extracted in the Laboratorio de Chimica at University of Sao Paulo. Zircon were separated using the magnetic and the liquid methods. Zircon were arranged in row and covered by expody resin before to be polished to reveal the internal structure. The catholumisence and transmitted images were used to choose the spots.

SHRIMP Geochronology

Age determinations on the SHRIMP were performed according to the standard procedures described in Compston et al. (1984), Williams (1998), Stern (1998) and Sircombe (2000). The analyses were performed using the configuration presented below:

- Primary beam analytical conditions: Kohler aperture = 120 µm; spot size = 30 µm and O_2 beam density = ~2.5–7 ηA (dependent of brightness aperture).
- Secondary beam analytical conditions: source slit = 80 µm; mass resolutions for 196 (Zr_2O), ^{206}Pb, ^{207}Pb, ^{208}Pb, ^{238}U, ^{248}(ThO) and ^{254}(UO) ranging between 5,000 and 5,500 (1%); and residues < 0.025; energy slit = open.

During acquisition, raster time was 2 minutes with spot size = 50 µm, plus 0.5 minutes of burning time, fixed at the center. Analytical ratio was 1 standard to 4 zircon samples.

Data was reduced using SQUID 1.06. Common lead corrections used ^{204}Pb according to Stacey & Kramer (1975). Temora 2 was taken as the ^{206}Pb/^{238}U age reference (416.78 Ma, Black et al. 2004), and SL13 zircon (238 ppm) was used as the U composition reference. Measurements of Temora 2, Z6266 and OG1 standards at the Geochronological Research Center of the University of São Paulo (CPGeo – USP) yield concordia ages of 416.7±2.3 (n=18, MSWD=0.105), 561.9±1.0 (n=53, MSWD=0.14) and 3462.6±5.1 Ma (n=16, MSWD=0.119), respectively (Sato et al. 2014). These ages are comparable to international standard ages reported by Black et al. (2004), Stern & Amelin (2003) and Stern et al. (2009), indicating high accuracy and precision of the SHRIMP method in use at the CPGeo. More details about analytical procedures, data acquisition and processing are presented by Sato et al. (2014).

Lu-Hf isotopes

All Lu–Hf zircon analyses were carried out on a Neptune multicollector inductively coupled plasma mass spectrometer equipped with an Analyte G2 excimer laser ablation system.

Lu–Hf isotopic analyses were performed in the same zircon grains that were previously dated by U-Pb, as close as possible to the location of the original spot for U-Pb analyses.

The laser spot parameters were: 39 µm in diameter; ablation time of 60s; repetition rate of 7 Hz and He was used as the carrier gas. The 9 isotopes: 171Yb, 173Yb, 174(Hf+Yb+Lu), 175Lu, 176(Hf+Yb+Lu), 177Hf, 178Hf, 179Hf and 181Ta were collected simultaneously, on Faraday cups.

The analysis rourtin consist of:

- A blanck analysis
- Two standard GJ
- Eleven measurements
- Two standard GJ

The data correction are as follow:

- The blank is only monitored, not subtracted;
- Yb mass bias correction (βYb) is based on the $^{173}Yb/^{171}Yb$ ratio;
- Hf mass bias correction (βHf) is based on the $^{179}Hf/^{177}Hf$ ratio;
- Lu mass bias correction adopts: βLu = βYb;
- At the end, a Python program renormalizes the sample's 176Hf /177Hf ratio, based on the difference between the average value of the GJ standard and its expected value (0.282015; Y.S. Liu et al., 2010).
- This Python program calculates εHf, tDM etc. using formulas from Yang et al., 2007.

Appedix. Table - ***Appendix. Table 1*** *– Modal abundance (% vol.) of granitoids in Capo Vaticano Promontory. Mineral abbreviations by Siivola and Schimd, 2007.*

Sample name	Rock type	Pl	Cum	Hbl	Bt	Qrz	Chl	Ep	Aln	Zrn	Ap	Ilm	Ms	Orto
CVP18	*Hybrid quartz-diorite*	80.00	5.00	7.50	1.50	1.00	3.00	-	-	0.50	0.50	1.00	-	-
CVP16	*Hybrid quartz-diorite*	80.5	1	6	5	2	2	0.5	-	-	-	2	-	-
CVP15	*Hybrid quartz-diorite*	89	-	-	5	3	-	-	-	1	1	1	-	-
CVP20	*Quartz-diorite*	75	-	2	15	4.5	-	2	1	0.2	0.2	0.1	-	-
CVP21	*Quartz-diorite*	65	-	7	12	10	-	5	0.5	0.2	0.1	0.2	-	-
CVP22	*Quartz-diorite*	74	-	5.5	8.5	5	1	4.5	-	0.5	0.5	0.5	-	-
CVP27	*Quartz-diorite*	65	-	5	17	10	-	0.2	-	0.2	-	0.1	-	2.5
CVP30	*Quartz-diorite*	53	-	15	20	5	1	3	1	0.5	0.5	1	-	-
CVP31	*Quartz-diorite*	67	-	5	15	10	-	2	-	0.5	-	0.5	-	-
CVP32	*Quartz-diorite*	70	-	5	12.5	7.5	-	5	-	-	-	-	-	-
CVP12	*Quartz-diorite*	61	-	-	20	14	-	1	-	0.5	0.3	0.2	1	2
CVP10	*Tonalite*	55	-	-	23	16	-	1	-	0.5	0.2	0.3	2	2
CVP11	*Tonalite*	60	-	-	25	10	-	2	2	0.5	-	0.4	0.1	-
CVP13	*Tonalite*	60	-	-	20	15	-	2	1	0.3	0.2	0.5	1	-
CVP14	*Tonalite*	55	-	-	27.7	15	-	1	-	0.1	0.1	0.1	1	-
CVP24	*Tonalite*	54	-	-	25	15	-	3	-	0.3	0.2	0.1	0.4	2
CVP26	*Tonalite*	57	-	-	25	15	-	2	0.5	0.2	0.1	0.1	0.1	-
CVP28	*Tonalite*	45	-	5.5	25	17	-	5	2	0.2	0.2	0.1	-	-
CVP29	*Tonalite*	58	-	0.1	17	20	0.1	3	1	0.5	0.1	0.2	-	-
CVP33	*Tonalite*	36.5	-	7.5	38	15	-	2.5	-	0.2	0.3	-	-	-
CVP34	*Tonalite*	60	-	-	15	20	-	3.5	-	0.5	0.5	0.5	-	-
CVP35	*Tonalite*	60	-	-	23	15	-	1	-	0.5	-	0.5	-	-
CVP38	*Tonalite*	55	-	2	25	15	-	2	-	0.4	0.5	0.1	-	-
CVP39	*Tonalite*	60	-	3	15	18	-	3	-	0.5	-	0.5	-	-
CVP40	*Tonalite*	52	-	-	18	25	-	2	-	0.5	0.5	1	1	-
CVP41	*Tonalite*	58	-	-	20	15	-	1	1	0.5	1	0.5	3	-
CVP42	*Tonalite*	60	-	-	22	10	-	3	1	0.5	1	0.5	2	-
CVP1	*Leuco-tonalite*	62	-	-	5	25	-	-	-	0.5	-	-	5	2.5
CVP3	*Leuco-tonalite*	55.5	-	-	8	30	-	-	-	0.5	-	-	5	1
CVP4	*Leuco-tonalite*	60	-	-	15.5	20	-	-	-	0.5	0.5	-	3	0.5

***Appendix. Table 2**– Microprobe analysis of Amphibole in the Capo Vaticano Promontory rocks.*

Rock type	Hybrid quartz-diorite						
Sample name	CVP16						
Mineral acronym	*Anf. 1.1*	*Anf. 1.2*	*Anf. 1.3*	*Anf. 1.4*	*Anf. 1.6*	*Anf. 1.7*	*Anf1./Pl2 contact*
SiO_2	29.46	40.48	41.43	40.84	40.93	33.70	40.89
TiO_2	0.27	0.23	0.15	0.18	0.17	2.81	0.17
Al_2O_3	18.86	17.65	17.08	17.95	17.21	18.25	17.96
FeO	23.17	18.01	17.96	18.14	18.61	18.34	18.11
MnO	0.09	0.27	0.25	0.24	0.22	0.10	0.23
MgO	14.01	7.49	7.84	7.20	7.29	11.93	7.28
CaO	0.30	11.23	11.39	11.31	11.54	3.35	11.35
Na_2O	0.04	1.31	1.16	1.29	1.31	0.09	1.20
K_2O	0.32	0.36	0.34	0.38	0.43	3.30	0.45
F	0.08	0.07	0.15	0.03	0.05	0.27	0.10
Cl	0.01	0.13	0.08	0.08	0.17	0.69	0.11
Cr_2O_3		0.01	0.00	0.01	0.03		
Tot	86.61	97.24	97.84	97.65	97.95	92.83	97.85

Rock type	S. Maria quartz-diorite								
Sample name	CVP20								
Mineral acronym	*Anf .1.3*	*Anf .1.4*	*Anf. 2.1*	*Anf. 2.2*	*Anf. 2.3*	*Anf. 2.4*	*Anf.2.5*	*Anf .3.1*	*Anf .3.2*
SiO_2	45.87	46.09	45.44	46.12	43.13	43.57	46.52	52.76	46.1
TiO_2	0.8518	0.8507	0.6691	0.542	0.3759	0.36	0.4439	0.0137	0.6361
Al_2O_3	9.88	9.82	10.03	10.15	12.12	12.14	10.31	20.17	10.44
FeO	17.62	17.84	18.2	18.09	16.56	16.93	18.05	7.54	18.45
MnO	0.6565	0.6175	0.576	0.6025	0.4643	0.4556	0.5589	0.2135	0.6669
MgO	9.57	9.41	9.42	9.42	7.6	7.64	9.21	3.32	9.15
CaO	11.39	11.64	11.66	11.55	10.48	10.62	11.59	2.34	11.34
Na_2O	0.9622	0.7851	0.9389	0.9357	0.7439	0.826	0.8011	3.53	1.057
K_2O	0.6743	0.7587	0.8474	0.806	1.46	1.45	0.9674	4.87	0.7172
F	0.0646	0.0529	0.0557	0.0884	0.0392		0.0576	0.042	0.0233
Cl	0.036	0.0234	0.0703	0.0688	0.1094	0.0531	0.0407	0.0367	0.0328
Cr_2O_3	0.0343		0.0036		0.0217		0.0045		0.0153
Tot	97.61	97.89	97.91	98.37	93.10	94.04	98.55	94.84	98.63

Rock type	S. Maria quartz-diorite			Briatico quartz-diorite				
Sample name	CVP20			CVP27				
Mineral acronym	*Anf .3.4*	*Anf .3.5*	*Anf. 3.6*	*Anf 1.1*	*Anf . 1.2*	*Anf 1.3*	*Anf 1.4*	*Anf 2.2*
SiO_2	46.34	45.32	47.44	40.07	42.19	41.35	34.65	43.89
TiO_2	0.5013	0.5531	0.5016	0.5512	0.1316	0.054	0.7258	0.338
Al_2O_3	9.43	11.21	10.43	16.76	16.81	21.04	19.95	14.04
FeO	17.95	18.07	17.51	18.61	19	18.58	19.52	17.09
MnO	0.5554	0.5256	0.5267	0.5943	0.5671	0.4517	0.2502	0.5714
MgO	9.97	8.9	8.8	7.3	7.03	5.62	12.09	8.8
CaO	11.8	11.79	11.26	11.09	11.24	9.66	0.221	11.18
Na_2O	0.7888	0.8559	0.7465	1.2585	1.2643	1.337	0.0925	1.1156
K_2O	0.8195	1.04448	0.9366	0.5512	0.475	1.0671	6.48	0.0506
F	0.0749	0.1563	0.0891	0.0185	0.0841	0	0.1218	0.105
Cl	5	0.0563	0.0078	0.1763	0.1464	0.1723	0.1392	0.0893
Cr_2O_3		0.009	0.0298			0.0162	0.0107	
Tot	103.2299	98.4907	98.2781	96.98	98.94	99.35	94.25	97.27

Rock type	Briatico quartz-diorite							
Sample name	CVP27							
Mineral acronym	*Anf 2.4*	*Anf 2.5*	*Anf 3.1*	*Anf 3.2*	*Anf 3.4*	*Anf 3.5*	*Anf 3.6*	*Anf 3.7*
SiO_2	40.08	39.74	49.07	45.21	50.7	52.57	53.62	53.69
TiO_2	1.4029	1.44	0.186	0.1932	0.1662	0.0581	0	0.0386
Al_2O_3	16.54	16.29	8.42	12.23	6.34	4.5	1.832	1.55
FeO	16.22	16.82	14.45	17.01	14.54	13.5	21.78	21.08
MnO	0.2813	0.776	0.6013	0.7009	0.7431	0.7285	2.13	1.73
MgO	9.17	9.44	12.31	10	13.36	14.67	15.7	16.23
CaO	3.96	3.94	11.06	11.11	11.19	11.41	2	2.13
Na_2O	0.4016	0.3716	0.7643	1.0793	0.5818	0.4169	0.1527	0.1558
K_2O	5.89	5.9	0.1531	0.4524	0.1436	0.0859	0.0311	0.0292
F	0.1218	0.1448	0.0407	0.0521	0.0675	0.0422	0.0159	0.0596
Cl	0.1047	0.1562	0.236	0.1003	0.0221	0.0427	0.0111	0.0254
Cr_2O_3		0.0036	0.0082	0.0054	0.0291	0.0091	0.0009	0.0106
Tot	94.17	95.02	97.30	98.14	97.88	98.03	97.27	96.73

Rock type	Briatico quartz-diorite						
Sample name	CVP27						
Mineral acronym	*Anf 3.8*	*Anf 3.9*	*Anf 3.10*	*Anf 5.2*	*Anf.5.3*	*Anf 6.2*	*Anf 6.3*
SiO_2	45.29	43.59	46.84	46.14	44.03	42.07	37.52
TiO_2	0.3582	0.1537	0.092	0.3075	0.4459	0.263	0.7979
Al_2O_3	12.16	16.22	10.89	11.74	13.63	15.92	18.71
FeO	16.63	15.65	15.65	16.43	17.27	17.86	17.56
MnO	0.7285	0.5442	0.5784	0.0754	0.6979	0.5623	0.2102
MgO	10.02	8.94	11.21	10.25	8.91	7.83	11.43
CaO	11.06	11.15	11.25	11.35	10.98	11.43	0.1532
Na_2O	1.0496	1.1534	0.8962	0.979	1.1219	1.2008	0.1357
K_2O	0.4988	0.536	0.29	0.4256	0.5032	0.6853	6.7
F	0	0	0.0253	0.0894	0.1256	0.0475	0.0728
Cl	0.0424	0.1538	0.1038	0.0754	0.1034	0.1704	0.1256
Cr_2O_3	0.0326	0.0235	0	0.0027	0	0.0081	0.0402
Tot	97.87	98.11	97.83	97.87	97.82	98.05	93.46

Rock type	Tonalite							
Sample name	CVP33							
Mineral acronym	*Anf. 1.1*	*Anf. 1.2*	*Anf. 1.3*	*Anf. 1.4*	*Anf. 1.5*	*Anf. 1.6*	*Anf. 1.7*	*Anf. 2.1*
SiO_2	43.84	44.71	45.37	45.85	43.07	43.11	42.75	46.29
TiO_2	0.7791	0.6904	0.8053	0.679	0.7364	0.4003	0.2639	0.7428
Al_2O_3	10.81	11.49	10.89	10.33	11.4	13.05	15.24	10.8
FeO	18.29	18.85	18.32	17.93	18.11	18.78	19	18.43
MnO	0.5506	0.5709	0.5481	0.5374	0.5035	0.4755	0.5184	0.5884
MgO	8.41	8.69	8.91	9.41	9.39	7.85	6.98	9.08
CaO	11.45	11.62	11.74	11.8	10.13	11.5	11.6	11.45
Na_2O	0.8288	0.9205	0.8062	0.7813	0.7558	0.9362	1.0901	0.8556
K_2O	1.0577	0.92	0.8053	0.7883	1.78	1.1321	0.8471	0.7801
F	0.0169	0.1012	0.0373	0.1044	0.103	0.1272	0	0.0537
Cl	0.0717	0.0671	0.0843	0.0703	0.0717	0.106	0.186	0.0906
Cr_2O_3	0	0.126	0.0135	0.0162	0.0395	0	0.0171	0.0126
Tot	96.10	98.76	98.33	98.30	96.09	97.47	98.49	99.17

Rock type	Tonalite							
Sample name	CVP33							
Mineral acronym	*Anf. 2.2*	*Anf. 2.3*	*Anf. 2.4*	*Anf. 2.5*	Anf 2.6	Anf 2.7	Anf 3.1	Anf 3.2
SiO_2	45.85	46.08	44.95	43.46	45.47	45.89	44.72	44.98
TiO_2	0.7521	0.7667	1.434	0.3878	0.69	0.87	0.70	0.53
Al_2O_3	9.96	10.03	10.37	11.12	10.13	10.18	10.83	11.31
FeO	17.96	18.18	17.81	17.98	18.13	18.02	18.20	18.48
MnO	0.5979	0.6195	0.5279	0.5192	0.61	0.52	0.57	0.60
MgO	9.31	9.48	8.94	9.09	9.59	9.42	9.24	8.92
CaO	11.65	11.53	11.38	11.49	11.58	11.64	11.51	11.46
Na_2O	0.7873	0.9312	0.7758	0.8953	0.87	0.82	0.84	0.94
K_2O	0.7819	0.7277	0.7457	0.9167	0.74	0.87	1.02	0.93
F	0.0181	0.1019		0.1198	0.08	0.00	0.13	0.05
Cl	0.0734	0.0266	0.0749	0.0624	0.07	0.04	0.04	0.09
Cr_2O_3	0	0	0.0189	0	0.03	0.00	0.04	0.02
Tot	97.74	98.47	97.03	96.04	97.99	98.28	97.84	98.33

Rock type	Tonalite							
Sample name	CVP33							
Mineral acronym	Anf 3.3	Anf 3.4	Anf 3.5	Anf 3.6	Anf 3.7	Anf. 4.1	Anf. 4.2	Anf. 4.3
SiO_2	44.51	44.31	43.33	43.76	42.57	42.51	44.16	45.04
TiO_2	0.50	0.49	0.473	0.3863	0.1942	0.2539	0.3272	0.5176
Al_2O_3	11.41	11.65	12.5	12.7	14.61	14.36	12.75	11.34
FeO	18.53	18.35	18.27	18.78	19.27	18.6	18.33	17.34
MnO	0.52	0.46	0.5166	0.4934	0.5059	0.4721	0.5025	0.5629
MgO	8.75	8.75	8.06	8.51	7.43	7.39	8.24	8.7
CaO	11.71	11.58	11.74	11.7	11.63	11.36	11.59	11.25
Na_2O	0.85	0.90	0.8068	0.9236	1.07	1.01	0.957	0.907
K_2O	0.89	1.21	1.29	1.28	0.9126	1.0942	0.9353	0.7913
F	0.08	0.00	0.0305	0.0542	0.209	0.0846	0	0
Cl	0.10	0.12	0.081	0.1091	0.092	0.0842	0.0827	0.0719
Cr_2O_3	0.02	0.00	0.0593	0	0	0.0126	0.0297	0.0189
Tot	97.87	97.82	97.16	98.70	98.49	97.23	97.90	96.54

Rock type	Tonalite							
Sample name	CVP33							
Mineral acronym	Anf. 4.4	Anf. 4.5	Anf. 4.6	Anf. 4.7	Anf. 4.8	Anf. 4.9	Anf. 4.10	Anf. 4.11
SiO_2	45.94	45.03	45.36	46.31	45.82	43.96	44.52	44.12
TiO_2	0.1389	0.614	0.4909	0.2833	0.5074	0.5449	0.2173	0.411
Al_2O_3	11.58	11.47	10.91	10.71	10.87	12.36	11.59	12.2
FeO	18.11	18.07	18.01	17.89	17.72	18.64	18.3	18.59
MnO	0.5373	0.5389	0.5775	0.5408	0.5214	0.5557	0.5088	0.51
MgO	8.83	8.98	9.1	9.45	9.28	8.31	8.89	8.52
CaO	11.82	11.75	11.64	11.69	11.73	11.59	11.74	11.76
Na_2O	1.0028	0.8834	0.9318	0.8487	0.8801	0.8578	0.8487	0.91
K_2O	0.3547	0.9613	0.7696	0.6005	0.7487	1.24	0.9898	1.22
F	0.0764	0.105	0.0552	0.0868	0.0238	0.1236	0.1002	0.1203
Cl	0.0469	0.0999	0.0703	0.0407	0.0595	0.0906	0.072	0.1226
Cr_2O_3	0.0126	0.0441	0	0.009	0.0162	0.0333	0.0054	0.0288
Tot	98.45	98.55	97.92	98.46	98.18	98.31	97.78	98.51

Rock type	Tonalite							
Sample name	CVP33							
Mineral acronym	Anf. 4.12	Anf. 4.13	Anf. 4.14	Anf. 4.15	Anf. 4.16	Anf. 4.17	Anf. 4.18	Anf. 4.19
SiO_2	44.47	44.07	43.69	43.8	43.71	54.01	51.34	43.17
TiO_2	0.4031	0.452	0.3204	0.3203	0.3383	0.0364	0.0624	0.2451
Al_2O_3	12.55	12.38	13.32	13.14	12.9	1.0185	4.01	13.8
FeO	18.34	18.28	18.25	18.47	18.44	16.24	16.36	18.71
MnO	0.5304	0.5274	0.5213	0.496	0.5158	0.6585	0.5929	0.5295
MgO	8.39	8.57	7.98	8.05	8.25	12.63	11.64	7.9
CaO	11.63	11.61	11.67	11.75	11.63	12.46	12.26	11.67
Na_2O	0.8667	0.8882	0.9512	0.9553	0.8879	0.1137	0.316	1.0556
K_2O	1.1355	1.0252	1.07596	1.074	1.0913	0.0401	0.2109	0.8808
F	0.0226	0.0774	0.0572	0.052	0.0466	0.0092	0.0936	0.058
Cl	0.0735	0.1033	0.0892	0.0689	0.1045	0.0016	0.0551	0.1045
Cr_2O_3	0	0.0027	0.0181	0.0334	0	0.0182	0	0
Tot	98.41	97.99	97.94	98.21	97.91	97.24	96.94	98.12

Rock type	Tonalite							
Sample name	CVP33							
Mineral acronym	Anf. 5.1	Anf. 5.2	Anf. 5.3	Anf. 5.4	Anf. 5.5	Anf. 5.7	Anf. 6.1	Anf. 6.2
SiO_2	44.01	44.81	45	44.26	44.31	43.47	44.62	45.07
TiO_2	0.5237	0.5685	0.61	0.723	0.9535	0.9535	0.9568	0.9656
Al_2O_3	11.73	10.68	11.02	11.25	11.72	12.03	11.27	11.13
FeO	18.06	18.12	18.2	18.15	18.33	17.96	18.29	18.09
MnO	0.5223	0.5793	0.5794	0.589	0.5931	0.52	0.4973	0.5406
MgO	8.67	9.19	9.13	9.03	8.9	8.62	8.97	8.96
CaO	11.59	11.54	11.5	11.54	11.31	11.35	11.72	11.17
Na_2O	0.8459	0.8367	0.8616	0.9031	0.8759	0.9089	0.8223	0.7819
K_2O	1.1428	0.9448	0.8901	0.723	0.9535	0.953	0.9568	0.9656
F	0.0731	0.0705	0.0659	0.0279	0.0601	0	0.0361	0.0361
Cl	0.072	0.0971	0.0689	0.1033	0.0861	0.08	0.0876	0.0642
Cr_2O_3	0.0731	0.0235	0.0217	0.054	0	0.0072	0.0045	0.0009
Tot	97.31	97.46	97.95	97.35	98.09	96.85	98.23	97.77

Rock type	Tonalite							
Sample name	CVP33							
Mineral acronym	Anf. 6.3	Anf. 6.5	Anf. 6.6	Anf. 6.8	Anf. 6.10	Anf. 6.14	Anf. 6.15	Anf. 7.4
SiO_2	44.88	44.83	44.67	43.9	44.72	44.94	43.81	44.98
TiO_2	0.548	0.51	0.6277	0.28	0.4148	0.601	0.5921	0.6404
Al_2O_3	11.82	11.43	11.26	13.56	11.74	12	12.09	11.36
FeO	18.26	18.37	18.35	18.98	18.33	18.46	18.84	18.11
MnO	0.5199	0.51	0.5357	0.5481	0.4928	0.5102	0.5402	0.5382
MgO	8.77	8.95	8.85	7.7	8.83	8.51	8.48	8.89
CaO	11.26	11.33	11.1	10.97	10.92	11.78	11.33	11.75
Na_2O	0.8709	0.841	0.8722	1.0461	0.7956	0.8074	0.8768	0.8506
K_2O	1.042	0.8802	1.063	0.8562	1.0138	1.1807	1.1901	1.08783
F	0.0612	0.0567	0.0964	0.0188	0.0232	0.0863	0.0971	0.1478
Cl	0.0783	0.0673	0.0923	0.0845	0.0485	0.407	0.1047	0.0813
Cr_2O_3	0.0279	0	0.0036	0.0188	0.0315	0.0099	0.0081	0
Tot	98.14	97.78	97.52	97.96	97.36	99.29	97.96	98.44

Rock type	Tonalite						
Sample name	CVP33						
Mineral acronym	Anf. 7.5	Anf. 7.6	Anf. 7.8	Anf. 7.9	Anf. 7.11	Anf. 7.12	Anf. 7.13
SiO_2	44.6	44.53	44.37	45	45.68	45.6	45.39
TiO_2	0.4127	0.6076	0.5822	0.6142	0.5436	0.5386	0.4385
Al_2O_3	13.2	11.41	11.77	11.45	11.74	11.01	11.58
FeO	18.22	18.72	18.64	18.5	17.96	17.93	17.3
MnO	0.5162	0.5475	0.5072	0.5342	0.5412	0.5354	0.4883
MgO	8.12	8.99	8.61	8.77	9.36	9.3	9.43
CaO	11.38	11.63	11.67	11.52	11.74	11.68	11.55
Na_2O	0.9419	0.8543	0.8301	0.7971	0.7683	0.7971	0.5865
K_2O	0.8533	0.9496	1.14	0.9738	0.7926	0.901	0.9099
F	0	0.148	0.038	0.006	0.1075	0.1	0.0284
Cl	0.0893	0.1174	0.0844	0.0705	0.0674	0.0564	0.0784
Cr_2O_3	0.0208	0.0252	0.0343	0.0298	0.0036	0.0424	0.0216
Tot	98.35	98.53	98.28	98.27	99.30	98.49	97.80

Rock type	Mafic microgranular enclave							
Sample name	CVP23E (S.Maria)							
Mineral acronym	*Anf. 1.1 (Incl.)*	*Anf. 1.2 (Incl.)*	*Anf. 2.1 (Incl.)*	*Anf. 2.2 (Incl.)*	*Anf. 3.1 (Incl.)*	*Anf. 5.1 (Incl.)*	*Anf. 5.2 (Incl.)*	*Anf. 5.3 (Incl.)*
SiO_2	46.1	44.08	43.86	44.13	43.38	43.07	44.06	43.08
TiO_2	0.2435	0.2193	0.5915	0.6766	0.7309	0.5926	0.4762	0.4933
Al_2O_3	11.42	14.13	13.68	12.72	13.98	14.2	12.75	13.98
FeO	16.47	16.56	17.2	17.41	17.23	17.19	17.7	17.34
MnO	0.5679	0.4876	0.4745	0.5707	0.4548	0.5308	0.6352	0.5499
MgO	10.46	9.04	8.96	9.38	8.15	8.56	9.35	8.54
CaO	11.29	11.22	11.42	11.14	11.32	11.3	11.04	11.24
Na_2O	0.9901	1.2094	1.1523	1.1706	1.0797	1.1944	1.1364	1.1879
K_2O	0.4745	0.5247	0.7065	0.6512	0.7331	0.6774	0.6468	0.6879
F	0.1729	0.1597	0.0966	0.0548	0.1017	0.1985	0.0637	0.1096
Cl	0.0157	0.0817	0.0657	0.0814	0.595	0.0955	0.0627	0.0736
Cr_2O_3	0.0036	0.0073	0.0253	0.0135	0.0091	0.0252		
Tot	98.21	97.72	98.23	98.00	97.76	97.63	97.92	97.28

Rock type	Mafic microgranular enclave				Mafic microgranular enclave			
Sample name	CVP23E (S. Maria)				CVP25E (Briatico)			
Mineral acronym	*Anf. 6.1 (Incl.)*	*Anf. 6.2 (Incl.)*	*Anf. 7.1 (Incl.)*	*Anf. 7.2 (Incl.)*	*Anf. 1.1 (Incl.)*	*Anf. 1.2 (Incl.)*	*Anf. 2.1 (Incl.)*	*Anf. 2.2 (Incl.)*
SiO_2	43.98	43.4	43.89	43.46	45.55	44.81	46	45.6
TiO_2	0.6902	0.6933	0.6556	0.6574	0.4796	0.5706	0.8942	0.4221
Al_2O_3	13.13	13.71	12.9	13.88	11.03	12.02	10.49	11.43
FeO	17.05	17.5	17.24	16.89	17.69	17.2	17.68	17.33
MnO	0.5394	0.5382	0.5891	0.4996	0.5591	0.5847	0.5795	0.5203
MgO	9.16	8.98	9.29	8.91	9.47	8.97	9.82	9.26
CaO	11.14	11.4	11.09	11.28	11.71	11.82	11.84	11.76
Na_2O	1.14	1.1942	1.1638	1.1931	0.7804	0.8211	0.7586	0.7928
K_2O	0.6979	0.7641	0.6619	0.5943	0.9285	0.8915	0.8942	0.9918
F	0.0407	0.1593	0.1274	0.175	0.0546	0.1043	0.0049	0.0796
Cl	0.0689	0.0454	0.083	0.0439	0.0578	0.0937	0.0625	0.0781
Cr_2O_3		0.0153	0.0379	0.0307		0.0226	0.0208	0.0027
Tot	97.64	98.40	97.73	97.61	98.31	97.91	99.04	98.27

Rock type	Mafic microgranular enclave							
Sample name	CVP25E (Briatico)							
Mineral acronym	*Anf. 3.1 (Incl.)*	*Anf. 3.2 (Incl.)*	*Anf. 4.1*	*Anf. 2.2*	*Anf. 4.3*	*Anf. 4.5*	*Anf. 4.6*	*Anf. 5.1*
SiO_2	45.79	46.26	45.16	45.85	45.06	44.51	44.4	44.83
TiO_2	0.4201	0.5867	0.4776	0.5569	0.3179	0.6051	0.3724	0.4212
Al_2O_3	11.07	10.52	11.52	10.54	11.86	11.29	12.65	12.06
FeO	17.14	16.79	17.7	17.43	17.41	17.23	17.02	17.75
MnO	0.582	0.5865	0.546	0.5593	0.5349	0.56	0.5537	0.5765
MgO	9.38	9.91	9.14	9.63	9.12	9.07	8.84	9.09
CaO	11.89	11.61	11.66	11.82	11.84	11.4	11.62	11.88
Na_2O	0.7247	0.6853	0.8226	0.7764	0.8338	0.8539	0.8831	0.6253
K_2O	0.9647	0.9589	1.0558	1.0168	0.9728	1.0716	0.939	1.092
F	0.0858	0.0345	0.0222	0.0846	0.1254	0.0721	0.118	0
Cl	0.0766	0.0454	0.1327	0.0594	0.1156	0.0781	0.0813	0.0796
Cr_2O_3	0.0036	0		0	0.0253	0.0063	0.0117	0.018
Tot	98.13	97.99	98.24	98.32	98.22	96.75	97.49	98.42

Rock type	Mafic microgranular enclave							
Sample name	CVP25E (Briatico)							
Mineral acronym	*Anf. 5.2*	*Anf. 5.3*	*Anf. 6.1*	*Anf. 6.2 (Incl.)*	*Anf. 7.1 (Incl.)*	*Anf. 7.2 (Incl.)*	*Anf. 8.2*	*Anf. 8.3*
SiO_2	43.25	44.31	45.52	44.82	46.26	45.44	46.96	46.82
TiO_2	0.2829	0.2725	0.6566	0.5406	0.4965	0.58	0.6388	0.5863
Al_2O_3	14.58	13.43	10.72	11.47	10.46	11.1	9.66	9.8
FeO	17.98	15.11	17.22	17.04	17.31	17.35	17.38	17.18
MnO	0.5728	0.3563	0.588	0.5322	0.609	0.5797	0.5694	0.5915
MgO	7.98	6.19	9.57	9.17	9.88	9.58	10.06	10.16
CaO	11.73	7.55	11.84	11.64	11.84	11.74	11.69	11.71
Na_2O	1.1027	0.5428	0.78	0.8613	0.7979	0.8109	0.7196	0.8096
K_2O	0.7848	0.9394	1.0189	0.9882	0.9784	1.0422	0.8102	0.8375
F	0.1169	0	0.0303	0.1898	0.0718	0.0717	0.0816	0.0999
Cl	0.0797	0.1056	0.0703	0.0828	0.0813	0.0453	0.0829	0.0798
Cr_2O_3	0.0081	0.009		0	0.0135	0	0.0072	0.0289
Tot	98.47	88.82	98.01	97.33	98.80	98.34	98.66	98.70

Rock type	Mafic microgranular enclave							
Sample name	CVP25E (Briatico)							
Mineral acronym	*Anf. 8.4*	*Anf. 11.1*	*Anf. 11.2*	*Anf. 11.3*	*Anf. 11.4*	*Anf. 11.1*	*Anf. 11.2*	*Anf. 12.1*
SiO_2	45.61	45.63	46.26	46.66	43.35	44.15	45.7	44.29
TiO_2	0.5346	0.4812	0.8858	0.5656	0.2073	0.2622	0.43	0.5817
Al_2O_3	11.07	11.65	9.93	9.79	14.67	13.56	10.62	12.46
FeO	17.7	17.63	17.3	16.75	18.34	17.93	17.14	17.86
MnO	0.5773	0.5373	0.6073	0.6047	0.6115	0.5689	0.5587	0.5817
MgO	9.62	9.22	10.16	10.24	7.94	8.62	9.75	8.8
CaO	11.78	11.64	11.7	11.64	11.74	11.79	11.79	11.83
Na_2O	0.8141	0.7985	0.7263	0.7499	1.0851	0.9679	0.7875	0.8501
K_2O	1.0027	1.0494	0.8858	0.8745	0.7889	0.886	0.8974	1.0542
F	0.089	0.0731	0.1082	0.1304	0.0816	0.0605	0	0.0558
Cl	0.075	0.0844	0.0563	0.083	0.1032	0.0844	0.0924	0.0766
Cr_2O_3	0	0	0.226	0	0.0135	0.0054	0.0226	0.0234
Tot	98.87	98.79	98.85	98.09	98.93	98.89	97.79	98.46

Rock type	Mafic microgranular enclave								
Sample name	CVP25E (Briatico)								
Label	*Anf. 12.2*	*Anf. 15.1*	*Anf. 15.2*	*Anf. 15.3*	*Anf.1/pl1*	*Anf.2/pl1*	*Anf.5/pl1*	*Anf.8/pl1*	*Anf.11/pl1*
SiO_2	45.85	46.41	45.52	45.75	41.34	42.81	36.45	44.43	44.52
TiO_2	0.6028	0.4476	0.4079	0.4766	0.2014	0.2715	1.0732	0.5419	0.4939
Al_2O_3	10.45	10	9.78	10.48	13.86	15.13	18.3	11.7	12.12
FeO	17.29	17.1	16.93	17.68	16.45	18.17	20.22	17.37	17.56
MnO	0.572	0.5752	0.5436	0.569	0.531	0.5822	0.3181	0.5489	0.554
MgO	9.84	10.16	8.87	9.84	6.9	7.74	10.09	9.12	8.97
CaO	11.47	11.65	11.3	11.75	9.66	11.53	0.0705	11.29	11.85
Na_2O	0.7195	0.718	0.5677	0.7585	0.9299	1.1637	0.0956	0.866	0.8612
K_2O	0.9441	0.8658	0.8468	0.9586	0.5371	0.875	9.28	1.0874	1.178
F	0.1959	0.0647	0.0223	0.0929	0.031	0.0452	0.0452	0.1064	0.0796
Cl	0.0313	0.0595	0.0643	0.0861	0.1003	0.0905	0.0905	0.1312	0.0765
Cr_2O_3	0.0063	0.024	0.0515	0.0045	0	0.0126	0.0126	0.0135	0.0199
Tot	97.97	98.07	94.90	98.45	90.54	98.42	96.05	97.21	98.28

Appendix. Table 3 – Microprobe analysis of biotite in CVP granitoids.

Rock	Hybrid quartz-diorite							
Sample	CVP16							
Label	Bt 1.2	Bt 1.3	Bt 1.4	Bt 1.5	Bt 1.6	Bt 2.1	Bt 2.2	Bt 3.1
SiO_2	35.58	35.38	35.38	35.6	35.6	35.41	35.45	35.98
TiO_2	1.443	1.4819	1.4819	1.5159	1.4714	1.5857	1.5357	1.519
Al_2O_3	17.72	17.74	17.74	17.91	17.79	18.67	17.65	18.29
FeO	16.2	15.34	15.34	15.99	16.1	15.81	16.33	15.8
MnO	0.026	0.0728	0.0728	0.064	0.0755	0.0728	0.0796	0.0646
MgO	11.97	12.24	12.24	12.23	12.24	11.53	12.04	12.08
CaO	0.0444	0	0	0.0077	0.0085	0.0664	0.0587	0.038
Na_2O	0.1598	0.1543	0.1543	0.1764	0.1812	0.1668	0.1406	0.1939
K_2O	8.97	9.04	9.04	9.14	9.12	9.35	8.92	9.26
BaO	0.4162	0.5251	0.5251	0.5588	0.625	0.4804	0.4557	0.4831
ZnO	0.0221	0.0204	0.0204	0.0377	0.0797	0.0329	0.0953	0.225
F	0.0884	0.0783	0.0783	0.0555	0.0845	0.0806	0.0666	0.076
Cl	0.1091	0.0967	0.0967	0.1029	0.1511	0.1028	0.0577	0.1123
Tot	92.75	92.17	92.17	93.39	93.53	93.36	92.88	94.12

Rock	Hybrid quartz-diorite				
Sample	CVP16				
Label	Bt 3.2	Bt 3.3	Bt 4.1	Bt 4.2	Bt 4.3
SiO_2	36.57	34.34	35.58	35.08	32.26
TiO_2	1.0724	1.5608	1.76	1.4217	1.626
Al_2O_3	19.84	18.07	17.85	17.82	18.14
FeO	13.3	17.67	17.37	17.31	19
MnO	0.0721	0.0847	0.0418	0.0882	0.1114
MgO	10.92	12.7	12.07	12.2	13.19
CaO	0.0642	0.106	0.0298	0.0735	0.1459
Na_2O	0.3209	0.1569	0.158	0.1574	0.1526
K_2O	8.333	7.64	9.39	9.29	5.06
BaO	0.432	0.4558	0.49	0.554	0.338
ZnO	0.033	0.0488	0.0358	0.0548	0.032
F	0.0594	0.0733	0.0865	0.591	0.0497
Cl	0.0939	0.0687	0.1213	0.1183	0.078
Tot	91.11	92.975	94.983	94.759	90.184

Rock	Quartz-diorite							
Sample	CVP27							
Label	Bt 1.1	Bt 1.2	Bt 2.2	Bt 2.3	Bt 3.1	Bt 3.2	Bt 3.3	Bt 4.1
SiO_2	35.26	35.05	35.3	35.42	34.87	33.66	34.34	33.82
TiO_2	1.95	1.77	2.26	0.721	1.667	2.48	1.67	2.49
Al_2O_3	18.26	18.17	17.82	21.77	18.43	18.04	19.71	17.65
FeO	18.44	18.31	17.82	15.07	17.47	17.74	16.43	18.37
MnO	0.2568	0.2065	0.1802	0.1721	0.165	0.2208	0.1495	0.2406
MgO	10.95	11.17	11.14	10.92	10.99	9.62	10.46	11.05
CaO	0.046	0.068	0.0496	0.0551	0.0143	0.1662	0.1228	0.0798
Na_2O	0.1841	0.161	0.1593	0.1646	0.1015	0.0886	0.1343	0.14
K_2O	9.44	9.6	9.68	9.76	9.79	9.32	9.66	8.4
BaO	0.3505	0.3431	0.311	0.2499	0.3606	0.4442	0.3729	0.3157
ZnO	0.0361	0.0292	0.0041	0.0705	0.0698	0.0717	0.0458	0.0761
F	0.0452	0.0434	0.0533	0.0282	0.0473	0.0198	0.0354	0.0522
Cl	0.104	0.1598	0.1473	0.1435	0.1506	0.1548	0.1523	0.1475
Tot	95.32	95.08	94.92	94.54	94.13	92.03	93.28	92.83

Rock	Quartz-diorite			Quartz-diorite				
Sample	CVP27			CVP20				
Label	Bt 4.2	Bt 4.3	Bt 4.4	Bt 2.1	Bt 2.2	Bt 3.1	Bt 3.2	Bt 4.1
SiO_2	35.19	34.41	32.05	35.21	35.89	35.04	38.35	35.21
TiO_2	2.17	1.77	1.3	2.13	1.71	2.4	1.002	1.89
Al_2O_3	17.77	17.24	16.41	16.82	17.37	16.26	18.74	16.51
FeO	17.97	16.84	19.81	20.43	19.48	21.09	16.34	19.94
MnO	0.1951	0.2347	0.1315	0.3614	0.2737	0.3913	0.2657	0.3241
MgO	10.88	10.87	14.06	9.48	9.53	9.49	7.65	9.97
CaO	0.0515	0.0573	0.6933	0.0822	0.258	0.1796	0.9988	0.3041
Na_2O	0.177	0.1644	0.2086	0.0569	0.0282	0.0585	1.51	0.0813
K_2O	9.5	9.09	0.2086	9.47	8.16	8.75	7.87	8.6
BaO	0.3636	0.3764	0.0187	0.2995	0.081	0.1466	0.071	0.2184
ZnO	0.0693	0.058	0.0436	0.0994	0.0745	0.0654	0.0147	0.0806
F	0.0367	0.0406	0	0.0394	0.0396	0.0406	0.0346	0.0564
Cl	0.1738	0.1275	0.0284	0.0402	0.0808	0.0618	0.075	0.0496
Tot	94.55	91.28	84.96	94.52	92.98	93.97	92.92	93.23

Rock	Tonalite							
Sample	CVP29							
Label	Bt 1.3	Bt 1.4	Bt 1.6	Bt 1.7	Bt 1.8	Bt 2.1	Bt 2.3	Bt 2.5
SiO_2	35.11	35.04	35.3	35.15	34.82	35.14	35.36	35.31
TiO_2	2.19	2.37	2.09	2.19	2.78	2.4	2.25	2.39
Al_2O_3	17.67	17.58	17.67	18.04	17.96	17.7	18	17.92
FeO	18.75	18.45	18.47	18.55	18.54	18.08	18.29	18.68
MnO	0.265	0.2569	0.2474	0.2541	0.22	0.2305	0.2098	0.2124
MgO	10.5	10.77	10.73	10.33	10.55	10.32	10.58	10.61
CaO	0.0434	0.0263	0.0468	0	0.0921	0	0.0341	0.0078
Na_2O	0.109	0.1056	0.1138	0.1195	0.1316	0.1049	0.1376	0.1066
K_2O	10.07	10.04	9.83	10.04	9.13	9.8	10.13	9.91
BaO	0.3484	0.3425	0.3566	0.3919	0.2953	0.356	0.3163	0.312
ZnO	0.025	0.0358	0.0765	0.0411	0.0535	0.043	0.0415	0.0599
F	0.0433	0.0386	0.0349	0.0354	0.0447	0.044	0.0486	0.0475
Cl	0.133	0.1454	0.1084	0.1377	0.0867	0.1052	0.1347	0.1022
Tot	95.26	95.20	95.07	95.28	94.70	94.32	95.53	95.67

Rock	Tonalite			Tonalite				
Sample	CVP29			CVP33				
Label	Bt 3.1	Bt 3.2	Bt 5.3	Bt 1.1	Bt 1.2	Bt 1.3	Bt 2.1	Bt 2.2
SiO_2	35.65	35.57	34.65	35.2	35.4	35.14	35.2	35.23
TiO_2	2.26	2.15	1.558	1.86	2.02	2.18	2.2	2.37
Al_2O_3	17.99	18	17.78	17.39	17.75	17.24	17.07	17.22
FeO	18.62	18.82	19.4	20.62	19.9	19.98	20.53	20.35
MnO	0.2465	0.2074	0.2115	0.3145	0.2608	0.3229	0.2608	0.3227
MgO	10.42	10.63	11.07	9.51	9.56	9.59	9.73	9.57
CaO	0	0	0.0685	0.0172	0.0371	0.0631	0.0156	0.0363
Na_2O	0.1342	0.1345	0.1058	0.0713	0.0674	0.0834	0.0904	0.1007
K_2O	9.86	10.01	9.06	9.9	9.99	9.88	9.63	9.6
BaO	0.3694	0.2931	0.2218	0.3144	0.3165	0.3567	0.3513	0.2816
ZnO	0.071	0.0059	0.0317	0.0338	0.0363	0.0463	0.0765	0.0245
F	0.0496	0.0572	0.0391	0.0437	0.0347	0.0515	0.0154	0.0204
Cl	0.1115	0.1517	0.138	0.0912	0.1144	0.068	0.0943	0.0928
Tot	95.78	96.03	94.33	95.37	95.49	95.00	95.26	95.22

Rock	Tonalite							
Sample	CVP33							
Label	Bt 2.3	Bt 2.4	Bt 2.6	Bt 2.7	Bt 3.1	Bt 4.1	Bt 4.2	Bt 4.3
SiO_2	34.56	35.45	35.01	34.74	34.63	35.23	35.26	35.03
TiO_2	2.51	2.54	2.13	2.82	2.33	1.87	2.17	1.6618
Al_2O_3	16.72	17.14	18.47	17.32	17.06	3	16.8	16.77
FeO	20.26	19.8	19.89	20.31	20.68	20.74	20.77	20.61
MnO	0.31	0.301	0.3209	0.3585	0.377	0.3247	0.3448	0.3168
MgO	9.3	9.74	8.73	8.94	903	9.94	9.94	10.23
CaO	0.1536	0	0.0379	0.0557	0.0246	0.0047	0.0181	0.1572
Na_2O	0.1856	0.1162	0.0711	0.0994	0.0567	0.0773	0.1122	0.1867
K_2O	9.25	9.68	9.57	9.9	9.81	9.99	9.6	9.4
BaO	0.3204	0.294	0.3669	0.3123	0.3955	0.3833	0.3517	0.2529
ZnO	0.0358	0.0964	0.032	0.0587	0.0505	0.0099	0.0314	0.062
F	0.0191	0.0363	0.0228	0.0337	0.0416	0.0402	0.0459	0.0571
Cl	0.105	0.0819	0.0572	0.1004	0.0879	0.0928	0.1005	0.1068
Tot	93.73	95.28	94.71	95.05	988.54	81.70	95.54	94.84

Rock	Tonalite						Tonalite	
Sample	CVP33						CVP35	
Label	Bt 4.4	Bt 4.5	Bt 4.6	Bt 5.1	Bt 5.2	Bt 5.3	Bt 1.2	Bt 1.3
SiO_2	34.98	34.79	34.53	34.88	35.2	34.73	35.01	35.13
TiO_2	1.5087	1.88	1.69	1.92	2.11	1.0981	2.65	2.96
Al_2O_3	17.12	17.43	17.11	17.15	17.6	18.12	17.02	17.41
FeO	20.11	20.08	20.74	20.71	19.87	20.62	19.95	19.89
MnO	0.2799	0.3193	0.3692	0.3316	0.323	0.3445	0.246	0.2265
MgO	10.22	10.15	9.61	9.52	9.39	9.69	9.5	9.48
CaO	0.1551	0.0205	0.0189	0.0406	0.0153	0.0586	0.0453	0.0259
Na_2O	0.1437	0.0837	0.08	0.0842	0.1247	0.0981	0.1001	0.1048
K_2O	9.27	9.84	9.59	9.57	9.69	9.79	10.06	9.99
BaO	0.2608	0.2538	0.3907	0.2833	0.3926	0.3125	0.4043	0.4124
ZnO	0.0609	0.0463	0.0686	0.0315	0.0239	0.0827	0.0973	0.0744
F	0.0504	0.0309	0.0541	0.0312	0.0256	0.0405	0.0828	0.0788
Cl	0.1038	0.1192	0.0989	0.0634	0.1036	0.1192	0.0417	0.0525
Tot	94.26	95.04	94.35	94.62	94.87	95.10	95.21	95.84

Rock	Tonalite							
Sample	CVP35							
Label	Bt 1.4	Bt 1.5	Bt 2.1	Bt 2.4	Bt 3.2	Bt 3.3	Bt 3.5	Bt 3.6
SiO_2	35.08	35.4	35.18	35.15	34.86	34.66	34.96	35.6
TiO_2	3	2.12	3.09	2.65	1.96	2.24	1.78	1.78
Al_2O_3	17.4	17.91	17.23	17.04	17.82	17.43	17.56	18.61
FeO	19.58	18.94	20	20.49	19.47	19.26	19.59	18.4
MnO	0.2288	0.2291	0.2543	0.2114	0.1988	0.2512	0.263	0.2192
MgO	9.55	10.07	9.65	9.73	10.13	9.81	10.11	9.6
CaO	0.0014	0.0506		0.0159	0.07	0.0358	0.0277	0.033
Na_2O	0.0868	0.0425	0.0709	0.0603	0.0614	0.0562	0.0373	0.028
K_2O	9.81	9.93	9.83	9.6	9.85	9.83	9.79	10.05
BaO	0.4686	0.4255	0.4658	0.45	0.3218	0.3715	0.3374	0.4313
ZnO	0.0067	0.0537	0.0537		0.0201	0.0609	0.0611	0.0476
F	0.0706	0.0769	0.052	0.0586	0.0575	0.08	0.0865	0.0919
Cl	0.0756	0.0526	0.0355	0.071	0.0294	0.0464	0.0448	0.0759
Tot	95.36	95.30	95.91	95.53	94.85	94.13	94.65	94.97

Rock	Tonalite							
Sample	CVP38							
Label	Bt 1.2	Bt 2.3	Bt 4.2	Bt 4.3	Bt 4.4	Bt 5.2	Bt 6.1	Bt 6.2
SiO_2	35.01	35.13	35.08	35.4	35.18	35.15	34.86	34.66
TiO_2	2.65	2.96	3	2.12	3.09	2.65	1.96	2.24
Al_2O_3	17.02	17.41	17.4	17.91	17.23	17.04	17.82	17.43
FeO	19.95	19.89	19.58	18.94	20	20.49	19.47	19.26
MnO	0.246	0.2265	0.2288	0.2291	0.2543	0.2114	0.1988	0.2512
MgO	9.5	9.48	9.55	10.07	9.65	9.73	10.13	9.81
CaO	0.0453	0.0259	0.0014	0.0506		0.0159	0.07	0.0358
Na_2O	0.1001	0.1048	0.0868	0.0425	0.0709	0.0603	0.0614	0.0562
K_2O	10.06	9.99	9.81	9.93	9.83	9.6	9.85	9.83
BaO	0.4043	0.4124	0.4686	0.4255	0.4658	0.45	0.3218	0.3715
ZnO	0.0973	0.0744	0.0067	0.0537	0.0537		0.0201	0.0609
F	0.0828	0.0788	0.0706	0.0769	0.052	0.0586	0.0575	0.08
Cl	0.0417	0.0525	0.0756	0.0526	0.0355	0.071	0.0294	0.0464
Tot	95.21	95.84	95.36	95.30	95.91	95.53	94.85	94.13

Rock	Tonalite					Tonalite		
Sample	CVP38					CVP42		
Label	Bt 6.4	Bt 6.5	Bt 6.6	Bt 6.10	Bt 6.11	Bt 1.1	Bt 1.3	Bt 2.2
SiO_2	34.96	35.6	35.18	35.45	34.9	34.96	35.14	35.13
TiO_2	1.78	1.78	2.17	0.6269	2.06	1.79	1.37	1.98
Al_2O_3	17.56	18.61	17.11	18.13	17.23	17.79	17.86	17.69
FeO	19.59	18.4	19.31	18.25	18.67	19.22	18.98	18.6
MnO	0.263	0.2192	0.2744	0.255	0.2496	0.1552	0.173	0.15
MgO	10.11	9.6	10.54	11.55	10.43	10.44	10.35	10.9
CaO	0.0277	0.033	0.0182	0.0362	0.0738	0.0266	0.1058	0.0415
Na_2O	0.0373	0.028	0.1244	0.1061	0.1171	0.0907	0.0995	0.1053
K_2O	9.79	10.05	9.8	9.59	9.74	9.68	9.32	9.77
BaO	0.3374	0.4313	0.457	0.1947	0.3586	0.5127	0.5648	0.6489
ZnO	0.0611	0.0476	0.0744	0.0408	0.0816	0.0642	0.0547	0.0865
F	0.0865	0.0919	0.0459	0.0565	0.0537	0.0862	0.0931	0.0739
Cl	0.0448	0.0759	0.0511	0.067	0.0791	0.0642	0.076	0.0666
Tot	94.65	94.97	95.16	94.35	94.04	94.88	94.19	95.24

Rock	Tonalite					Tonalite		
Sample	CVP42					CVP10		
Label	Bt 2.3	Bt 2.5	Bt 3.1	Bt 3.2	Bt 3.3	Bt 1.2	Bt 1.3	Bt 2.1
SiO_2	35.51	35.83	34.68	34.96	35.08	35.48	35.34	34.9
TiO_2	1.6189	2.14	1.68	2.3	2.53	1.84	2.72	2.71
Al_2O_3	17.99	18.44	17.75	17.64	18	17.67	17.19	17.11
FeO	18.5	17.7	18.5	18.68	17.24	20.03	19.78	20.4
MnO	0.0999	0.1081	0.1575	0.1609	0.1302	0.2907	0.2774	0.2909
MgO	11	11.01	10.88	10.44	11.12	9.74	9.59	9.19
CaO	0.046	0.0306	0.0168	0.0273	0.0053	0.0175	0.0735	0
Na_2O	0.0927	0.094	0.102	0.1209	0.0981	0.0825	0.0661	0.0916
K_2O	9.8	9.74	9.8	9.65	9.19	10.11	9.89	9.77
BaO	0.6396	0.5302	0.5886	0.5898	0.535	0.2933	0.189	0.1692
ZnO	0.0895	0.032	0.0494	0.0369	0.0528	0.0213	0.0165	0.0238
F	0.0866	0.0802	0.0639	0.0729	0.0636	0.0517	0.046	0.0454
Cl	0.0528	0.0761	0.0558	0.0712	0.0775	0.1314	0.085	0.091
Tot	95.53	95.81	94.32	94.75	94.12	95.76	95.26	94.79

Rock	Leuco-tonalite							
Sample	CVP4							
Label	Bt 1.1	Bt 1.2	Bt 2.1	Bt 2.2	Bt 2.3	Bt 2.4	Bt 3.1	Bt 3.2
SiO_2	34.2	35.03	35.26	34.84	34.15	34.9	34.26	34.67
TiO_2	2.57	2.32	2.55	2.57	1.69	2.3	2.71	2.65
Al_2O_3	17.61	18.05	18.08	17.6	18.2	17.88	17.84	17.48
FeO	20.05	20	21.21	20.23	19.94	19.89	20.87	20.4
MnO	0.2883	0.2897	0.3019	0.3108	0.3067	0.2769	0.3062	0.2868
MgO	9.07	9.23	8.91	9.43	9.67	9.52	9.2	9.25
CaO	0.0376	0.0144	0.1073	0.0313	0.0372		0.0702	0.0211
Na_2O	0.1037	0.0759	0.0498	0.0885	0.0553	0.0992	0.115	0.0919
K_2O	9.99	9.97	9.53	10.01	10.11	10.14	9.98	10.09
BaO	0.1851	0.1177	0.0914	0.1019	0.1213	0.1461	0.0899	0.1741
ZnO	0.0772	0.0561	0.0639	0.0186	0.0217	0.0801	0.0501	0.065
F	0.1018	0.0984	0.0734	0.0736	0.0988	0.0871	0.0912	0.0791
Cl	0.068	0.0913	0.0634	0.1051	0.1005	0.0974	0.0895	0.0772
Tot	94.35	95.34	96.29	95.41	94.50	95.42	95.67	95.34

Rock	MME							
Sample	CVP23E							
Label	Bt 1.1	Bt 1.2	Bt 2.1	Bt 2.2	Bt 3.1	Bt 4.1	Bt 4.2	Bt 4.3
SiO_2	33.33	34.81	35.05	34.02	33.83	34.48	35.33	34.8
TiO_2	2.19	2.4	1.6096	0.2205	1.76	2.95	2.17	1.3476
Al_2O_3	16.56	17	17.34	18.26	17.21	17.13	17.26	19.19
FeO	19.4	19.51	19.08	18.17	19.96	19.51	19.18	17.64
MnO	0.254	0.1808	0.2121	0.2166	0.2574	0.2608	0.2102	0.2224
MgO	11.47	10.5	11.09	11.93	10.58	10.04	10.67	10.81
CaO	0.0045	0.0186	0.0562	0.0818	0.0828	0.015	0.0106	0.0743
Na_2O	0.1234	0.1473	0.1221	0.1138	0.1154	0.1209	0.1544	0.1018
K_2O	9.03	9.53	9.46	8.92	8.07	9.77	9.82	9.55
BaO	0.3605	0.3623	0.4178	0.1918	0.3033	0.3874	0.359	0.2839
ZnO	0.0363	0.0556	0.0346	0.0494	0.0289	0.0692	0.0305	0.0248
F	0.0632	0.0624	0.0671	0.0701	0.0551	0.0357	0.0685	0.0597
Cl	0.1145	0.0624	0.0901	0.0796	0.115	0.0959	0.0993	0.0828
Tot	92.94	94.64	94.63	92.32	92.37	94.86	95.36	94.19

Rock	MME		MME					
Sample	CVP23E		CVP23E					
Label	Bt 4.4	Bt 4.5	Bt 1.1	Bt 1.2	Bt 1.3	Bt 1.4	Bt 1.5	Bt 1.7
SiO_2	34.85	35.06	35.66	36.04	36.08	35.94	36.13	35.86
TiO_2	1.3937	2.14	2.68	1.79	1.96	1.8	1.74	1.77
Al_2O_3	19.15	17.39	18.29	17.39	17.07	17.25	17.99	16.91
FeO	17.46	18.7	16.51	18.51	17.33	17.66	18.13	18.02
MnO	0.1888	0.244	0.2769	0.326	0.2529	0.2891	0.337	0.2557
MgO	10.74	10.55	10.47	10.79	11.08	10.74	10.09	11.26
CaO	0.0414	0.0294	0.1407	0.0694	0.1292	0.1312	0.137	0.0456
Na_2O	0.0954	0.175	0.1853	0.1167	0.1588	0.1473	0.1863	0.0917
K_2O	9.76	9.75	9.57	9.45	9.19	9.03	9.55	9.35
BaO	0.3193	0.3952	0.2501	0.2704	0.228	0.157	0.1707	0.1312
ZnO	0.0598	0.091	0.0272	0.0779	0.0312	0.0428	0.0145	0.0562
F	0.0605	0.0604	0.0493	0.0654	0.052	0.0642	0.0533	0.0522
Cl	0.0716	0.0916	0.0699	0.0869	0.1166	0.0824	0.0885	0.1398
Tot	94.19	94.68	94.18	94.98	93.68	93.33	94.62	93.94

Rock	MME							
Sample	CVP25E							
Label	Bt 1.8	Bt 1.9	Bt 2.2	Bt 2.4	Bt 2.5	Bt 2.6	Bt 2.8	Bt 3.1
SiO_2	35.69	35.96	35.37	45.1	44.86	43.65	29.41	38.08
TiO_2	1.92	2.03	1.7	0.7541	0.6793	0.7563	1.76	1.5263
Al_2O_3	17.99	18	17.02	14.86	9.8	11.52	14.12	16.73
FeO	17.12	16.94	18.87	16.03	18.29	18.18	18.52	18.41
MnO	0.2541	0.3209	0.4054	0.2673	0.6102	0.5959	0.3278	0.3056
MgO	11.05	10.77	11.04	9.04	8.62	8.67	11.96	4.64
CaO	0.0737	0.0337	0.0018	0.1434	10.85	11.8	0.1755	0.097
Na_2O	0.1337	0.0765	0.108	0.067	0.6332	0.8137	0.1127	0.0648
K_2O	9.88	9.97	9.79	7.36	1.0988	1.24	9.64	9.56
BaO	0.1815	0.2914	0.2589	0.2171			0.2417	0.1666
ZnO	0.0528	0.0475	0.2589	0.058			0.0467	0.0544
F	0.062	0.0486	0.0467	0.041	0.0282	0.0119	0.0675	0.0125
Cl	0.0528	0.0823	0.0714	0.055	0.1687	0.1107	0.1142	0.0823
Tot	94.46	94.57	94.94	93.99	95.64	97.35	86.50	89.73

Rock	MME				
Sample	CVP25E				
Label	Bt 3.2	Bt 3.5	Bt 3.6	Bt 4.1	Bt 4.2
SiO_2	35.66	43.02	35.48	35.13	35.76
TiO_2	1.661	0.8266	1.5169	1.5456	1.621
Al_2O_3	16.72	10.7	16.8	16.75	16.49
FeO	18.22	17.89	18.8	18.97	18.487
MnO	0.3075	0.6132	0.3322	0.3802	0.317
MgO	10.9	9.33	10.99	10.81	10.78
CaO	0.1177	11.87	0.0848	0.0281	0.0807
Na_2O	0.1108	0.8921	0.959	0.1054	0.1078
K_2O	9.55	1.0657	9.57	9.8	9.25
BaO	0.1477	0.0106	0.2474	0.3207	0.3172
ZnO	0.0481	0.0516	0.0504	0.0598	0.0456
F	0.0044	0.0029	0.0723	0.0538	0.0558
Cl	0.1227	0.1108	0.0575	0.0744	0.1119
Tot	93.57	96.38	94.96	94.03	93.42

***Appendix. Table 4** – Microprobe analysis of Plagioclase in CVP granitoids.*

Rock	Hybrid quartz-diorites							
Sample	CVP16							
Label	Pl1.2	Pl1.4	Pl1.5	Pl2.1	Pl2.2	Pl2.3	Pl2.4	Pl3.2
SiO_2	54.95	55.36	54.22	55.11	55.47	56.3	55.23	54.8
TiO_2			0.0707		0.0192	0.0359	0.0509	0.0317
Al_2O_3	28.78	28.66	28.39	28.33	28.74	26.17	28.7	29.19
FeO	0.0255	0.0171	0.0524	0.2271	0.0213	0.0171	0.0412	0.1066
MnO	0.0067	0.0164	0.0046		0.0082	0.0059	0.0119	
Na_2O	5.4	5.63	5.69	5.86	5.6	5.88	5.33	5.37
MgO								
CaO	10.51	10.2	10.48	9.97	10.32	9.79	10.4	10.88
K_2O	0.036	0.0275	0.084	0.0258	0.043	0.0568	0.0576	0.037
SrO	0.1397	0.065	0.0919	0.0715	0.1073	0.105	0.0689	0.1075
BaO	0.0739	0.0261		0.0106		0.0517		0
Tot	99.92	100.00	99.08	99.61	100.33	98.41	99.89	100.52
Ab %	51.02	50.57	48.977	54.324	44.201	48.807	48.401	64.664
An %	48.782	45.687	50.57	45.47	55.446	50.643	50.24	34.956
Or %	0.1984	3.7433	0.4535	0.2062	0.3537	0.5504	1.3594	0.3803

Rock	Hybrid quartz-diorites						
Sample	CVP16						
Label	Pl3.3	Pl4.1	Pl4.2	Pl4.3	Pl5.1	Pl5.2	Pl5.3
SiO_2	55.25	54.73	53.94	55.6	62.94	57.74	54.87
TiO_2	0.0314	0.0416	0.0309	0.0575			
Al_2O_3	28.94	28.59	29.48	28.38	23.05	26.95	28.97
FeO	0.0526	0.0284			0.0171	0.0099	
MnO	0.0062	0.0017	0.0051	0.0046	0.0036	0.0197	
Na_2O	5.37	5.61	4.89	5.76	9.15	6.63	5.3
MgO							
CaO	10.55	9.34	11.15	9.63	3.82	8.23	10.52
K_2O	0.1289	0.6303	0.0455	0.192	0.0968	0.0484	0.0224
SrO	0.0544	0.1568	0.0605	0.0858	0.0061	0.0907	0.1131
BaO	0.0347	0.0033	0.0615	0.0744			0.0113
Tot	100.42	99.13	99.66	99.78	99.08	99.72	99.81
Ab %	51.214	50.152	44.128	51.392	80.797	59.145	47.627
An %	46.19	46.141	55.602	47.48	18.64	40.571	52.24
Or %	2.5963	3.7075	0.2702	1.1272	0.5624	0.2841	0.1324

Rock	Quartz-diorite							
Sample	CVP20 (S.Maria)							
Label	Pl1.1	Pl1.2	Pl1.4	Pl1.5	Pl1.6	Pl1.7	Pl2.1	Pl2.2
SiO_2	55.2	57.27	50.1	60.69	55.62	54.4	56.21	55.14
TiO_2	0.0445		0.0289		0.043	0.0071		0.058
Al_2O_3	28.37	26.31	30.31	21.71	28.2	29.2	27.92	28.84
FeO	0.0412	0.0311	0.1657	0.0736	0.1079	0.1178	0.0398	0.0567
MnO	0.004	0.0013	0.0563				0.0024	0.03
Na_2O	5.61	4.33	3.77	1.44	5.69	5.13	6.02	5.48
MgO							0.03	
CaO	10.03	8.07	11.28	3.7	9.68	10.65	9.36	10.37
K_2O	0.1752	3.46	2.32	11.65	0.1221	0.1844	0.062	0.0679
SrO	0.0672	0.0613	0.0619	0.0349	0.0811	0.1121	0.0289	0.0863
BaO		0.2559	0.0134	0.3258	0.0404	0.0078	0	0
Tot	99.54	99.79	98.11	99.62	99.58	99.81	99.67	100.13
Ab %	49.788	39.129	32.698	12.915	51.171	46.065	53.591	48.689
An %	49.189	40.299	54.063	18.337	48.106	52.846	46.045	50.914
Or %	1.0231	20.573	13.24	68.748	0.7225	1.0895	0.3632	0.3969

Rock	Quartz-diorite					Quartz-diorite		
Sample	CVP20 (S. Maria)					CVP27 (Briatico)		
Label	Pl2.3	Pl3.2	Pl3.3	Pl3.4	Pl3.5	Pl1.1	Pl1.2	Pl1.3
SiO_2	57.12	57.1	57.26	62.64	56.27	55.47	54.88	61.42
TiO_2			0.0141		0.0104			0.0099
Al_2O_3	27.4	27.34	27.29	23.73	28	28.52	29.12	24.27
FeO	0.061	0.1107	0.0067	0.0512	0.454	0.0157	0.213	0.0199
MnO		0.0043		0.0064			0.0175	
Na_2O	6.4	6.23	6.16	8.84	5.91	5.63	5.35	7.18
MgO								
CaO	8.74	8.89	8.92	4.27	9.52	10.24	10.84	6.61
K_2O	0.1163	0.1025	0.1042	0.1357	0.0775	0.068	0.024	0.0286
SrO	0.1237	0.079	0.0681	0.1099	0.0651	0.0717	0.0992	0.0808
BaO	0.0616	0.052	0.034	0.0173	0.0345	0.0277		0.008
Tot	100.02	99.91	99.86	99.80	100.34	100.04	100.54	99.63
Ab %	56.606	55.575	55.208	78.307	52.666	49.676	47.112	66.166
An %	42.717	43.823	44.177	20.902	46.88	49.929	52.749	33.661
Or %	0.6768	0.6016	0.6145	0.7909	0.4544	0.3948	0.1391	0.1734

Rock	Quartz-diorite							
Sample	CVP27 (Briatico)							
Label	Pl1.4	Pl1.5	Pl1.6	Pl1.7	Pl2.1	Pl2.2	Pl2.3	Pl2.4
SiO_2	59.21	57.86	59.25	58.5	59.2	54.25	58.93	58.71
TiO_2	0.0439	0.034			0.0223	0.0484		
Al_2O_3	26.11	26.68	25.85	25.95	26.39	29.07	25.46	26.37
FeO	0.0157	0.037		0.24	0.0426	0.1321	0.3111	0.0796
MnO		0.0365	0.0117	0.0054			0.0028	0.0083
Na_2O	7.26	6.77	7.44	6.46	7.13	5.26	7.69	5.11
MgO				0.03				
CaO	7.39	7.97	7.1	5.67	7.57	10.59	6.89	9.21
K_2O	0.0347	0.0865	0.0486	2.1	0.0579	0.0533	0.0684	0.1061
SrO	0.0881	0.0329	0.1189	0.0433	0.0619	0.0802	0.0914	0.1072
BaO	0.0479	0.0471		0.0773		0.0479	0.006	
Tot	100.20	99.55	99.82	99.08	100.47	99.53	99.45	99.70
Ab %	63.872	60.279	65.289	58.861	62.812	47.187	66.624	49.76
An %	35.928	39.214	34.43	28.549	36.852	52.498	32.986	49.56
Or %	0.2009	0.5068	0.2806	12.59	0.3356	0.3146	0.3899	0.6798

Rock	Quartz-diorite							
Sample	CVP27 (Briatico)							
Label	Pl3.1	Pl3.2	Pl3.3	Pl3.5	Pl4.1	Pl4.2	Pl4.6	Pl4.7
SiO_2	54.87	54.88	61.26	51.54	54.81	55.25	58.31	56.87
TiO_2		0.0023		0.0486	0	0.0224		
Al_2O_3	28.72	28.6	24.3	27.29	28.68	28.63	25.65	26.24
FeO		0.0128	0.0214	2.06	0.0427	0.0569	0.3096	0.2893
MnO		0.0029		0.0015	0.0028	0.0227	0.0031	0.0191
Na_2O	5.31	5.56	8.25	5.1	5.45	5.59	6.17	5.66
MgO								
CaO	10.47	10.11	5.25	9.77	10.54	10.33	5.44	7.98
K_2O	0.0947	0.0646	0.0976	0.5326	0.0525	0.0801	2.44	2.34
SrO	0.0737	0.0869	0.1047	0.1012	0.0811	0.0781	0.0933	0.0695
BaO	0.0108	0		0.0881			0.1635	0.1247
Tot	99.55	99.32	99.28	96.53	99.66	100.06	98.58	99.59
Ab %	47.589	49.69	73.56	47.007	48.192	49.246	57.227	48.754
An %	51.853	49.93	25.868	49.763	51.503	50.289	27.882	37.984
Or %	0.5584	0.3799	0.5726	3.2301	0.3055	0.4643	14.891	13.262

Rock	Quartz-diorite							
Sample	CVP27 (Briatico)							
Label	Pl4.9	Pl4.11	Pl4.12	Pl5.1	Pl5.2	Pl5.3	Pl5.4	Pl5.5
SiO_2	55.24	58.83	55.53	60.29	53.7	56.84	52.95	55.23
TiO_2	0.0121		0.0133	0.0299	0.013	0.0274		
Al_2O_3	28.38	25.82	28.22	24.81	29.64	27.56	30.16	28.37
FeO	0.2085	0.3256	0.2316		0.0347	0.0362	0.0058	0.0536
MnO	0.0057			0.0042	0.0245	0.0756		
Na_2O	5.7	7.26	5.94	7.18	4.84	6.4	4.54	5.64
MgO								
CaO	10.2	7.09	9.69	6.97	11.56	9.03	11.99	9.98
K_2O	0.0605	0.3243	0.0816	0.0653	0.0096	0.0756	0.0725	0.0798
SrO	0.0729	0.1256	0.0374	0.1022	0.0999	0.108	0.1035	0.0834
BaO		0.0412	0.0031		0.0476	0.0248		0.055
Tot	99.88	99.82	99.75	99.45	99.969	100.18	99.822	99.492
Ab %	50.104	63.733	52.342	64.833	43.082	55.945	40.487	50.324
An %	49.546	34.394	47.185	34.779	56.862	43.62	59.087	49.208
Or %	0.3499	1.8732	0.4731	0.388	0.0562	0.4348	0.4254	0.4685

Rock	Tonalite							
Sample	CVP42							
Label	Pl1.2	Pl1.3	Pl1.4	Pl1.5	Pl1.10	Pl1.11	Pl1.12	Pl1.13
SiO_2	54.65	53.38	60.58	56.59	54.8	55.37	54.03	58.8
TiO_2	0.0079				0.0353	0.0006	0.0086	0.0274
Al_2O_3	29.29	30.17	25.14	28.15	28.29	28.93	29.89	26.27
FeO	0.1277	0.0879	0.0327	0.0056	0.0369	0.0255	0.0255	0.0611
MnO	0.004	0.0009	0.0092		0.0051			0.0124
Na_2O	5.15	4.51	7.8	5.97	5.73	5.35	4.77	7.12
MgO							0.03	
CaO	11.04	12	6.13	9.57	10.14	10.3	11.46	7.46
K_2O	0.0266	0.035	0.0425	0.0818	0.07	0.055	0.0343	0.0631
SrO	0.0288	0.1013	0.0929	0.0464	0.1207	0.1071	0.0592	0.0834
BaO			0.0269		0.0219	0.0174		
Tot	100.33	100.29	99.85	100.41	99.25	100.16	100.31	99.90
Ab %	45.704	40.397	69.547	52.775	50.354	48.294	42.875	63.099
An %	54.141	59.397	30.203	46.749	49.241	51.379	56.922	36.533
Or %	0.1553	0.2063	0.2493	0.4758	0.4048	0.3267	0.2029	0.3679

Rock	Tonalite							
Sample	CVP42							
Label	Pl2.1	Pl2.2	Pl2.3	Pl2.4	Pl3.1	Pl3.2	Pl3.3	Pl3.4
SiO_2	54.65	56	55.31	56.76	62.27	52.51	55.43	61.94
TiO_2		0.0206	0.0584	0.0051	0.07			
Al_2O_3	28.93	28.27	29.1	27.94	23.99	30.68	28.45	24.09
FeO	0.0284	0.0284	0.1575	0.0554	0.0227	0.0128	0.0752	0.0156
MnO		0.0006		0.0074	0.0218	0.0249	0.0015	0.012
Na_2O	5.25	5.82	5.4	6.21	8.86	4.33	5.78	8.66
MgO								
CaO	10.71	9.85	8.28	9.36	4.88	12.25	10.08	4.93
K_2O	0.0318	0.0576	1.21	0.0551	0.0583	0.0428	0.0507	0.1051
SrO	0.0911	0.0937	0.1446	0.0822	0.0749	0.0609	0.1209	0.0647
BaO	0.002				0.0333	0.0289		0.0324
Tot	99.69	100.14	99.66	100.48	100.28	99.94	99.99	99.85
Ab %	46.92	51.5	50.131	54.385	76.412	38.913	50.775	75.61
An %	52.893	48.165	42.477	45.298	23.257	60.834	48.932	23.786
Or %	0.187	0.3354	7.3912	0.3175	0.3308	0.2531	0.293	0.6038

Rock	Tonalite							
Sample	CVP42							
Label	Pl3.5	Pl3.6	Pl3.7	Pl3.8	Pl3.9	Pl3.10	Pl3.11	Pl4.1
SiO_2	57.72	54.99	55.56	60.86	54.66	54.44	54.84	57.15
TiO_2			0.0026					0.0026
Al_2O_3	27.28	29.01	28.26	24.88	29.38	29.32	29	27.73
FeO	0.071	0.0752	0.0582	0.2046	0.0412	0.0171	0.0909	0.0142
MnO			0.0036	0.0054	0.0052		0.0089	0.0072
Na_2O	6.5	5.51	5.86	7.91	5.05	5.02	5.5	6.2
MgO								
CaO	8.64	10.64	9.94	6.06	11.26	11.18	10.6	8.95
K_2O	0.0552	0.0755	0.0404	0.098	0.048	0.0232	0.0584	0.0698
SrO	0.0488	0.0953	0.0586	0.0578	0.119	0.0461	0.0636	0.1185
BaO		0.026	0.0072		0.0254	0.0263	0.0511	0.0186
Tot	100.32	100.42	99.79	100.08	100.59	100.07	100.21	100.26
Ab %	57.467	48.167	51.496	69.856	63.733	52.342	64.833	43.082
An %	42.212	51.399	48.27	29.574	34.394	47.185	34.779	56.862
Or %	0.3211	0.4343	0.2336	0.5695	1.8732	0.4731	0.388	0.0562

Rock	Tonalite							
Sample	CVP42							
Label	Pl4.2	Pl4.3	Pl4.4	Pl4.5	Pl5.1	Pl5.2	Pl5.3	Pl5.4
SiO_2	59.78	55.22	53.95	60.73	54.89	55.37	55.28	58.96
TiO_2						0.0117	0.0142	0.0026
Al_2O_3	26.04	28.91	28.98	24.26	28.9	28.93	29.03	26.31
FeO		0.0398	0.1051	0.2924	0.0752		0.0355	0.1251
MnO		0.055	0.0025	0.0079		0.0084		0.0038
Na_2O	7.5	5.56	4.94	8.65	5.43	5.39	5.44	7.03
MgO								
CaO	6.75	10.26	9.16	5.31	10.32	10.28	10.37	7.44
K_2O	0.0909	0.0499	0.8615	0.0859	0.0472	0.0513	0.0361	0.0544
SrO	0.1008	0.089	0.1057	0.0708	0.109		0.0355	0.1251
BaO	0.0152	0.0366	0.0074	0.0448	0.0512	0.0613	0.1162	0.066
Tot	100.28	100.22	98.11	99.45	99.82	100.10	100.36	100.12
Ab %	55.945	40.487	50.324	64.016	49.185	48.539	48.597	62.896
An %	43.62	59.087	49.208	35.718	50.106	51.157	51.191	36.784
Or %	0.4348	0.4254	0.4685	0.2668	0.709	0.304	0.2122	0.3202

Rock	Tonalite							
Sample	CVP10							
Label	Pl1.1	Pl1.2	Pl1.3	Pl1.4	Pl1.5	Pl3.1	Pl3.2	Pl3.3
SiO_2	54.16	55.35	56.63	55.5	56.55	55.8	57.37	55.97
TiO_2	0.0166				0.0042	0.0243	0.0294	
Al_2O_3	29.13	28.85	27.62	28.32	27.44	28.24	27.42	28.05
FeO	0.0355	0.0454	0.0425	0.0156	0.1534		0.1434	
MnO		0.0085		0.0191		0.022	0.0046	
Na_2O	5.23	5.59	6.42	5.54	6.36	5.77	6.37	5.93
MgO								
CaO	11.03	10.45	8.94	9.98	8.87	9.72	8.63	9.39
K_2O	0.0506	0.1013	0.1119	0.0945	0.1241	0.1195	0.1456	0.0671
SrO	0.0232	0.0493	0.0998	0.0826	0.1009	0.086	0.1253	0.1155
BaO	0.009	0	0.0025	0	0.002	0.0594	0.0541	0
Tot	99.68	100.44	99.87	99.55	99.60	99.84	100.29	99.52
Ab %	46.045	48.901	56.149	49.833	56.069	51.426	56.699	53.122
An %	53.662	50.516	43.207	49.608	43.211	47.873	42.448	46.483
Or %	0.2931	0.5831	0.6439	0.5593	0.7199	0.7008	0.8527	0.3955

Rock	Tonalite							
Sample	CVP11							
Label	Pl3.4	Pl3.5	Pl3.6	Pl3.7	Pl3.8	Pl4.1	Pl4.2	Pl4.3
SiO_2	56.88	55.42	57.59	62.18	78.57	55.56	54.85	56.14
TiO_2			0.0218			0.0159	0.0006	0.0425
Al_2O_3	27.4	28.65	26.78	23.14	14.41	28.32	29	28.27
FeO	0.0284	0.0753	0.0554	0.175		0.0767	0.0227	0.0099
MnO		0.0187	0.0071		0.0126		0.0043	0.0072
Na_2O	6.36	5.55	6.53	9.13	3.33	5.73	5.18	5.79
MgO								
CaO	8.81	9.52	8.03	4.31	4.39	9.59	10.59	9.62
K_2O	0.1466	0.5011	0.2471	0.1002	0.3686	0.2281	0.1074	0.0818
SrO	0.119	0.0911	0.0885	0.0177	0.0873	0.1069	0.072	0.0196
BaO	0.0219	0.0546	0.0121	0	0.0684	0	0	0.0234
Tot	99.77	99.88	99.36	99.05	101.24	99.63	99.83	100.00
Ab %	56.16	49.818	58.67	78.859	55.514	51.254	46.655	51.882
An %	42.989	47.222	39.869	20.572	40.442	47.403	52.708	47.635
Or %	0.8518	2.9596	1.4608	0.5695	4.0432	1.3425	0.6365	0.4823

Rock	Tonalite								
Sample	CVP11								
Label	Pl5.1rim	Pl5.1core	Pl5.1rim	Pl5.2rim	Pl5.2int	Pl5.2rim	Pl6.1rim	Pl6.1core	Pl6.1rim
SiO_2	57.26	57.2	55.8	56.88	55.47	56.03	55.39	55.78	55.88
TiO_2					0.0011				0.0833
Al_2O_3	26.67	27.32	28.57	27.56	28.48	28.1	28.52	27.75	28.35
FeO	0.0185	0.0085	0.0781	0.0569	0.0498	0.0853	0.0384	0.0298	0.0427
MnO	0.0533		0.0145	0.0145		0.0069	0.0145	0.0063	
Na_2O	6.05	6.44	5.56	6.36	5.65	5.85	5.65	5.66	5.77
MgO									
CaO	8.74	8.6	10.06	8.94	10	9.5	9.92	9.32	9.46
K_2O	0.2149	0.1061	0.0921	0.1265	0.1128	0.1929	0.1292	0.4981	0.1267
SrO	0.0671	0.1098	0.0906	0.0655	0.1036	0.0607	0.1078	0.0777	0.0087
BaO	0	0.0377	0	0.0188	0.0363	0.0476	0	0.0383	0
Tot	99.07	99.82	100.27	100.02	99.90	99.87	99.77	99.16	99.72
Ab %	54.895	57.183	49.733	55.87	50.221	52.108	50.371	50.817	52.071
An %	43.822	42.198	49.725	43.398	49.119	46.761	48.871	46.24	47.176
Or %	1.283	0.6199	0.542	0.7312	0.6597	1.1306	0.7579	2.9425	0.7523

Rock	Tonalite							
Sample	CVP38							
Label	Pl1.1	Pl1.2	Pl1.3	Pl1.4	Pl1.5	Pl1.6	Pl2.1	Pl2.2
SiO_2	61.28	56.34	60.97	60.45	56.04	56.74	60.43	56.14
TiO_2		0.003		0.0102	0.0229		0.9309	
Al_2O_3	24.82	28.16	24.91	24.93	28.47	27.71	24.38	28.01
FeO	0.017	0.0426		0.0582	0.0468	0.1206	0.2695	0.0341
MnO			0.0026			0.0149		0.0099
Na_2O	8.11	5.93	7.97	7.96	5.65	6.15	8.05	5.79
MgO								
CaO	5.92	9.64	5.56	6.28	9.87	8.92	5.27	9.69
K_2O	0.065	0.0361	0.2818	0.1039	0.0352	0.0852	0.3048	0.0902
SrO	0.0597	0.0869	0.1068	0.0066	0.0852	0.0798	0.0358	0.0914
BaO	0.0127	0.072	0.0144	0.0656				0.015
Tot	100.28	100.31	99.82	99.86	100.22	99.82	99.67	99.87
Ab %	70.99	52.567	70.984	69.225	50.776	55.23	72.115	51.678
An %	28.636	47.222	27.365	30.18	49.016	44.267	26.089	47.793
Or %	0.3744	0.2106	1.6514	0.5945	0.2081	0.5034	1.7966	0.5297

Rock	Tonalite							
Sample	CVP38							
Label	Pl2.3	Pl2.4	Pl2.5	Pl2.6	Pl2.7	Pl2.9	Pl2.10	Pl3.1
SiO_2	54.54	57.3	61.44	53.43	54.73	54.94	55.92	55.22
TiO_2			0.0308		0.0148		0.0339	
Al_2O_3	29.03	27.42	24.43	29.47	29	28.98	27.88	28.63
FeO	0.0454	0	0.0227	0.1178	0.1532	0.2426	0.1788	0.0355
MnO	0.0155	0.0042		0.0074			0.0017	0.0017
Na_2O	5.32	6.36	8.3	4.86	5.26	5.41	6.17	5.69
MgO								
CaO	10.67	8.92	5.24	11.29	10.68	10.29	8.66	10.2
K_2O	0.0712	0.1248	0.1606	0.0805	0.0652	0.0687	0.2635	0.0627
SrO	0.0738	0.0902	0.0909	0.0592	0.0932	0.0739	0.0417	0.0935
BaO	0.0671	0.028	0	0	0	0.0481	0.0248	0.0311
Tot	99.83	100.25	99.72	99.31	100.00	100.05	99.17	99.96
Ab %	47.234	55.93	73.443	43.58	46.945	48.557	55.441	50.054
An %	52.35	43.348	25.622	55.945	52.672	51.037	43.001	49.583
Or %	0.4159	0.7221	0.935	0.475	0.3829	0.4057	1.5579	0.3629

Rock	Tonalite							
Sample	CVP38							
Label	Pl3.2	Pl3.3	Pl3.4	Pl3.5	Pl3.6	Pl3.7	Pl3.8	Pl3.9
SiO_2	57.2	56.87	55.62	60.15	56.09	56.71	55.3	55.17
TiO_2			0.0305	0.0138				
Al_2O_3	26.94	27.57	27.97	25.56	28.25	27.48	28.35	28.36
FeO	0.0227	0.0213	0.051		0.0681	0.0255		0.0511
MnO	0.0077				0.0173	0.0025	0.0037	0.0022
Na_2O	6.1	6.3	5.84	7.61	5.95	6.26	5.75	5.49
MgO								
CaO	8.34	9.08	9.66	6.62	9.56	8.96	9.86	9.86
K_2O	0.7084	0.0439	0.0773	0.1662	0.0628	0.0465	0.0593	0.0687
SrO	0.0505	0.0481	0.084	0.0907	0.076	0.1261	0.0757	0.1011
BaO	0.0543		0.0498		0.0604	0.0402	0	0.0202
Tot	99.42	99.93	99.38	100.21	100.13	99.65	99.40	99.12
Ab %	54.587	55.524	52.008	66.886	52.775	55.685	51.167	49.983
An %	41.242	44.222	47.539	32.153	46.858	44.043	48.486	49.606
Or %	4.1711	0.2546	0.453	0.9612	0.3665	0.2722	0.3472	0.4115

Rock	Tonalite						
Sample	CVP38						
Label	Pl3.10	Pl3.11	Pl4.1	Pl4.2	Pl4.3	Pl4.4	Pl4.5
SiO_2	53.56	61.11	58.76	54.02	55.44	56.31	70.56
TiO_2	0.0294	0.0277	0.0277			0.0108	
Al_2O_3	29.64	24.52	26.22	29.25	28.83	28.26	19.55
FeO	0.1006	0.1448	0.0454	0.0412	0.0412	0.0042	0.0213
MnO	0.0046	0.0091		0.005			
Na_2O	4.85	8.22	7.21	3.71	5.65	6	6.2
MgO							
CaO	11.28	5.72	7.51	10.24	10.28	9.29	4.85
K_2O	0.0608	0.0893	0.0397	2.13	0.0953	0.0663	0.0819
SrO	0.0709	0.0981	0.1259	0.0749	0.0561	0.0836	0.0488
BaO	0.0053	0	0	0.0356	0.0913	0.0047	0.021
Tot	99.60	99.94	99.94	99.51	100.48	100.03	101.33
Ab %	43.602	71.855	63.323	34.447	49.59	53.68	69.398
An %	56.038	27.631	36.448	52.54	49.86	45.929	29.999
Or %	0.3597	0.5136	0.2294	13.013	0.5504	0.3903	0.6032

Rock	Tonalite							
Sample	CVP35							
Label	Pl1.1	Pl1.2	Pl1.3	Pl1.4	Pl1.5	Pl1.6	Pl2.1	Pl2.4
SiO_2	56.85	63.73	56.99	58.09	57.54	60.98	65.18	57.41
TiO_2	0.0675	0	0.0029	0.0319	0	0.0248		0.0314
Al_2O_3	27.93	23.42	28.08	27.02	27.51	24.78	22.24	27.42
FeO	0.0128	0.0711	0.051			0.0384		0.0427
MnO	0.0111		0.005		0.0145	0.0042	0.0036	
Na_2O	6.18	9.12	6.06	6.73	6.42	8.22	9.95	6.63
MgO								
CaO	9.1	4.04	9.34	8.41	8.66	5.35	2.95	8.76
K_2O	0.0628	0.0688	0.0482	0.0379	0.0827	0.1606	0.0603	0.0604
SrO	0.0899	0.0857	0.1028	0.0842	0.1167	0.0547	0.1056	0.0587
BaO		0.0336	0.0266	0.0706	0.0186	0.0419		0.0594
Tot	100.30	100.57	100.71	100.47	100.36	99.65	100.49	100.47
Ab %	54.933	80.016	53.852	59.023	57.016	72.859	85.629	57.599
An %	44.699	19.587	45.866	40.758	42.5	26.204	14.029	42.055
Or %	0.3673	0.3972	0.2818	0.2187	0.4833	0.9366	0.3415	0.3453

Rock	Tonalite							
Sample	CVP35							
Label	Pl2.5	Pl2.6	Pl2.7	Pl3.1	Pl3.2	Pl3.3	Pl3.4	Pl3.5
SiO_2	56.63	62.2	57.15	57.38	55.94	56.42	56.72	55.88
TiO_2			0.002	0.0091				9.21
Al_2O_3	28.08	24.06	27.95	27.28	28.22	28.12	27.8	27.7
FeO	0.0369	0.0014	0.0696	0.0469		0.0355		0.0284
MnO	0.0155	0.0002				0.0043	0.0185	
Na_2O	6.26	8.85	6.22	6.5	5.96	6.15	6.17	6.21
MgO				0.0469		0.0355		0.0284
CaO	9.38	5	9.16	8.47	9.58	9.09	9.26	0.1026
K_2O	0.044	0.0913	0.0696	0.126	0.0671	0.0621	0.0612	0.0379
SrO	0.1006	0.0981	0.144	0.0833	0.0806	0.0708	0.0753	0.0976
BaO	0.0626		0.077	0.017	0.0746	0.0666	0.047	0.0068
Tot	100.61	100.30	100.84	99.96	99.92	100.05	100.15	99.30
Ab %	54.566	75.815	54.91	57.709	52.752	54.842	54.47	98.702
An %	45.182	23.67	44.686	41.555	46.857	44.793	45.175	0.9011
Or %	0.2524	0.5146	0.4043	0.7361	0.3908	0.3644	0.3555	0.3964

Rock	Tonalite				Tonalite			
Sample	CVP35				CVP33			
Label	Pl3.6	Pl3.7	Pl3.8	Pl3.9	Pl1.1	Pl1.2	Pl1.3	Pl1.4
SiO_2	56.63	57.42	53.96	56.55	55.52	55.83	55.52	55.52
TiO_2	0.0294	0.0153	0.017		0.0566	0	0	0.0817
Al_2O_3	27.57	27.61	29.15	28.08	28.5	28.53	28.73	28.98
FeO	0.0384	0.0341	0.0142	0.0326	0.0823	0.0241	0.0895	0.0171
MnO	0.0004							0.0018
Na_2O	6.26	6.42	5.12	5.97	5.58	5.89	5.48	5.49
MgO	0.0384							
CaO	8.96	8.82	10.66	9.56	10.02	9.79	10.1	10.21
K_2O	0.0837	0.0707	0.0773	0.0861	0.0619	0.1015	0.1212	0.0541
SrO	0.1089	0.0642	0.0931	0.1032	0.0876	0.0393	0.0819	0.1047
BaO		0.0308	0.0109	0.0394			0.0284	
Tot	99.72	100.49	99.10	100.42	99.91	100.20	100.15	100.46
Ab %	55.564	56.611	46.286	52.787	50.01	51.818	49.188	49.16
An %	43.948	42.978	53.254	46.712	49.625	47.595	50.097	50.521
Or %	0.4888	0.4102	0.4598	0.5009	0.365	0.5875	0.7158	0.3187

Rock	Tonalite							
Sample	CVP33							
Label	P2.1	P2.2	P2.3	P2.4	Pl3.1	Pl3.2	Pl3.3	Pl3.4
SiO_2	55.35	55.03	56.28	59.04	56.95	56.88	54.73	56.34
TiO_2	0.0345	0.013	0.0062	0.0133	0.0029			
Al_2O_3	28.74	28.28	28.56	26.51	27.47	27.89	29.32	28.12
FeO		0.0071	0.0142	0.1052	0.0412	0.071	0.0497	0.0511
MnO		0.0036	0.019					
Na_2O	5.63	5.44	5.59	6.89	6.39	6.05	5.17	5.99
MgO								
CaO	10.22	10.18	10.07	7.79	8.68	9.05	10.92	9.58
K_2O	0.0429	0.1014	0.283	0.1927	0.0672	0.3453	0.0781	0.1258
SrO	0.1133	0.0586	0.0949	0.0485	0.0605	0.1154	0.087	0.089
BaO	0.0646	0.0151	0.0261	0.0103	0.0058	0.051	0	0.0476
Tot	100.20	99.13	100.94	100.60	99.67	100.45	100.35	100.34
Ab %	49.797	48.867	49.291	60.857	56.897	53.643	45.932	52.698
An %	49.953	50.533	49.067	38.023	42.709	44.342	53.612	46.574
Or %	0.2497	0.5993	1.6419	1.1199	0.3937	2.0145	0.4565	0.7282

Rock	Tonalite							
Sample	CVP33							
Label	Pl3.5	Pl3.6	Pl4.1	Pl4.2	Pl4.3	Pl4.4	Pl4.5	Pl5.1
SiO_2	56.74	61.77	55.87	55.85	55.98	55.43	54.76	57
TiO_2	0.0111	0.0317	0.0221		0.0479	0.0144		
Al_2O_3	27.91	24.88	28.56	28.45	28.47	28.94	29.52	27.6
FeO	0.0497	0.1337	0.0128	0.0655	0.0014	0.0399	0.0427	0.0526
MnO	0.0143	0.0002				0.0047		
Na_2O	6.05	8.22	5.73	5.68	5.76	5.33	5.16	6.13
MgO								
CaO	9.5	5.69	9.9	10.04	10.01	10.45	10.82	9.02
K_2O	0.1146	0.0713	0.0338	0.0534	0.1103	0.0516	0.0507	0.0501
SrO	0.0724	0.0845	0.0955	0.0983	0.107	0.0855	0.0622	0.0853
BaO	0.0174	0.0509	0.0779	0.0009	0.0123	0.0204	0.0034	0
Tot	100.48	100.93	100.30	100.24	100.50	100.37	100.42	99.94
Ab %	53.186	72.034	51.056	50.43	50.686	47.852	46.185	54.99
An %	46.151	27.554	48.746	49.259	48.675	51.844	53.517	44.714
Or %	0.6629	0.4111	0.1982	0.312	0.6386	0.3048	0.2986	0.2957

Rock	Tonalite			Tonalite				
Sample	CVP33			CVP29				
Label	Pl5.2	Pl5.3	Pl5.4	Pl1.2	Pl1.3	Pl1.4	Pl1.5	Pl1.6
SiO_2	56.42	56.41	55.93	55.89	59.61	55.39	61.24	55.35
TiO_2			0.0334		0.0104		0.031	0.0108
Al_2O_3	27.83	28.18	28.27	27.86	24.97	28.08	24.02	28.18
FeO	0.0441	0.0199	0.0028	0.0099	0.027	0.0426	0.0512	0.0355
MnO	0.0045	0.0104			0.0077		0.0264	0.0026
Na_2O	6.06	5.76	5.78	5.72	7.59	5.52	8.25	5.52
MgO								
CaO	9.46	9.58	9.6	10.19	6.8	10.26	5.56	10.4
K_2O	0.0517	0.0802	0.0362	0.0645	0.0528	0.0937	0.0643	0.061
SrO	0.1028	0.0874	0.1081	0.0603	0.0941	0.0784	0.111	0.0671
BaO	0.032	0.0046	0.0442		0.0014	0.0525		0.0444
Tot	100.01	100.13	99.80	99.79	99.16	99.52	99.35	99.67
Ab %	53.526	51.861	52.031	50.204	66.682	49.061	72.593	48.819
An %	46.174	47.664	47.755	49.423	33.013	50.391	27.035	50.826
Or %	0.3005	0.4751	0.2144	0.3725	0.3052	0.548	0.3723	0.355

Rock	Tonalite							
Sample	CVP29							
Label	Pl1.7	Pl1.8	Pl1.9	Pl2.1	Pl2.2	Pl2.3	Pl2.4	Pl2.5
SiO_2	60.67	55.32	54.72	59.74	55.67	61.57	55.92	62.67
TiO_2			0.0357	0.0424		0.0268	0.013	
Al_2O_3	24.32	28.2	28.58	25.43	28.45	24.69	28.56	23.79
FeO	0.1634		0.0852	0.0057	0.0114	0.0356	0.0497	0.01
MnO	0.0017	0.0058	0.0136	0.009	0.0023			0.0061
Na_2O	8.04	5.57	5.3	7.86	5.79	8.16	5.72	8.77
MgO								
CaO	5.81	10.06	10.78	6.56	9.9	5.78	10.21	4.56
K_2O	0.1848	0.3037	0.079	0.1386	0.0869	0.0756	0.1006	0.0809
SrO	0.2098	0.0502	0.0698	0.0376	0.0923	0.0835	0.0972	0.0875
BaO	0.0572	0.0025	0.0332	0.0507	0	0.0571	0	0.0216
Tot	99.46	99.51	99.70	99.87	100.00	100.48	100.67	100.00
Ab %	70.699	49.166	46.865	67.898	51.158	71.555	50.051	77.316
An %	28.232	49.07	52.675	31.315	48.337	28.009	49.369	22.215
Or %	1.0692	1.7639	0.4596	0.7878	0.5052	0.4362	0.5792	0.4693

Rock	Tonalite							
Sample	CVP29							
Label	Pl2.6	Pl2.7	Pl3.1	Pl3.2	Pl3.3	Pl3.4	Pl3.5	Pl3.6
SiO_2	56.12	56.09	59.96	55.33	55.55	55.04	77.51	55.73
TiO_2			0.0045	0.0142		0.0288		0.0197
Al_2O_3	28.49	28.16	25.17	29.1	28.96	29.22	13.89	28.02
FeO	0.0341	0.3122	0.1321	0.0795	0.0326	0.088		0.0838
MnO	0.025			0.0011	0.0012	0.004		0.0013
Na_2O	5.67	5.69	7.96	5.45	5.67	5.25	4.47	5.97
MgO								
CaO	9.91	9.47	6.49	10.6	10.15	9.53	2.05	9.84
K_2O	0.1222	0.5014	0.0572	0.073	0.0869	0.6819	2.47	0.0963
SrO	0.0776	0.0907	0.1013	0.0792	0.1277	0.0957	0.0458	0.1129
BaO		0.045		0.02	0.0266		0.1251	0.0256
Tot	100.45	100.36	99.88	100.75	100.61	99.94	100.56	99.90
Ab %	50.505	50.564	68.715	47.994	50.017	47.88	61.842	52.045
An %	48.779	46.504	30.96	51.583	49.478	48.028	15.673	47.403
Or %	0.7162	2.9317	0.3249	0.423	0.5044	4.0919	22.485	0.5524

Rock	Tonalite							
Sample	CVP29							
Label	Pl3.7	Pl4.1	Pl4.2	Pl4.3	Pl4.4	Pl4.5	Pl5.1	Pl5.2
SiO_2	56.85	55.1	60.53	55.48	80.31	62.05	60.8	60.5
TiO_2	0.0113	0.0212		0.0254	0.0181		0.0017	0.0087
Al_2O_3	27.93	28.96	25.43	28.52	14.33	24.71	25.57	24.45
FeO	0.1561	0.061		0.005	0.0314	0.044	0.152	0.0368
MnO	0.0062		0.0121	0.0076	0.0202	0.0034		
Na_2O	6.29	5.35	7.84	5.47	3.15	7.99	7.62	7.26
MgO								
CaO	9.17	10.57	6.54	9.89	4.77	5.32	6.74	5.18
K_2O	0.0654	0.0644	0.0823	0.3937	0.0253	0.3977	0.0537	1.52
SrO	0.0675	0.0925	0.0381	0.056	0.0028	0.0865	0.0466	0.1113
BaO	0.0245	0.0701	0.0685	0	0.0089	0	0	1.52
Tot	100.57	100.29	100.54	99.85	102.67	100.60	100.98	100.59
Ab %	55.174	47.626	68.126	48.864	54.286	71.393	66.96	65.273
An %	44.449	51.997	31.404	48.822	45.427	26.268	32.729	25.736
Or %	0.3775	0.3772	0.4706	2.3141	0.2869	2.3382	0.3105	8.9919

Rock	Tonalite					Leuco-tonalite		
Sample	CVP29					CVP4		
Label	Pl5.3	Pl5.4	Pl5.5	Pl5.6	Pl5.7	Pl1.1	Pl1.2	Pl1.3
SiO_2	55.61	60.01	53.67	55.22	55.35	59.47	55.91	58.37
TiO_2	0.0192	0.0212	0.01			0.0175		0.0651
Al_2O_3	28.75	25.91	30.28	28.56	29.01	25.43	28.8	26.44
FeO	0.044	0.0355	0.0752	0.0227	0.0469	0.0283	0.0014	
MnO		0.0105			0.0001	0		0.0086
Na_2O	5.59	7.59	4.72	5.28	5.54	7.59	5.87	6.81
MgO						0.2318	0.1751	0.1712
CaO	10.2	6.84	11.73	10.14	10.32	6.69	9.7	7.79
K_2O	0.061	0.0355	0.0514	0.7164	0.0576	0.1194	0.1239	0.3698
SrO	0.1205	0.0677	0.0658	0.1371	0.0716	0.0856	0.11	0.0553
BaO	0.0279	0.0538	0.0892	0.0146	0.0264		0.0242	0.0435
Tot	100.42	100.57	100.69	100.09	100.42	99.66	100.71	100.12
Ab %	49.615	66.619	42.008	46.501	49.11	66.781	51.893	59.957
An %	50.028	33.176	57.691	49.348	50.554	32.527	47.386	37.9
Or %	0.3562	0.205	0.301	4.1511	0.336	0.6912	0.7207	2.1423

Rock	Leuco-tonalite							
Sample	CVP4							
Label	Pl1.4	Pl1.5	Pl2.1	Pl2.2	Pl2.3	Pl2.4	Pl2.5	Pl4.1
SiO_2	56.13	59.2	59.75	55.97	60.13	55.91	59.52	89.52
TiO_2			0.0263	0.0277		0.0343		
Al_2O_3	27.97	26.08	25.62	28.33	25.38	28.26	25.76	7.74
FeO	0.0157	0.01	0.0071	0.0255	0.0085	0.0085	0.01	
MnO								
Na_2O	6.02	7.18	7.51	5.75	7.57	5.85	7.45	2.08
MgO	0.296	0.3678						
CaO	9.49	7.22	6.98	9.97	6.57	9.76	6.83	2.14
K_2O	0.1068	0.1004	0.1463	0.1143	0.1352	0.0594	0.0607	0.0229
SrO	0.0923	0.0422	0.0857	0.0616	0.0701	0.11	0.0901	0.0529
BaO	0.0083	0.0227		0.0215	0.0117	0.0624		0.0178
Tot	100.13	100.22	100.13	100.27	99.88	100.05	99.72	101.57
Ab %	53.112	63.903	65.513	50.729	67.053	51.85	66.139	63.46
An %	46.268	35.509	33.647	48.607	32.159	47.803	33.507	36.08
Or %	0.62	0.588	0.8397	0.6635	0.788	0.3464	0.3546	0.4597

Rock	Leuco-tonalite							
Sample	CVP4							
Label	Pl1.4	Pl1.5	Pl2.1	Pl2.2	Pl2.3	Pl2.4	Pl2.5	Pl4.1
SiO_2	56.13	59.2	59.75	55.97	60.13	55.91	59.52	89.52
TiO_2			0.0263	0.0277		0.0343		
Al_2O_3	27.97	26.08	25.62	28.33	25.38	28.26	25.76	7.74
FeO	0.0157	0.01	0.0071	0.0255	0.0085	0.0085	0.01	
MnO								
Na_2O	6.02	7.18	7.51	5.75	7.57	5.85	7.45	2.08
MgO	0.296	0.3678						
CaO	9.49	7.22	6.98	9.97	6.57	9.76	6.83	2.14
K_2O	0.1068	0.1004	0.1463	0.1143	0.1352	0.0594	0.0607	0.0229
SrO	0.0923	0.0422	0.0857	0.0616	0.0701	0.11	0.0901	0.0529
BaO	0.0083	0.0227		0.0215	0.0117	0.0624		0.0178
Tot	100.13	100.22	100.13	100.27	99.88	100.05	99.72	101.57
Ab %	53.112	63.903	65.513	50.729	67.053	51.85	66.139	63.46
An %	46.268	35.509	33.647	48.607	32.159	47.803	33.507	36.08
Or %	0.62	0.588	0.8397	0.6635	0.788	0.3464	0.3546	0.4597

Rock	Leuco-tonalite							
Sample	CVP4							
Label	Pl4.2	Pl4.3	Pl4.4	Pl4.5	Pl4.6	Pl5.1	Pl5.2	Pl5.3
SiO_2	60.06	56.3	59.35	66.08	59.97	55.22	55.68	58.81
TiO_2	0.0251	0			0.0368	0.0232	0.0153	
Al_2O_3	25.45	28.09	26.13	19.68	25.68	28.75	28.34	25.79
FeO	0.037	0.0185		0.0354		0.0057		0.0199
MnO								0.0059
Na_2O	7.75	6	7.28	8.13	7.48	5.54	5.65	7.22
MgO								
CaO	6.43	9.5	7.25	0.4127	6.78	10.18	9.79	7.12
K_2O	0.0979	0.1386	0.071	3.99	0.1586	0.0911	0.087	0.1126
SrO	0.0757	0.0579	0.0863	0.0517	0.0615	0.0896	0.103	0.0854
BaO	0.0356	0	0.0119	0.6753	0.0036	0.0324		
Tot	99.96	100.11	100.18	99.06	100.17	99.93	99.67	99.16
Ab %	68.176	52.906	64.237	74.021	66.014	49.352	50.822	64.3
An %	31.257	46.29	35.351	2.0764	33.065	50.114	48.663	35.04
Or %	0.5667	0.8041	0.4122	23.903	0.921	0.534	0.5149	0.6598

Rock	Leuco-tonalite				MME			
Sample	CVP4				CVP25E			
Label	Pl6.1	Pl6.2	Pl6.3	Pl6.4	Pl1.2	Pl1.3	Pl1.4	Pl1.6
SiO_2	60.14	59.74	64.62	68.5	55.58	55.49	55.16	56.59
TiO_2	0.0122	0.0045		0.0082		0.0665		0.0455
Al_2O_3	25.86	25.75	22.62	20.46	28.13	27.66	28.16	27.57
FeO				0.0071		0.0099	0.088	0.0709
MnO			0.0151				0.0075	
Na_2O	7.48	7.48	9.28	7.54	5.82	5.56	5.55	6.12
MgO								
CaO	7.01	6.81	3.18	3.92	10.07	9.09	10.37	9.27
K_2O	0.0858	0.141	0.5107	0.0638	0.0344	0.6255	0.0781	0.0353
SrO	0.056	0.0657	0.1021	0.0428	0.1075	0.1113	0.0415	0.0801
BaO	0.021		0.021		0.0401	0	0.0428	0.06
Tot	100.67	99.99	100.35	100.54	99.78	98.61	99.50	99.84
Ab %	65.555	65.985	81.595	77.348	51.02	50.57	48.977	54.324
An %	33.95	33.197	15.451	22.222	48.782	45.687	50.57	45.47
Or %	0.4948	0.8184	2.9546	0.4306	0.1984	3.7433	0.4535	0.2062

Rock	MME						
Sample	CVP25E						
Label	Pl2.1	Pl2.2	Pl2.3	Pl3.1	Pl3.2	Pl3.3	Pl3.4
SiO_2	54.19	55.26	54.8	60.2	59.35	55.73	55.33
TiO_2	0.0331		0.0059	0.0426		0.0026	
Al_2O_3	29.38	28.5	28.22	25.41	26.06	27.8	28.63
FeO		0.1376	0.027	0.2456	0.2329	0.278	0.2837
MnO	0.02	0.0068	0.0119	0.012	0.0043	0.0095	
Na_2O	5	5.56	5.51	7.79	7.35	5.79	5.72
MgO							
CaO	11.35	10.44	10.35	6.46	7.19	9.45	9.96
K_2O	0.0608	0.0953	0.2352	0.0407	0.0657	0.4461	0.0661
SrO	0.042	0.0589	0.0075	0.1383	0.0648	0.086	0.0444
BaO		0.0071		0.0101		0.0398	0.0253
Tot	100.08	100.07	99.17	100.35	100.32	99.63	100.06
Ab %	44.201	48.807	48.401	68.414	64.664	51.214	50.766
An %	55.446	50.643	50.24	31.351	34.956	46.19	48.848
Or %	0.3537	0.5504	1.3594	0.2352	0.3803	2.5963	0.386

Rock	MME							
Sample	CVP23E							
Label	Pl1.1	Pl1.2	Pl1.3	Pl1.4	Pl1.6	Pl1.8	Pl1.9	Pl2.1
SiO_2	54.39	53.75	54.83	66.25	56.84	58.82	61.36	54.22
TiO_2			0.004	0.0006	0.0133		0.0581	0.0707
Al_2O_3	29.24	29.77	28.79	19.61	27.65	25.7	24.76	28.39
FeO	0.0908	0.0113	0.0525	0.8206	0.1176	0.0752	0.1476	0.0524
MnO	0.0286			0.0075	0.0146	0.0005		0.0046
Na_2O	5.13	4.75	5.45	6.83	6.13	7.55	8.19	5.69
MgO							0.03	
CaO	10.99	11.43	10.64	0.1422	9.23	6.97	5.76	10.48
K_2O	0.0488	0.0848	0.0429	6.38	0.2364	0.0076	0.0771	0.084
SrO	0.0552	0.0747	0.1049	0.0472	0.0896	0.0729	0.0931	0.0919
BaO				0.2359	0.0226	0.0232		
Tot	99.97	99.87	99.91	100.32	100.34	99.22	100.48	99.08
Ab %	45.66	42.708	47.984	61.496	53.838	66.19	71.693	49.322
An %	54.054	56.79	51.767	0.7075	44.796	33.767	27.863	50.199
Or %	0.2858	0.5017	0.2485	37.797	1.3661	0.0438	0.4441	0.4791

Rock	MME							
Sample	CVP23E							
Label	Pl2.2	Pl2.3	Pl2.4	Pl3.1	Pl3.2	Pl3.3	Pl4.1	Pl4.2
SiO_2	55.53	55.85	61.16	55.16	55.51	61.75	52.53	57.86
TiO_2		0.0395	0.0417			0.0313		0.0037
Al_2O_3	28.78	28.18	24.86	28.81	28.71	25	30.63	26.8
FeO	0.0269	0.0227	0.1433	0.051	0.0624	0.0313	0.0793	0.0355
MnO				0.0256			0.0027	
Na_2O	5.54	5.73	8.1	5.47	5.55	7.92	4.34	6.59
MgO								
CaO	10.28	9.85	5.77	10.41	10.36	5.92	12.34	8.41
K_2O	0.0446	0.0395	0.0711	0.0601	0.0807	0.0737	0.0623	0.0552
SrO	0.0802	0.0751	0.0981	0.0685	0.0422	0.0754	0.0499	0.0383
BaO			0.0181			0.0113		0.039
Tot	100.28	99.79	100.26	100.06	100.32	100.81	100.03	99.83
Ab %	49.244	51.165	71.458	48.57	48.993	70.463	38.75	58.455
An %	50.495	48.603	28.129	51.079	50.538	29.105	60.884	41.223
Or %	0.2609	0.2321	0.4127	0.3511	0.4687	0.4314	0.366	0.3222

Rock	MME							
Sample	CVP23E							
Label	Pl4.3	Pl4.4	Pl4.5	Pl4.6	Pl4.7	Pl5.1	Pl5.2	Pl5.3
SiO_2	55.21	63.22	56.56	54.32	53.6	54.72	55.2	61.56
TiO_2	0.0113				0.0073		0.0124	
Al_2O_3	28.75	24.44	27.35	28.17	29.14	28.61	28.54	24.35
FeO	0.0723	0.3236	0.2864	0.19	0.343	0.1348	0.0397	0.4226
MnO			0.0002		0.009	0.0056		0.0204
Na_2O	5.44	7.54	6.07	5.37	5.08	5.47	5.54	8.34
MgO								
CaO	10.44	5	7.63	10.09	10.79	10.03	10.35	5.25
K_2O	0.0583	0.1337	0.988	0.1373	0.388	0.1271	0.0798	0.1205
SrO	0.0672	0.131	0.1396	0.1354	0.0661	0.0664	0.1045	0.0589
BaO		0.0429		0.0462	0.0628	0.0247		0.0051
Tot	100.05	100.83	99.02	98.46	99.49	99.19	99.87	100.13
Ab %	48.366	72.563	55.503	48.659	63.733	49.296	48.975	73.672
An %	51.293	26.59	38.553	50.523	34.394	49.95	50.561	25.628
Or %	0.3411	0.8466	5.9442	0.8186	1.8732	0.7537	0.4642	0.7004

Rock	*MME*			
Sample	CVP23E			
Label	Pl6.1	Pl6.2	Pl6.3	Pl6.4
SiO_2	52.57	57.07	61.54	61.33
TiO_2				0.0037
Al_2O_3	30.32	27.41	24.1	24.47
FeO	0.0156	0.0723	0.1391	0.3577
MnO	0.0035			0.0231
Na_2O	4.43	6.5	8.49	8.36
MgO				
CaO	12.12	8.82	5.15	5.43
K_2O	0.047	0.0628	0.0477	0.131
SrO	0.0533	0.1098	0.0858	0.095
BaO	0.0689	0.0247		0.0196
Tot	99.63	100.07	99.55	100.22
Ab %	39.701	56.941	74.688	73.033
An %	60.022	42.697	25.036	26.214
Or %	0.2771	0.362	0.2761	0.753

Table 5– Epidote minero-chemical analysis of main lithotypes in Capo Vaticano Promontory.

Rock	Quartz-diorite							
Sample	CVP20 (S.Maria)							
Label	EP1.1	EP1.2	EP1.3	EP1.4	EP1.5	EP1.6	EP1.7	EP2.1
SiO_2	38.75	38.86	38.67	38.17	38.65	38.76	38.24	38.82
TiO_2	0.069	0.0847	0.1887	0.053	0.0546	0.1199	0.1355	0.0878
Al_2O_3	25.65	25.75	26.32	24.28	25.48	25.99	26.07	26.71
FeO	11.18	10.94	9.74	12.57	11.38	10.01	9.93	9.58
MnO	0.2038	0.1754	0.3103	0.4084	0.2731	0.28	0.2498	0.5096
MgO								
CaO	22.57	22.75	22.01	22.03	22.15	22.26	22.46	22.4
La_2O_3	0.0228		0.0137	0.0195	0.0434			
Ce_2O_3			0.0439	0.0223	0.0055	0.0018	0.0081	
Y_2O_3		0.0561	0.3608			0.00875	0.2082	
Tot	98.45	98.62	97.66	97.55	98.04	97.43	97.30	98.11

Rock	Quartz-diorite			Tonalite				
Sample	CVP20 (S. Maria)			CVP42				
Label	EP2.2	EP2.3	EP2.4	EP2.1	EP2.2	EP2.3	EP3.1	EP3.2
SiO_2	38.43	37.87	38.89	38.38	38.19	38.1	35.93	32.73
TiO_2	0.0384	0.0039		0.1022	0.1018		0.0326	0.1588
Al_2O_3	25.54	21.85	27.07	25.29	25.77	25.39	24.31	19.99
FeO	10.7	16.12	9.13	11.53	11.12	11.16	10.46	11.98
MnO	0.223	0.026	0.3006				0.0289	0.4682
MgO				0.2318	0.1751	0.1712	0.296	0.3678
CaO	22.52	23.14	23.45	22.81	22.74	23.33	19.71	13.73
La_2O_3	0.0986	0.0068		0.0957		0.0434	0.8448	3.26
Ce_2O_3			0.0121	0.0952	0.0163	0.0382	1.78	7.21
Y_2O_3	0.0345		0.0649	0.685			0.8151	0.4018
Tot	97.58	99.02	98.92	99.22	98.11	98.23	94.21	90.30

Rock	Tonalite							
Sample	CVP42							
Label	EP3.3	EP3.4	EP3.5	EP3.6	EP3.7	EP3.8	EP3.9	EP3.10
SiO_2	33.12	35.51	38.25	37.94	36.26	34.05	33.43	38.43
TiO_2	0.2079	0.0119			0.0789	0.684	0.1577	0.1052
Al_2O_3	20.71	23.69	26.44	26.2	24.24	21.12	20.28	25.11
FeO	11.62	10.79	10.47	10.53	10.73	11.45	11.69	10.9
MnO	0.4469	0.0918			0.041	0.3971	0.5221	
MgO	0.3882	0.3013	0.2025	0.192	0.3067	0.3948	0.3881	0.2186
CaO	14.66	19.46	23.02	23.41	19.85	14.8	13.77	21.95
La_2O_3	2.78	1.21			0.7516	2.22	3.69	0.3257
Ce_2O_3	5.98	2.78	0.593	0.0258	1.69	5.83	7.38	0.6749
Y_2O_3	0.5379	0.2526			0.7604	0.5782	0.4328	
Tot	90.45	94.10	98.98	98.30	94.71	91.52	91.74	97.71

Rock	Tonalite							
Sample	CVP42							
Label	EP3.11	EP3.12	EP4.1	EP4.2	EP4.3	EP4.4	EP4.5	EP4.6
SiO_2	38.58	38.86	33.33	35.95	38.52	33.52	36.77	36.81
TiO_2	0.1988	0.0588	0.2176	0.0691	0.0583	0.1106	0.0828	0.0904
Al_2O_3	25.06	25.95	20.22	23.44	25.9	20.9	24.09	24.69
FeO	11.92	11.22	11.74	10.83	10.54	11.51	10.84	10.46
MnO			0.5798	0.0891		0.3625	0.035	0.0349
MgO	0.2469	0.1914	0.4277	0.3156	0.1905	0.4006	0.2883	0.2975
CaO	22.81	22.9	13.83	18.83	23.02	14.96	19.51	20.44
La_2O_3	0.0137	0.0137	3.56	1.139	0.0023	2.83	0.9971	0.6632
Ce_2O_3			7.64	2.67	0.0379	6.3	2.2	1.31
Y_2O_3			0.3251	0.764		0.4725	0.5458	0.6486
Tot	98.83	99.19	91.87	94.10	98.27	91.37	95.36	95.44

Rock	Tonalite				Tonalite			
Sample	CVP42				CVP29			
Label	EP4.7	EP4.8	EP4.9	EP4.10	EP1.1	EP1.2	EP1.3	EP1.4
SiO_2	38.86	38.66	38.58	38.38	35.19	34.91	36.5	34.4
TiO_2	0.0355	0.0608	0.0375	0.0915	0.1516	0.1937	0.1333	0.2873
Al_2O_3	25.77	25.9	26.18	26.34	21.75	22.11	24.12	21.32
FeO	10.77	10.82	10.51	10.32	11.1	11.03	10.56	11.68
MnO					0.2236	0.2318	0.2495	0.297
MgO	0.1933	0.1803	0.1892	0.3033	0.328	0.2841	0.1314	0.3556
CaO	22.98	23.2	23.26	23.19	16.8	17.39	19.88	16.56
La_2O_3	0.0252				3.16	2.08	1.21	2.95
Ce_2O_3	0.0031		0.0423		5.67	4.71	2.66	6.14
Y_2O_3					0.0823	0.2336	0.0828	0.1986
Tot	98.64	98.82	98.80	98.62	94.456	93.173	95.527	94.189

Rock	Tonalite							
Sample	CVP29							
Label	EP1.5	EP1.6	EP1.7	EP1.8	EP1.9	EP1.10	EP1.11	EP1.12
SiO_2	35.44	36.69	34.38	35.98	37.98	40.24	38.29	36.91
TiO_2	0.2366	0.1219	0.3097	0.1786	0.1253	0.1278	0.054	0.0593
Al_2O_3	22.44	23.61	21.5	23.19	25.34	24.64	25.54	23.81
FeO	10.83	11	11.11	10.76	10.69	9.75	10.56	10.92
MnO	0.2227	0.1863	0.2438	0.2253	0.2582	0.264	0.2095	0.2423
MgO	0.233	0.116	0.3398	0.1833				
CaO	17.67	19.72	16.71	18.55	22.91	21.05	23.21	20.62
La_2O_3	1.88	2.24	2.64	2.58	0.0114		0.0457	0.887
Ce_2O_3	4.32	2.9	5.26	3.93	0.2325	0.002		1.95
Y_2O_3	0.1125		0.2098	0.0379	0.11		0.073	
Tot	93.3848	96.5842	92.7031	95.6151	97.657	96.074	97.982	95.399

Rock	Tonalite							
Sample	CVP29							
Label	EP1.13	EP1.16	EP2.1	EP2.2	EP2.3	EP2.4	EP2.5	EP2.6
SiO_2	38.49	38.06	37.99	38.45	35.22	38.92	37.45	37.56
TiO_2	0.164	0.1539	0.1054	0.0706	0.0677	0.1684	0.9164	0.2435
Al_2O_3	25.65	25.75	25.53	25.82	25.55	25.96	20.65	19.95
FeO	10.47	10.49	10.66	10.61	10.94	10.49	17.06	17.65
MnO	0.2429	0.2422	0.2864	0.2554	0.2272	0.2438	0.1774	0.1733
MgO								0.7706
CaO	22.83	22.67	22.55	23.19	23.01	23.12	22.14	21.09
La_2O_3	0.0616		0.0251			0.0183		0.0067
Ce_2O_3			0.0042	0.0071			0.036	
Y_2O_3			0.0345	0.0041		0.0199		
Tot	97.9085	97.3661	97.1856	98.4072	95.015	98.94	98.43	97.444

Rock	Tonalite							
Sample	CVP29							
Label	EP2.7	EP2.8	EP2.9	EP2.10	EP2.11	EP2.12	EP2.13	EP2.14
SiO_2	38.37	38.26	38.41	38.82	37.87	38.36	38.17	38.42
TiO_2	0.2058	0.1384	0.2291	0.0514	0.1329	0.0862	0.0647	0.0878
Al_2O_3	25.6	25.32	25.6	25.52	24.88	24.94	24.46	25.15
FeO	11.14	10.89	10.53	10.97	11.14	10.92	11.04	11.13
MnO	0.3295	0.3326	0.3529	0.3296	0.3275	0.3504	0.3292	0.3446
MgO							0.4572	
CaO	11.14	22.13	22.67	22.74	21.89	22.19	21.12	22.35
La_2O_3		0.0365				0.0411		
Ce_2O_3		0.0516			0.0504	0.0584	0.4572	0.0326
Y_2O_3		0.2585	0.0794	0.0574	0.2783	0.1772	0.2065	0.0644
Tot	86.7853	97.4176	97.8714	98.4884	96.569	97.123	96.305	97.579

Rock	Tonalite							
Sample	CVP29							
Label	EP2.15	EP2.16	EP2.17	EP2.18	EP2.19	EP2.20	EP2.21	EP2.22
SiO_2	37.86	39.52	37.82	38.06	37.93	37.98	37.89	37.48
TiO_2	0.4212	0.0601	0.1389	0.1035	0.0511	0.11	0.1097	0.0257
Al_2O_3	21.97	25.29	24.96	24.73	25.01	25.16	25.05	24.63
FeO	15.07	11.3	10.44	10.82	10.68	10.75	10.68	10.45
MnO	0.1067	0.2844	0.2064	0.2109	0.2088	0.2554	0.2498	0.3053
MgO	0.0641							
CaO	22.41	22.53	20.98	22.1	21.92	22.19	21.93	21.36
La_2O_3		0.0342	0.05	0.0592	0.041		0.0387	0.0182
Ce_2O_3	0.0257	0.0092	0.3359	0.1258	0.1963	0.1669	0.1629	0.2371
Y_2O_3			1.0379	0.3623	0.6572	0.6384	0.5826	1.32
Tot	97.9277	99.0279	95.9691	96.5717	96.694	97.251	96.694	95.826

Rock	Tonalite							
Sample	CVP29							
Label	EP2.23	EP2.24	EP2.25	EP2.26	EP2.27	EP2.28	EP2.30	EP2.31
SiO_2	37.61	37.33	37.36	38.22	35.42	38.63	38.39	37.75
TiO_2	0.3199	0.0903	0.0433	0.1074	0.1438	0.1222	0.1091	0.4897
Al_2O_3	24.32	24.21	24.17	25.05	25.57	26.96	25.03	22.21
FeO	10.17	10.73	10.86	10.7	10.45	11.22	11.47	14.4
MnO	0.3199	0.3566	0.2903	0.3154	0.2989	0.296	0.2705	0.1712
MgO								
CaO	21.26	20.71	21.54	22.4	22.56	21.61	22.97	22.62
La_2O_3	0.0501	0.0885	0.1181	0.0637	0.0296	0.009		
Ce_2O_3	0.318	0.4208	0.4579	0.035	0.0231	0.0056	0.0742	0.0037
Y_2O_3	0.9739	1.2438	0.7069	0.2133	0.0862			0.0308
Tot	95.3418	95.18	95.5465	97.1048	94.582	98.853	98.314	97.675

Rock	Tonalite						
Sample	CVP29						
Label	EP3.1	EP3.2	EP3.3	EP3.4	EP3.5	EP3.6	EP3.7
SiO_2	44.6	38.36	38.42	37.89	37.78	38.11	37.58
TiO_2	0.3206	0.0647	0.1199	0.4427	0.2109	0.0563	0.1982
Al_2O_3	19.77	25.58	25.66	21.07	21.47	24.93	22.09
FeO	13.78	10.74	10.62	16.18	16.15	11.95	14.72
MnO	0.0075	0.2752	0.2887	0.0346	0.1385	0.4023	0.0877
MgO							
CaO	17.39	23.13	23.05	22.48	22.44	22.42	22.54
La_2O_3	0.0543				0.0158		0.0068
Ce_2O_3	0.032			0.054		0.0142	
Y_2O_3	0.0451		0.0094				
Tot	95.9995	98.1499	98.168	98.1513	98.205	97.883	97.223

Rock	Tonalite							
Sample	CVP42							
Label	EP1.2	EP1.3	EP1.4	EP1.5	EP1.6	EP1.7	EP1.8	EP1.9
SiO_2	35.3	33.5	31.1	31.31	33.45	32.91	34.02	32.52
TiO_2	0.0096	0.2454	0.5251	0.4848	0.2407	0.1954	0.2888	0.3233
Al_2O_3	25.15	19.9	16.09	16.17	20.04	18.78	20.75	18.73
FeO	7.49	11.69	14.32	14.36	11.55	11.84	11.11	12.8
MnO	0.2022	0.3259	0.4416	0.4275	0.3377	0.4243	0.3017	0.3973
MgO		0.4392	1.4602	1.3478	0.4654	0.9465	0.412	0.7385
CaO	21.06	14.34	9.95	10.19	14.17	9.81	14.64	12.45
La_2O_3	0.7654	4.43	5.78	6.05	4.39	5.16	4.06	4.67
Ce_2O_3	1.39	8.17	11.25	11.28	8.46	9.81	7.61	8.76
Y_2O_3	0.0332	0.0706	0.2127	0.0482	0.1883	0.0675	0.0732	0.2486
Tot	91.40	93.11	91.13	91.67	93.29	89.94	93.27	91.64

Rock	Tonalite			Tonalite				
Sample	CVP42			CVP33				
Label	EP1.10	EP1.11	EP1.12	EP1.2	EP1.3	EP1.4	EP1.5	EP1.6
SiO_2	34.69	36.26	35.87	37.1	37.25	37.33	37.11	37.38
TiO_2	0.1917	0.0514	0.0701	0.1519	0.09	0.1716	0.0839	0.0149
Al_2O_3	21.46	23.81	23.35	25.94	25.96	26.24	26.17	26.3
FeO	11.08	9.54	9.46	10	10.12	9.61	9.1	9.36
MnO	0.3491	0.2756	0.2358	0.2468	0.3062	0.2	0.3753	0.2459
MgO	0.3158	0.01	0.0776					
CaO	16.41	18.89	18.28	22.56	22.55	22.74	21.83	21.82
La_2O_3	3.32	2.22	2.47		0.0137	0.0161	0.0412	
Ce_2O_3	5.61	4.24	4.52		0.006	0.034	0.039	0.183
Y_2O_3	0.1865		0.0852	0.0239			0.0412	0.1783
Tot	93.61	95.30	94.42	94.46	93.17	95.53	94.19	93.38

Rock	Tonalite							
Sample	CVP33							
Label	EP1.8	EP1.9	EP1.10	EP1.11	EP1.12	EP1.14	EP2.1	EP2.2
SiO_2	36.77	37.13	37.22	38.46	38.52	38.65	38.19	38.16
TiO_2	0.1164	0.0448	0.1164	0.1681	0.1097	0.1141	0.0999	0.1078
Al_2O_3	25.92	25.88	22.99	25.63	26	26.23	25.74	25.9
FeO	10.37	10.71	9.93	10.38	9.68	9.48	9.83	10.28
MnO	0.2322	0.2197	0.3429	0.3394	0.2665	0.2923	0.2056	0.2454
MgO								
CaO	22.53	22.84	22.39	22.63	22.12	22.81	22.83	22.42
La_2O_3		0.0046	0.0046				0.0046	
Ce_2O_3		0.0143	0.011		0.0126	0.0417		
Y_2O_3	0.0053	0.0163	0.1689		0.098	0.0853		
Tot	96.58	92.70	95.62	97.66	96.07	97.98	95.40	97.91

Rock	Tonalite							
Sample	CVP33							
Label	EP2.3	EP2.4	EP2.5	EP2.6	EP2.7	EP2.8	EP2.9	EP2.10
SiO_2	38.31	38.39	38.47	38.36	38.57	38.4	38.54	38
TiO_2	0.1987	0.1798	0.1275	0.1962	0.0748	0.1199	0.1066	0.0622
Al_2O_3	25.44	25.76	26.15	26.14	26.11	26.08	26.3	25.96
FeO	10.33	10.07	10.15	10.04	10.14	9.68	9.8	9.54
MnO	0.2536	0.2338	0.2037	0.1916	0.1936	0.1688	0.2048	0.2023
MgO								
CaO	22.63	22.4	22.93	22.94	23.12	23.44	22.92	22.74
La_2O_3		0.0274					0.0275	
Ce_2O_3	0.0331					0.0476	0.0287	0.001
Y_2O_3	0.0557	0.1106						
Tot	97.37	97.19	98.41	95.01	98.94	98.43	97.44	86.79

Rock	Tonalite							
Sample	CVP33							
Label	EP3.2	EP3.3	EP3.4	EP3.5	EP3.6	EP3.7	EP3.8	EP3.9
SiO_2	37.64	37.93	38.01	37.98	38.03	38.53	38.31	38.15
TiO_2	0.0889	0.0803	0.0972	0.0596	0.1103	0.1569	0.0926	0.0866
Al_2O_3	25.04	25.31	25.35	25.46	25.07	26.02	25.85	26.03
FeO	10.78	11.01	10.84	10.62	10.71	10	10.12	10.22
MnO	0.3337	0.2967	0.297	0.3061	0.1541	0.198	0.2352	0.2227
MgO								
CaO	22.66	22.69	22.57	22.4	23.2	23.05	22.9	22.48
La_2O_3	0.057		0.0251		0.0137		0.0023	
Ce_2O_3	0.0525	0.0177		0.0301	0.0422		0.0229	0.0107
Y_2O_3	0.1664	0.0564	0.1225	0.0178	0.0108		0.0157	0.0355
Tot	99.03	95.97	96.57	96.69	97.25	96.69	95.83	95.34

Rock	Tonalite							
Sample	CVP33							
Label	EP3.10	EP3.12	EP 4.1	EP 4.2	EP 4.3	EP 4.4	EP 1.1	EP1.2
SiO_2	38.19	37.65	38.48	38.3	38	38.3	38.76	38.37
TiO_2	0.0741	0.0671	1.2835	0.1	0.1156	0.3288	0.1182	0.0612
Al_2O_3	25.95	25.74	23.5	25.97	25.22	26.36	25.85	25.72
FeO	10.34	10.08	12.02	10.18	10.5	9.65	10.55	10.34
MnO	0.1849	0.2782	0.2564	0.213	0.3054	0.322	0.3065	0.3085
MgO		0.7558				0.0053		
CaO	22.41	21.28	22.75	22.33	22.48	22.19	23.05	22.95
La_2O_3		0.0091	0.0229	0.0526			0	0.0527
Ce_2O_3		0.0355		0.0237	0.0042	0.0397		0.0104
Y_2O_3	0.101	0.0977		0.0506			0.133	0.0458
Tot	95.18	95.55	97.10	94.58	98.85	98.31	97.68	96.00

Rock	Tonalite					MME		
Sample	CVP33					CVP23E (S.Maria)		
Label	EP 1.5	EP 1.6	EP 1.7	EP 1.8	EP 1.9	EP2.1	EP2.2	EP2.3
SiO_2	38.35	37.98	38.39	38.16	37.88	38.5	38.45	36.64
TiO_2	0.1044	0.1054	0.1079	0.0486	0.0696	0.0386	0.06	0.2604
Al_2O_3	26	25.64	26.31	26.11	25.51	25.31	25.21	19.7
FeO	10.09	9.9	9.57	9.65	10.46	11.44	11.65	17.67
MnO	0.3085	0.2887	0.3337	0.3034	0.278	0.3112	0.3369	0.1955
MgO								
CaO	22.95	22.13	22.83	22.63	23.14	23.35	22.98	22.38
La_2O_3	0.0527	0.0687	0.039	0.0619	0.0709	0.0091	0.0274	
Ce_2O_3	0.0104	0.256	0.0887	0.1202	0.0432	0.0134		0.0409
Y_2O_3	0.077	0.1786	0.0529	0.1053	0.0821	0.0138		
Tot	98.15	98.17	98.15	98.21	97.88	98.74	98.088	97.602

Rock	MME							
Sample	CVP23E (S. Maria)							
Label	EP2.4	EP3.1	EP3.2	EP3.3	EP4.1	EP4.2	EP4.3	EP4.4
SiO_2	35.31	38.32	38.44	38.25	38.04	37.14	38.39	38.37
TiO_2	0.2837	0.1136	0.0391	0.0992	0.1386	0.073	0.0946	0.0763
Al_2O_3	16.89	25.27	25.37	25.82	24.89	24.26	25.65	25.4
FeO	21.09	11.35	11.01	10.26	11.49	11.28	11	11.05
MnO	0.1248	0.2443	0.3062	0.2888	0.2676	0.3315	0.2647	0.3123
MgO								
CaO	21.93	22.94	23.16	22.74	23.06	21.46	22.95	23.12
La_2O_3		0.0319		0.0504		0.5202		0.0159
Ce_2O_3	0.021			0.0246	0.0405	1.1047	0.0259	
Y_2O_3		0.0876			0.1164			
Tot	98.787	98.178	97.831	97.542	98.169	97.638	97.451	98.171

Rock	MME					MME		
Sample	CVP23E (S. Maria)					CVP25E (Briatico)		
Label	EP5.1	EP5.2	EP6.2	EP6.3	EP6.4	EP1.1	EP1.2	EP1.3
SiO_2	38.39	38.05	38.08	38.45	38.38	38.65	38.33	38.34
TiO_2	0.1245	0.1451	0.1527	0.124	0.1404	0.1445	0.2595	0.1119
Al_2O_3	25.26	25.21	24.42	24.95	25.2	25.39	25.59	26.17
FeO	11.59	11.24	12.09	11.11	11.2	11.08	10.9	9.86
MnO	0.4102	0.4621	0.324	0.3576	0.3132	0.3934	0.3614	0.3058
MgO								
CaO	22.99	22.86	22.46	22.57	23.06	23.06	22.58	22.78
La_2O_3	0.0274						0.064	0.0023
Ce_2O_3	0.0127	.	0.0002	0.036	0.0276	0.022	0.0034	0.0219
Y_2O_3	0.0151	0.0855			0.0118			0.0102
Tot	98.28	98.189	92.29	96.879		98.74	98.088	97.602

Rock	MME							
Sample	CVP25E (Briatico)							
Label	EP2.1	EP2.2	EP2.3	EP3.1	EP3.82	EP3.3	EP3.6	EP4.2
SiO_2	38.43	38.26	37.88	38.11	38.48	38.34	37.51	38.44
TiO_2	0.1017	0.0491		0.1076	0.1278	0.0444	0.1173	0.0534
Al_2O_3	26.45	26.3	25.81	25.73	26.64	26.77	25.84	26.79
FeO	10.37	10.29	11.12	10.42	9.58	9.23	11.26	9.4
MnO	0.2574	0.2476	0.2785	0.2673	0.3109	0.2925	0.2832	0.1977
MgO								
CaO	23.15	22.98	22.74	22.88	23.03	22.94	22.44	23.24
La_2O_3		0.0206	0.0023	0.0274		0.0207		
Ce_2O_3	0.0274	0.031						0.0164
Y_2O_3								0.0336
Tot	98.787	98.178	97.831	97.542	98.169	97.638	97.451	98.171

Rock	MME			
Sample	CVP25E (Briatico)			
Label	EP4.3	EP5.1	EP5.2	EP5.3
SiO_2	38.61	38.2	36.2	37.54
TiO_2	0.0536	0.0917	0.0814	0.2525
Al_2O_3	26.53	26.2	24.67	25.19
FeO	9.72	10.02	9.61	11.52
MnO	0.2447	0.2496	0.2348	0.6838
MgO				
CaO	23.09	23.05	21.46	21.69
La_2O_3	0.032			0.0023
Ce_2O_3		0.378		
Y_2O_3			0.0341	
Tot	98.28	98.189	92.29	96.879

Sample	CVP15	CVP16	CVP20	CVP21	CVP22	CVP30	CVP32	CVP24	CVP26	CVP27
Rock-type	Hybrid Qrt-diorite	Hybrid Qrt-diorite	Qrt-diorite	Qrt-diorite	Qrt-diorite	Qrt-diorite	Qrt-diorite	Qrt-diorite	Qrt-diorite	Qrt-diorite
SiO_2	54.6	53.35	62.25	59.61	60.84	58.19	59.89	62.55	60.87	59.46
Al_2O_3	23.6	23.29	18.03	18.49	18.41	19.33	18.86	18.04	18.84	19.53
FeO_{tot}	4.94	6.03	5.27	6.33	5.61	6.02	5.80	5.25	5.59	5.31
CaO	7.29	7.07	5.37	5.93	5.76	6.63	6.12	4.97	5.49	6.38
MgO	2.61	3.11	2.56	3.15	3.05	3.39	3.23	2.49	2.55	2.96
Na_2O	3.85	3.75	2.94	2.77	2.83	2.80	2.48	2.95	2.96	2.94
K_2O	1.82	1.95	2.37	2.35	2.25	2.22	2.30	2.55	2.5	2.15
TiO_2	1.04	1.18	0.79	0.91	0.81	0.94	0.88	0.79	0.81	0.79
MnO	0.04	0.05	0.10	0.1	0.10	0.11	0.10	0.09	0.07	0.11
P_2O_5	0.02	0.02	0.18	0.23	0.21	0.23	0.21	0.20	0.19	0.25
SrO	0.05	0.05	0.03	0.02	0.03	0.04	0.04	0.03	0.03	0.04
BaO	0.14	0.14	0.08	0.1	0.09	0.08	0.08	0.08	0.09	0.08
LOI	1.23	1.51	2.61	1.38	1.73	1.56	1.58	1.52	1.23	1.87
Total	100	100.46	101.33	98.97	101.46	100.51	100.06	100.74	98.73	101.51
ASI	1.1	1.11	1.06	1.04	1.06	1.02	1.07	1.09	1.08	1.05
Ba	1175	1255	779	889	807	787	823	768	768	781
Cr	20	30	10	20	20	20	20	10	20	20
Cs	1.32	1.26	1.94	0.61	0.76	0.6	0.7	1.69	2.27	0.97
Ga	31.1	29.5	24.9	23.3	25.1	25.1	26.1	26	24.6	26.3
Hf	8.7	5.9	5.1	4.9	4.2	4.8	4.3	4.5	4.9	4.4
Nb	9.7	11.7	13.8	13.5	12.7	10.8	11.1	12.7	11.8	5.8
Rb	63.2	61.4	81.2	78	72	70	78.7	94.7	89.3	70.6
Sr	497	485	298	286	304	336	318	292	297	328
Ta	0.4	0.4	0.7	0.4	0.4	0.5	0.5	0.7	0.6	0.4
Th	3.64	1.8	8.06	1.01	1.57	1.9	2.83	17.1	10.75	0.99
U	0.44	0.34	0.75	0.4	0.45	0.33	0.46	1.25	1.59	0.56
V	187	197	109	117	121	132	137	109	101	128
Y	4.5	3.6	30	23.9	28.5	28.6	37.1	24.1	23.1	7.1
Zr	355	235	199	196	178	199	182	186	197	185
Rb/Ba	0.05	0.05	0.10	0.09	0.09	0.09	0.10	0.12	0.12	0.09
Rb/Sr	0.13	0.13	0.27	0.27	0.24	0.21	0.25	0.32	0.30	0.22
La	27.6	18.5	36.5	11.5	15	25.2	24.3	74.9	53.1	14.3
Ce	49.9	29.2	69.9	25.5	32.8	51.8	55.5	141.5	103.5	29
Pr	5.36	3.16	8.26	3.96	4.65	6.71	7.61	16.05	11.95	3.76
Nd	19.6	11.5	33.7	19.7	23.3	30.6	36.3	62.6	46.9	16.7
Sm	2.78	1.82	7.56	5.22	6.35	7.21	8.67	11	8.31	3.5
Eu	2.19	1.93	1.38	1.46	1.36	1.65	1.69	1.68	1.54	1.1
Gd	1.72	1.17	6.14	5.13	6.1	6.04	7.76	7.27	6.39	3
Tb	0.2	0.13	0.94	0.8	0.92	0.99	1.17	0.93	0.85	0.37
Dy	0.94	0.64	5.46	4.79	5.69	5.41	7.01	4.94	4.66	1.87
Ho	0.17	0.14	0.99	0.91	1.04	1.01	1.38	0.89	0.89	0.27
Er	0.38	0.38	2.78	2.62	2.95	2.96	3.66	2.51	2.37	0.54
Tm	0.07	0.06	0.41	0.34	0.42	0.42	0.55	0.35	0.3	0.08
Yb	0.44	0.41	2.37	1.98	2.15	2.26	2.76	1.93	1.91	0.35
Lu	0.09	0.08	0.36	0.29	0.32	0.35	0.45	0.29	0.25	0.06
ΣREE	111.44	69.12	176.75	84.2	103.05	142.61	158.81	326.84	242.92	74.9
Eu/Eu*	3.06	4.04	0.61	0.61	0.66	0.76	0.62	0.57	0.64	1.03
La_N/Yb_N	42.29	30.42	10.38	3.91	4.7	7.51	5.93	26.16	18.74	27.54

Appendix. Table 6 – *Geochemical analysis (major (%vol) and trace element (ppm)) of hybrid quartz-diorites, quartz-diorite, tonalite, leuco-tonalite and MME in the CVP area.*

Sample	CVP10	CVP11	CVP13	CVP14	CVP28	CVP29	CVP31	CVP33	CVP34	CVP35
Rock-type	Tonalite	Tonalite	Tonalite	Tonalite	Tonalite	Tonalite	Tonalite	Tonalite	Tonalite	Tonalite
SiO_2	64.46	61.11	63.76	62.74	61.02	61.51	57.96	60.93	62.25	66.92
Al_2O_3	17.34	18.29	17.72	17.53	18.29	18.46	19.44	18.31	17.9	16.83
FeO_{tot}	4.80	6.14	4.93	5.51	5.52	5.21	6.18	5.59	5.79	3.83
CaO	4.68	5.3	4.80	4.97	5.79	5.78	6.15	5.94	5.15	4.61
MgO	2.15	2.54	2.18	2.56	2.88	2.81	3.36	2.66	2.43	1.90
Na_2O	2.79	2.87	2.97	2.78	2.77	2.81	2.94	2.84	2.73	3.06
K_2O	2.61	2.48	2.47	2.63	2.47	2.16	2.60	2.42	2.53	1.90
TiO_2	0.78	0.83	0.76	0.84	0.84	0.85	0.90	0.87	0.83	0.63
MnO	0.08	0.1	0.06	0.10	0.09	0.08	0.10	0.10	0.08	0.05
P_2O_5	0.18	0.2	0.21	0.23	0.21	0.21	0.21	0.20	0.21	0.15
SrO	0.03	0.02	0.04	0.03	0.03	0.04	0.04	0.03	0.02	0.03
BaO	0.09	0.11	0.08	0.09	0.09	0.08	0.10	0.09	0.1	0.08
LOI	1.23	1.1	1.17	1.39	1.16	2.23	1.31	1.14	1.02	1.11
Total	99.8	100.31	101.3	100.98	101.58	100.83	100.51	100.88	100.57	100.45
ASI	1.1	1.08	1.1	1.07	1.04	1.06	1.04	1.03	1.09	1.1
Ba	817	990	793	902	821	743	903	782	842	776
Cr	10	20	10	10	20	10	20	10	20	10
Cs	1.05	1.34	0.84	1.06	2.07	0.9	0.7	0.76	0.81	0.74
Ga	23.2	23.7	24.1	26.9	25	24.9	27.3	23.9	24.5	22.7
Hf	5.1	5.8	6	5.9	4.4	6	5.8	5.1	6.2	4.1
Nb	12.4	13.2	16.6	15.2	12	11.8	13.8	12.7	11.8	9.6
Rb	88.4	86.8	85.7	93.5	91.1	74.8	85	77.4	92.1	63
Sr	295	317	315	306	300	332	313	298	306	300
Ta	0.5	0.6	0.4	0.5	0.6	0.6	0.4	0.5	0.7	0.2
Th	9.43	12.15	11.5	8.89	3.1	7.17	19.25	8.33	11.8	11.35
U	0.66	0.68	0.83	0.73	0.96	0.64	0.48	0.46	0.5	0.74
V	87	106	88	116	131	109	141	117	107	75
Y	14.3	14.1	15.5	15.5	30	26.3	32.7	30.3	16	9.2
Zr	190	219	239	241	193	239	229	208	251	166
Rb/Ba	0.11	0.09	0.11	0.10	0.11	0.10	0.09	0.10	0.11	0.08
Rb/Sr	0.30	0.27	0.27	0.31	0.30	0.23	0.27	0.26	0.30	0.21
La	51.3	73.4	58	48.6	22.4	50.8	130.5	41.6	50.8	64.4
Ce	99.7	135	111.5	92.9	45.5	96	247	79.9	101.5	114
Pr	10.95	15.05	12.55	10.35	5.57	10.85	25.9	9.17	11.3	12.4
Nd	41.1	54.7	47.3	41	24.9	42.9	94.8	36.3	39.8	46.2
Sm	6.69	8.07	8.24	6.81	6.28	8.57	13.8	7.57	6.37	6.07
Eu	1.6	1.65	1.54	1.51	1.3	1.47	1.61	1.57	1.57	1.4
Gd	4.35	4.99	4.88	4.5	6.11	6.98	8.65	6.73	4.7	3.83
Tb	0.57	0.61	0.64	0.62	1.01	1.02	1.23	1.11	0.55	0.45
Dy	3.02	3.08	3.05	3.1	5.63	5.48	6.3	5.85	2.81	2.02
Ho	0.59	0.53	0.55	0.56	1.02	1.03	1.23	1.19	0.58	0.33
Er	1.42	1.31	1.41	1.4	3.03	2.51	3.31	3.33	1.46	0.91
Tm	0.23	0.17	0.23	0.19	0.43	0.34	0.46	0.45	0.21	0.13
Yb	1.2	0.98	1.12	1.05	2.1	1.61	2.54	2.48	1.42	0.83
Lu	0.17	0.13	0.19	0.14	0.29	0.2	0.34	0.34	0.21	0.11
ΣREE	222.89	299.67	251.2	212.73	125.57	229.76	537.67	197.59	223.28	253.08
Eu/Eu*	0.9	0.79	0.74	0.83	0.64	0.58	0.45	0.67	0.87	0.88

LaN/YbN	*28.82*	*50.49*	*34.91*	*31.2*	*27.54*	*21.27*	*34.63*	*11.3*	*24.11*	*52.31*
Sample	*CVP38*	*CVP39*	*CVP40*	*CVP41*	*CVP42*	*CVP4*	*CVP1*	*CVP2*	*CVP3*	
Rock-type	Tonalite	Tonalite	Tonalite	Tonalite	Tonalite	Tonalite	Tonalite	Tonalite	Tonalite	
SiO_2	62.09	61.00	60.69	66.77	62.52	68.57	68.27	68.00	68.39	
Al_2O_3	18.12	18.27	18.71	16.74	18.26	16.06	16.39	16.4	16.5	
FeO_{tot}	5.10	5.46	5.77	4.2	4.93	3.56	3.53	3.81	3.83	
CaO	5.35	5.87	5.52	4.74	5.35	3.89	3.90	3.88	3.9	
MgO	2.74	2.97	2.68	1.9	2.69	1.59	1.54	1.65	1.65	
Na_2O	2.75	2.82	2.82	2.81	2.74	3.19	3.38	3.22	3.24	
K_2O	2.53	2.35	2.56	1.93	2.25	2.34	2.20	2.27	2.29	
TiO_2	0.87	0.82	0.85	0.59	0.81	0.49	0.50	0.5	0.5	
MnO	0.08	0.10	0.09	0.06	0.06	0.06	0.05	0.05	0.05	
P_2O_5	0.22	0.20	0.18	0.15	0.22	0.15	0.14	0.12	0.12	
SrO	0.04	0.03	0.03	0.02	0.03	0.03	0.04	0.03	0.03	
BaO	0.10	0.09	0.09	0.08	0.13	0.06	0.06	0.07	0.07	
LOI	1.55	1.41	1.11	1.03	1.26	0.9	1.01	0.97	0.98	
Total	100.35	100.54	98.86	99.44	100.65	100.89	101.74	100.29	99.43	
ASI	1.07	1.03	1.08	1.1	1.1	1.11	1.13	1.13	1.10	
Ba	935	799	860	656	1265	545	550	668	502	
Cr	20	20	20	20	20	10	10	10	10	
Cs	0.78	0.98	1.13	0.78	0.93	0.61	0.9	0.67	0.86	
Ga	25.7	24.2	23.4	22.3	24.9	21.4	21.9	19.4	22.7	
Hf	5.6	5.4	5.1	4.1	4.3	3.8	4.8	4.6	5.3	
Nb	10.8	12.1	11.6	8.2	8.4	10.4	10.9	9.8	12	
Rb	85.6	76.2	86.3	68.8	71.6	86	88.6	83.2	81.6	
Sr	315	294	289	282	312	295	325	291	304	
Ta	0.3	0.5	0.5	0.4	0.2	0.8	1.1	0.9	0.9	
Th	9.06	5.89	7.57	2.09	0.91	9.26	12.15	13.25	9.24	
U	0.42	0.47	0.63	0.35	0.42	1.27	1.58	1.47	1.21	
V	114	129	102	81	121	60	61	62	63	
Y	13.4	31.4	16.4	10.4	12.5	15.9	21	21.4	26.3	
Zr	229	223	204	148	173	148	166	164	186	
Rb/Ba	0.09	0.10	0.10	0.10	0.06	0.16	0.16	0.12	0.16	
Rb/Sr	0.27	0.26	0.30	0.24	0.23	0.29	0.27	0.29	0.27	
La	55.3	35.5	35.6	11.6	16	36.1	44.6	44.5	32.7	
Ce	102.5	71.4	69.1	22.4	29.8	68.5	86.4	84.4	61.1	
Pr	11.25	8.69	8.22	2.59	3.55	7.81	9.44	9.69	7.19	
Nd	40.5	38.1	33.3	11	16	29.9	37.2	36.5	27.5	
Sm	5.84	8.28	5.57	2.22	3.77	5.19	6	6.24	5.43	
Eu	1.36	1.57	1.32	1.24	1.4	1.11	1.28	1.25	1.37	
Gd	4.09	7.32	4.26	2.48	3.07	3.66	4.14	4.78	4.43	
Tb	0.51	1.07	0.56	0.36	0.45	0.55	0.68	0.72	0.76	
Dy	2.94	6.51	3	2.09	2.46	3.08	3.8	4	4.57	
Ho	0.5	1.19	0.62	0.39	0.45	0.54	0.71	0.73	0.92	
Er	1.39	2.92	1.73	0.95	1.15	1.63	2.15	2.11	2.7	
Tm	0.18	0.45	0.23	0.14	0.17	0.24	0.33	0.32	0.41	
Yb	0.98	2.32	1.42	0.88	0.73	1.33	2.13	2.2	2.46	
Lu	0.15	0.36	0.21	0.1	0.13	0.19	0.33	0.3	0.36	
ΣREE	227.49	185.68	165.14	58.44	79.13	159.83	199.19	197.74	151.9	

*Eu/Eu**	0.85	0.61	0.82	1.61	1.25	0.77	0.85	0.69	0.78
La_N/Yb_N	38.04	10.31	16.9	8.88	14.77	18.29	14.11	13.63	8.96

Sample	*CVP16E*	*CVP21E*	CVP23E	CVP25E
Rock-type	MME	MME	MME	MME
SiO_2	57.28	54.53	53.86	54.50
Al_2O_3	17.62	19.58	21.32	19.09
FeO_{tot}	7.63	7.88	7.97	8.29
CaO	7.99	7.71	5.64	7.15
MgO	5.73	4.09	4.50	4.22
Na_2O	0.99	2.76	3.06	2.61
K_2O	1.59	2.08	2.14	2.72
TiO_2	0.78	0.97	1.10	0.99
MnO	0.15	0.15	0.12	0.19
P_2O_5	0.16	0.12	0.16	0.12
SrO	0.01	0.03	0.03	0.02
BaO	0.06	0.08	0.08	0.07
LOI	1.86	1.29	3	1.91
Total	96.2	98.84	100.97	101.54
ASI	1	0.95	1.22	0.95
Ba	589	742	815	655
Cr	160	40	40	20
Cs	1.09	0.54	0.83	2.04
Ga	18.8	24.4	31.2	23.3
Hf	3.2	4.6	3.4	3.9
Nb	8.1	10.3	15.8	11.1
Rb	58.5	63.2	84	93
Sr	236	344	341	266
Ta	0.3	0.3	0.6	0.5
Th	0.5	0.72	1.06	0.45
U	0.27	0.32	0.49	0.48
V	194	181	165	180
Y	27.2	67.5	18.5	56.8
Zr	129	173	134	145
Rb/Ba	0.10	0.09	0.10	0.14
Rb/Sr	0.25	0.18	0.25	0.35
La	21.2	20.6	28.1	10.4
Ce	59.6	53.7	57.5	28.4
Pr	9.11	9.08	7.16	5.25
Nd	37.8	49	30.9	29.5
Sm	6.97	13.8	6.95	10
Eu	2.37	2.12	1.11	1.89
Gd	5.4	14.8	5.26	9.59
Tb	0.79	2.34	0.7	1.68
Dy	4.67	13.5	3.52	10.85
Ho	0.96	2.75	0.71	2.04
Er	2.64	7.52	1.83	5.82
Tm	0.39	0.99	0.25	0.88

Yb	2.92	6.03	1.5	5.28
Lu	0.41	0.77	0.23	0.74
ΣREE	155.23	197	145.72	122.32
*Eu/Eu**	1.18	0.45	0.56	0.59
La_N/Yb_N	4.89	2.3	12.62	1.32

Appendix. Table7– Sr, Nd and Pb whole-rock isotopic data for the main granitoids in CVP area.

Sample	Rock type	Rb (ppm)	Sr (ppm)	$^{87}Rr/^{86}Sr$	$^{87}Sr/^{86}Sr$	$^{87}Sr/^{86}Sr_{298}$
CVP27	Qrz-drt	70.6	328	0.62328	0.7126	0.709956
CVP30	Qrz-drt	70	336	0.60326	0.7123	0.709758
CVP33	Qrz-drt	77	298	0.74828	0.7134	0.71019
CVP21	Qrz-drt	78	286	0.78978	0.7132	0.70981
CVP12	Ton	84	318	0.76495	0.7133	0.710036
CVP13	Ton	86	315	0.73064	0.7135	0.710158
CVP28	Ton	91	300	0.87844	0.7135	0.709767
CVP42	Ton	72	312	0.66824	0.7126	0.709802
CVP3	Leu-ton	81.6	304	0.77734	0.7135	0.710157
CVP24	Ton	94.7	292	0.93924	0.7139	0.709907
CVP29	Ton	74.8	332	0.65243	0.7129	0.710142
CVP35	Ton	63	300	0.6081	0.7126	0.71007
CVP39	Ton	76.2	294	0.75055	0.7130	0.709773
CVP41	Ton	68.8	282	0.70648	0.7128	0.709788
CVP23E	Enclave	84	341	0.71337	0.7134	0.710338
CVP25E	Enclave	93	266	1.01255	0.7140	0.70969

Sample	Sm (ppm)	Nd (ppm)	$^{147}Sm/^{144}Nd$	$^{143}Nd/^{144}Nd$	$^{143}Nd/^{144}Nd_{298}$	εNd_{298}	TDM.2stg
CVP27	3.5	16.7	0.12664	0.512181	0.511934	-6.26	1.511
CVP30	7.2	30.6	0.14218	0.512186	0.511909	-6.75	1.55
CVP33	7.6	36.3	0.12651	0.512154	0.511907	-6.78	1.552
CVP21	5.22	19.7	0.16011	0.512226	0.511914	-6.65	1.542
CVP12	7.7	50.5	0.09213	0.512094	0.511914	-6.64	1.541
CVP13	8.2	47.3	0.10475	0.512117	0.511913	-6.67	1.543
CVP28	6.3	24.9	0.15288	0.512224	0.511926	-6.42	1.523
CVP42	3.8	16	0.14351	0.512154	0.511874	-7.43	1.602
CVP3	5.43	27.5	0.11931	0.512133	0.5119	-6.91	1.562
CVP24	11	62.6	0.14292	0.512119	0.511912	-6.69	1.545
CVP29	8.57	42.9	0.12071	0.512143	0.511907	-6.77	1.551
CVP35	6.07	46.2	0.07939	0.512071	0.511916	-6.6	1.538
CVP39	8.28	38.1	0.13132	0.512172	0.511916	-6.61	1.539
CVP41	2.22	11	0.12195	0.512191	0.511953	-5.88	1.482
CVP23E	7	30.9	0.13688	0.512155	0.511888	-7.15	1.581
CVP25E	10	29.5	0.20484	0.512297	0.511897	-6.97	1.567

Sample	$^{206}Pb/^{204}Pb$	2SD	$^{207}Pb/^{204}Pb$	2SD	$^{208}Pb/^{204}Pb$	2SD
CVP27	18.269	0.005	15.653	0.006	38.329	0.016
CVP30	18.048	0.008	15.617	0.01	38.094	0.03
CVP33	18.089	0.009	15.616	0.009	38.554	0.021
CVP21	-	-	-	-	-	-
CVP12	18.028	0.004	15.603	0.004	38.386	0.009
CVP13	18.275	0.008	15.638	0.007	39.004	0.018
CVP28	18.388	0.004	15.657	0.005	38.48	0.013
CVP42	18.025	0.006	15.604	0.006	37.97	0.014
CVP3	-	-	-	-	-	-
CVP24	-	-	-	-	-	-
CVP29	-	-	-	-	-	-
CVP35	-	-	-	-	-	-
CVP39	-	-	-	-	-	-
CVP41	-	-	-	-	-	-
CVP23E	18.398	0.005	15.661	0.005	38.496	0.014
CVP25E	18.302	0.009	15.644	0.007	38.321	0.019

Grain Spot	Location	U (ppm)	Th (ppm)	Th/U(ppm)	$^{204}Pb/^{206}Pb$	± (%)	$^{208}Pb^*/^{206}Pb^*$	± (%)	$^{208}Pb^*/^{232}Th$	± (%)	$^{206}Pb^*/^{238}U$	± (%)	$^{207}Pb^*/^{235}U$	± (%)	$^{207}Pb^*/^{206}Pb$	± (%)	Dates (Ma)*					
																	208/232	± (1σ)	206/238	± (1σ)	207/206	± (1σ)
CVP23E - Enclave																						
1.1	CePUZ	191	151	0.79	1.4E-3	19	0.229	6.0	0.01303	5.9	0.04635	1.0	0.3439	11	0.05381	11	262	15	296	4	363	249
2.1	MPCZ	171	73	0.43	2.0E-3	17	0.125	10.6	0.01307	10.8	0.04601	1.6	0.3315	18	0.05226	18	262	28	292	5	297	404
4.1	MPCZ	236	150	0.64	1.6E-3	17	0.193	6.7	0.01359	6.5	0.04626	1.2	0.3364	12	0.05274	12	273	18	294	4	318	263
13.1	MPCZ	156	99	0.64	1.8E-3	20	0.190	7.7	0.01341	8.1	0.04623	1.7	0.3421	15	0.05368	15	269	22	294	5	357	340
3.1	MPCZ	238	134	0.56	1.1E-3	18	0.179	4.7	0.01469	4.9	0.04767	1.0	0.3533	9	0.05374	9	295	14	301	3	360	213
6.1	MPUZ	119	72	0.61	3.8E-3	15	0.169	21.2	0.01214	16.7	0.04538	2.1	0.3206	27	0.05124	27	244	41	290	7	252	613
11.1	OPUZ	233	162	0.69	1.1E-3	19	0.200	4.3	0.01295	4.5	0.04637	1.0	0.3378	10	0.05284	10	260	12	296	3	322	234
7.1	MPCZ	130	77	0.59	1.4E-3	23	0.175	7.6	0.01338	8.0	0.04649	1.6	0.3422	11	0.05338	11	269	21	295	5	345	257
8.1	CePUZ	177	131	0.74	2.1E-3	17	0.223	8.4	0.01335	7.9	0.04578	1.4	0.3394	16	0.05377	16	268	21	291	5	361	365
15.1	CePUZ	140	97	0.69	1.8E-3	19	0.214	10.0	0.01338	9.0	0.04467	1.2	0.3267	16	0.05305	16	269	24	283	4	331	361
11.2	CePUZ	135	90	0.67	2.1E-3	19	0.210	11.0	0.01389	9.9	0.04558	1.3	0.3282	20	0.05222	20	279	27	288	4	295	454
10.1	EPUZ	121	51	0.42	3.1E-3	17	0.120	30.8	0.01244	21.8	0.04542	1.8	0.3208	28	0.05122	28	250	54	289	7	251	643
12.1	MPBZ	278	248	0.89	1.0E-3	18	0.266	3.1	0.01343	3.5	0.04662	1.4	0.3423	9	0.05325	9	270	9	298	5	340	197
14.1	MPBZ	223	294	1.32	1.3E-3	20	0.408	3.5	0.01391	3.8	0.04643	1.4	0.3425	10	0.05349	10	279	11	296	5	350	234

Grain Spot	Location	U (ppm)	Th (ppm)	Th/U(ppm)	$^{204}Pb/^{206}Pb$	± (%)	$^{208}Pb^*/^{206}Pb^*$	± (%)	$^{208}Pb^*/^{232}Th$	± (%)	$^{206}Pb^*/^{238}U$	± (%)	$^{207}Pb^*/^{235}U$	± (%)	$^{207}Pb^*/^{206}Pb$	± (%)	Dates (Ma)*					
																	208/232	± (1σ)	206/238	± (1σ)	207/206	± (1σ)
CVP25E - Enclave																						
1.1	MPOZ	636	294	0.46	4.8E-4	19	0.132	3.0	0.01323	3.2	0.04798	1.0	0.3462	4	0.05232	4	266	9	302	3	300	93
4.1	EPOZ	148	79	0.54	3.4E-3	14	0.172	19.7	0.01454	14.5	0.04691	1.7	0.3439	26	0.05317	26	292	42	296	5	336	591
2.1	MPHD	443	471	1.06	1.3E-3	23	0.320	4.1	0.01373	4.4	0.04719	1.0	0.3449	13	0.05300	12	276	12	297	3	329	284
4.2	CePHB	225	204	0.91	2.1E-3	15	0.269	7.7	0.01292	6.9	0.04510	1.4	0.3225	16	0.05187	16	260	18	284	4	280	360
6.1	MFOZ	209	183	0.87	4.1E-3	11	0.276	12.3	0.01438	9.7	0.04695	1.9	0.3455	27	0.05337	27	289	28	296	5	345	619
8.1	EFOZ	207	144	0.70	2.4E-3	31	0.205	15.8	0.01327	15.8	0.04667	1.8	0.3327	27	0.05170	27	266	42	294	5	272	619
9.1	MFOZ	304	300	0.99	1.1E-3	18	0.283	3.0	0.01305	3.3	0.04700	1.0	0.3406	9	0.05256	9	262	9	296	3	310	215
3.1	EPOZ	264	149	0.57	1.3E-3	17	0.175	8.2	0.01394	7.3	0.04650	1.0	0.3401	11	0.05304	11	280	20	293	3	331	249
3.2	CePBZ	203	188	0.93	3.2E-3	13	0.293	6.4	0.01361	6.7	0.04441	1.7	0.3152	22	0.05147	22	273	18	280	5	262	495
7.1	MPOZ	243	153	0.63	1.8E-3	16	0.195	7.6	0.01406	7.3	0.04688	1.6	0.3404	14	0.05266	14	282	20	295	5	314	322
12.1	EFOZ	227	128	0.57	1.7E-3	18	0.169	12.2	0.01329	10.2	0.04603	1.1	0.3291	15	0.05185	15	267	27	290	3	279	343
14.1	MPOZ	176	112	0.64	2.1E-3	17	0.199	9.0	0.01391	8.5	0.04584	2.1	0.3334	19	0.05275	19	279	24	289	6	318	425
13.1	CeFBZ	587	778	1.33	1.8E-3	16	0.415	3.3	0.01455	3.6	0.04804	1.0	0.3470	14	0.05239	14	292	11	302	3	303	320
11.1	MFHD	676	995	1.47	5.6E-4	18	0.451	1.1	0.01415	1.5	0.04774	0.8	0.3482	5	0.05290	5	284	4	301	2	324	103
10.1	MFHD	462	540	1.17	1.0E-3	26	0.359	3.4	0.01384	3.7	0.04655	1.0	0.3394	10	0.05288	10	278	10	293	3	324	237
5.1	MPBZ	194	227	1.17	2.4E-3	15	0.374	5.7	0.01507	5.7	0.04877	1.9	0.3629	16	0.05397	16	302	17	307	6	370	358

Appendix. Table 8. *U-Pb SHRIMP data of zircon of Capo Vaticano granitoids.*

Grain Spot	Location	U (ppm)	Th (ppm)	Th/U(ppm)	$^{204}Pb/^{206}Pb$	± (%)	$^{208}Pb^*/^{206}Pb^*$	± (%)	$^{208}Pb^*/^{232}Th$	± (%)	$^{206}Pb^*/^{238}U$	± (%)	$^{207}Pb^*/^{235}U$	± (%)	$^{207}Pb^*/^{206}Pb$	± (%)	Dates (Ma)*					
																	208/232	± (1σ)	206/238	± (1σ)	207/206	± (1σ)
CVP30 QUARTZ-DIORITE																						
1.1	EPOZ	311	213	0.68	1.6E-3	15	0.211	7.3	0.01359	6.6	0.04551	1.2	0.3320	11	0.05291	11	273	18	287	3	325	248
7.1	EPOZ	252	155	0.62	1.7E-3	17	0.189	8.0	0.01407	7.6	0.04729	1.1	0.3452	14	0.05293	14	282	21	298	3	326	309
2.1	MPOZ	210	126	0.60	2.3E-3	14	0.194	9.8	0.01431	8.7	0.04553	1.6	0.3263	17	0.05197	17	287	25	287	5	284	391
5.1	MPOZ	251	179	0.71	1.7E-3	16	0.208	5.3	0.01330	5.7	0.04690	1.3	0.3425	14	0.05297	14	267	15	295	4	327	320
6.1	MPOZ	699	501	0.72	3.8E-4	18	0.223	1.5	0.01457	1.9	0.04839	1.1	0.3569	4	0.05350	4	292	5	305	3	350	84
9.1	MPOZ	459	369	0.81	1.4E-3	26	0.253	6.3	0.01407	6.4	0.04625	1.2	0.3375	13	0.05292	13	282	18	291	3	326	285
11.1	MPOZ	216	137	0.64	1.3E-3	20	0.197	8.3	0.01386	7.5	0.04619	1.0	0.3355	10	0.05268	10	278	21	291	3	315	225
8.1	MPOZ	260	178	0.68	1.1E-3	29	0.216	7.3	0.01398	7.3	0.04573	1.4	0.3346	12	0.05307	12	281	20	288	4	332	280
10.1	EPOZ	230	143	0.62	1.1E-3	19	0.194	6.6	0.01396	6.2	0.04601	1.4	0.3310	10	0.05219	10	280	17	290	4	294	218
3.1	MPOZ	377	192	0.51	1.5E-3	16	0.144	8.4	0.01297	7.7	0.04730	1.0	0.3394	10	0.05204	10	260	20	298	3	287	222
4.1	EPOZ	461	139	0.30	5.1E-4	20	0.091	7.1	0.01446	6.5	0.04929	0.9	0.3587	5	0.05278	5	290	19	310	3	320	106
12.1	CeRHB	94	71	0.75	2.4E-3	19	0.223	11.4	0.01327	10.4	0.04625	1.9	0.3345	27	0.05245	27	266	28	291	5	305	605

Grain Spot	Location	U (ppm)	Th (ppm)	Th/U(ppm)	$^{204}Pb/^{206}Pb$	± (%)	$^{208}Pb^*/^{206}Pb^*$	± (%)	$^{208}Pb^*/^{232}Th$	± (%)	$^{206}Pb^*/^{238}U$	± (%)	$^{207}Pb^*/^{235}U$	± (%)	$^{207}Pb^*/^{206}Pb$	± (%)	Dates (Ma)*					
																	208/232	± (1σ)	206/238	± (1σ)	207/206	± (1σ)
CVP27 QUARTZ-DIORITE																						
3.1	MPOZ	278	117	0.42	2.0E-4	1.2	0.164	2.2	0.01767	2.5	0.04664	0.8	0.3375	2	0.05536	1	354	9	294	2.4	306	51
14.1	MPOZ	173	110	0.64	2.2E-4	1.6	0.248	2.1	0.01759	2.5	0.04695	0.9	0.3355	3	0.05505	2	353	9	296	2.6	278	70
15.1	MPHB	105	50	0.48	4.4E-4	2.1	0.239	2.9	0.02276	3.8	0.04709	1.0	0.3419	5	0.05907	2	455	17	297	2.9	314	118
6.1	MFOZ	184	105	0.57	3.2E-4	1.5	0.224	2.2	0.01778	2.8	0.04710	1.2	0.3370	4	0.05658	1	356	10	297	3.5	281	76
12.1	MPOZ	213	126	0.59	5.7E-5	1.4	0.230	2.8	0.01776	2.9	0.04717	1.0	0.3416	2	0.05336	1	356	10	297	3.0	308	42
5.1	CePOZ	194	180	0.93	4.5E-4	4.1	0.337	2.3	0.01704	2.3	0.04769	1.3	0.3594	6	0.06124	4	342	8	300	3.7	398	126
2.1	CePHB	129	48	0.37	3.0E-4	1.8	0.190	2.9	0.02360	3.6	0.04767	0.9	0.3431	4	0.05653	2	471	17	300	2.8	294	90
13.1	MFOZ	532	398	0.75	1.5E-4	1.0	0.244	1.3	0.01516	1.7	0.04778	0.9	0.3470	2	0.05480	1	304	5	301	2.6	314	36
4.1	CePOZ	241	196	0.82	1.3E-4	1.4	0.298	1.6	0.01698	1.9	0.04791	0.9	0.3478	2	0.05450	1	340	7	302	2.5	314	49
7.1	EPOZ	261	210	0.81	2.3E-4	1.3	0.292	1.5	0.01681	1.9	0.04806	0.9	0.3454	3	0.05547	1	337	6	303	2.5	291	56
1.1	MPOZ	136	81	0.59	3.8E-4	1.8	0.249	2.4	0.01971	3.1	0.04836	0.9	0.3531	4	0.05852	2	395	12	304	2.8	327	96
8.1	MPOZ	230	162	0.70	4.0E-4	1.5	0.276	2.0	0.01844	2.6	0.04844	1.3	0.3498	4	0.05826	2	369	10	305	3.7	302	84
11.1	CePOZ	167	68	0.40	3.9E-5	1.7	0.189	2.5	0.02241	2.5	0.04861	0.9	0.3609	2	0.05440	2	448	11	306	2.7	364	45
10.1	MPOZ	269	190	0.71	3.6E-4	2.5	0.266	2.1	0.01828	2.3	0.04985	1.0	0.3671	4	0.05874	2	366	9	314	3.1	346	89

Grain Spot	Location	U (ppm)	Th (ppm)	Th/U(ppm)	$^{204}Pb/^{206}Pb$	± (%)	$^{208}Pb^*/^{206}Pb^*$	± (%)	$^{208}Pb^*/^{232}Th$	± (%)	$^{206}Pb^*/^{238}U$	± (%)	$^{207}Pb^*/^{235}U$	± (%)	$^{207}Pb^*/^{206}Pb$	± (%)	Dates (Ma)*					
																	208/232	± (1σ)	206/238	± (1σ)	207/206	± (1σ)
CVP42 TONALITE																						
1.1	CoRHB	22	25	1.13	2.2E-3	25	0.358	6.9	0.14908	7.1	0.48802	2.0	11.5684	8	0.17192	7	2809	187	2562	42	2576	125
1.2	ORHB	129	63	0.49	2.3E-3	20	0.160	15.6	0.01476	13.5	0.04624	1.3	0.3318	21	0.05204	21	296	40	291	4	287	470
3.2	CePHB	97	53	0.54	1.9E-3	21	0.177	14.5	0.01488	12.5	0.04723	1.8	0.3403	20	0.05226	20	299	37	297	5	297	459
3.1	EPOZ	218	125	0.57	8.6E-4	23	0.184	4.8	0.01470	4.9	0.04716	1.0	0.3434	10	0.05281	10	295	14	297	3	321	219
4.2	CePCZ	238	161	0.68	9.9E-4	20	0.217	6.7	0.01475	6.2	0.04782	1.0	0.3489	11	0.05292	11	296	18	301	3	325	257
4.1	EPOZ	190	97	0.51	3.1E-3	19	0.186	15.8	0.01685	14.4	0.04767	2.0	0.3504	24	0.05331	24	338	48	300	6	342	552
5.1	EPOZ	392	234	0.60	6.4E-4	20	0.189	6.7	0.01447	6.2	0.04720	0.9	0.3403	7	0.05228	7	290	18	297	3	298	161
6.1	MPOZ	189	117	0.62	1.1E-3	21	0.200	4.8	0.01483	5.2	0.04729	1.4	0.3506	10	0.05378	10	298	15	298	4	362	231
7.1	MPOZ	306	165	0.54	6.0E-4	23	0.173	5.8	0.01468	5.5	0.04731	0.9	0.3441	4	0.05275	4	295	16	298	3	318	98
11.1	MPOZ	204	55	0.27	1.7E-3	20	0.117	15.8	0.02021	13.6	0.04837	1.6	0.3546	16	0.05316	16	404	54	305	5	336	360
8.1	MEQOZ	189	109	0.57	1.3E-3	22	0.190	6.1	0.02021	13.6	0.04857	1.1	0.3480	11	0.05197	11	313	20	306	3	284	259
10.1	MEQOZ	170	84	0.49	1.5E-3	19	0.175	8.3	0.01657	7.9	0.04833	1.1	0.3592	14	0.05391	14	332	26	304	3	367	319
9.1	EPOZ	209	127	0.61	1.7E-3	18	0.176	9.3	0.01314	8.5	0.04699	1.1	0.3370	16	0.05201	16	264	22	296	3	286	369
11.2	CePHB	431	135	0.31	6.3E-4	20	0.094	9.8	0.01393	8.5	0.04814	0.9	0.3496	7	0.05267	7	280	24	303	3	314	161

Grain Spot	Location	U (ppm)	Th (ppm)	Th/U(ppm)	$^{204}Pb/^{206}Pb$	± (%)	$^{208}Pb^*/^{206}Pb^*$	± (%)	$^{208}Pb^*/^{232}Th$	± (%)	$^{206}Pb^*/^{238}U$	± (%)	$^{207}Pb^*/^{235}U$	± (%)	$^{207}Pb^*/^{206}Pb$	± (%)	Dates (Ma)*					
																	208/232	± (1σ)	206/238	± (1σ)	207/206	± (1σ)
CVP28 TONALITE																						
1.1	EPOZ	120	55	0.46	2.6E-3	17	0.135	20.8	0.01322	16.3	0.04646	1.3	0.3309	19	0.05165	19	265	43	293	4	270	441
3.1	EPOZ	320	145	0.45	5.6E-4	23	0.151	4.9	0.01498	4.8	0.04675	0.9	0.3369	4	0.05226	4	301	14	295	3	297	92
4.1	CePOZ	448	300	0.67	9.9E-4	17	0.212	4.2	0.01501	4.3	0.04898	1.4	0.3564	6	0.05278	6	301	13	308	4	319	140
5.2	EPOZ	287	158	0.55	1.8E-3	16	0.169	7.8	0.01453	7.5	0.04890	1.4	0.3614	10	0.05360	10	291	22	308	4	354	225
7.1	EPOZ	283	204	0.72	6.4E-4	22	0.228	2.9	0.01453	3.1	0.04735	0.9	0.3389	6	0.05191	6	292	9	298	3	282	144
8.1	EPOZ	361	362	1.00	9.5E-4	17	0.313	3.7	0.01421	3.7	0.04704	1.1	0.3427	8	0.05283	8	285	11	296	3	322	187
9.1	MPOZ	194	132	0.68	2.3E-3	17	0.210	12.9	0.01403	10.7	0.04674	1.8	0.3422	18	0.05310	18	282	30	294	5	333	413
10.1	MPOZ	335	198	0.59	1.6E-3	16	0.190	8.8	0.01475	7.8	0.04728	1.3	0.3381	14	0.05186	13	296	23	298	4	279	308
11.1	EPOZ	340	211	0.62	1.6E-3	22	0.177	7.4	0.01304	7.9	0.04699	1.1	0.3382	13	0.05220	13	262	21	296	3	294	306
2.1	CePOZ	230	137	0.60	5.1E-4	28	0.177	3.7	0.01360	3.9	0.04747	1.0	0.3523	6	0.05382	6	273	11	299	3	364	133
12.1	MPOZ	187	135	0.72	1.4E-3	20	0.219	6.4	0.01373	6.3	0.04654	1.3	0.3385	13	0.05275	13	276	17	293	4	318	287
13.1	CePHD	426	171	0.40	8.7E-4	18	0.119	9.4	0.01345	8.2	0.04661	1.1	0.3372	7	0.05247	7	270	22	294	3	306	167
6.1	EPOZ	406	229	0.56	5.7E-4	19	0.169	3.0	0.01401	3.2	0.04840	0.9	0.3494	5	0.05236	5	281	9	305	3	301	106
5.1	CePHB	114	73	0.64	2.4E-3	18	0.183	13.2	0.01286	11.7	0.04646	1.8	0.3403	21	0.05313	21	258	30	293	5	334	483

Grain Spot	Location	U (ppm)	Th (ppm)	Th/U(ppm)	$^{204}Pb/^{206}Pb$	± (%)	$^{208}Pb^*/^{206}Pb^*$	± (%)	$^{208}Pb^*/^{232}Th$	± (%)	$^{206}Pb^*/^{238}U$	± (%)	$^{207}Pb^*/^{235}U$	± (%)	$^{207}Pb^*/^{206}Pb$	± (%)	Dates (Ma)*					
																	208/232	± (1σ)	206/238	± (1σ)	207/206	± (1σ)
CVP13 TONALITE																						
1.1	MPOZ	1188	423	0.36	1.7E-4	19	0.107	1.6	0.01472	1.8	0.05039	0.9	0.3643	1	0.05242	1	295	5	317	3	304	26
6.1	MPOZ	294	138	0.47	4.4E-4	27	0.148	3.7	0.01424	3.8	0.04652	0.9	0.3338	4	0.05205	4	286	11	293	3	288	87
9.1	MPOZ	1043	451	0.43	2.2E-4	20	0.131	2.4	0.01460	2.4	0.04980	0.8	0.3589	2	0.05227	2	293	7	313	2	297	49
12.1	MPOZ	661	99	0.15	4.7E-4	18	0.046	9.8	0.01402	8.7	0.04764	0.9	0.3465	4	0.05275	4	281	24	300	3	318	93
5.1	EPOZ	396	196	0.49	9.8E-4	16	0.148	6.7	0.01396	6.1	0.04802	0.9	0.3502	7	0.05288	7	280	17	302	3	324	152
3.1	EPOZ	854	335	0.39	2.3E-4	20	0.116	2.0	0.01353	2.2	0.04742	1.0	0.3404	2	0.05206	2	272	6	299	3	288	45
7.1	EPOZ	442	266	0.60	8.0E-4	18	0.193	6.2	0.01350	5.7	0.04557	0.9	0.3420	7	0.05444	7	271	15	287	2	389	160
2.1	EPOZ	413	199	0.48	5.4E-4	19	0.145	4.3	0.01377	4.2	0.04712	0.9	0.3429	5	0.05278	5	276	12	297	3	319	111
8.1	EPOZ	952	441	0.46	2.8E-4	19	0.142	2.6	0.01404	2.7	0.04719	0.8	0.3462	3	0.05321	3	282	7	297	2	338	65
11.1	OPOZ	380	142	0.37	7.8E-4	39	0.112	12.1	0.01337	11.8	0.04609	1.0	0.3332	11	0.05243	11	268	31	290	3	304	251
14.1	CePOZ	324	225	0.69	9.7E-4	19	0.208	4.8	0.01346	4.8	0.04643	0.9	0.3334	11	0.05208	11	270	13	293	3	289	249
4.1	MPOZ	265	136	0.51	7.6E-4	20	0.161	4.2	0.01397	4.4	0.04596	1.2	0.3317	6	0.05235	6	280	12	290	3	301	134
12.2	OPHB	216	38	0.18	2.0E-3	20	0.047	47.6	0.01206	34.9	0.04670	1.4	0.3449	17	0.05355	17	242	84	294	4	352	381
10.1	EEQOZ	245	93	0.38	3.3E-4	33	0.116	4.4	0.01359	4.6	0.04572	1.3	0.3281	5	0.05205	5	273	13	288	4	288	114

Grain Spot	Location	U (ppm)	Th (ppm)	Th/U(ppm)	$^{204}Pb/^{206}Pb$	± (%)	$^{208}Pb^*/^{206}Pb^*$	± (%)	$^{208}Pb^*/^{232}Th$	± (%)	$^{206}Pb^*/^{238}U$	± (%)	$^{207}Pb^*/^{235}U$	± (%)	$^{207}Pb^*/^{206}Pb$	± (%)	Dates (Ma)*					
																	208/232	± (1σ)	206/238	± (1σ)	207/206	± (1σ)
CVP35 TONALITE																						
9.1	MPOZ	114	81.4	0.71	3.2E-4	41	0.294	2.4	0.01766	2.8	0.04416	0.0	0.3135	5	0.05150	4	353	11	279	4	263	100
4.1	EPOZ	339	359	1.06	1.5E-4	35	0.374	1.8	0.01525	2.0	0.04458	0.0	0.3165	2	0.05150	2	305	6	281	2	263	45
3.1	MPBZ	211	282	1.34	2.0E-4	38	0.441	1.3	0.01451	1.8	0.04543	0.0	0.3318	3	0.05296	3	293	5	286	3	327	57
11.1	OPHB	80	45.1	0.56	6.2E-4	41	0.320	3.1	0.02518	3.7	0.04566	0.0	0.3225	8	0.05122	8	499	23	288	5	251	185
2.1	EPOZ	215	147	0.68	2.4E-4	33	0.250	1.8	0.01620	2.0	0.04573	0.0	0.3257	3	0.05166	3	323	7	288	3	270	63
10.1	CePUZ	154	185	1.20	1.2E-4	58	0.427	1.6	0.01584	1.9	0.04618	0.0	0.3353	3	0.05266	3	319	6	291	3	314	58
7.1	EPOZ	309	282	0.91	8.2E-5	50	0.316	1.4	0.01593	1.6	0.04746	0.0	0.3422	2	0.05228	2	319	5	299	3	298	39
5.1	EPUZ	705	104	0.15	3.5E-5	58	0.069	3.2	0.02283	2.8	0.04990	0.0	0.3589	1	0.05216	1	448	11	314	3	293	25
8.1	EPOZ	1017	505	0.50	4.5E-5	38	0.197	1.2	0.01921	1.5	0.04993	0.0	0.3609	1	0.05243	0.8	383	6	314	3	304	19
12.1	EPOZ	79	39.5	0.50	1.2E-3	38	0.374	3.9	0.03826	4.6	0.05308	0.1	0.3869	14	0.05287	13	758	47	333	10	323	300
1.1	EPUZ	440	141	0.32	2.2E-4	38	0.166	3.0	0.02708	3.4	0.05429	0.1	0.4043	4	0.05402	3	546	20	341	7	372	61
6.1	EPUZ	185	52.3	0.28	4.8E-4	41	0.192	3.8	0.03720	3.9	0.05681	0.1	0.4258	6	0.05436	6	745	38	356	5	386	133

Grain Spot	Location	U (ppm)	Th (ppm)	Th/U(ppm)	$^{204}Pb/^{206}Pb$	± (%)	$^{208}Pb^*/^{206}Pb^*$	± (%)	$^{208}Pb^*/^{232}Th$	± (%)	$^{206}Pb^*/^{238}U$	± (%)	$^{207}Pb^*/^{235}U$	± (%)	$^{207}Pb^*/^{206}Pb$	± (%)	Dates (Ma)*					
																	208/232	± (1σ)	206/238	± (1σ)	207/206	± (1σ)
CVP39 TONALITE																						
8.1	EPOZ	136	70.6	0.52	1.6E-4	50	0.214	2.5	0.01781	2.9	0.04459	1.4	0.3216	3	0.05231	3	357	10	281	4	299	64
1.1	EPOZ	220	152	0.69	2.0E-4	35	0.251	1.8	0.01582	2.2	0.04483	1.1	0.3238	3	0.05239	2	317	7	283	3	303	56
6.1	EPOZ	123	82.9	0.68	8.3E-5	71	0.269	2.1	0.01755	2.3	0.04507	1.0	0.3310	3	0.05326	2	352	8	284	3	340	54
3.1	EPOZ	260	183	0.70	1.2E-4	41	0.244	2.6	0.01544	2.7	0.04561	0.9	0.3337	2	0.05306	2	310	8	288	3	331	42
10.1	EPOZ	420	384	0.91	3.7E-4	88	0.297	3.9	0.01468	4.5	0.04644	1.1	0.3372	13	0.05266	13	295	13	293	3	314	296
11.1	MPOZ	355	232	0.65	7.1E-5	50	0.233	1.6	0.01611	1.8	0.04647	1.0	0.3374	2	0.05267	2	323	6	293	3	315	35
12.1	MPOZ	248	145	0.58	4.9E-5	71	0.232	1.8	0.01813	1.9	0.04691	0.9	0.3400	2	0.05256	2	363	7	296	3	310	38
7.1	MPOZ	205	122	0.59	1.6E-4	45	0.245	3.1	0.01896	3.2	0.04697	1.1	0.3446	3	0.05321	2	380	12	296	3	338	57
9.1	EPOZ	272	239	0.88	---	---	0.320	1.4	0.01667	1.6	0.04708	0.9	0.3424	2	0.05275	1	334	5	297	3	318	29
4.1	EPOZ	145	48.6	0.34	-4.8E-5	100	0.198	2.7	0.02739	2.9	0.04736	1.3	0.3466	3	0.05308	2	546	15	298	4	332	52
5.1	EPOZ	232	124	0.53	4.5E-4	24	0.206	2.1	0.01816	2.8	0.04759	1.2	0.3527	4	0.05375	3	364	10	300	3	361	75
2.1	EPOZ	292	171	0.58	1.1E-4	45	0.223	1.7	0.01752	2.0	0.04760	0.9	0.3409	2	0.05193	2	351	7	300	3	283	43

Grain Spot	Location	U (ppm)	Th (ppm)	Th/U(ppm)	$^{204}Pb/^{206}Pb$	± (%)	$^{208}Pb^*/^{206}Pb^*$	± (%)	$^{208}Pb^*/^{232}Th$	± (%)	$^{206}Pb^*/^{238}U$	± (%)	$^{207}Pb^*/^{235}U$	± (%)	$^{207}Pb^*/^{206}Pb$	± (%)	Dates (Ma)*					
																	208/232	± (1σ)	206/238	± (1σ)	207/206	± (1σ)
CVP3 LEUCOTONALITE																						
2.1	CePBZ	137	166	1.21	2.8E-4	41	0.429	2.9	0.01583	3.4	0.04623	1.7	0.3349	4	0.05254	4	318	11	291	5	309	85
10.1	EPOZ	190	127	0.67	3.5E-5	100	0.262	2.2	0.01754	2.1	0.04632	1.0	0.3325	3	0.05206	3	351	7	292	3	288	63
1.1	EPOZ	375	222	0.59	6.1E-5	50	0.211	1.6	0.01612	1.7	0.04661	1.0	0.3346	2	0.05205	1	323	6	294	3	288	31
4.1	MPOZ	170	115	0.68	2.2E-4	41	0.267	4.2	0.01796	4.2	0.04681	1.0	0.3377	3	0.05231	3	360	15	295	3	299	69
5.1	MPOZ	265	205	0.77	9.3E-5	50	0.285	1.6	0.01678	1.9	0.04725	1.1	0.3363	2	0.05163	2	336	6	298	3	269	43
3.1	EPOZ	327	311	0.95	9.7E-5	41	0.329	1.2	0.01575	1.6	0.04726	1.0	0.3379	2	0.05184	2	316	5	298	3	279	36
9.1	MPOZ	241	165	0.69	1.5E-4	41	0.251	1.8	0.01687	2.2	0.04741	1.3	0.3442	3	0.05265	2	338	7	299	4	314	51
6.1	MPHB	88	53	0.59	4.6E-4	41	0.301	3.3	0.02344	3.8	0.04774	1.7	0.3443	7	0.05230	7	468	18	301	5	299	166
8.1	MPOZ	204	108	0.53	2.5E-5	113	0.223	2.1	0.01950	2.3	0.04784	1.2	0.3458	2	0.05242	2	390	9	301	4	304	40
7.1	MPOZ	349	106	0.30	1.5E-4	35	0.122	2.5	0.01860	2.7	0.04795	1.0	0.3453	2	0.05223	2	373	10	302	3	296	44

Cells marked'-'. ^{204}Pb below detection limit.

* Radiogenic Pb: Corrected for common Pb with a composition appropriate to the age of the spot using 204Pb.

Location codes: O - overgrowth, E - edge, Ce - centre, Co - core, P - Prism, EQ - equant, F - Fragmented, R- Rounded, CZ - concentric zonation, BZ - banded zonation, UZ - appears unzoned, HB - homogenous bright, HD - homogenoud dark

Appendix. Table 9 – Hf isotopic data in zircon by LA-ICPMS for CVP granitoids.

Spot	$^{176}Hf/^{177}Hf$	± 2 se	$^{176}Lu/^{177}Hf$	± 2 se	εHf (0)	εHf (T1)	T DM (Ga)	εHf DM(T)
CVP27 - Quartz-diorite								
CVP-27 1.1	0.28238	0.00002	0.00118	0.00004	-13.8	-7.3	1720	9.9
CVP-27 2.1	0.28246	0.00002	0.00056	0.00002	-10.9	-4.4	1530	10.6
CVP-27 3.1	0.2821	0.0003	0.00149	0.00009	-10	-10	2400	7
CVP-27 4.1	0.2821	0.0003	0.00122	0.00008	-23	-16	2300	8
CVP-27 5.1	0.28235	0.00003	0.00141	0.00007	-14	-7	1790	9.7
CVP-27 6.1	0.28243	0.00004	0.000684	0.000006	-11	-5	1600	10.3
CVP-27 7.1	0.2823	0.0002	0.0014	0.0001	-15	-9	1900	9
CVP-27 8.1	0.28251	0.00002	0.0009	0.00004	-9.4	-2.8	1440	10.9
CVP-27 10.1	0.28235	0.00004	0.00116	0.00002	-14	-7	1800	9.7
CVP-27 11.1	0.28239	0.00003	0.00086	0.00004	-13	-6	1700	10
CVP-27 12.1	0.28246	0.00001	0.000849	0.000006	-11	-4.6	1540	10.6
CVP-27 13.1	0.28172	0.00008	0.0029	0.0003	-36	-30	3200	4.5
CVP-27 14.1	0.28238	0.00002	0.00071	0.00002	-13.8	-7.4	1720	9.9
CVP-27 15.1	0.2821	0.0002	0.00174	0.00008	-23	-17	2400	7
CVP30 - Quartz-diorite								
CVP-30 1.1	0.28242	0.000009	0.00082	0.000006	-12.5	-6.3	1640	10.2
CVP-30 2.1	0.2823	0.0001	0.00131	0.00003	-15	-8	1800	9
CVP-30 3.1	0.2822	0.0002	0.00195	0.00004	-21	-15	2200	8
CVP-30 4.1	0.28252	0.00005	0.00102	0.00004	-8	-1	1400	11.1
CVP-30 5.1	0.28241	0.00003	0.00088	0.00002	-12	-5	1660	10.1
CVP-30 6.1	0.28242	0.00002	0.00109	0.00003	-12.4	-5.9	1630	10.2
CVP-30 7.1	0.28252	0.00002	0.00101	0.00004	-9.1	-2.7	1430	11
CVP-30 8.1	0.28243	0.00002	0.00096	0.00002	-12.1	-5.9	1620	10.3
CVP-30 9.1	0.2824	0.00001	0.00072	0.00001	-13	-6.8	1670	10.1
CVP-30 10.1	0.2822	0.0001	0.00107	0.00003	-21	-15	2200	8.1
CVP-30 11.1	0.28225	0.00006	0.00176	0.00006	-18	-12	2000	8.8
CVP42 - Tonalite								
CVP-42 1.1	0.28116	0.00002	0.0005708	0.0000007	-57.1	-0.6	3040	5.1
CVP-42 1.2	0.28237	0.00001	0.000572	0.000005	-14.1	-7.8	1740	9.86
CVP-42 2.1	0.28243	0.00008	0.0004	0.0001	-11	-5	1600	10.3
CVP-42 2.2	0.28239	0.00001	0.000512	0.000002	-13.5	-7.6	1710	10
CVP-42 3.1	0.28239	0.00002	0.000516	0.000009	-13.5	-7.1	1700	10
CVP-42 3.2	0.28245	0.00002	0.00048	0.00002	-11.5	-5.1	1570	10.5
CVP-42 4.1	0.28229	0.00009	0.00086	0.00003	-16	-10	1900	9.2
CVP-42 4.2	0.28226	0.00004	0.00135	0.00002	-17	-11	2000	8.9
CVP-42 5.1	0.2824	0.00002	0.00076	0.00001	-13	-6.6	1670	10.1
CVP-42 6.1	0.28237	0.00002	0.000593	0.000005	-14.2	-7.8	1740	9.8
CVP-42 7.1	0.28233	0.00001	0.00086	0.00002	-15.8	-9.4	1840	9.5
CVP-42 8.1	0.282437	0.000009	0.000614	0.000001	-11.9	-5.3	1590	10.39
CVP-42 9.1	0.2824	0.00002	0.000928	0.000009	-13.1	-6.7	1680	10.1
CVP-42 10.1	0.28243	0.00004	0.00087	0.00002	-11	-4	1600	10.4
CVP-42 11.2	0.28242	0.00004	0.00114	0.00003	-11	-5	1600	10.2
CVP-42 11.1	0.28235	0.00002	0.00066	0.00004	-14.8	-8.3	1780	9.7

Spot	$^{176}Hf/^{177}Hf$	± 2 se	$^{176}Lu/^{177}Hf$	± 2 se	εHf (0)	εHf (T1)	T DM (Ga)	εHf DM(T)
CVP35 - Tonalite								
CPV-35 1.1	0.28236	0.00004	0.00059	0.00002	-13	-6	1730	9.9
CPV-35 12.1	0.28241	0.00002	0.000535	0.000001	-12.8	-5.6	1630	10.2
CPV-35 3.1	0.28233	0.00004	0.00127	0.00007	-15	-9	1850	9.4
CPV-35 5.1	0.28236	0.00001	0.00096	0.00002	-14.7	-8	1770	9.74
CPV-35 6.1	0.28238	0.00003	0.001	0.00002	-13	-5	1690	10
CPV-35 7.1	0.28228	0.00003	0.00118	0.00003	-17	-11	1940	9.1
CPV-35 8.1	0.28216	0.00006	0.00155	0.00003	-21	-14	2200	8.1
CPV-35 9.1	0.28235	0.00003	0.00076	0.00003	-14	-8	1800	9.6
CPV-35 10.1	0.28234	0.00007	0.00106	0.00005	-14	-8	1800	9.6
CPV-35 11.1	0.28241	0.00003	0.00063	0.00001	-12	-6	1670	10.1
CVP39 - Tonalite								
CPV-39 1.1	0.28243	0.00001	0.00079	0.00001	-12.1	-6.1	1620	10.3
CPV-39 2.1	0.28235	0.00002	0.00102	0.00001	-15.1	-8.7	1800	9.6
CPV-39 3.1	0.2829	0.0003	0.0014	0.00009	3	9	600	14
CPV-39 4.1	0.28253	0.00004	0.00076	0.00003	-8	-1	1390	11.1
CPV-39 12.1	0.2826	0.0001	0.00071	0.00002	-7	0	1300	11.3
CPV-39 6.1	0.28241	0.00002	0.00113	0.00008	-12.9	-6.8	1670	10.1
CPV-39 7.1	0.28263	0.00004	0.00082	0.00002	-4	1	1200	11.9
CPV-39 9.1	0.2823	0.0002	0.00134	0.00008	-15	-8	1800	9
CPV-39 10.1	0.2824	0.0001	0.00118	0.00007	-12	-6	1700	10.1
CPV-39 11.1	0.2824	0.00003	0.00085	0.00005	-12	-6	1670	10.1
CVP33 - Tonalite								
CVP-33 1.1	0.28219	0.00003	0.00196	0.00004	-20	-14	2150	8.4
CVP-33 2.1	0.2823	0.00003	0.00111	0.00005	-16	-9	1900	9.3
CVP-33 3.1	0.2821	0.0002	0.0015	0.00008	-24	-17	2400	7
CVP-33 4.1	0.282441	0.000002	0.00133	0.00002	-11.72	-5.48	1598	10.37
CVP-33 5.1	0.28238	0.00002	0.00108	0.00002	-14	-7.7	1740	9.9
CVP-33 6.1	0.2824	0.0001	0.00102	0.00003	-11	-4	1600	10
CVP-33 7.1	0.2824	0.0002	0.00114	0.00004	-12	-5	1600	10
CVP-33 9.1	0.28235	0.00001	0.00103	0.00001	-14.8	-8.6	1790	9.7
CVP-33 10.1	0.28226	0.00001	0.001018	0.000006	-18	-11.7	1990	9
CVP-33 11.1	0.28224	0.00008	0.00084	0.00003	-18	-11	2000	8.8
CVP-33 12.1	0.28236	0.00007	0.00098	0.00005	-13	-7	1800	9.8
CVP28 - Tonalite								
CVP-28 1.1	0.28221	0.00002	0.001233	0.000007	-19.9	-13.7	2110	8.5
CVP-28 2.1	0.28217	0.00007	0.0017	0.00002	-20	-14	2200	8.2
CVP-28 3.1	0.28232	0.00002	0.00093	0.00002	-16	-9.7	1860	9.4
CVP-28 4.1	0.28239	0.00004	0.00098	0.00003	-13	-6	1700	10
CVP-28 5.1	0.28243	0.00005	0.00072	0.00005	-11	-5	1600	10.3
CVP-28 5.2	0.28239	0.00001	0.00084	0.00001	-13.4	-6.8	1690	10
CVP-28 6.1	0.282416	0.000007	0.000854	0.000009	-12.6	-6.1	1640	10.21
CVP-28 7.1	0.2821	0.0001	0.00184	0.00004	-22	-16	2300	7.7

Spot	$^{176}Hf/^{177}Hf$	± 2 se	$^{176}Lu/^{177}Hf$	± 2 se	εHf (0)	εHf (T1)	T DM (Ga)	εHf DM(T)
CVP13 - Tonalite								
CVP-13 1.1	0.2822	0.00002	0.001427	0.000009	-20.1	-13.5	2110	8.5
CVP-13 2.1	0.28222	0.00003	0.00124	0.00001	-19	-12	2090	8.6
CVP-13 3.1	0.28215	0.00002	0.001452	0.000007	-21.9	-15.6	2230	8.1
CVP-13 4.1	0.28224	0.00001	0.001256	0.000008	-18.7	-12.5	2030	8.8
CVP-13 5.1	0.28212	0.00004	0.00152	0.00008	-22	-16	2300	7.8
CVP-13 6.1	0.28231	0.00006	0.00105	0.00005	-15	-9	1900	9.3
CVP-13 7.1	0.28221	0.00005	0.00108	0.00004	-19	-13	2100	8.5
CVP-13 8.1	0.28226	0.00004	0.00095	0.00002	-17	-11	2000	8.9
CVP-13 9.1	0.2821	0.0001	0.0019	0.00004	-21	-15	2200	8
CVP-13 10.1	0.28233	0.00001	0.00094	0.00002	-15.7	-9.6	1850	9.5
CVP-13 10.2	0.28236	0.00005	0.00068	0.00005	-14	-8	1800	9.7
CVP-13 11.1	0.2822	0.0001	0.0013	0.00003	-18	-12	2100	8.6
CVP-13 12.1	0.28216	0.00009	0.00164	0.00004	-21	-14	2200	8.1
CVP-13 12.2	0.2822	0.0001	0.00133	0.00002	-20	-14	2200	8
CVP-13 13.1	0.28224	0.00003	0.00098	0.00002	-18.9	-12.7	2050	8.7
CVP3 - Leucotonalite								
CVP-3 1.1	0.2823	0.00002	0.001168	0.000006	-16.8	-10.6	1920	9.2
CVP-3 2.1	0.2823	0.0001	0.00097	0.00005	-15	-9	1800	9
CVP-3 3.1	0.28236	0.00001	0.00105	0.00001	-14.5	-8.2	1770	9.7
CVP-3 4.1	0.28244	0.00001	0.000348	0.000009	-11.9	-5.5	1600	10.4
CVP-3 5.1	0.28227	0.00003	0.001094	0.000008	-17	-11	1980	9
CVP-3 6.1	0.28238	0.00002	0.001045	0.000002	-14	-7.6	1730	9.9
CVP-3 7.1	0.282402	0.000009	0.000526	0.000005	-13.1	-6.6	1670	10.11
CVP-3 8.1	0.28234	0.00003	0.00105	0.00002	-14	-8	1820	9.5
CVP-3 9.1	0.28232	0.00002	0.00096	0.00001	-16	-9.6	1860	9.4
CVP-3 10.1	0.28241	0.00002	0.000635	0.000009	-12.7	-6.5	1660	10.2
CVP25E - Enclave								
CVP-25E 1.1	0.28226	0.00001	0.001256	0.000005	-18.3	-11.9	2000	8.9
CVP-25E 2.1	0.28215	0.00009	0.00187	0.00005	-21	-15	2200	8
CVP-25E 3.1	0.2826	0.0002	0.0012	0.00006	-5	1	1200	12
CVP-25E 3.2	0.2827	0.0002	0.00119	0.00008	-1	4	1000	12
CVP-25E 4.1	0.2824	0.00002	0.000629	0.000009	-13	-6.7	1670	10.1
CVP-25E 4.2	0.2821	0.0004	0.0013	0.0002	-10	-10	2300	8
CVP-25E 5.1	0.28234	0.00004	0.00156	0.00003	-14	-8	1810	9.6
CVP-25E 6.1	0.28228	0.00006	0.00101	0.00003	-16	-10	1900	9.1
CVP-25E 7.1	0.28228	0.00001	0.00103	0.00002	-17.3	-11	1940	9.11
CVP-25E 8.1	0.28238	0.00002	0.00089	0.00003	-13.9	-7.6	1730	9.9
CVP-25E 9.1	0.28227	0.00001	0.00109	0.00001	-17.6	-11.3	1960	9
CVP-25E 10.1	0.2812	0.0005	0.006	0.0004	-50	-40	4000	0

Spot	$^{176}Hf/^{177}Hf$	± 2 se	$^{176}Lu/^{177}Hf$	± 2 se	εHf (0)	εHf (T1)	T DM (Ga)	εHf DM(T)
CVP23E - Enclave								
CPV-23E 1.1	0.28234	0.00003	0.00148	0.00003	-14	-8	1810	9.6
CPV-23E 2.1	0.28234	0.00001	0.001058	0.000003	-15.4	-9.3	1830	9.5
CPV-23E 3.1	0.28244	0.00002	0.00082	0.00002	-11.8	-5.4	1590	10.4
CPV-23E 4.1	0.28232	0.00004	0.00104	0.00003	-15	-9	1860	9.4
CPV-23E 5.1	0.28245	0.00002	0.000653	0.000002	-11.4	-5.2	1570	10.5
CPV-23E 6.1	0.28237	0.00003	0.00089	0.00002	-13	-7	1750	9.8
CPV-23E 7.1	0.28229	0.00008	0.00093	0.00003	-16	-10	1900	9.1
CPV-23E 8.1	0.28226	0.00002	0.00134	0.00003	-18	-12	2000	8.9
CPV-23E 9.1	0.28232	0.000004	0.00137	0.00002	-16	-10	1870	9.38
CPV-23E 10.1	0.28235	0.00002	0.001146	0.000009	-14.9	-8.8	1800	9.6
CPV-23E 11.1	0.2824	0.00002	0.00063	0.00002	-13	-6.7	1670	10.1
CPV-23E 11.2	0.28228	0.00005	0.00131	0.00005	-16	-10	2000	9.1
CPV-23E 12.1	0.28228	0.00002	0.00137	0.00007	-17.5	-11.3	1960	9.1
CPV-23E 13.1	0.28232	0.00002	0.0012	0.00004	-15.9	-9.7	1860	9.4
CPV-23E 14.1	0.28216	0.00008	0.00141	0.00005	-21	-15	2200	8.1
CPV-23E 15.1	0.28216	0.00008	0.00191	0.00005	-21	-15	2200	8.1